Performance prediction and hydraulic design of intakes with particular reference to the formation of free surface vortices

Eugene Chang

Thesis submitted for the degree of Ph. D.

October, 1978

SUMMARY

"Performance prediction and hydraulic design of intakes with particular reference to the formation of free surface vortices"

Eugene Chang

Thesis submitted for the degree of Ph.D. 1978

This thesis describes work carried out on the hydraulic design of intakes and the scaling of free surface vortices. The aims were to 1) consider the economics involved when deciding whether or not to conduct a model study, 2) obtain a better understanding of vortex formation, 3) provide comprehensive data on various aspects of intake design, 4) derive scaling laws for modelling surface vortices.

Chapter 2 discusses the first aim, and shows that it is important to get the hydraulic design correct at an early stage. In certain circumstances a model study is advisable to be certain of trouble-free performance of the whole scheme. Examples of adverse effects of bad design are discussed in terms of loss in hydraulic performance, mechanical damage and cost of delays.

As regards the second aim, it is suggested that the boundary layer is the source of vorticity, with the suction pipe as the major contributor for the common rectangular sump geometry with a vertically suspended pump and symmetrical approach flow. The experimental results obtained for various sump geometries have been explained using these new ideas.

Comprehensive data on sump design has been obtained using a suction pipe with a bellmouth of diameter 244 mm placed at the end of a rectangular channel. The results have been plotted to show the variation of critical submergence with bellmouth velocity, and it is deduced that some optimum sump dimensions are dependent on the latter.

A new mathematical form of a consistent scaling law has been developed, based on a Froude and Reynolds number contribution, which assumes that the model:prototype velocity ratio is a function of scale only. Analysis of results from four geometrically similar rigs shows that other parameters are also involved. However, a series of curves has been obtained giving the appropriate scaling velocity for operating models in a certain size range.

KEYWORDS: INTAKE DESIGN, PUMP SUMPS, HYDRAULIC MODELS, PHYSICAL MODELLING, VORTEX FORMATION.

CONTENTS

ACKNOWLEDGEMENTS

I would like to thank Dr. A. J. Cochran for the valuable discussions I had with him, and for his constant interest and encouragement during the supervision of this research project.

The associate academic supervisor was Dr. A. E. Kramer.

Mr. M. J. Prosser was the industrial supervisor, and his help is gratefully acknowledged. Numerous other colleagues at BHRA, including the Library Staff, the Photography Section and Central Services Group have contributed in one way or another, and I am indebted to them for their assistance. In particular, I am grateful to Mr. G. A. J. Young who initiated the project and to Mr. A. Clarke who assisted with some of the experimental work, especially that described in Chapter 7.

Mrs. Lynn Pavey produced the excellent tracings of many of the line diagrams, and the IHD office helped in the initial preparation of the thesis.

Finally, I wish to thank Mrs. Sue Thompson for typing the thesis with such diligence and efficiency.

NOMENCLATURE

A	Cross-sectional area of intake
b	Coefficient of Reynolds number contribution to consistent scaling law
C	Distance from sump floor to bellmouth lip (floor clearance)
C_D	Discharge coefficient
D	Bellmouth diameter
d	Suction pipe diameter (external)
F	Froude number - $V/(gl)^{\frac{1}{2}}$
g	Acceleration due to gravity
H	Total depth (S + C) or pump head
K	Kolf number $\Gamma r/Q$
k	Froude scale multiplying factor
L	Length of approach channel
l	Characteristic length, e.g. water depth, intake diameter
p	Pressure
Q	Discharge, flow rate
R	Reynolds number Vl/ν
r, θ, z,	Cylindrical polar co-ordinates
S	Submergence (water surface to bellmouth)
$\mathcal{S}$	Strouhal number = nd/V_W, n = frequency of vortex shedding
s	Scale ratio l_m/l_p
t	Time
u	Radial velocity component
V	Velocity
v	Tangential velocity component
W	Sump channel width

$\overline{We}$	Weber number = $V(\rho l/\sigma)^{\frac{1}{2}}$
w	Axial velocity component
X	Distance from endwall to bellmouth lip (endwall clearance)
x	Distance along sidewall
x, y, z	Rectangular co-ordinates
Γ	Circulation at radius r
δ	Boundary layer thickness
ζ	Vorticity
μ	Dynamic viscosity
ν	Kinematic viscosity
ρ	Density
σ	Surface tension
ψ	Stream function
Ω	Angular velocity

Subscripts (not included above)

c	Critical length parameter for onset of air entrainment
m	Model
p	Prototype
θ	Tangential component

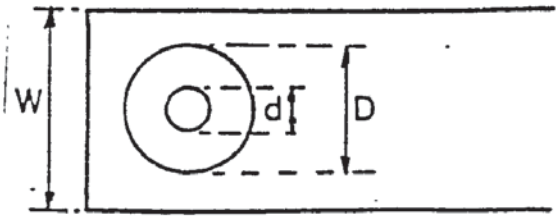

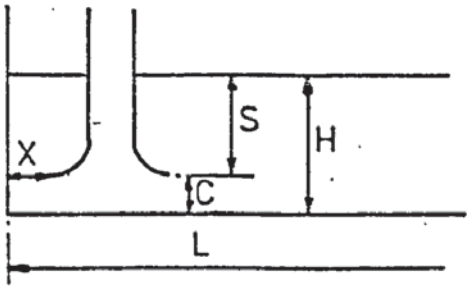

CHAPTER 1

INTRODUCTION

1.1 General background

New civil engineering works commissioned by Government agencies, public bodies and private industry are being built all the time. A large and important part of these such as dams, power stations and water supply systems involve the flow of some fluid from a source to an intake and from there to a discharge point via various hydraulic structures, pipework and machinery. There must be appropriate design features for each of these for safe, efficient and economic operation of the complete scheme.

In some cases, design features for new hydraulic schemes can be based on well-founded standard designs. General design guidelines, for example, for pump sumps and intakes are to be found in refs. 1 and 2. These are based on the existing knowledge and experience of pump manufacturers, end-users, hydraulic laboratories and consulting engineers. Furthermore, some standard situations are amenable to theoretical treatment, often supplemented by empirical results, thus giving a practicable design.

However, it is often the case with hydraulic structures that the real-life situation (called the prototype) in a particular project is, of necessity, unique in that it does not conform to any known standard situation. This may be due to peculiarities in the local topography or geological structure or to constraints imposed by existing works or permanent physical features. Although it may be possible to eliminate some of the more obvious hydraulic problems at the design stage, these are very often not appreciated or considered early enough. Furthermore, it is not easy to foresee the undesirable flow phenomena which can arise in complex flow situations, and it is

then only prudent to conduct a hydraulic model study.

Fig. 1.1 shows in simplified form the possible sequence of events that can occur between the original 'felt need' for a scheme to the final handover of the completed project. Various outcomes are possible, depending on whether the design is standard or non-standard, and whether or not a model study is commissioned. The relative length of each path gives an indication of the time taken for final handover, and shows the extra time and hence delay involved when a model study is not undertaken. This is discussed further in Chapter 2.

The use of scale models to reproduce flow conditions on proposed or existing hydraulic structures is a well-established technique. They have been successfully used in a wide variety of situations, including irrigation schemes, intakes in hydro-electric schemes, pump sumps for sewage stations or power stations, spillway design and offshore structures. For proposed schemes, they serve not only to predict the performance but can also provide useful design data in lieu of actual field measurements; modifications can be readily carried out on the model to optimise the hydraulic design. For existing schemes which are not operating satisfactorily or which require extension, effective modifications can be tested on a model before installation on the prototype. Obviously a cut-and-try method on the prototype would be prohibitively expensive.

One undesirable phenomenon which occurs all too frequently is vortex formation and its associated swirl. This can occur whenever fluid with a free surface is drawn into an intake, either by pumping or by gravity. Surface vortex formation can lead to air entrainment which causes loss in pump performance as well as mechanical damage to the pump. The swirl associated with vortex motion can cause overloading of the drive motor. In situations requiring continuous duty, e.g. cooling water supply for

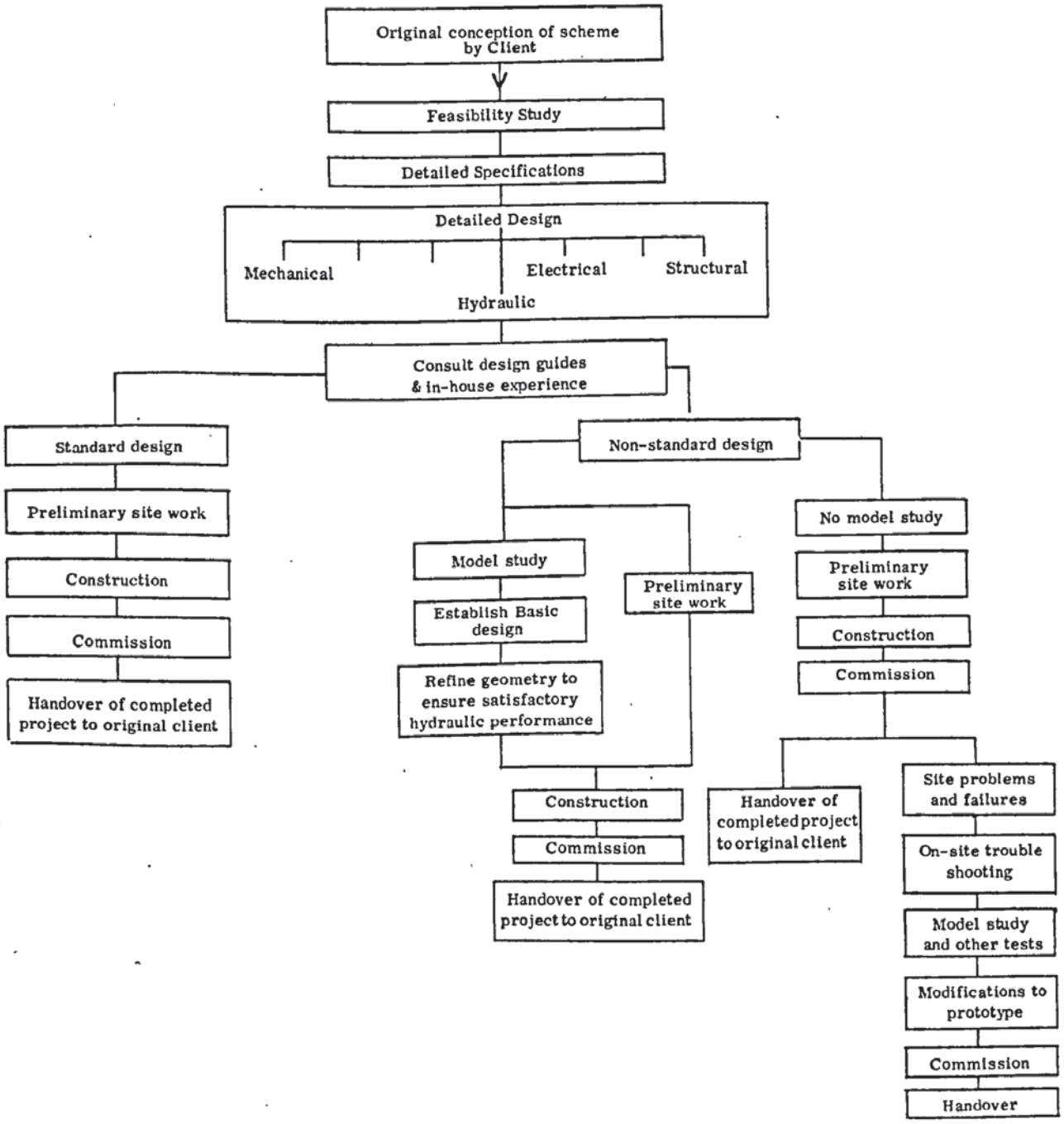

Fig. 1.1 Design history of a new civil engineering scheme: possible routes from original conception to handover of completed project. The relative length of each complete path gives an indication of the time taken for final handover.

steam turbines it is essential to have trouble-free operation of the pumps. A more recent example is the emergency core cooling system of a nuclear reactor, which must operate reliably and efficiently in the event of a loss of coolant accident. Where only intermittent pump operation occurs, e.g. land drainage, then a slight loss in performance may be acceptable.

1.2 Necessity for the project

Although hydraulic models are undoubtedly of great value to the design engineer, the interpretation of them needs to be treated with care. With a complex flow phenomenon such as vortex formation which involves several forces, it is not possible to ensure complete geometric, kinematic and dynamic similarity between model and prototype if the same fluid, i.e. water is used in both, and so a compromise has to be made. There is, however, still a conflict of opinion on the best scaling laws to use in order to accurately reproduce vortices on the model.

The choice of the linear scale and the velocity scale for the model is an important one. If the model velocity is too low, then severe vortices may not be observed whereas too high a velocity may produce vortices which entrain air on the model but do not do so on the prototype. This can lead to over-conservative recommendations to prevent air entrainment and hence extra expense which becomes particularly significant when scaled up for very large schemes. Alternatively, high model velocities give rise to surface distortion and high levels of turbulence which can inhibit air-entraining vortices.

One way of resolving this problem would be to locate a prototype situation where vortex formation could be easily observed and controlled, and then to build one or two geometrically similar scale models. This approach was considered early on in the project, but enquiries to various

members of BHRA produced no suitable prototype location. Indeed, on looking through previous literature, there is an obvious lack of prototype data. The main reason is that vortices are normally "designed out", and in any prototype where strong surface vortices do occur, the vortices are not planned, let alone controllable. Where there is any likelihood of damage to the hydraulic machinery, then anti-vortex devices would be designed and installed, (see Chapter 7 for an example of this). This explains the difficulty in finding a suitable prototype where systematic tests could be made. Thus tests were carried out on laboratory scale experimental rigs.

Also of importance in ensuring satisfactory prototype performance is the question of optimum design of pump sumps and intakes. There is general agreement on the basic dimensions for a rectangular pump sump but a range of uncertainty still exists, especially over the submergence required by an intake to avoid air-entraining vortices. If these dimensions could be more closely defined, this would lead to savings in construction costs and improved pump performance.

In view of the uncertainties indicated above in the areas of velocity scaling for free surface vortices and the hydraulic design of intakes, BHRA Fluid Engineering initiated a research project on these problem areas. The aim was to carry out systematic work on an intake design whose geometric shape and physical size were as close as possible to practical configurations. This is in contrast to much of the work described in the published literature in this field, most of which is either based on idealised or simplified geometries, or is based on specific schemes with unusual design features.

1.3 Relevance of the project to the sponsoring organisation

BHRA is an independent, non-profit distributing research association and undertakes both basic and contract research for industry and Government departments in the general field of fluid engineering. Since its inception in 1947, it has been actively involved in hydraulic model studies for numerous schemes throughout the world, especially those involving hydraulic structures and intakes of one sort or another.

Although it has satisfactorily completed these model studies - there has been no adverse feedback from site operators after commissioning of the prototype - the scaling of vortices has always been a subjective matter, with engineers having their own preferred test procedure. On the design side, BHRA has recently been involved in a design guide for intakes (1)*, and the work discussed in the following Chapters provides supporting material for this.

Thus, this research project is a logical extension of an important aspect of BHRA's activities, with the aim of better modelling of vortex phenomena and improved performance of hydraulic intakes at minimum cost to the client.

1.4 Scope and aims of the project

Hydraulic intakes occur in a wide variety of different configurations, and it was decided to concentrate on a single vertical bellmouth intake in a rectangular channel, a configuration commonly found in pump sumps.

Experimental work was initially carried out with a single bellmouth intake of diameter 244mm and suction pipe diameter 6" (nominal) to provide

---

* Numbers in brackets refer to references listed at the end of the thesis.

the bulk of the information on sump design. Some tests were then repeated with geometrically similar channels with a bellmouth 61mm in diameter (1.5" nominal suction pipe), 122mm in diameter (3" nominal suction pipe diameter) and 488mm diameter (12" nominal suction pipe diameter) in order to provide information on scaling laws. These were then supplemented by work on an actual model study of a multiple pump sump consisting of four vertical bellmouth intakes in a rectangular sump.

Thus, experimental work on horizontal intakes is beyond the scope of this project, though some of the results are equally applicable to these intakes in a qualitative manner. Furthermore, only free surface vortices have been considered in detail, though other undesirable phenomena such as swirl and submerged vortices which also affect the performance of a particular intake are discussed.

The aims of the research project can be summarised as follows :-

1) to consider the economic factors involved when deciding whether or not to conduct a model study for a proposed or existing design.

2) to obtain a better understanding of the mechanism responsible for the formation and development of vortices.

3) to provide comprehensive experimental data on various aspects of intake design including pump sumps, especially with regard to the occurrence of surface vortices, and to compare this data with predictions from a recently developed mathematical model, (3b)

4) to derive satisfactory scaling laws for modelling free surface vortices.

CHAPTER 2

ECONOMIC CONSIDERATIONS

2.1 Introduction

Design features for new hydraulic structures or for extensions to existing works can be based on standard designs. However, any deviation from a standard situation gives rise to uncertainty over the hydraulic performance of the intake. One can then either take a risk and proceed with construction or carry out a model test beforehand to be sure of satisfactory prototype performance. A model study necessarily involves extra costs and possible delay in completion of the scheme. However, the actual cost of a model study is a very small percentage of the total prototype cost. Furthermore, without a model study, hydraulic problems could appear on the prototype which would give rise to substantial extra costs for the entire scheme, out of all proportion to the relative size and cost of construction of the intake itself. Thus the model costs must be balanced against the potential savings arising from increased performance and reliability of operation. Any possible delays due to a model study can be minimised by adequate planning at an early stage.

As mentioned earlier, there is uncertainty in the correct scaling law for air-entraining vortices, and this leads to conservative recommendations in the design of anti-vortex devices. Thus, precise knowledge of the scaling law could lead to savings in design modifications as well as reducing the testing time and hence costs for a model study.

The table below lists the costs that can be incurred when conducting and not conducting a model study prior to construction. This comparison only applies to non-standard situations. Where a design closely follows that of a previous design known to function satisfactorily then a model study

is not necessary and none of the costs under "No Model Study" should apply. Similarly, for small schemes where the costs under "No Model Study" are very small, it may be more economic to construct first and modify later, if necessary, without incurring the cost of a model study.

Model Study	No Model Study
a) Cost of model study	a) Loss in performance
b) Cost of design modifications	b) Mechanical damage
c) Extra design office work	c) Delays in commissioning/ production
d) Possible delays in completion	d) Increased cost of installing design modifications after commissioning.

It should be noted that sump design affects both the initial capital cost of a project and the subsequent running costs (fuel, labour, maintenance, rent for land usage). In the past, the emphasis has been on minimising initial costs. Now however, with increasing fuel costs and size of pump units more attention should be paid to running costs. For example, a drop in efficiency of 1% can lead to extra costs which, in a few years, can exceed the initial capital cost of the pump. Furthermore, the running costs of an installation can exceed the initial capital cost of the entire pumping scheme within a 10-year period (4). Discounted cash flow techniques are a useful way of comparing the total costs (i.e. capital and running costs) of alternative schemes (5).

In the following sections, some of the costs summarised in the table above are discussed and illustrated by specific examples where possible. Only economic costs and savings are discussed, though better design can also lead to social benefits in the form of improved recreation facilities, reduction of accident hazards and less environmental noise. In fact, the possible adverse impact on the environment of some schemes may outweigh

strictly economic considerations of the necessity for a model study.

2.2 Costs arising from adverse flow conditions if no model study is carried out.

2.2.1 Loss in performance

If no model study is carried out, then there is the possibility that the sump design itself will not give optimum pump performance. Several authors (6, 7) have shown that small changes in the position of a pump within a sump can lead to changes in head and efficiency, though power input remains relatively constant.

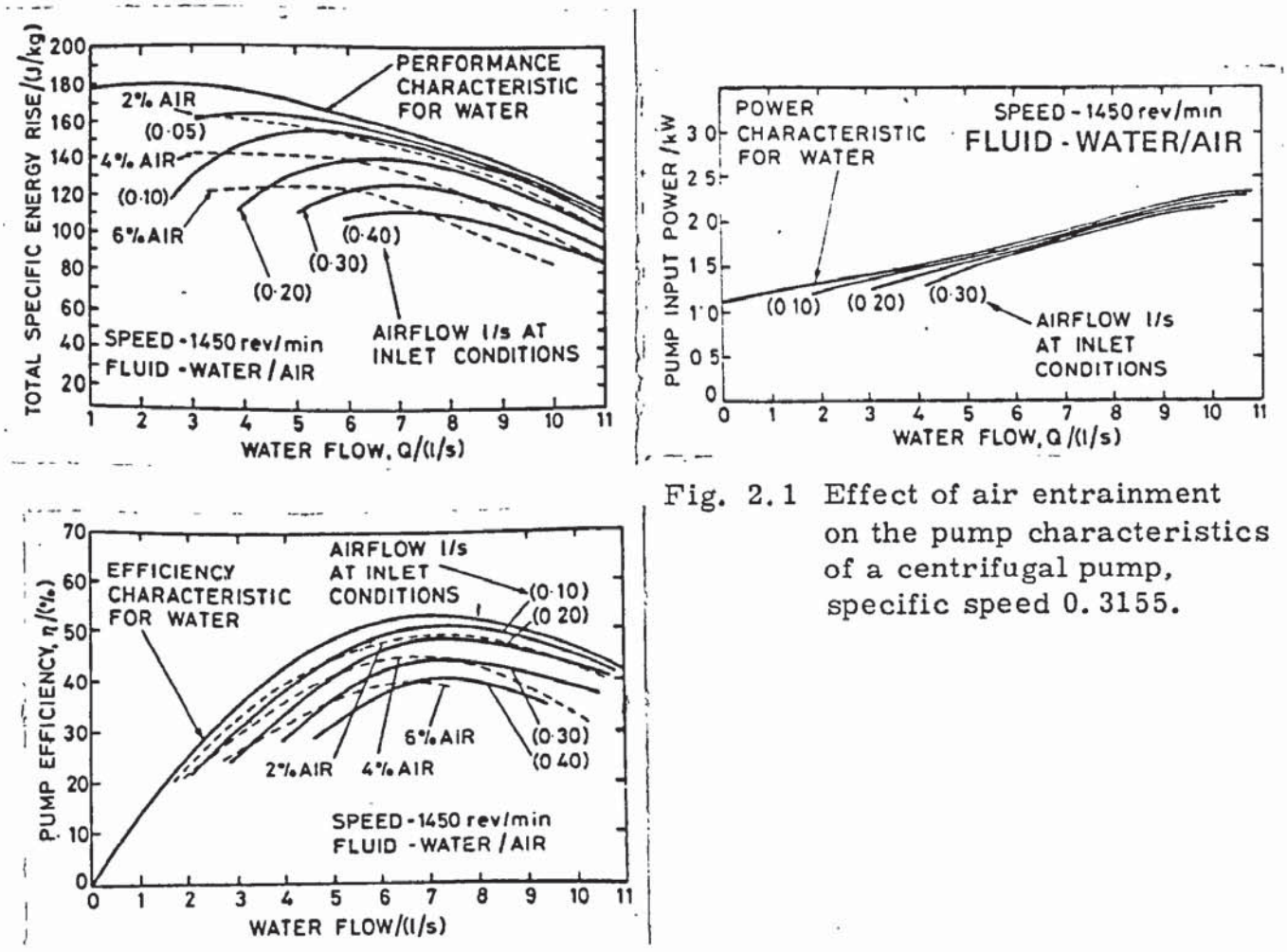

Fig. 2.1 Effect of air entrainment on the pump characteristics of a centrifugal pump, specific speed 0.3155.

If undesirable flow phenomena such as vortices and swirl are also present, then further loss in performance may result. A few studies have been made on the effect of entrained air on pump performance and these are reviewed in ref. 8. Fig. 2.1 shows some typical results from Merry (9) for a centrifugal pump of specific speed 0.3155 with up to 6% of

air by volume introduced into the pump inlet. This leads to a drop in efficiency of up to 15%. The air-to-water volumetric ratio associated with a vortex is difficult to assess accurately, but estimates range from less than 0.01% (10) up to 15% (11, 12) for strong vortices at low submergences. At the higher end of this range, depriming of the pump may occur.

If the volume of air entrained by a vortex is less than 1%, then the effect on pump performance seems to be very small. However, increased noise and vibration can result as the air bubbles collapse in regions of higher pressure. Submerged vortices and swirl also increase noise and vibration levels. Mayo (13) quotes results showing a direct relationship between noise measured near a pump/turbine shaft and loss in hydraulic efficiency.

Noise and vibration will also accelerate the rate of wear of any pump unit. This will inevitably affect the pump characteristics, as shown in Fig. 2.2 (14), as well as increasing maintenance costs. Excessive noise and vibration can also lead to mechanical damage, as discussed in the next section.

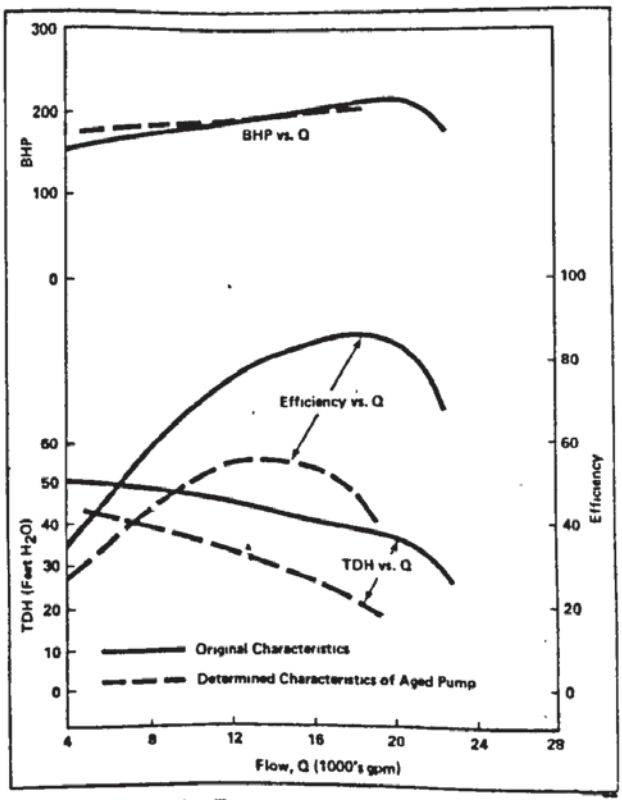

Fig. 2.2 Effect of ageing on pump characteristics. BHP: Brake Horse Power TDH = Total Discharge Head

The increased costs due to loss in pump performance can be found by considering the power input required to obtain a discharge Q at head H.

$$\text{Power input required} = \frac{QH\rho g}{\eta}$$

ρ = relative density of fluid

η = pump efficiency

$$\text{direct cost per unit pumped} = \frac{H\rho g}{\eta} \cdot \text{unit cost of electrical input}$$

(Indirect costs arise from depreciation, interest and maintenance costs). Thus a drop in efficiency leads to increased pumping costs, for delivery at a given head. In practice, the head-discharge curve also changes for a worn pump, leading to a drop in head and also in the flow-rate delivered by the pump (fig. 2.3)

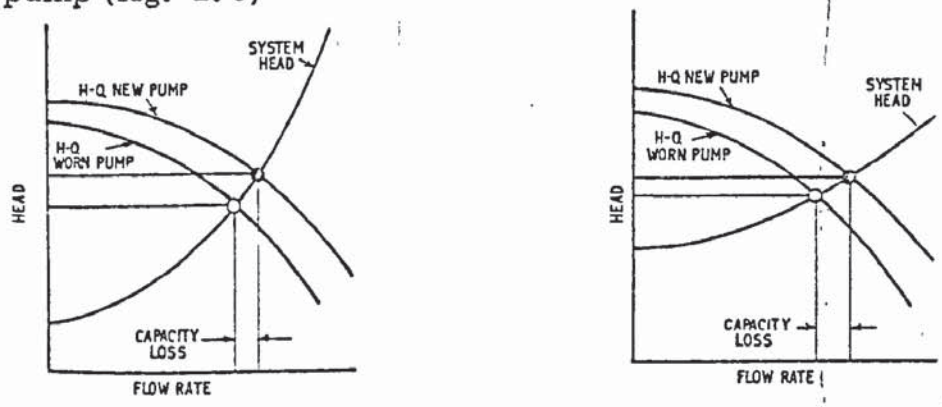

Fig. 2.3 Head-discharge curves for a new and worn pump, showing the loss in capacity for two different systems.

2.2.2 Mechanical damage

It is now well established that poor hydraulic design can lead to mechanical damage such as shaft failure (15), fracture of impeller blades (16) and gearbox failure (17). The basic causes of these are excessive vibration levels, uneven blade loading and cavitation damage. Costs are then incurred not only through repair work but also through delays in commissioning and stoppages in production. If the original design engineer or pump manufacturer is no longer available for consultation, then the

subsequent delay can make the total costs of repair work plus downtime more expensive than the initial capital cost of the equipment. It is difficult to generalise on the costs that can be incurred, but more likely than not they will exceed the cost of a model study when large pumping units are involved.

In the example of ref. 17 which is also discussed in Chapter 7, the cost of recommended modifications to the civil design and mechanical support found to be necessary after commissioning was an order of magnitude greater than the cost of the model study. This does not take into account the costs incurred due to either the delay of several months in commissioning the nuclear power station or the constant movement of technical personnel to and from site.

2.2.3 Delays in commissioning

The economic consequences of delays in completing a particular project vary considerably with the purpose of the project, but are particularly high in the case of electricity generating plants and water supply for production plants such as liquified natural gas plant. The extra costs arise from a) interest charges on tied capital which is not providing any income; b) the cost of alternative fuel supplies in the case of generating plant, leading to higher running costs; c) the cost of tying up staff who were either expecting to finish the project or staff who were expecting to start work on site.

As an example, take the case of a new 1300 MW generating station costing £400 million which has been delayed by 12 months through bad hydraulic design of the cooling water system. At least half this sum is tied up in capital investment which is producing no return through the sale of electricity. Thus, if interest rates are 8%, then this represents a

loss of £16 million a year. A second cause of increased costs is that less efficient plant then has to be kept in use for a year longer. This reserve plant could consume up to 50% more fuel than a modern plant for the same amount of electricity generated. The 1977/78 figures for generating costs, including capital charges and fuel and operating costs are given below (18) :

Fuel	Generating cost per kW/hr
Nuclear	0.76p
Coal	1.23p
Oil	1.42p

Thus, for a 1300 MW coal-fired station, the average generating costs for a 75% load factor would be £105 million a year, so that if a less efficient plant is used, generating costs are increased by several million pounds. The extra costs are greatest where the commissioning of a nuclear power staion with relatively low generating costs is delayed, and an older, oil-fired station has to be kept in service instead. The third factor to consider, that of prolonged commitment of staff to the project and the enforced idleness of some staff can also add considerable sums to the total cost of delay, the exact amount depending on the scale of the project.

Thus, to summarise for this particular example, delays in completing a project on time can have severe financial consequences. The extra costs incurred in one year's delay can add up to a significant percentage of the original construction costs. As further illustration of this, the cost overruns due to delays in completion of four advanced gas-cooled nuclear reactor power stations are given in the table below (19) :

	Dungeness 'B'	Hinckley Point 'B'	Hartlepool	Heysham
Date of original estimate	1965	1966	1968	1970
Originally expected date of completion of commissioning	1971	1973	1974	1976
Assumed commercial operation date of No. 1 reactor	1980	1977	1981	1981
Original estimate at prices at dates given above	£89m	£95m	£92m	£142m
Cost overrun as % of original estimate (excluding effects of inflation)	120%	33%	87%	35%
Estimated costs to completion based on prices at July 1977	£320m	£147m	£252m	£273m

It should be noted that the effects of delays are not always as great as the above examples would suggest. For example, Steenbras pumped storage scheme, whose purpose is to provide 180MW of electricity during peak hours, will substantially reduce the need for power imports from alternative sources. The savings are expected to be around £700,000 a year (20) so that any delay in completion of this project would represent a loss of this amount per year. Although this sum is less than the millions of pounds involved with power stations, it is still much greater than the cost of a model study plus modifications. This is discussed in the next section.

2.3 Cost of model and modifications

The cost of a model study varies greatly depending on the physical

size to be modelled, the complexity of the test programme and on the nature of the organisation carrying out the study. University departments, pump manufacturers and private laboratories all conduct model studies but would differ in their charging system and time for completion of the project. For example, universities may be able to use research assistants to help on model studies, and pump manufacturers could incorporate the cost of a model study into the total contract price when tendering for the supply of certain pumps.

For schemes such as pumped storage schemes requiring a large amount of civil engineering works, the total cost can run into millions of pounds, e.g. the cost of Steenbras pumped storage scheme is about £30 million, as quoted in ref. 20. By comparison, the model study (21) cost approximately £40,000. On top of this should be added the cost of the recommended anti-vortex grids, which is estimated to be £15,000. Thus, the total cost of the model plus subsequent modifications is a very small percentage of the total prototype cost. This is further borne out by costs for the model and prototype on the Turlough Hill pumped storage scheme (22), where the cost of model plus anti-vortex grid was less than 0.2% of the cost of the whole scheme, including civil works, mechanical and electrical equipment and overheads.

For pump sumps, the civil works are less extensive, though the sump may form part of a larger scheme, e.g. cooling water supply. The cost of model studies in this case is typically in the range £9,000 - £20,000. Modifications to the original design arising from the model study may include small geometry changes such as the addition of guiding vanes or splitter walls which would add a negligible amount to the total cost. On the other hand, modifications may actually lead to savings in construction costs by showing some features to be redundant or sump

lengths to be too long, e.g. ref. 23, where it was found that a reduction in sump length from 12m to 8m was in no way detrimental to hydraulic performance, thus saving a volume of 350m^3 of excavation, i.e. a reduction of 33$\frac{1}{3}$% in sump volume.

In the model study discussed in Chapter 7, modifications to the sump were found necessary after the sump had been designed and built. The cost of just the civil works required for these modifications would probably be around £50,000, which is several times the model study cost, and a significant proportion of the original construction cost for the sump and pumphouse. This underlines the importance of getting the hydraulic design correct at an early stage, and how much more economical it is to undertake a model study before, rather than after, completion of the project.

2.4 Conclusions

This Chapter has discussed the importance of good hydraulic design and the various factors involved in deciding whether or not to conduct a model study. It has been stated that for standard designs or relatively small schemes, a model study may not be necessary. However, for non-standard designs, a model study at the design stage can ensure satisfactory hydraulic performance on the prototype. Otherwise, if no model study is undertaken, and hydraulic conditions on site are unsatisfactory, then extra costs can be incurred due to loss in pump performance, increased mechanical wear and hence increased maintenance costs, and delays in reaching the design output. These costs are compared in Fig. 2.4 which is based on estimates for the hypothetical example of a 1300 MW power station discussed in 2.2.3. Actual values for any given scheme may vary considerably from these, depending on size and application.

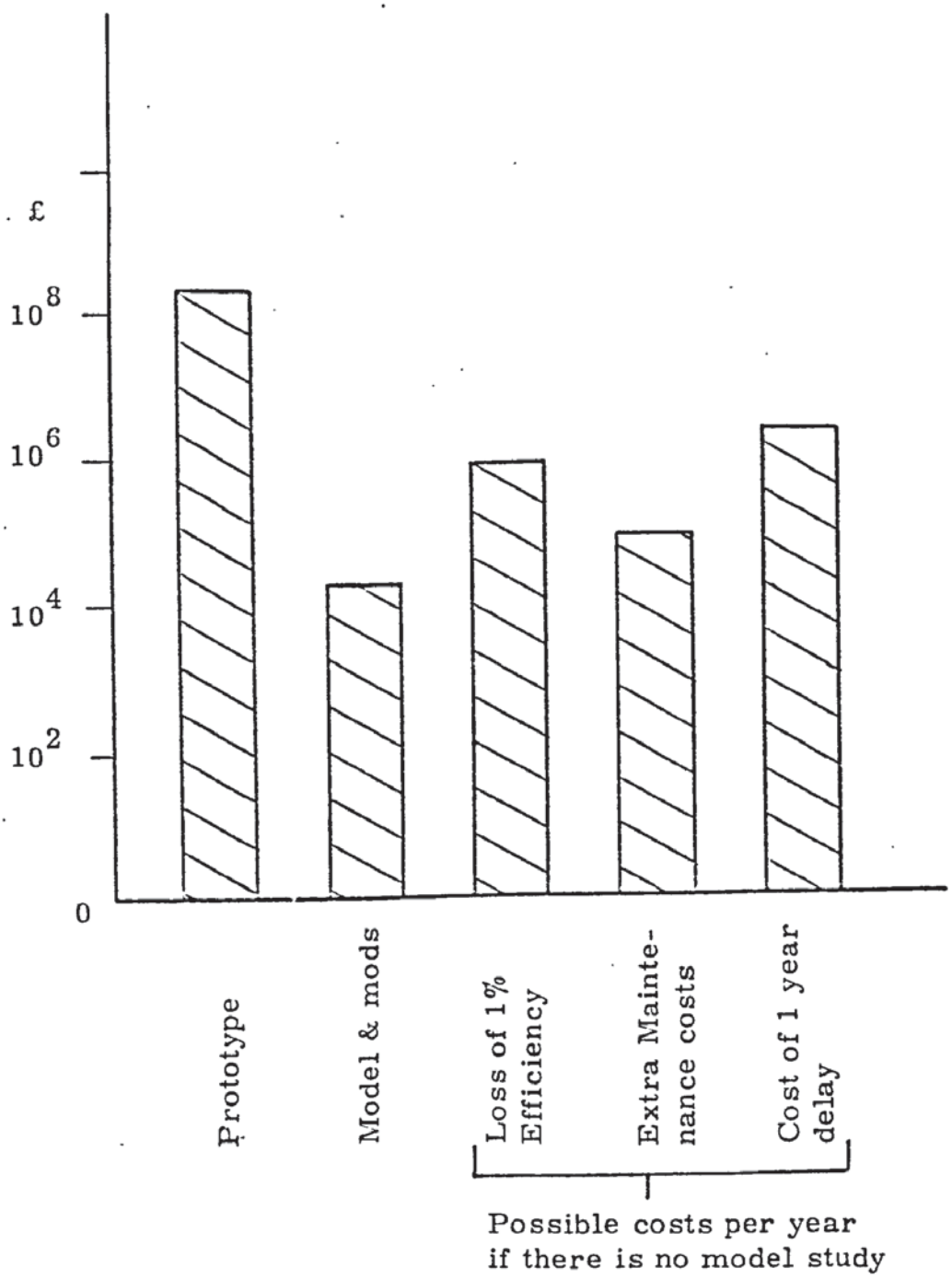

Fig. 2.4 Comparison of cost of prototype, model study and modifications, and possible annual costs due to bad hydraulic design if no model study is carried out.

On the basis of data obtained from several real-life schemes it is concluded that the cost of a model study is a very small percentage of the prototype costs and that although extra design modifications suggested by the model tests may be necessary, it is also possible that the results of a model study can lead to savings in construction costs. Furthermore, there are potential savings arising from increased performance and reliability of operation. Savings in running costs are becoming increasingly important with the constant rise in fuel prices.

Savings are also possible if the scaling laws were known more precisely, though it is impossible to generalise on the actual sums involved. The current practice is to operate models with a certain safety margin, so that anti-vortex devices or sump geometries may be over-designed. In the extreme case, anti-vortex grids may be completely redundant if the safety margin is too great. If this is the case for the Steenbras pumped storage scheme referred to earlier, then it means that an extra expenditure of £15,000 has been incurred because of uncertainty in the scaling laws. In fact, for this particular scheme, it is proposed to conduct prototype tests on the grid size and beam spacing to determine the degree of redundancy if any, in the design of the anti-vortex grids (21). Prototype data will then also be available for comparison with model data.

CHAPTER 3

THEORETICAL BACKGROUND

3.1 Summary

The mathematical analysis of the onset of vortices and their subsequent development is far from complete. Even in the simpler, axisymmetric case of drain vortices in cylindrical tanks, the basic equations become exceedingly complex when realistic boundary conditions are imposed. Accurate solution of these equations requires a detailed knowledge of velocity gradients, and these are difficult to determine experimentally. In the present area of interest, rectangular sumps, there has been noticeably little work carried out.

The following sections describe various approaches to understanding vortex formation :

Section 3.2 Mathematical description using the Navier-Stokes equation; it is shown that this approach has limited application to the more complex situation of vortices in rectangular geometries;

Section 3.3 Dimensional analysis to find the important parameters which are involved;

Section 3.4 Essentially qualitative considerations of the origin of the vorticity necessary for vortex formation; the application of these ideas to a suction pipe in a rectangular channel shows the pipe to be the major source of vorticity;

Section 3.5 Use of a mathematical model developed by Swainston (3) and based on potential flow round a point sink.

Section 3.6 Finally, the introduction and development of a new consistent

scaling law based on both the Froude and Reynolds number, which shows how a general scaling law could be derived by conducting experiments with different size rigs. The implications of the law on the form of the experimental results is also described.

3.2 Mathematical description of vortex motion from the Navier-Stokes equation.

It is of interest first of all to consider the mathematical description of a vortex. In the work reviewed in this section, the mathematical treatment has been simplified by assuming axisymmetric flow conditions. Despite uncertainty over the form of velocity gradients and boundary conditions, limited success has been achieved in describing some of the features of vortex motion, including velocity distribution and surface profiles. There also exists a large body of work on atmospheric vortices (24), but these introduce problems of compressibility and heat convection which are not relevant to the type of vortex presently under consideration.

The starting point of any mathematical treatment of the flow of an incompressible viscous fluid is the Navier-Stokes equation which is, in vector form :

$$\frac{D\underline{V}}{Dt} = \underline{F} - \frac{1}{\rho} \nabla p - \nu \nabla \wedge (\nabla \wedge \underline{V})$$

where $\frac{D\underline{V}}{Dt}$ is the total differential $\frac{d\underline{V}}{dt} + (\underline{V}.\nabla)\underline{V} = \frac{d\underline{V}}{dt} + u\frac{d\underline{V}}{dr}$

$$+ \frac{v}{r}\frac{d\underline{V}}{d\theta} + w\frac{d\underline{V}}{dz}$$

in cylindrical polar co-ordinates (r, θ , z) with components of $\underline{V}$ (u,v, w,), and $\underline{F}$ is an external body force per unit mass acting on the fluid, e. g.

where Coriolis force is important, $\underline{F} = -2\,\underline{\Omega} \wedge \underline{V}$

If axial symmetry is assumed, then the Navier-Stokes equation expressed in cylindrical polar co-ordinates becomes, in component form:

$$u\frac{du}{dr} + w\frac{du}{dz} - \frac{v^2}{r} = -\frac{1}{\rho}\frac{dp}{dr} + \nu\left(\frac{d^2u}{dr^2} + \frac{1}{r}\frac{du}{dr} - \frac{u}{r^2} + \frac{d^2u}{dz^2}\right)$$

$$u\frac{dv}{dr} + w\frac{dv}{dz} + \frac{uv}{r} = \nu\left(\frac{d^2v}{dr^2} + \frac{1}{r}\frac{dv}{dr} - \frac{v}{r^2} + \frac{d^2v}{dz^2}\right)$$

$$u\frac{dw}{dr} + w\frac{dw}{dz} = -\frac{1}{\rho}\frac{dp}{dz} + \nu\left(\frac{d^2w}{dr^2} + \frac{1}{r}\frac{dw}{dr} + \frac{d^2w}{dz^2}\right)$$

whilst continuity requires :

$$\frac{\partial(ru)}{\partial r} + \frac{\partial(rw)}{\partial z} = 0$$

There have been various attempts to solve these equations. One approach is to start with an infinite flow field with axisymmetric stagnation point flow superimposed on the tangential velocity distribution of a free vortex so that

$$u = -ar \qquad v = \frac{\Gamma_\infty}{2\pi r} \qquad w = 2az \qquad (a = \text{const.})$$

This represents an exact solution of the Navier-Stokes equation, where Γ_∞ is the constant circulation of a free vortex centred around the z-axis. However, this solution requires v to be infinite when r = 0. Another exact steady-state solution for v which is regular at the origin (due to Burgers Ref. 25) is

$$v = \frac{\Gamma_\infty}{2\pi r}\left(1 - e^{-ar^2/2\nu}\right)$$

To maintain this vortex new circulation is continuously brought in from infinity towards the axis by the stagnation point flow. Developing this further, Rott (26) defined a "viscous radius"

$$r^* = \sqrt{2\nu/a}$$

such that for $r \gg r^*$ the form of v reduces to that of a free (inviscid) vortex whilst for $r \simeq r^*$ the effect of viscosity is significant leading to departure from the free vortex velocity distribution. As $r \to 0$, rigid body rotation is obtained. This essentially describes a Rankine vortex.

This implies that the viscous effect is restricted to a cylinder of radius of order r^*, and that the solution applies to a viscous vortex core with stagnation point flow irrespective of the flow at infinity. Thus, Rott applied the solution to the bathtub vortex, representing the flow by a sink at a distance h from an infinite plane (representing the free surface) plus its image to give a free surface stagnation point. (This method was developed by Swainston for rectangular sumps - see 3.5). The effect of the bottom and sidewalls was neglected. The total pressure drop from infinity to the centre of the core which causes a surface dimple to appear, is then

$$\Delta p = \frac{\log 2 \; \rho \Gamma_\infty^2 a}{8 \nu \pi^2}$$

He gives a rough estimate for the critical value of h for the dimple to become air-entraining as

$$\left(\frac{h}{d}\right)^2 = \frac{\Gamma_\infty^2 \sqrt{2} \log 2}{16 \pi^2 \nu h \sqrt{gh}}$$ where d is the outlet diameter.

A more general class of exact solutions can be obtained by assuming

$$u = u(r) \qquad v = v(r) \qquad w = zw(r)$$

Donaldson and Sullivan (27) found it necessary to have the z-dependence of the axial velocity to keep v finite at the axis. One of the many solutions for a range of Reynolds numbers, based on u and the tank radius, is shown in fig. 3.1 together with the special limiting case of Burgers' solution. Sullivan's solution shows reverse axial flow, and this has been observed both in laboratory experiments and in hurricanes and tornadoes. Various other solutions were obtained satisfying the boundary conditions that u, v vanish at the axis and w is zero at the tank walls.

Fig. 3.1 Comparison of Burgers' (25)(on the left) and Donaldson's (27) solutions for the streamlines and variation along a radius of velocity components of a vortex with $R = -\infty$ and with tank radius assumed infinite.

By introducing the variable (r/z), the Navier-Stokes equation in component form reduces to three ordinary differential equations (28), with axial velocity $w = \frac{1}{r} f(r/z)$. By assuming $u \ll v$, and neglecting derivatives with respect to z compared with those with respect to r, then the circulation becomes constant on every conical surface, $r/z = \text{const}$,

which may explain the almost conical shape of a dimple vortex. However, these solutions also imply that $v \simeq w$, which is not true in practice for a drain vortex.

The form of the surface profile has been obtained (29) from the radial component of the Navier-Stokes equation by using solutions from Einstein and Li (30) for the tangential component equation. The main assumptions for these were that vertical velocities were negligible compared with horizontal velocities and that the velocity distribution at the drain outlet, was uniform. Expressions for the regions near and away from the vortex core for the surface profile were found to give reasonable agreement with experiment.

Another approach consists of introducing dimensionless quantities to obtain two partial differential equations in ψ and Γ (31), which, however, cannot be solved exactly. It is interesting to note that three dimensionless parameters emerge from this method: a radial Reynolds number $Q/\nu l$, a Rossby number $Q/\Gamma r$ and a ratio of characteristic lengths. Refs. (26) and (28) above are special cases of this where special forms for ψ and Γ were assumed. A series expansion of ψ and Γ can be made to attempt to solve the equations for small Rossby numbers, and the first order solution thus obtained is essentially that in Ref. (30).

However, higher order solutions require considerably more effort and also restrict the form of permissible axial boundary conditions. Granger (32) follows a similar approach, but with a series expansion in powers of radial Reynolds number instead of the Rossby number, and Anwar (33) applied the solution for a weak vortex, with the assumptions that Γ did not depend on z/h, and that $(r_o/h)^2$ was very small. His experimental results agreed best with the numerical solutions for the

velocity distributions in which the axial velocity was taken as zero at the axis of symmetry.

The rapid growth of a vortex core is considered in Ref. (34). By assuming a form for u, the other two velocity components and hence the change in surface profile with time for a inviscid fluid can also be found. Sample results are shown in fig. 3.2

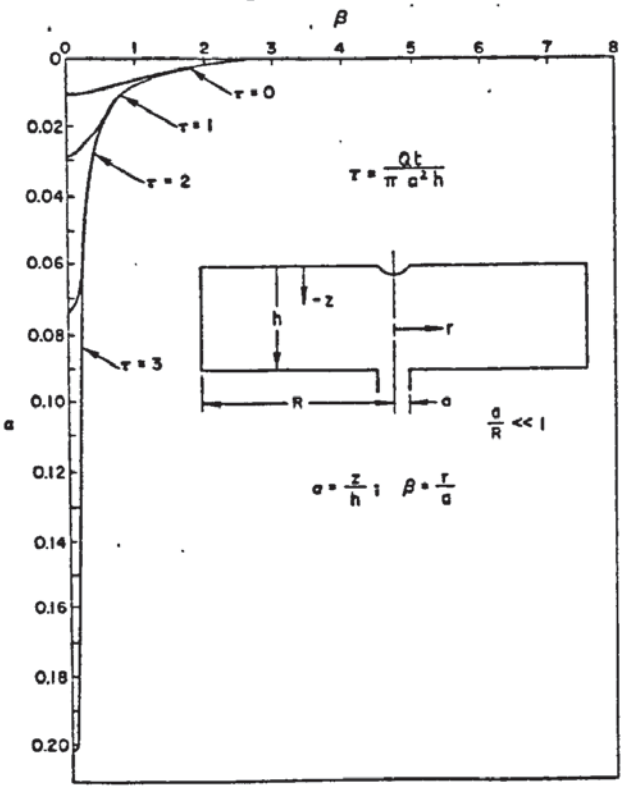

Fig. 3.2 Time history of the formation of a vortex core, starting with a surface dimple ($\tau = 0$) and growing with time into a deep dimple with tail ($\tau = 3$). Vertical and horizontal axes are non-dimensionalised depth and radius respectively.

To sum up, there have been a few attempts to solve the Navier-Stokes equation to describe vortex formation in an axisymmetric situation. These often assume forms for various velocity components and velocity gradients, some of which do not hold in practice. Thus, it seems that this mathematical approach could not be readily applied to other intakes such as rectangular pump sumps which do not possess axisymmetry.

3.3 Dimensional analysis

Let us assume that vortex formation is a function of the following variables :

$$f(S,\ C,\ X,\ W,\ L,\ d,\ D,\ V,\ \rho\ ,\ \mu\ ,\ \sigma\ ,\ g) = 0$$

where V represents a mean velocity. It is assumed also that there is no time dependence, i.e. steady flow conditions exist.

Using Buckingham's theorem with ρ, D, and V as the basic parameters we obtain a function of 9 dimensionless groups (π - parameters) as follows :

Parameter	Formula	Name	Physical significance
π_1	$\frac{S}{D}$		Geometric parameters
π_2	$\frac{C}{D}$		
π_3	$\frac{X}{D}$		
π_4	$\frac{W}{D}$		
π_5	$\frac{L}{D}$		
π_6	$\frac{d}{D}$		
π_7	$\frac{VD}{\nu}$	Reynolds Number R	$(\frac{\text{inertial force}}{\text{viscous force}})$
π_8	$V\sqrt{\frac{\rho\ D}{\sigma}}$	Weber Number We	$(\frac{\text{inertial force}}{\text{surface tension force}})^{\frac{1}{2}}$
π_9	$\frac{V}{\sqrt{gD}}$	Froude Number F	$(\frac{\text{inertial force}}{\text{gravitational force}})^{\frac{1}{2}}$

Taking the critical submergence as the dependent variable, S_c can be expressed as :

$$\frac{S_c}{D} = f\left(\frac{C}{D}, \frac{X}{D}, \frac{W}{D}, \frac{L}{D}, \frac{d}{D}, R, We, F\right)$$

Although the length parameters are non-dimensionalised using D, any other length could equally well have been chosen. Also, the analysis gives no indication of whether V represents V_d, V_D, or V_w.

This is a useful technique but must be applied with care. It is important to include all the quantities which it is thought are involved in vortex formation. The analysis may show one of the quantities to be unnecessary, since it has a dimension which no other quantity has. (However, this could also be due to the omission of a variable). Numerical factors such as 2 or π do not affect the general result. The final result gives no indication of the form or power of the functional expressions or of the relative importance of the dimensionless groups.

3.4 Mechanisms for the generation of vorticity

3.4.1 Introduction

When the flow in the main body of a fluid is irrotational, the basic mechanism responsible for the generation of vorticity is boundary shear, either at a solid/liquid boundary or between two fluid layers. These shear layers give rise to velocity gradients within the fluid, often with high local values, and the resulting vorticity, if sufficiently organised, can cause a vortex to appear. This process is further aided by amplification of vorticity which occurs when a vortex filament is stretched, as occurs when fluid is drawn down into the intake. This has the effect of concentrating vorticity which is initially diffused into a relatively small core.

When the main flow is rotational, additional sources of vorticity exist. Ways of physically creating and maintaining this type of flow with asymmetric approach conditions are described in chapter 4.

3.4.2 Growth of the boundary layer

The two major sources of boundary layer growth are firstly, the walls and floor of the sump, and secondly, the cylindrical surface of the suction pipe.

The flow along the sump boundaries can be approximated to that past a flat plate which is placed parallel to the direction of the main flow. For this situation, the boundary layer thickens as fluid progresses along the plate, due to diffusion of vorticity away from the solid boundary and its thickness, δ , is given by

$$\frac{\delta_{plate}}{x} = \frac{5.83}{R_x^{\frac{1}{2}}} \qquad R_x = \frac{V_w x}{\nu}$$

where x is the distance travelled along the plate by the fluid, V_w is the mean velocity of the main flow. However, for $R_x > 1.2 \times 10^5$, transition to a turbulent boundary layer occurs and

$$\frac{\delta_{plate}}{x} = \frac{0.38}{R_x^{1/5}}$$

This transition occurs earlier if the approach flow is unsteady or otherwise disturbed, e.g. by surface roughness on the plate or its leading edge.

The flow past the suction pipe itself is a source of vorticity, and is similar to steady flow past a cylinder or pipe. In this case, a laminar boundary layer develops, starting from the upstream stagnation point, and thickens gradually until it separates from the cylinder, producing shed

vortices downstream with a frequency depending on the Strouhal number, S, of the flow. For $R_d = \frac{V_w d}{\nu}$ between 10^2 and 10^5 (where d is cylinder diameter) $S \simeq 0.2$. This is the same mechanism which produces the regular von Karman street behind cylinders, though for high Reynolds numbers ($3 \times 10^5 < R_d = \frac{V_w d}{\nu} < 3 \times 10^6$) the downstream pattern becomes less distinct as the transition to turbulent flow occurs. The vortices are shed in discrete cells along the length of the cylinder, the length of each cell being called the "correlation length". For $150 < R_d < 10^5$, the correlation length is 2d to 3d (35). The absolute value decreases with increasing R_d and depends also on turbulence, length/diameter ratio and surface roughness. Greater than $R_d = 10^5$, the correlation length drops to 0.5d.

Assuming steady, potential flow outside the boundary layer, then the laminar boundary layer thickness at the point of separation from the pipe is given by (36)

$$\frac{\delta_{pipe}}{d} = \frac{2.26}{R_d^{\frac{1}{2}}}$$

Again, transition to a turbulent boundary layer occurs when $R_d > 5 \times 10^5$ or earlier if the upstream flow is turbulent or if there is surface roughness on the cylinder. In this case separation is delayed, but the value of δ is not known.

There are obvious differences between the steady flow past a cylinder and the restricted flow past a suction pipe when there is an endwall, together with suction through one end, i.e. the bellmouth. Although the closeness of the endwall prevents the formation of a vortex street, it encourages the ingestion of separated boundary-layer fluid in the wake behind the suction pipe. The shape of the bellmouth and the suction through

the pipe introduce three-dimensional flow effects, which have not been considered in the case of steady flow past a cylinder. However, provided there is a sufficient length of cylindrical pipe submerged, then it is still valid to compare the two situations in a qualitative manner.

Sources of vorticity not associated with a solid boundary are shear layers in the fluid, and the boundary layer at the free surface. The former occurs when fluid layers within the body of the fluid are accelerated down towards the intake, whilst fluid near the surface continues downstream, and are decelerated by the presence of the suction pipe and end-wall. The velocity gradients at the shear layer are a source of diffuse vorticity, and only become important as the depth of water decreases. These layers, however, tend to be unstable, and are not considered further with reference to rectangular pump sumps.

3.4.3 Contribution to the vorticity from the boundary layer

Since the velocity at any solid boundary must be zero because of viscosity, velocity gradients will be present in the boundary layer which are a source of vorticity, ζ . This can be seen in a simplified two-dimensional analysis:

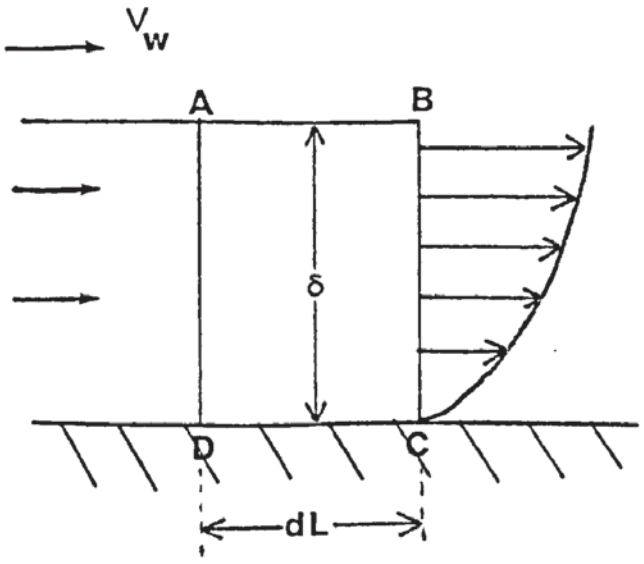

Consider one section labelled ABCD of the boundary layer in the approach flow at one side-wall of the channel. Then the circulation round the section ABCD is

$$\Gamma = \oint V \, ds = V_w \, dL.$$

But from Stokes' theorem,

$$\Gamma = \int_S \underline{\zeta} \cdot \underline{dS} = \zeta_A \, \delta \, dL$$

where ζ_A represents an average vorticity distributed in the entire boundary layer.

Therefore,

$$\zeta_A = \frac{V_w}{\delta}$$

with due regard taken of the sense of rotation. For example the vorticity vectors derived from boundary layer flow along the sump sidewalls are opposite in direction to each other.

Although it is well known that the boundary layer is a source of vorticity, the above analysis has not been applied to the case of vorticity shed from a suction pipe, as far as the author is aware. This will be described in the following paragraphs. The values of δ considered above all depend on a Reynolds number, and thus vary with velocity and geometric paramters. Thus, assuming a laminar boundary layer, the contribution to the vorticity from the flow past a suction pipe with bellmouth diameter D is given by

$$\zeta_{pipe} = \frac{V_w}{2.26d} \left(\frac{V_w d}{\nu}\right)^{\frac{1}{2}} = \frac{V_w^{3/2}}{2.26\,(\nu d)^{\frac{1}{2}}}$$

$$= \frac{0.308}{(H/D.\,W/D)^{3/2}\,(\nu d)^{\frac{1}{2}}} \; V_D^{3/2}$$

where H, W and V_D are the depth, channel width and bellmouth velocity respectively.

Similar expressions for vorticity ζ, can be derived for δ_{plate}, the only effect being to change the values of the exponents. Thus

$$\zeta_{\text{plate (laminar)}} = \frac{V_w}{5.83x}\left(\frac{V_w x}{\nu}\right)^{\frac{1}{2}} = \frac{V_w^{3/2}}{5.83\,(\nu x)^{\frac{1}{2}}}$$

$$= \frac{0.119}{(H/D.\,W/D)^{3/2}\,(\nu d)^{\frac{1}{2}}\,(x/d)^{\frac{1}{2}}}\,V_D^{3/2}$$

$$\zeta_{\text{plate (turbulent)}} = \frac{V_w}{0.38x}\left(\frac{V_w x}{\nu}\right)^{1/5} = \frac{V_w^{6/5}}{0.38x^{4/5}\,\nu^{1/5}}$$

$$= \frac{1.97}{(H/D.\,W/D)^{6/5}\,\nu^{1/5}\,(x/d)^{4/5}\,d^{4/5}}\,V_D^{6/5}$$

Then, to find the major source of vorticity, one must compare the relative contributions from the a) laminar boundary layer on a cylinder; b) laminar boundary layer on a flat plate and c) turbulent boundary layer on a flat plate. This has been done in fig. 3.3 for a suction pipe of diameter 160 mm for the range of V_w values covered in the experimental work. ζ has been drawn as a function of V_w so that it is independent of H/D. The graph shows that for a given pipe size and sump geometry, the dominant contribution to ζ arises from the suction pipe, whilst δ_{plate} being in the opposite direction, has a relatively small de-stabilising effect.

Thus, on the basis of the simplified analysis above, it has been shown that the suction pipe is the major source of vorticity in a rectangular pump sump, whilst the sidewalls have a small de-stabilising effect. This is borne out by the consistent direction of rotation of the vortices observed in the experiments behind the suction pipe. This is discussed further in chapter 6. It seems that an obvious solution to the vortex problem would be to remove the suction pipe completely, and abstract the flow through the floor or one wall. However, although the latter is done for some

Fig. 3.3 Graph of vorticity against channel velocity, showing the relative magnitudes arising from a pipe, plate (laminar boundary layer) and plate (turbulent boundary layer. Numerical values based on the 6" rig with suction pipe diameter 160 mm.

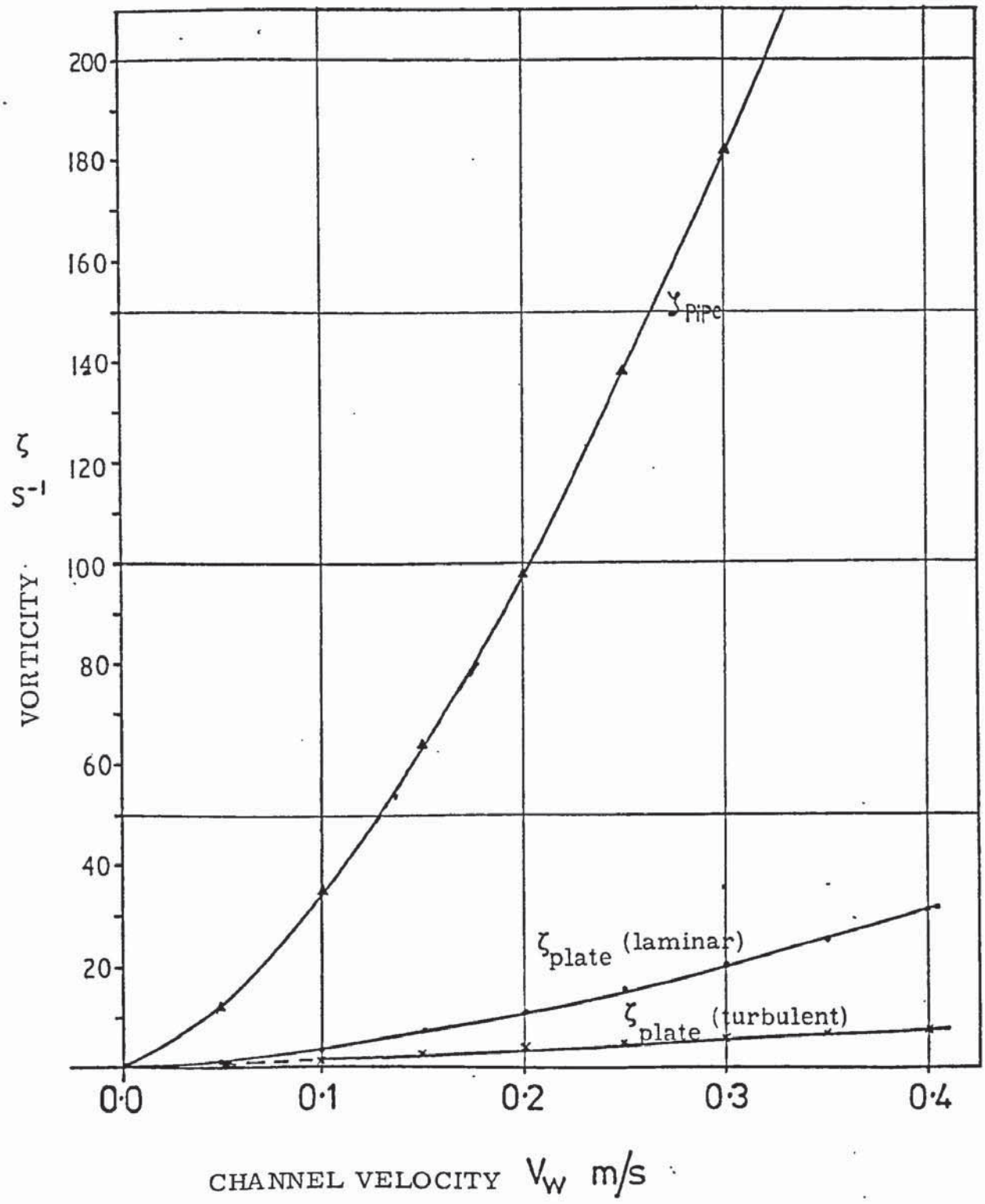

applications, with a subsequent reduction in vortex activity, there are increased costs involved in building a separate pumphouse to keep the pumps dry.

3.4.4 Onset of air entrainment

From the above it can be seen that vorticity from the boundary layer can cause a surface vortex to appear. The strength and persistence of this vortex depends on :

a) the magnitude of vorticity generated in the boundary layers; this depends on various factors discussed in 3.4.3

b) the degree of organisation of the vorticity so that the resultant magnitude of the local vorticity vectors will give rise to rotational motion; this depends on turbulence levels and correlation length of the shed vortices.

If both a) and b) are large, then the surface vortex will have a distinct tail which may develop into a complete air core, starting from the surface and extending into the intake. This will occur if a sufficiently large radial pressure gradient is developed by the rotating fluid so as to reduce the local pressure within the fluid to atmospheric. In other words, at any given water depth, the dynamic head must be sufficient to overcome the static head as well as losses due to viscosity. A qualitative treatment, however, of when air entrainment occurs is not possible due to a lack of detailed knowledge of the velocity distribution near the vortex core as well as boundary effects.

3.5 Mathematical modelling of vortex formation in rectangular sumps

Swainston (3) has proposed a simple mathematical model to describe and predict the onset of stable surface vortices. Of the various types of stagnation point that can arise from fluid moving normally to a plane surface, the type C stagnation point gathers fluid from all directions and directs it away from the surface (fig. 3.4)

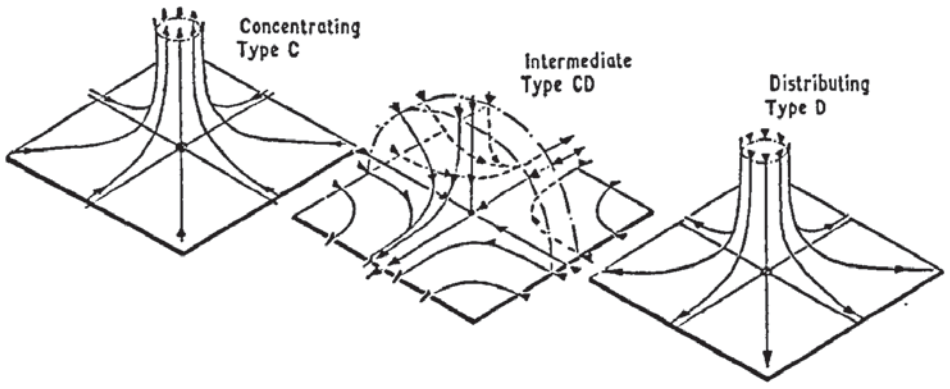

Fig. 3.4 Various types of stagnation point described by their effect on the boundary layer.

This seems to be the mechanism for generating submerged vortices from a sidewall or the floor where boundary layer fluid containing vorticity is drawn into a bellmouth placed at the end of a rectangular sump. Further potential flow calculations suggest that type C stagnation points can exist on the free surface, and are a necessary but insufficient condition for the onset of air-entraining vortices. This can be imagined by turning the type C diagram above upside down, so the boundary now represents the free surface. This approach predicts the existence of a maximum critical submergence, called the boundary submergence S_B, above which air-entraining vortices will not form. On the basis of 3.4.4 above, this means there comes a point when the vortex strength is insufficient to overcome the static head arising from the submergence S_B plus viscous losses.

By representing the flow through the bellmouth by a point sink, and the sump boundaries by planes of symmetry in appropriate combinations

of point sinks and their images. the location of the free surface stagnation points and the corresponding values of S_B can be found for a variety of geometric configurations. For example, wide, deep sumps can be represented by a basic unit of four sinks placed at the corners of a rectangle, (fig. 3.5)

Fig. 3.5 Arrangement of four point sinks as a basic unit in Swainston's mathematical model (3).

There is no flow normal to the two intersecting planes of symmetry, and so these can represent boundary surfaces. Quadrant 1 represents a sink near the floor and endwall of a deep, wide sump (sidewalls and surface at infinity), whereas quadrant 2 represents a sink near the free surface and endwall of a deep, wide sump (sidewalls and floor at infinity). The free surface stagnation points are then found by calculating the co-ordinates of points where all the velocity components are zero.

For a rectangular pump sump, the effect of the floor and sidewalls together must be included. This requires an infinite array of sinks in three dimensions. However, Swainston achieved satisfactory modelling by using up to 1500 point sinks, together with infinite plane sinks outside the central region of point sinks. He investigated the effect of varying floor clearance and width, and this is discussed further, together with experimental results in chapter 6.

There are certain limitations to this potential flow approach. Firstly, as the sump dimensions get closer to the size of the bellmouth and suction pipe, the latter have a significant effect on the flow, and the discharge can no longer be treated by a point sink. Secondly, ideal flow assumes that the fluid is non-viscous and irrotational. Thirdly, the effects of surface tension, surface turbulence and waves are not considered. This would lead to greater discrepancy between the mathematical model and experiment as the Froude number increases.

3.6 Scaling laws

3.6.1 Introduction

In order to correctly model a given fluid phenomenon, it is necessary to establish the predominant forces involved. The appropriate dimensionless groups are then formed and complete similarity is achieved by a) constructing a geometrically similar model and b) operating the model such that the values of the relevant dimensionless groups are maintained constant in both the model and the prototype.

For the case of vortex formation, dimensional analysis shows that it is necessary to keep the Froude, Reynolds and Weber numbers (F, R and We) simultaneously the same on model and prototype. This is impossible if the same fluid is used on both.

3.6.2 Scale-up with two dimensionless groups

One method commonly used to derive a scaling law empirically in the chemical engineering industry for scale-up of chemical processes is to assume that the dependant variable is a function of two dimensionless

groups only, the function taking the form of the product of powers of the two groups (37). Applying this extended principle of similarity to the dimensional analysis of 3.3, with submergence, S_c/D, as the dependant variable, (assuming that the other geometric parameters have been scaled correctly), and neglecting the influence of the Weber number, then a possible scaling law would take the form :

$$\frac{S_c}{D} = f(F, R)$$

$$= F^x R^y \qquad x, y \text{ are unknown dimensionless numbers.}$$

$$= \left(\frac{V_D}{\sqrt{gS_c}}\right)^x \cdot \left(\frac{V_D D}{\nu}\right)^y$$

$$\left(\frac{S_c}{D}\right)^{1+\frac{x}{2}} \propto V_D^{\,x+y} \; D^{y-\frac{1}{2}x}$$

Empirical results are then obtained from two or three different size models so that the following graphs can be drawn:

(i) $\log \frac{S_c}{D}$ against $\log V_D$ at constant D

(ii) $\log \frac{S_c}{D}$ against $\log (D)$ at constant V_D

These would be straight lines, the first of slope $\frac{x+y}{1+\frac{x}{2}}$, the second of slope $\frac{y-\frac{1}{2}x}{1+\frac{1}{2}x}$, from which values of x and y can be found. Hence S_c can be predicted for any given value of V and D. The relative importance of viscous and gravitational forces can also be judged by the relative values of x and y.

3.6.3 Derivation of a consistent scaling law

In practice, at BHRA and elsewhere, the procedure is to exaggerate flow velocities above that required by constancy of Froude number by increasing the Froude scale velocity by a certain multiplying factor, in order to reproduce viscous effects more closely. The degree of exaggeration is a subjective matter, but in general the multiplying factor is greater for smaller values of the scale ratio s. In order to derive an expression for a general scaling law which concurs with accepted practice, it is of most practical use to consider the velocity ratio, $\frac{V_m}{V_p}$, and to express it as a function of s only.

$$\frac{V_m}{V_p} = f(s)$$

so that $f(s) = s^{\frac{1}{2}}$ for simple Froude scaling

$= k_o s^{\frac{1}{2}}$ for multi-Froude scaling (k_o = a constant)

$= s^{-1}$ for simple Reynolds number scaling

$= s^{\frac{1}{2}} + a_o s^{-1}$ for a combination of Froude and Reynolds scaling, a_o being a constant to represent the Reynolds contribution to the scaling law. This new combination form would be a more realistic form, based on a knowledge of the forces involved in vortex formation.

However, one important requirement which has not been considered before as far as the author is aware is that there must be internal consistency in the form of the function f(s), such that the scaling law can be used both for scaling up from a model to a prototype (scale ratio s) and also in scaling down from the prototype to model (scale ratio 1 : s), see fig. 3.6.

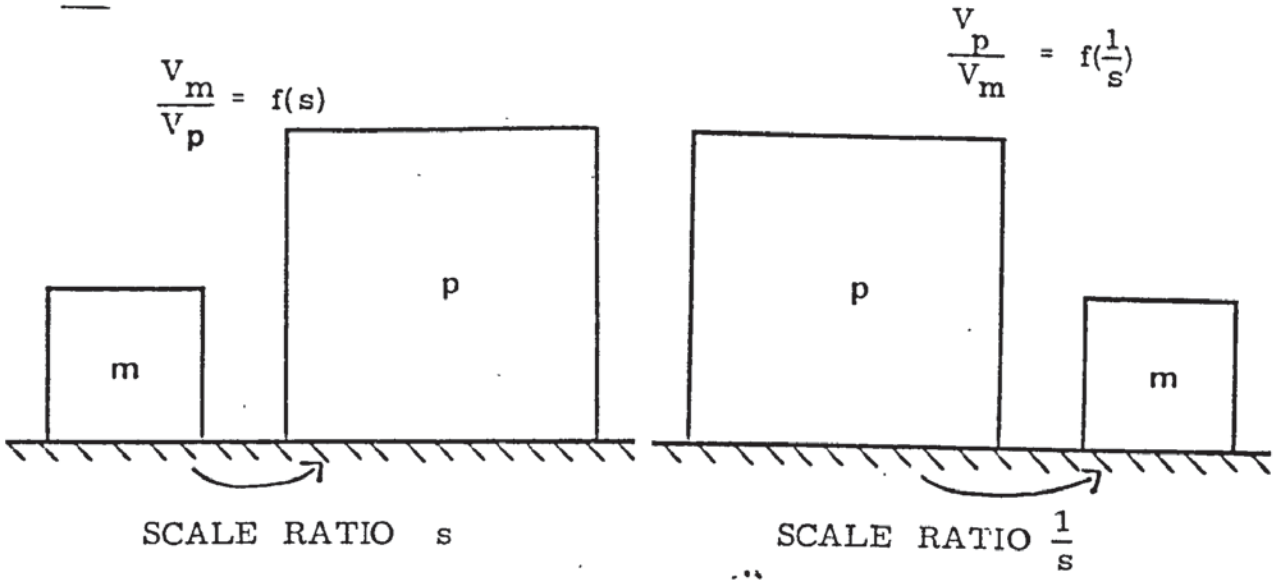

Fig. 3.6 Schematic representation of the requirement of internal consistency in any scaling law. Such a law can be used both for scaling up from a model to a prototype as well as scaling down from the prototype to the model.

Mathematically, this means that if

$$\frac{V_m}{V_p} = f(s)$$ then the inverse scaling requires that

$$\frac{V_p}{V_m} = f\left(\frac{1}{s}\right)$$

but $$\frac{V_m}{V_p} = \frac{1}{V_p/V_m}$$

This implies that the requirement on the form of f (s) is

$$f(s) = \frac{1}{f\left(\frac{1}{s}\right)}$$

Referring to the simple Froude and Reynolds scaling discussed above, it can be seen that $f(s) = s^{\frac{1}{2}}$ and $f(s) = s^{-1}$ satisfy the above consistency requirement. In fact, s raised to any power, including zero, would be acceptable.* However, multi-Froude scaling and the combination law

---

* It is interesting to note that the method described in section 3.6.2 is consistent and is equivalent to a simple power law with

$$f(s) = s^{\frac{\frac{1}{2}x - y}{x + y}}$$

are not consistent scaling laws, i.e. $f(s) = k_o s^{\frac{1}{2}} \neq \frac{1}{k_o s^{-\frac{1}{2}}}$ (unless $k_o = 1$)

and $f(s) = s^{\frac{1}{2}} + a_o s^{-1} \neq \frac{1}{s^{-\frac{1}{2}} + a_o s}$

One general class of functions which is internally consistent is

$$f(s) = \frac{g(s)}{g(\frac{1}{s})}$$

Then for simple Froude scaling, $g(s) = s^{\frac{1}{4}}$, so that

$$f(s) = \frac{s^{\frac{1}{4}}}{(\frac{1}{s})^{\frac{1}{4}}} = s^{\frac{1}{2}}$$

and for simple Reynolds scaling, $g(s) = s^{-\frac{1}{2}}$

3.6.4 Application to vortex formation in rectangular pump sumps

A multi-Froude scaling law to allow for Reynolds number effects is the general form used at BHRA, but this form, $f(s) = ks^{\frac{1}{2}}$, with k = constant, is not internally consistent. More important, however, is the fact that a combination law can now be used by expressing it in the following consistent form which takes both the Froude and the Reynolds number into consideration.

$$f(s) = \frac{as^{\frac{1}{4}} + b_o s^{-\frac{1}{2}}}{as^{-\frac{1}{4}} + b_o s^{\frac{1}{2}}}$$

$$= \left(\frac{a + b_o s^{-\frac{3}{4}}}{a + b_o s^{\frac{3}{4}}} \right) s^{\frac{1}{2}}$$

$$= \left(\frac{1 + bs^{-\frac{3}{4}}}{1 + bs^{\frac{3}{4}}} \right) s^{\frac{1}{2}} \quad \text{(by dividing numerator + denominator by a)}$$

The expression in brackets represents the k-factor or Froude scale multiplying factor used to exaggerate model velocities as discussed earlier.

One aim, therefore, of this project is to determine the value of b, and hence the k-factor over the scale range of 1 : 2 to 1 : 8 and then to generalise this for all model scales. In order to correlate the experimental results with a particular value of b and hence derive a general scaling law, the procedure which will be adopted will be :

a) plot the critical submergence S_c/D against bellmouth velocity V_D for the four sizes of rig available, labelled for convenience the 1.5", 3", 6" and 12" rigs after their nominal pipe diameter; this form of curve readily distinguishes the conditions under which various types of vortex form (see Fig. 5.15 for example).

b) taking the largest size available, the 12" rig, as the prototype, obtain average values of $\frac{V_6}{V_{12}}$, $\frac{V_3}{V_{12}}$, $\frac{V_{1.5}}{V_{12}}$ at various values of S_c/D.

c) substitute these values of V_m/V_p into the expression for f(s) to calculate b, using s = 1/2, 1/4 or 1/8 as appropriate.

Analysis of the results from the three rigs along these lines is described in 6.4.2

3.6.5 Assumptions and implications of the consistent scaling law

The following assumptions are inherent in the derivation described in sections 3.6.3 and 3.6.4:

(i) the scaling law is independent of any geometric parameters, so that V_m/V_p = f(s) only. This is based on accepted practice at BHRA, where the same modelling procedure is adopted for a wide

range of intakes regardless of their exact geometric configuration.

(ii) the Weber number contribution to vortex formation is negligible, so that only the Froude and Reynolds number have to be considered. In principle, surface tension effects could be allowed for by adding a further term to the scaling law :

$$f(s) = \frac{s^{\frac{1}{4}} + bs^{-\frac{1}{2}} + cs^{-\frac{1}{4}}}{s^{-\frac{1}{4}} + bs^{\frac{1}{2}} + cs^{\frac{1}{4}}}$$

(iii) The same fluid is used under the same physical conditions in both model and prototype so that physical properties such as ν and σ , and the value of g are the same.

The following points arise from the law :

(i) for positive values of b, the value of the k-factor increases steadily and continuously from 1 for s = 1 to infinity as s tends to zero. This is in agreement with subjective rule-of-thumb methods used at BHRA. A typical curve of k against s is shown in fig. 3.7 for b = 0.1. This gives values of k in reasonable agreement with accepted practice. There is a whole family of such curves for different values of b, ranging from the simple Froude scaling curve (b = 0) to simple Reynolds scaling (b = ∞).

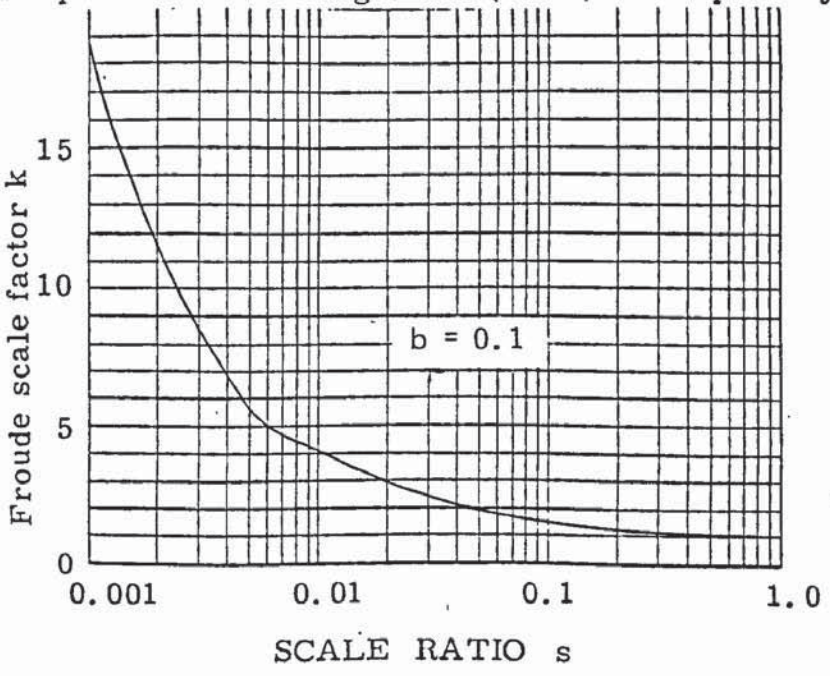

Fig. 3.7 Variation of Froude scale multiplying factor, k, with scale ratio s, for Reynolds number contribution b = 0.1

(ii) for $b < 0.5$, the velocity ratio f(s) is not a continuously increasing function of s but has a minimum in the range of interest, $0 < s < 1$. The variation of f(s) for various values of b is shown in fig. 3.8. When a minimum exists, then the S_c/D - V_D curves would not necessarily lie in order of size, e.g. if results from five rigs labelled 5, 4, 3, 2 and 1 in order of decreasing size are plotted, then the result may be as in fig. 3.9 where size 5 is treated as the prototype, and sizes 4 and 3 have $f(s) < 1$, sizes 2 and 1 have $f(s) > 1$.

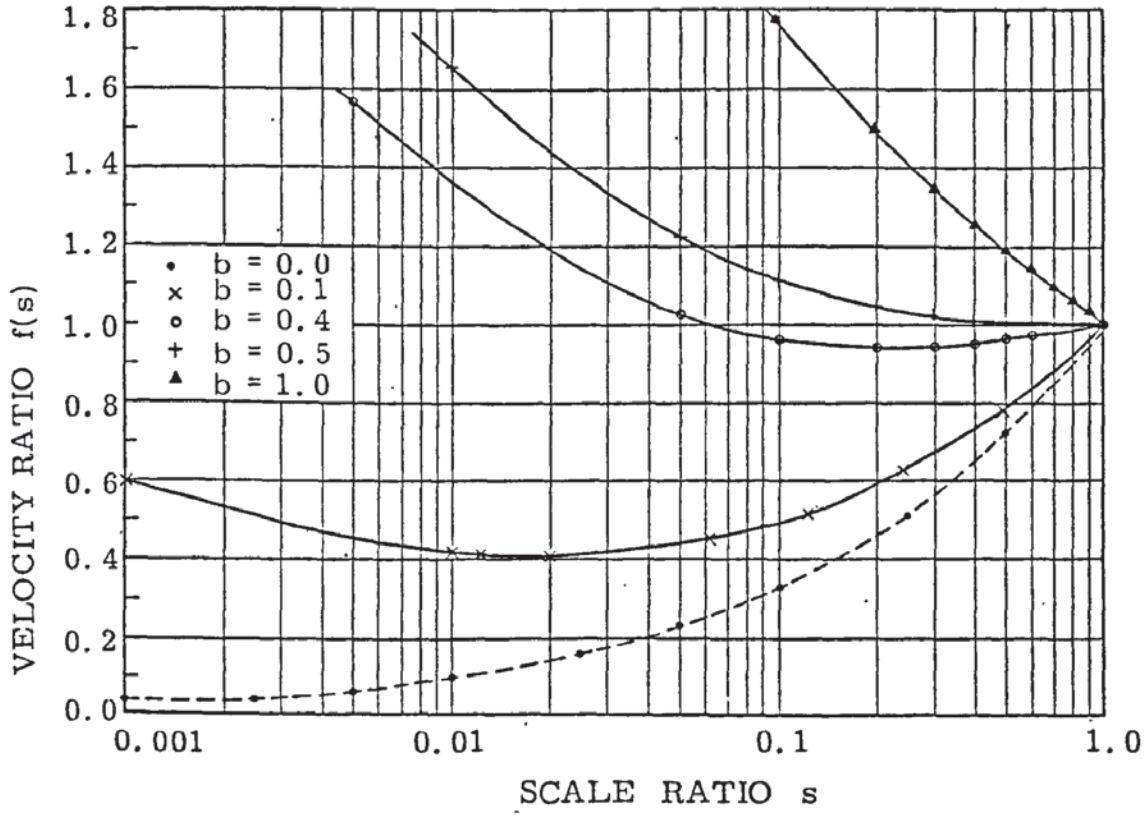

Fig. 3.8 Variation of ratio of model velocity to prototype velocity, f(s), with scale ratio s, for various values of b.

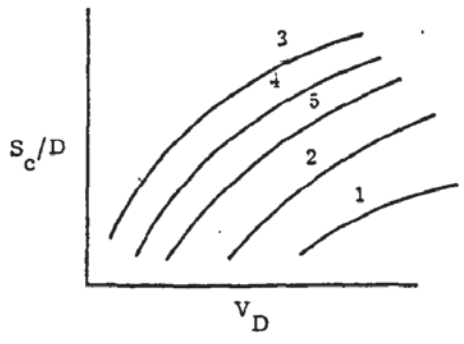

Fig. 3.9 Typical critical submergence-velocity curves for different size rigs when there is a minimum in f(s) i.e. for b less than 0.5.

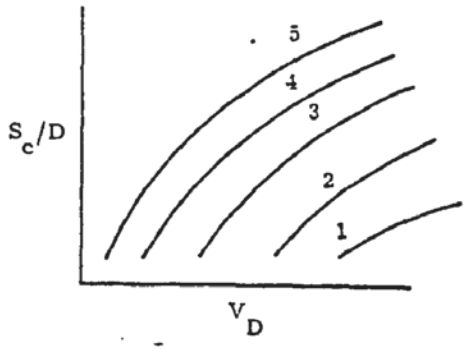

Fig. 3.10 Typical critical submergence-velocity curves for different size rigs when there is no minimum in f(s) i.e. for b greater than or equal to 0.5

(iii) For $b \geqslant 0.5$, no minimum exists in f(s). A typical curve showing the variation of f(s) with s is shown in fig. 3.8 for b = 1. S_c/D - V_D curves should now lie above each other in order of increasing size, since f(s) is always greater than 1 as shown in fig. 3.10. (Curves lying above each other in reverse order are possible, but only as a special case of (ii) above where the value of s is limited over a narrow range).

(iv) If f(s) is to be constant for a particular scale, then the S_c/D - V_D curves should never cross, but should remain "parallel" to each other in the sense that for a given S_c/D value, the velocities bear a constant ratio to each other over the range of S_c/D values, expect that if they do tend to a limit the asymptotic limit should be the same for all sizes so that the curves meet at infinity. (This is necessary anyway to ensure that all S_c/D values existing on a prototype are fully covered by the same range of S_c/D values on the model). Changes in the origin of the velocity axis can "de-cross" the curves should they cross over at any point(s), and this has been applied to the analysis of results in 6.4.2 to 'correct' velocities.

(v) for two different scale ratios s_1 and s_2, the law requires that

$$f(s_1)\, f(s_2) \neq f(s_1 s_2) \quad \text{and} \quad f(s_1) \,/\, f(s_2) \neq f\left(\frac{s_1}{s_2}\right)$$

Relating this to the three rig sizes 12", 6" and 1.5", this implies that, taking 12" as the prototype, 12" can be modelled either by 6" using $f(\frac{1}{2})$ or by 1.5" using f(1/8). However, the 12" cannot be correctly modelled by the 1.5" by first going from 12" to 6" using $f(\frac{1}{2})$ and then going from 6" to 1.5" using $f(\frac{1}{4})$ because :

$$f(\tfrac{1}{2}) = V_6 / V_{12} \quad \text{and} \quad f(\tfrac{1}{4}) = V_{1.5} / V_6$$

so that $f(\tfrac{1}{2})\, f(\tfrac{1}{4}) = V_{1.5} / V_{12} = f(1/8)$ which contradicts the initial requirement that $f(\tfrac{1}{2})\, f(\tfrac{1}{4}) \neq f(1/8)$. This restriction is illustrated in fig. 3.11

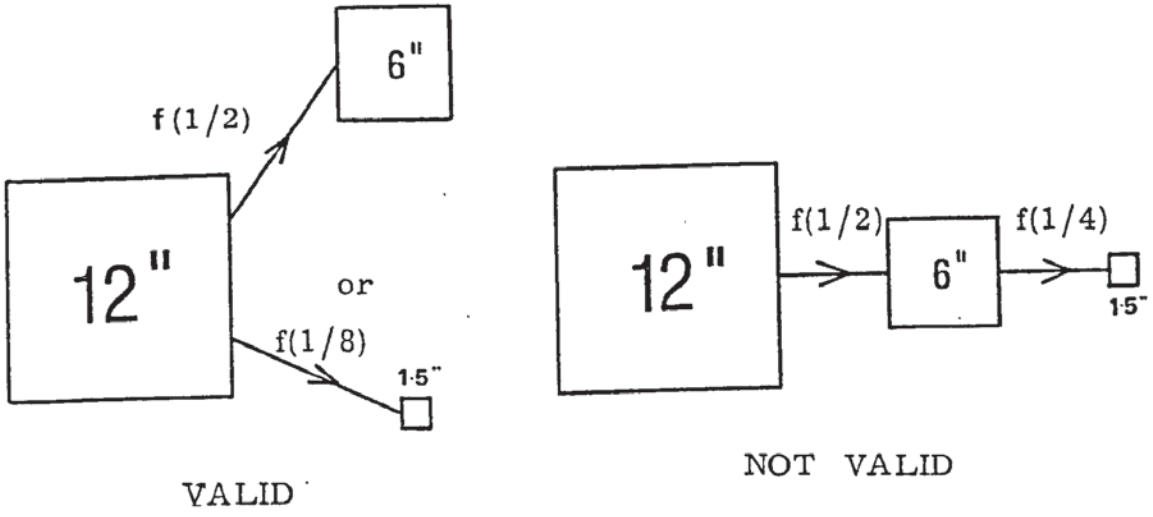

Fig. 3.11 Illustration of three ways of using a scaling law to model a 12" prototype, two of which are valid for the internally consistent combination scaling law, the third being invalid.

This property of the consistent scaling law is less relevant in practice since the "Valid" rather than the "Not valid" procedure is generally adopted. The implication for the analysis of the results is that only one size rig can be taken as the prototype, and this will be the 12" rig in this case.

CHAPTER 4

REVIEW OF PREVIOUS EXPERIMENTAL WORK

4.1 Introduction

The problem of vortex formation has been the subject of numerous papers for many years. Vortices occur in a wide variety of situations, e.g. as eddies shed from moving aeroplane wing tips; in various atmospheric phenomena such as tornadoes and waterspouts; at the intakes to gas turbines; in pump sumps and intakes for hydro-electric schemes; in hydrocyclones for single phase and two-phase separation; in the common bathtub and tea cup. They have been investigated both experimentally and theoretically for a wide range of geometries and flow conditions.

It is perhaps this ease of producing vortices in widely varying situations which has led to conflicting opinions on the subject, especially with regard to the scaling of vortices. Comparison between the work of different authors is made more difficult by the different forms of dimensionless parameters used and the variety of geometric configurations covered. In order to narrow the field of discussion, this chapter concentrates on relevant aspects of free surface vortex formation in cylindrical tanks and rectangular sumps, with a brief section on other forms of hydraulic intake. The literature describing specific examples of hydraulic intakes has not been reviewed because of its limited range of application.

The first section, 4.2, reviews work on cylindrical tanks where the vortices formed are relatively stable, and this, together with their axial symmetry, greatly simplifies both the experimental and theoretical treatment. (The latter has already been discussed in 3.2). This geometry has a few practical applications, e.g. sewage discharge control (38),

vortex amplifiers and other fluidic devices (39), hydrocyclones (40) and the design of emptying fuel tanks (41). Useful results have been obtained on various vortex parameters, some of which would be almost impossible to measure in a rectangular geometry where vortices tend to be more transient and unstable.

The second section, 4.3, reviews rectangular geometries which are more directly relevant to the current research project. Some of these geometries, however, have asymmetric inlets which act as a source of vorticity. The final section briefly discusses other forms of intakes found in practice.

4.2 Drain vortices in cylindrical tanks

4.2.1 Experimental configurations

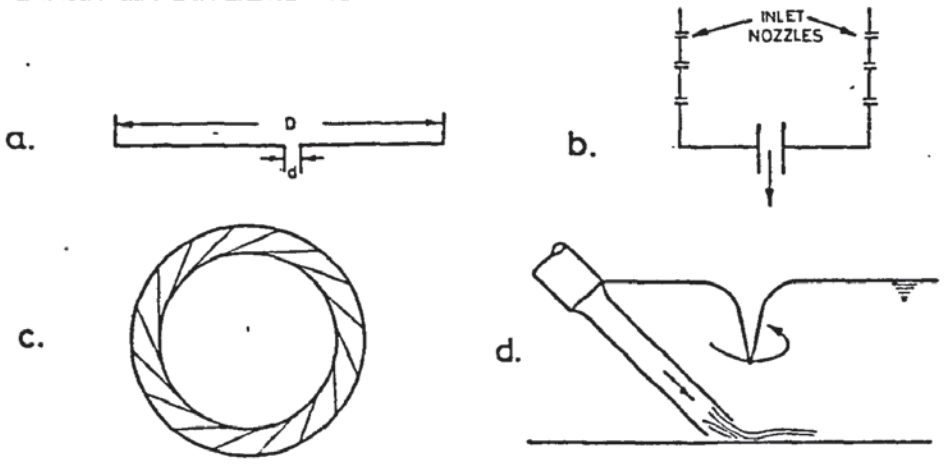

Fig. 4.1 Various experimental configurations for producing drain vortices in a cylindrical tank.

Amongst the various geometries adopted, the shallow cylindrical tank shown in fig. 4.1a was used by author's interested in the effects of the Earth's rotation, e.g. Shapiro (42) used D = 1.8m, Sibulkin (43) used D = 30 cm., Binnie (44) used a deeper tank with the outlet pipe protruding 33 cm. from the bottom. The tanks were filled with an initial rotation

either clockwise or anti-clockwise and allowed to drain slowly after various settling times. By taking appropriate precautions they eliminated external effects due to asymmetry, air currents, temperature changes, vibrations, etc.

Other arrangements are also shown in fig. 4.1. In fig. 4.1b, symmetrically placed inlet nozzles which could be swivelled round to produce flows ranging from purely radial to purely tangential were used to produce an initial circulation of known value (45). In fig. 4.1c, a concentric ring of adjustable guide vanes was used to control the inlet velocities and circulation (46). For all arrangements a very wide range of sizes was used, from 21 cm. to 200 cm. for the tank diameter, 1 cm. to 10 cm. for the outlet diameter and 1/12 to 1/2 of the tank diameter for the tank depth. This was partly because problems of scaling were also investigated by some authors.

Vortices are notoriously unstable, and any device introduced near a vortex core for flow measurements or visualisation should not disturb or distort the local flow pattern. Streak photography has been used, whereby suitable particles such as neutral density beads (Quck ref. 47), aluminium powder (Toyokura and Akaike ref. 48), or a dye globule (Granger ref. 32) are injected into the vortex flow and the subsequent motion is photographed using stroboscopic lighting. The length of the individual traces thus obtained gives a measure of the local velocity. More elaborate optical methods have been developed by Seddon and Anwar (49) and Berge (50) which allow flow measurements to be taken near the vortex core with little or no disturbance to the flow. Miniature propeller meters have been used (51) and provide a direct reading for flow measurement. However, they inevitably disturb the local flow patterns which could give misleading

results, especially for the complex conditions near the vortex core.

4.2.2 Effect of the Earth's rotation

From refs 42, 44, it can be confidently stated that the Coriolis force due to the earth's rotation is sufficiently strong to produce a vortex in an otherwise still body of water provided no other disturbing forces are present. This can only be achieved under well-controlled conditions. The sense of rotation is always anti-clockwise in the northern hemisphere when looking down at the outlet and clockwise in the southern hemisphere. Otherwise, in normal laboratory conditions, the Coriolis force is many orders of magnitude smaller than other forces present and can therefore be neglected. This result applies equally to rectangular pump sumps. In fact for a radial velocity of 100mm/s, the Coriolis force acting on a fluid element in BHRA's laboratories at Cranfield (latitude 52^{o}) is approximately 6×10^{-6} times that due to gravity.

4.2.3 Origin of vorticity

The experiments with drain vortices provide interesting results on the importance of the boundary layer as a source of vorticity. Shapiro observed that with initial clockwise filling of the tank, and a settling time of 4 hours before draining was started, a clockwise rotation was first observed which then changed to anticlockwise rotation. He attributes this to the growth of a viscous boundary layer on the tank bottom with its associated vorticity. This layer gradually acquires the Earth's anticlockwise angular velocity. Above the boundary layer the water has the same rotation as the initial swirl. As the water drains, the boundary layer is reached and a reversal of rotation is observed.

Silbulkin observed reversal for either direction of filling and attributes this to the vertical component of vorticity in the boundary layer. This component arises from the vertical (downward) velocity component of the fluid in the boundary layer as it flows through the outlet. The direction of the vertical component of vorticity is such that it induces a circulation of opposite direction to the initial circulation and increases in strength as more and more of the boundary layer liquid is present in the outflowing liquid. Thus, reversal occurs as the water level drops, irrespective of the direction of initial circulation. Kelly et al, however, consider that although this mechanism could reduce the intial circulation to zero, it would not be of sufficient strength to produce reversal (52). Instead, they suggest that circulation could be generated by surface waves produced by a mechanical shock to the system.

These explanations are necessarily qualitative, but they show how the boundary flow can contribute to the growth of a vortex. This is further confirmed both by Anwar (51) who artificially roughened the tank bottom and obtained a weaker vortex with much reduced tangential velocities, and by theoretical considerations in refs.53, 54.

4.2.4 Surface profile near the vortex core

Fig. 4.2 shows the profiles obtained by Anwar (51) for strong vortices. The theoretical curves are based on inviscid theory, i.e. they are hyperbolic in form but it can be seen that as the vortex core is approached, departures from the ideal form become more significant, with the measured profile usually higher than the theoretical one. Fig. 4.3 is due to Stevens and Kolf (38) who found the actual profile to be consistently higher that the theoretical one. Deviations from inviscid theory are to be expected

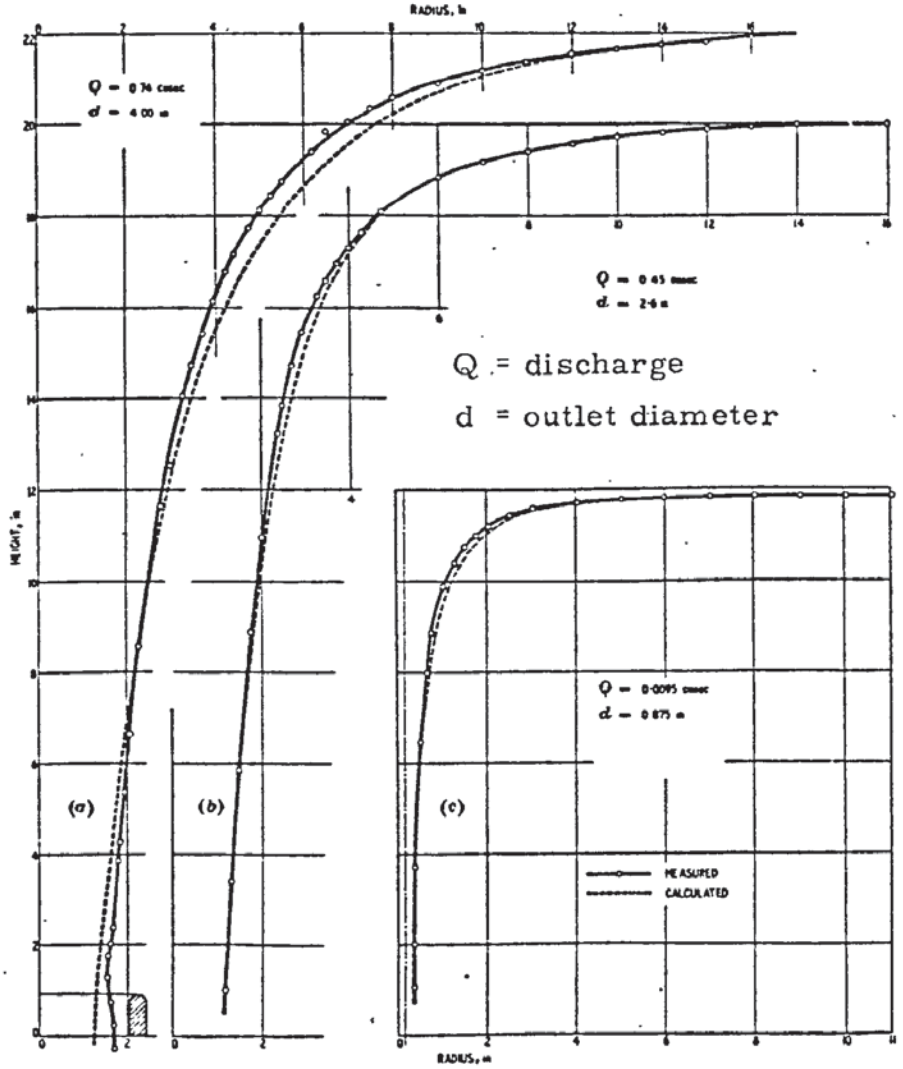

Fig. 4.2 Measured and calculated profiles for (a) large outlet pipe with high swirl and outlet projecting into tank, (b) large outlet pipe with high swirl and outlet level with bottom of tank, and (c) small outlet pipe with low swirl and outlet projecting into tank

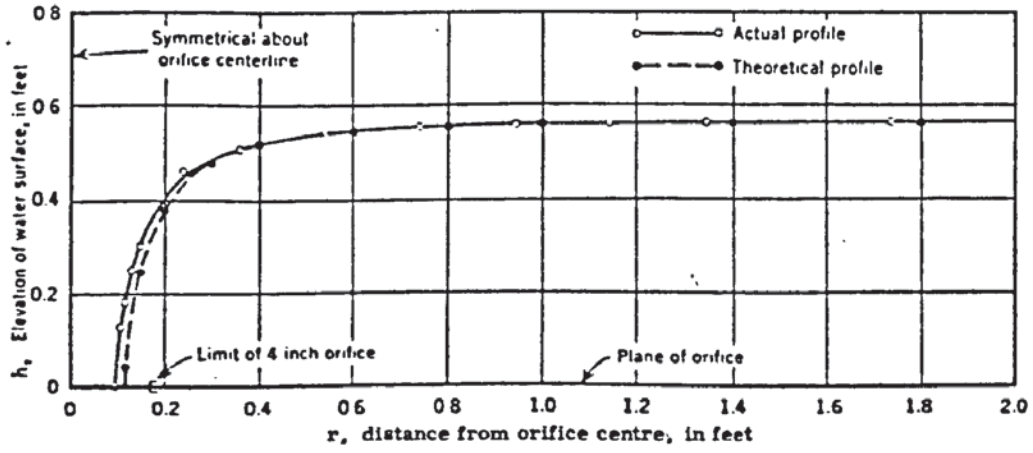

Fig. 4.3 Comparison of theoretical and actual water surface profiles
Discharge through a 4 inch orifice

due to two opposing factors : a) the depth of liquid h is not a constant near the axis of rotation and there is thus a reduction of flow area for the discharge. To satisfy the equation of continuity, this leads to higher velocities near the core and thus a greater drop in the liquid surface; b) as the velocity in the core increases, viscous shear forces also increase, reducing the outlet velocities. This reduction in discharge should lead to a greater depth of liquid remaining in the tank. Thus from fig. 4.3, viscous effects seem to predominate near the vortex core. These surface profiles were obtained from stable vortices and give only a general indication for vortices in rectangular geometries. These are described in 6.2.3.

4.2.5 Critical height (or depth) H_c

Springer and Patterson (45) investigated the dependence of the formation of an air-cored vortex on three factors: (a) strength of the vortex (its circulation), (b) submergence of the outlet (i.e. depth of water above outlet) and (c) outlet velocity. The general form of the H_c - V_d curves obtained in figs. 4.4 and 4.5 below agree with the work of other authors (55). In fig. 4.4 experiments were done first with an emptying tank and then with the outflow recirculated to the draining tank so that a constant depth was maintained for a particular set of observations. Where the outlet is flush with the tank floor, then water depth is the same as submergence.

It can be seen that in general, a vortex forms at greater depths of water for higher outlet velocities and increasing swirl. There seems to be a minimum velocity below which a vortex will not form at all. Similarly, above a certain value of outlet velocity, the critical height tends to a constant value independent of velocity. These are all features found

with rectangular pump sumps also. Note, however, that the values of non-dimensionalised critical submergence H_c/d are much higher for these cylindrical tanks.

It was also observed that if the outlet velocity was too large, it could produce surface turbulence which tended to unseat surface dimples, and so air-cored vortices were then formed at a lower level than for smaller values of outlet velocity.

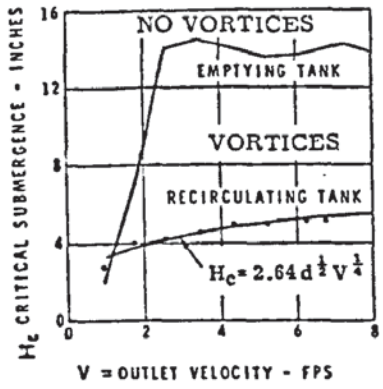

Fig. 4.4 Critical submergence versus tank outlet nozzle velocity for an emptying tank compared to a tank with recirculation.

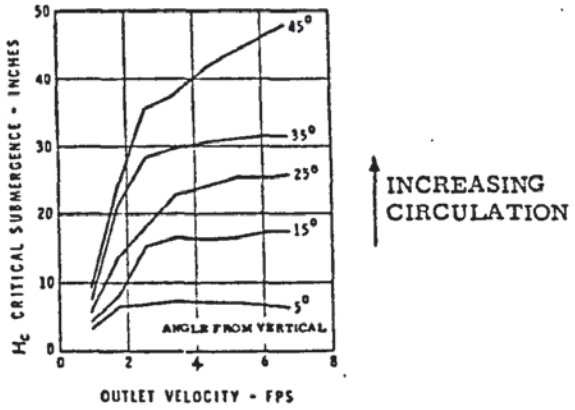

Fig. 4.5 Critical submergence versus tank outlet nozzle velocity for a recirculating tank with swirl induced by a single tilted supply nozzle.

Tank diameter 36" Outlet diameter d = 1.6"

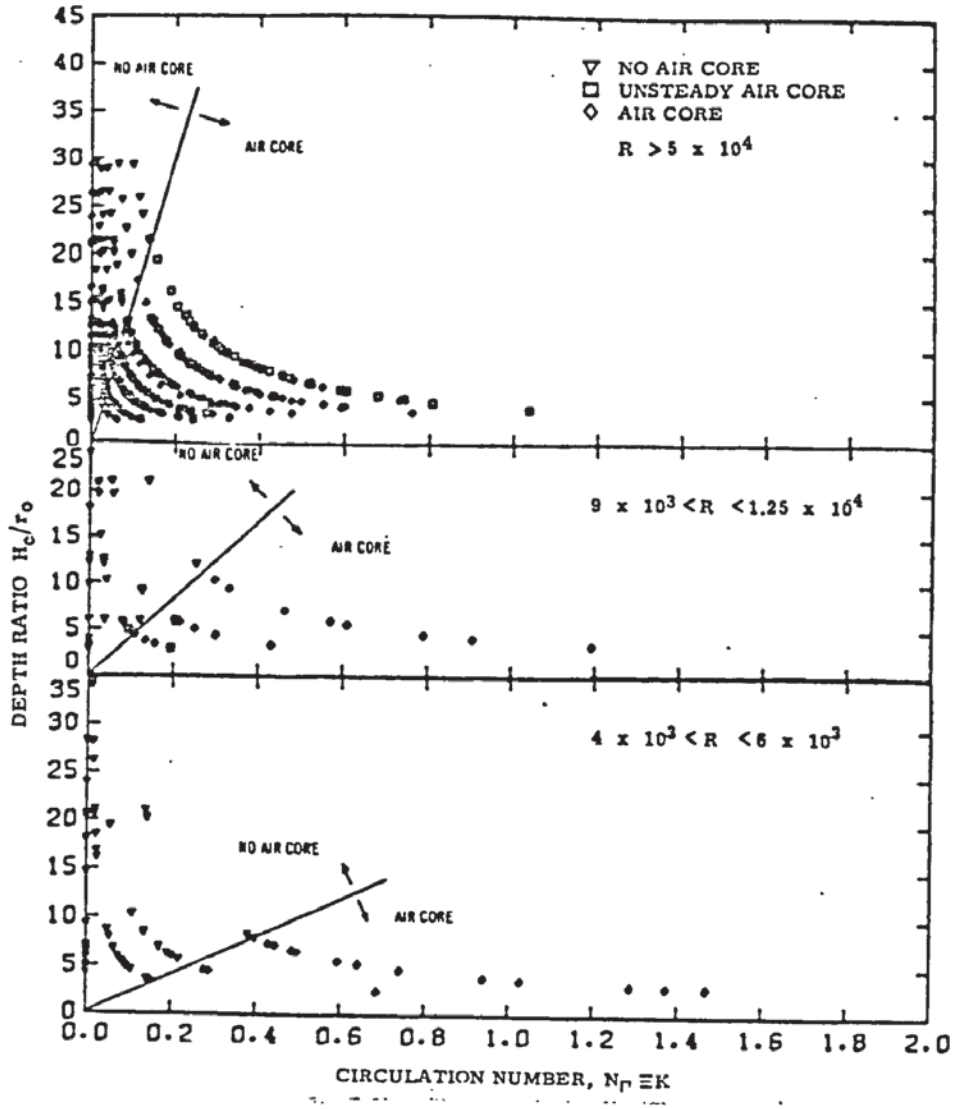

Fig. 4.6 Plots of critical depth against circulation (or Kolf) number for various ranges of Reynolds number, R, showing the different regions of air core formation.

Daggett (46) using the arrangement of Fig. 4.1c, did tests with 1.7m and 343 mm diameter tanks using various oils and glycerol solutions to obtain a range of viscosities and surface tensions. He assumed that the critical depth H_c, depended on the same parameters as the coefficient of discharge, C_D, i.e. $\frac{H_c}{r_o} = f(R, K)$ where r_o is the outlet radius, Reynolds number R was defined as $\frac{Q}{r_o \nu}$, Kolf number K as $\frac{\Gamma r_o}{Q}$, and with no dependence on Froude number, F. (There is a dependence on K whenever an initial circulation is imposed on the draining flow but this does not apply when the intake is symmetrically placed at the end of a

long rectangular channel with uniform approach flow).

C_D was found to be independent of R for $R > 5 \times 10^4$ and the same was assumed for H_c. Thus the following relations were deduced from the straight-line graphs of Fig. 4.6:

$$\frac{H_c}{r_o} = 35 \times 10^{-3}\ KR \qquad R < 5 \times 10^4$$

$$\frac{H_c}{r_o} = 150K \qquad R \geqslant 5 \times 10^4$$

These cannot be strictly correct because they predict $H_c = 0$ for zero circulation, contrary to experimental observations of both cylindrical and rectangular geometries.

4.2.6 Velocity distribution

(1) radial velocity u: This is very small near the core and thus difficult to measure accurately. Daggett found that u varied not only with r but also with z as shown in Fig. 4.7 contrary to assumptions in many theoretical analyses that $\frac{du}{dz} = 0$. Fig. 4.7 shows the variation with depth at different radial distances from the axis, though it should be noted that the velocities were measured with a miniature propeller meter.

The curves show that the radial velocities at the surface are low, but increase rapidly at lower levels nearer the outlet.

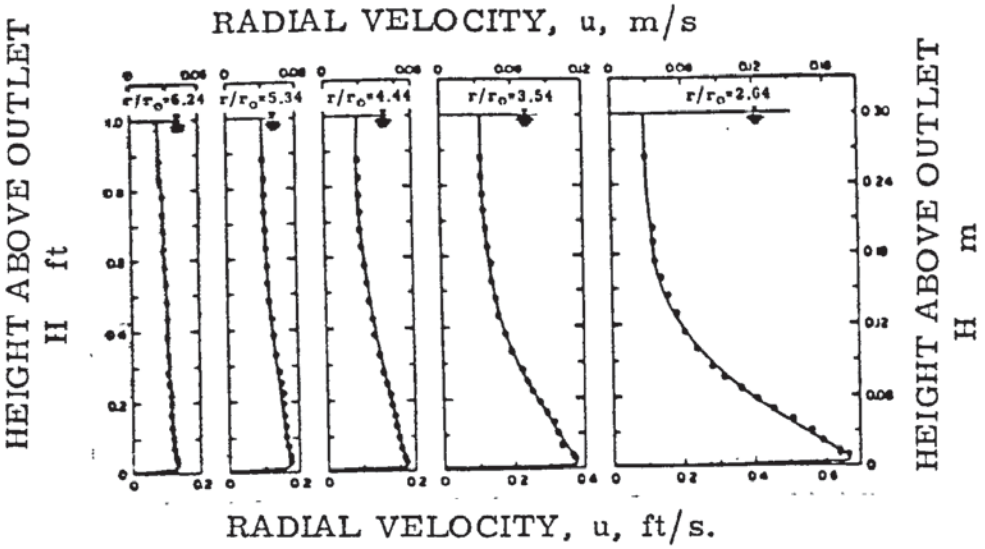

Fig. 4.7 Variation of radial velocity, u, with water height at different radii from the central discharge outlet for an air-cored vortex. Discharge = 0.019 m^3/s through 100 mm diameter outlet.

(2) tangential velocity v: Anwar has found the distribution to follow that of an ideal free vortex except near the vortex core where viscous shear retards the rotation, and v becomes progressively smaller than the ideal free vortex values. Measurements by Daggett (Fig. 4.8) show that v is independent of z (except near the tank bottom where boundary layer effects retard the flow) thus substantiating assumptions made in theoretical considerations.

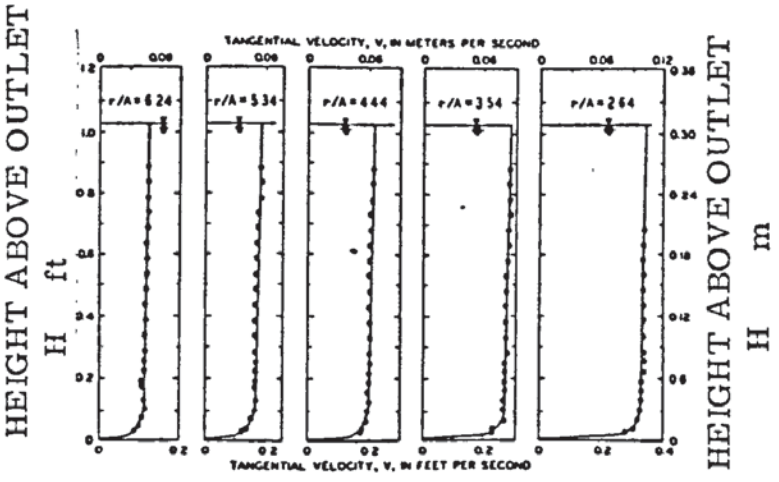

Fig. 4.8 Variation of tangential velocity, v, with water height at different radii for an air-cored vortex. Discharge = 0.019 m^3/s through 100 mm diameter outlet.

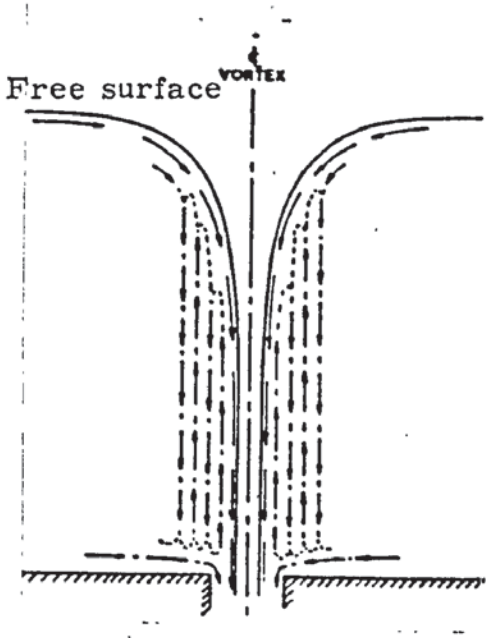

Fig. 4.9 Sketch of observed radial and vertical flow patterns near the core of a vortex.

(3) axial velocity w: These are also small, though Quick (47) has observed values of up to 10% of v, and so are by no means negligible. Upward as well as downward flows have been observed by several authors (Fig. 4.9), as well as predicted theoretically. Kamel (56) has shown that these upward axial components probably occur where the flow through the boundary layer formed at the tank bottom exceeds the discharge capacity of the outlet and so is forced upwards.

4.2.7 Effect of viscosity and surface tenstion on vortex flow

The effect of viscosity on surface profiles and air core formation has already been discussed above. There is no doubt that viscous effects become important near the vortex core where velocity gradients are highest.

As the Reynolds number decreases, so the relative importance of viscous forces increases. This can have the effect of preventing air entrainment as can be seen in Fig. 4.6 where significantly larger areas of no air core formation exist for the same range of H as R decreases from greater than 5×10^4 to about 5×10^3. This implies that if a model is constructed with too low a value of Reynolds number, no air core will be seen whilst an air core may be present in the prototype. This has important implications for deriving realistic scale laws.

The importance of surface tension and hence Weber number, has generally been considered to be negligible compared with gravitational and viscous forces, (except ref. 57), though there is little experimental evidence for this. Daggett uses fluid of the same kinematic viscosity but with surface tension differing by a factor of 3, and found no effect of this on the co-efficient of discharge. However, this does not necessarily mean that

surface tension has no effect on the formation of a deep dimple vortex, where the surface has a small radius of curvature at the vortex tip. Furthermore, when a model is operated at the Froude scale, the surface tension forces are not correctly scaled but are increased by the square of the scale factor. This much larger multiplying factor for the surface tension would then have a more noticeable effect than the factor of 3 which was tested by Daggett.

4.2.8 Scaling laws

The problem of scaling laws has been investigated intensively but no definitive result has yet been obtained. It can be seen that one scaling law for one geometry will not necessarily be appropriate for another. Even for a given geometry, e.g. a cylindrical tank in the case under consideration, one must be clear as to which parameter of the vortex flow is being modelled, whether it is C_D, H_c, Γ, depth of dimple, volume of air entrainment, frequency or duration of air entrainment, formation conditions of surface dimple, or the conditions of development of a dimple with tail into an air-cored vortex. The last is, of course, the one of greatest practical importance to model engineers. It should also be remembered that vortex shedding from a suction pipe or at a sharp corner is not present in the drain vortex case so different modelling criteria would apply.

Quick (58) using two geometrically similar tanks of diameter 540mm and 2160mm showed the dependence of C_D on K for a stable strong vortex, and argued that as K was a form of F, Froude scaling, i.e. velocity reduced by a factor $s^{-\frac{1}{2}}$ should apply for modelling the discharge of a vortex. Anwar agrees with this for a fully developed vortex provided $\frac{Q}{\nu H} > 10^3$.

On the other hand, Haindl (55) in investigating H_c at which an air entraining vortex began when a cylindrical tank of various diameters was slowly emptied, concludes that Reynolds scaling is appropriate, i.e. velocities increased by a factor s^{-1}. Froude scaling or equal model-prototype velocity would not agree with his results.

Between these two extremes, Polikovski and Perelman (59) suggested a "local" scaling of the vortex core according to R, and Froude scaling for the outer flow though it is difficult to see how this could be achieved in practice. Holtorff (29) also derived similar results theoretically, dividing the flow into two regions $r \geqslant r_o$ where Froude scaling applies, and $r < r_o$ where both F and R must be scaled.

Theoretical considerations by Kenn and Zanker (60) explain why an equal model-prototype velocity law may apply. They consider the ratio We : R, i.e. the ratio of viscous forces to surface tension forces and obtain a dimensionless number (capillary number) $\frac{\mu V}{\sigma}$ which is independent of length.

Rohan (61) discusses the effect of Froude scaling on viscous shear forces, and shows that tangential stresses on the model would be about $s^{-\frac{1}{2}}$ times greater than prototype, thus reducing angular velocities on the model and also reducing the likelihood of vortex formation on the model. Thus model velocities should be increased above Froude scale velocities, i.e. $V_m > V_p\, s^{\frac{1}{2}}$ by an amount depending on the ratio of R_p and R_m. (The subscripts m and p refer to model and prototype respectively.) This is not developed further to give actual numerical values but in general terms the procedure agrees with current practice at BHRA and elsewhere.

4.3 Vortex formation in rectangular sumps

4.3.1 Experimental configurations

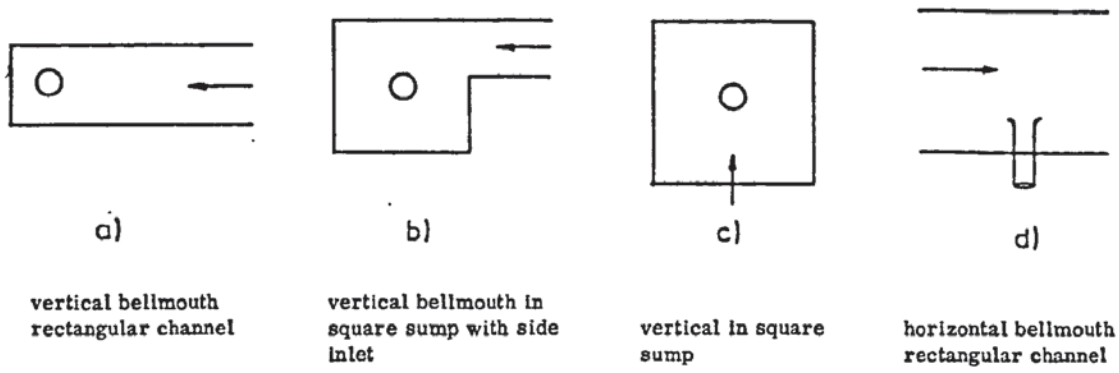

Fig. 4.10 Plan view of various sump geometries described in the published literature.

Most experimental studies have been with a vertical bellmouth intake in either a short rectangular sump or a square sump with a side-entry channel to produce asymmetric approach flow conditions (Fig. 4.10.) Amphlett (62) has studied the case of a horizontal bellmouth (surrounded by a ring of guide vanes to simulate different approach directions) in a rectangular channel. Laboratory experiments are usually done with a suction pipe to model the pump, so that the pump impeller is not modelled. This procedure thus neglects any pre-rotation effects from the prototype pump impeller. However, pre-rotation is not usually a significant factor on prototype installations when the pumps are running at or near best efficiency point. Most authors use a bellmouth attached to a straight suction pipe to represent the intake since this provides smoothly accelerated flow into the suction pipe. When no bellmouth is used, then $d = D$ and $V_d = V_D$. Fig. 4.11 gives details of systematic experimental work which has been done in the past on rectangular geometries.

Fig. 4.11

List of systematic tests carried out on various sump geometries.

(1 litre per sec = 0.035 ft^3/s = 13.1 UK gpm)

Sump Geometry	Author	Intake or Pump	Intake size d mm	D mm	Width W	Suction Velocity V_d m/s	V_p m/s	Discharge Q litres per sec.
Vertical intake, rectangular sump (fig. 4.10a)	Dicmas (63)	suction pipe	102	127	up to 5D		up to 1.83	up to 25.8
		prototype pumps		up to 1400	2D to 5D		up to 1.52	up to 2258
	Iversen (7)	suction pipe	102	171	2D to 5D		up to 1.26	up to 26.4
		prototype axial flow pump		464			0.97	164
	Markland and Pope (64)	suction pipe	66 66	185 119	about 3D 3D to 5D	up to 3.7		up to 12.2
	Raghunathan and Kar (65)	suction pipe	37.5	75	2D	up to 2.5		up to 2.8
Vertical intake, square sump with side inlet (fig. 4.10b)	Berge (66)	suction pipe (no bellmouth)	50	50	6D	up to 1.83		0.5 to 3.6
	Denny (67)	suction pipe	up to 762		up to 2.4m	up to 6.1		up to about 5.7
	Swainston (3)	suction pipe	19	?	254mm	up to 5.5		up to 1.6
	Wonsak (68)	suction pipe	42.4	70	1D to 2.5D	up to 1.2		up to 1.7
Vertical intake, square sump (fig. 4.10c)	Painter (12)	suction pipe (no bellmouth)	51	51	20D	up to 4.27		up to 8.5
horizontal intake, rectangular channel (fig. 4.10d)	Amphlett (62)	suction pipe (no bellmouth)	76.2	76.2	12D	up to 2		2.5 to 9

4.3.2 Criteria for defining critical submergence S_c

Individual authors have their own ways of defining the degree of air entrainment at the critical submergence and this makes direct comparison between authors difficult. Even in the results of an individual author, there may be considerable scatter. As Denny (67) states, "the boundary between vortex-forming and vortex-free conditions is not very precise". This highlights the difficulty of obtaining consistent results, and the importance of allowing sufficient time for a vortex to form.

For Denny (and subsequently used by Painter (12) and Hattersley (10)) S_c was defined as the submergence at which, "after a reasonable time at steady conditions of depth and flow, any air from the free water surface entered the intake, either continuously or intermittently through the agency of the vortex". This would correspond to a type 3 or 4 vortex in the classification given in chapter 6. Swainston (3) defines critical conditions "by the entrainment of small discrete bubbles". Dicmas (63) refined this to give two critical submergences, one when a few bubbles of air were intermittently pulled down from the vortex (type 3) and the other when open vortices formed with an audible sucking noise (type 4). The latter corresponds to the definition adopted in treating the results of the experiments described in chapters 5 and 6.

Iversen (7) actually measured the volume of air entrained and took S_c to be the value of the submergence at which the air volume was greater than zero, i.e. the level at which air first enters the suction pipe. However, this method is limited by the smallest quantity of entrained air which can be detected and could lead to underestimates of the submergence at which air is first entrained.

Markland and Pope's (64) experiments were done with a falling surface level (at a rate never greater than 5 cm. per min.) and the submergence at which the air core of a vortex (type 4) just passed into the bellmouth was noted. The level was then allowed to fall further and then rise again slowly to a submergence value at which vortex formation ceased. The latter was greater due to persistence of the vortex. These two values of submergence were then plotted in an S_c versus velocity head ($V_d^2/2g$) graph, and a curve of best fit drawn through the points. The authors admit some imprecision in this method, and suggest their results be used for qualitative comparisons rather than quantitative interpretation.

Raghunathan and Kar's paper (65) is concerned mainly with losses due to swirl in the suction pipe. They defined S_c as the water level at which air entrainment started, as shown by "the commencement of fluctuations of the manometric fluid in the manometers connected to the pressure tapping along the intake and simultaneous generation of noise in the intake pipe." This novel method could perhaps be developed to give a more reliable criterion than those based on subjective visual observations.

Duggins (69), in a paper on sump configurations for a submersible pump, observed the incidence of "vortex filaments" (submerged vortices) which could be easily seen between the sump floor and bellmouth intake. However, these filaments do not necessarily signal the start of air-entrainment by a free surface vortex and do not give any indication of the degree of entrainment.

Wonsak (68) expressed his results in terms of "pre-rotation intensity" 'a', which was the ratio of tangential velocity in the suction pipe (as measured by a vortometer) to the mean axial velocity V_d. This method

could be developed if combined with free surface observations to specify a minimum acceptable value of 'a', though swirl measurements taken with a vortometer can be misleading since the narrow tail of a vortex can pass between the vortometer vanes. If two contra-rotating cores are present, it is possible that little rotation of the vortometer blades will be seen, whereas local regions of non-zero swirl do in fact exist.

4.3.3 Importance of geometric parameters

It is now well known that sump geometry has an important influence on the incidence of vortices. The important dimensions to consider are 1) floor clearance, C, 2) sidewall clearance and hence width, W, 3) backwall clearance, X, 4) approach channel length, L, 5) submergence S, and 6) bellmouth shape. This section reviews the experimental work on these parameters. Although exact optimum values of the above dimensions are not known, basic guidelines for sump design, based on this work and field experience have evolved over the years (1, 2).

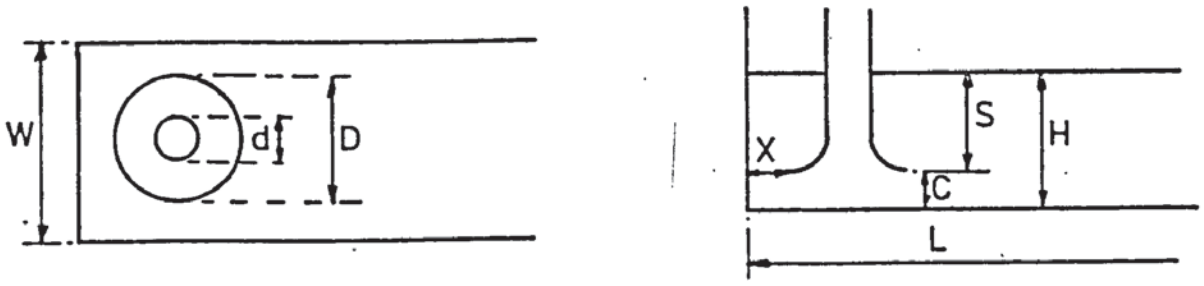

Diagram illustrating some of the common rectangular sump dimensions

Fig. 4.12 shows the variation of critical submergence, S_c/D, with floor clearance, C/D, for several rectangular geometries, though the geometries tested differ from basic standard designs. In general, S_c/D decreases as the floor clearance is increased. This can be accompanied

by a corresponding rise in total depth H. This trend is confirmed by several authors for several different rectangular geometries, though Berge, whilst agreeing with the decrease in S_c reports a decrease in H_c for the range $0.03 < C/H_c < 0.19$. Although the data plotted from Dicmas in Fig. 4.12 show an decreasing value of H, he quotes figures for X/D = 0.2 which follow the trend of the other curves for H. It would be of great interest, to determine whether or not there is a value of C at which a minimum value of H occurs.

Amphlett with his horizontal intake arrangement found that as C was increased, the coefficient of discharge, as defined by $Q/A(2gS)^{\frac{1}{2}}$, also increased for a given value of S_c and angle of approach.

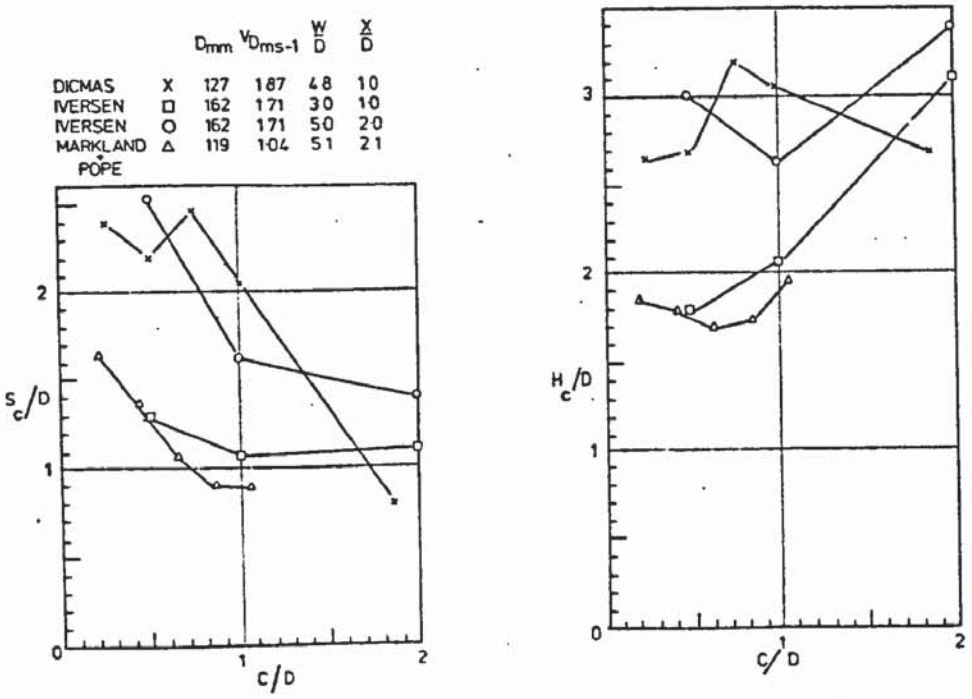

Fig. 4.12 Variation of critical submergence and depth, S_c/D and H_c/D, with floor clearance C/D, various authors.

Experiments involving changes in channel width, W, essentially relate to the effect of sidewall proximity, since most of the papers reviewed deal with suction intakes which were placed midway between the sidewalls. From fig. 4.13 it can be seen that S_c decreases with increasing W until a

value of W/D of about 3.6

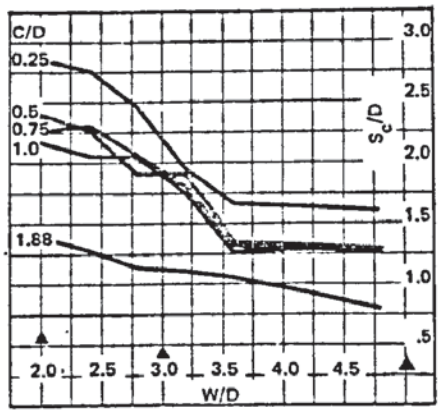

Fig. 4.13 Variation of critical submergence, S_c/D, for type 2/(3) vortices with width, W/D, and floor clearance C/D.
——X/D = 0.2, V_D = 1.87 m/s (Dicmas ref. 63)
▲ X/D = 0, V_D = 1.26 m/s C/D = 2 (Iversen ref. 7)

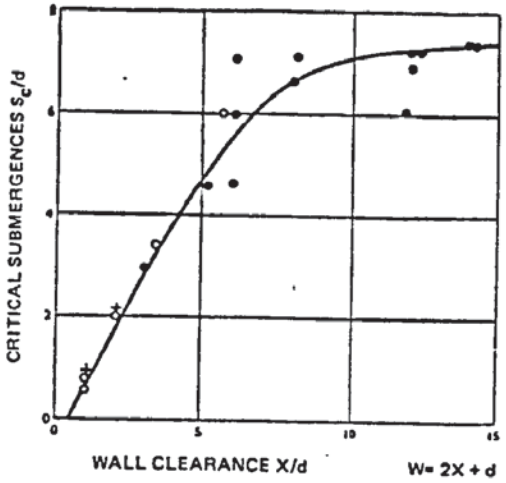

Fig. 4.14 Effect of wall clearance on critical submergence, S_c/D, for various size pipes situated centrally within similar square sumps. C/d = 1, V_d = 4.11 m/s. (Denny ref. 67)

Fig. 4.14 shows the results obtained from a square sump with swirl in the approach flow. Here, the opposite trend occurs with S_c increasing with W and wall clearance, X, until X is greater than 8 pipe diameters. It is uncertain, however, what the relative contributions of this are from a change in W and a change in X. Wonsak (68) also reports an increase in swirl as the width is increased.

As regards endwall clearance X, there is general agreement that the smaller X is, the less likelihood there will be of vortex formation. Bortzsonyi and Kajdi (70) found that the percentage of time when vortices were present decreased from 60% to 5% when X was decreased from 0.5D to 0.1D. It may be thought, then, that X = 0 gives the optimum performance. However, Dicmas found that head losses increase significantly for X below about 0.2D due to an uneven flow into the bellmouth as the end-

wall comes very close to it. Young (71) has gone as far as suggesting an empirical equation relating R, X, d and S_c which describes the results he obtained for a suction pipe 6.25 cms in diameter.

The approach channel length L is an important parameter in sump design since a certain length of straight is needed upstream of the suction pipe to ensure satisfactory flow conditions at the intake without incurring excessive construction costs. Most of the available literature describes work with sumps of a fixed length, ranging from 2D to 11D. As far as the author is aware, the paper by Wonsak (68) is the only one to give details of reduction in swirl when L is changed from 2D to 8D (fig. 4.15).

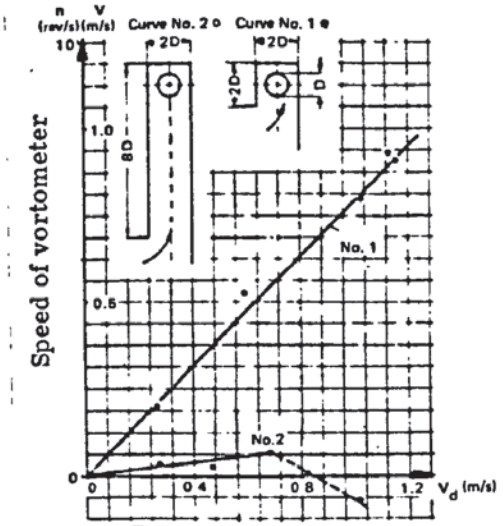

Fig. 4.15 Reduction in swirl as recorded by a decrease in speed of rotation of a vortometer, for channel length 8D as compared with 2D.

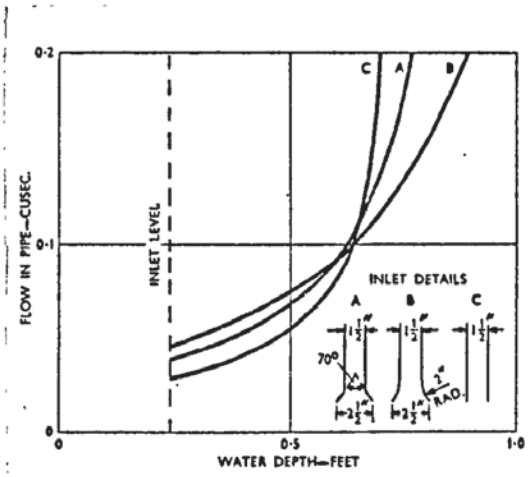

Fig. 4.17 Effect of conical and bell-mouth intake shapes in a 2 ft. square sump. W/d = 5.3, C/d = 1.9

Submergence S needs to be large enough to avoid air-entrainment. The minimum "safe" submergence to design for seems to be between 1D and 2D, depending on the value of V_D (see fig. 4.16). It should be noted that Dicmas' prototype readings are on the low side since he waited until the vortex was well-established before recording the result.

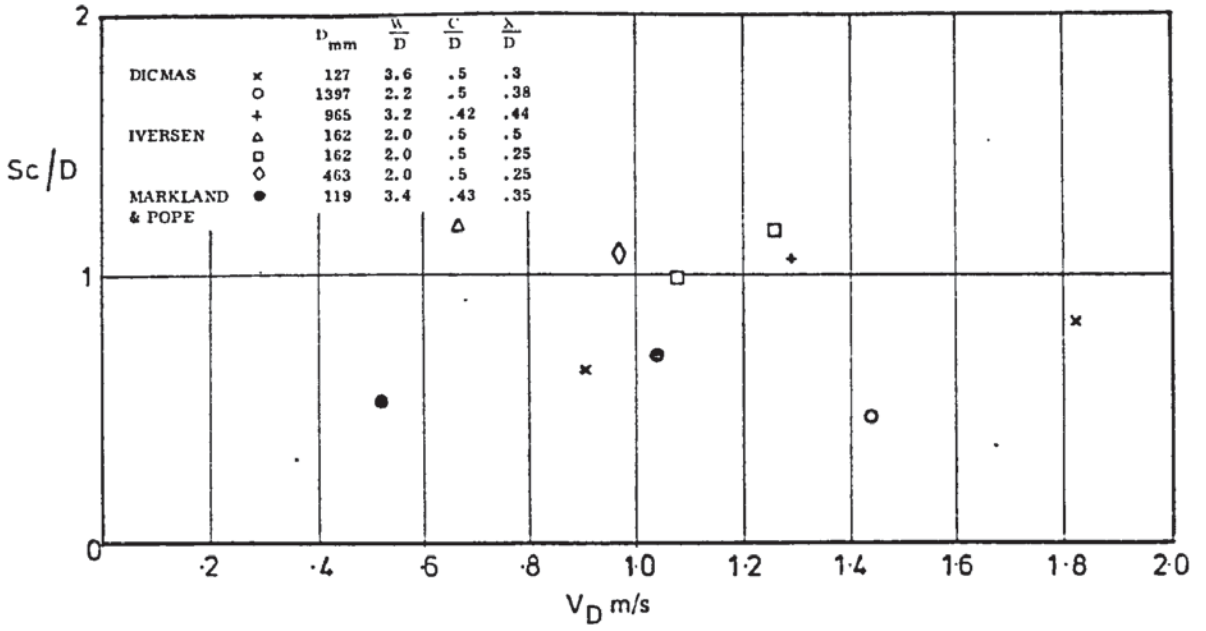

Fig. 4.16 Variation of critical submergence with bellmouth velocity for various sump geometries and bellmouth sizes. (Iversen's points refer to type 3 vortices).

There is a considerable variation in the size and shape of bellmouth used. The standard value of D/d met in practice is from 1.5 to 1.8, and refs. 64 and 66 report that a larger bellmouth gives smaller values of S_c/D. Fig. 4.17 shows the effect of different intake shapes with a constant suction pipe diameter. At lower flows, the bellmouth intake gives the lowest value of S_c whereas at higher flows, the straight suction pipe gives lowest S_c. However, this configuration is not used in practice, since flow separation would occur as the flow entered the pipe, leading to higher losses and a distorted velocity distribution at the pump impeller.

4.3.4 Comparison of recommended UK and USA design practice

The most comprehensive design data for pump sumps is to be found in refs. 1 and 2. Both of these are agreed on the importance of both the approach and local geometry in ensuring uniform flow conditions at the intake. The UK guide gives recommended dimensions in terms of bellmouth diameter, D, and assumes that V_D is usually similar for fixed

speed pumps (typically 4m/s for an axial flow pump) so that the variation of optimum dimensions with V_D is not discussed. On the other hand, the USA recommendations for various pump dimensions are given in inches for a range of flow rates from 3,000 to 300,000 US gpm (0.2 to 20m^3/s). In general, there is a power law relationship between flow rate and each sump dimension.

The similarities between the design recommendations can best be seen by taking a specific example. The table below compares the recommended dimensions for the single cell of a multiple pump sump in which D = 90 in. (2.29m), and the design flow rate of each pump was between 169,000 - 217,000 US gpm (10.7 to 13.7 m^3/s). This pump sump is discussed further in chapter 7.

Comparison of USA and UK recommendations and Kori 2 cooling water pump sump

	UK (1)	USA (2)	Kori 2 (72)
C/D floor clearance	0.50 to 0.75	0.52-0.59	0.52
W/D channel width	2.0 up to 3.0 possible	$\geqslant$2.6-2.8	2.4
X/D endwall clearance	$\simeq$ 0.25	$\leqslant$0.7-0.9	0.27
L/D channel length	3.25-9.25 depending on upstream bandscreen width.	$\geqslant$6.8-7.4	7.2
H/D depth	$>$ 2.0	$\geqslant$3.0-3.4	$\geqslant$2.4
V_W approach velocity	$<$0.3 m/s	$<$0.3 m/s	0.29-0.45 m/s

D = 2.29 m (90")

Q = 10.7 to 13.7 m^3/s (169,000 - 217,000 US gpm.)

It can be seen that some of the recommended dimensions are very similar, with ref. 2 more conservative in its recommendations for L and H. It also allows a larger value of X, though in common with ref. 1, it states that the lip of the bellmouth should be close to the endwall of the sump. However, since the USA recommendations depend on flowrate, larger discrepancies will occur for other values of flowrate. It should also be noted that individual pump manufacturers have their own "in-house" guidelines which do not necessarily agree with the above.

4.3.5 Scaling laws in rectangular sumps

It is generally agreed that some degree of exaggeration above Froude number scaling is required for dynamic similarity between model and prototype. However, Amphlett states that vortex formation depends only on Froude number if $R_R = V_d S/\nu \geqslant 3 \times 10^4$, whilst Surek (73) suggests a minimum figure of 2.2×10^5 for $R = \frac{V_W d_h}{\nu}$ (d_h = hydraulic diameter of channel = $\frac{4WH}{W+2H}$) above which Froude scaling is valid. This latter figure was derived from actual prototype installations which had proved themselves by trouble-free operation.

Denny and others (7, 66) agree that Froude scaling is correct for modelling surface dimples but that model and prototype velocities should be equal when considering air-entrainment. The only prototype evidence Denny quotes for this, however, comes from one spot observation on site. Otherwise, this "equal velocity rule" has only been verified for a limited range of pipe sizes in square sumps, and may be superseded by a different law for larger installations.

Dicmas, basing some tests on Iversen's prototype work with

D = 464 mm, obtained similar values of S_c/D by using the equal velocity rule for V_D and Froude scaling for V_W. This, however, meant exaggerating the value of W and so geometric similarity was not preserved.

In another approach to model testing, Hattersley (10) suggests that similar swirl parameters can be obtained in model and prototype provided $R\sqrt{f}$, where f is the Darcy friction factor, is greater than a critical value of about 2×10^3, and the model Froude number is equal to that of the prototype. Then, using a conventional friction factor chart, the scale is chosen so that with Froude scaling, the friction factor for the hydraulically smooth model is equal to that for the rough prototype. (The prototype R and friction factor need to be obtained first). This optimum model scale will be adjusted, in practice, by constraints such as available pipe diameter and laboratory space. The final step involves comparing the measured model velocity profile near the boundary with the corresponding prototype to calculate the increase (or decrease) over Froude scale velocities necessary for similarity.

Durgin and Hecker (74) consider it more likely that viscous effects become negligible asymptotically, rather than at a certain critical Reynolds number. They suggest the model should be operated at constant Froude number but at various Reynolds numbers by changing the water temperature. The prototype performance is then deduced by extrapolating the model behaviour to the prototype Reynolds number. It is difficult to generate sufficient model data with this method in order to extrapolate to prototype conditions with any confidence. Furthermore, with large bodies of water, there would inevitably be variations in temperature over the time intervals required for vortex observation. Nevertheless, the authors have successfully used this technique in hydraulic model studies of reactor

containment sumps.

Another recent paper (75) concludes that the scaling law (V_m/V_p) is a function of both the scale ratio and depth H/D. Using various values of D from 120 mm to 400 mm the authors were able to obtain results for scale ratios up to 1 : 4 (fig. 4.18). The results lie between Froude scale (shown for comparison) and equal velocity scaling. It is not clear what the form of the approach geometry was, or whether it was changed as D was changed to preserve geometric similarity.

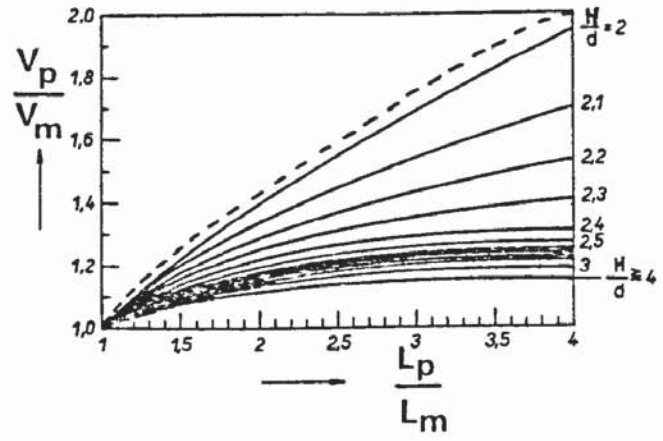

Fig. 4.18 Variation of velocity ratio V_p/V_m with scale ratio L_p/L_m for various water depths.
- - - - - - Froude scale

4.4 Other forms of hydraulic intake

A few papers on other commonly found intake geometries are included here for reasons of completeness. Because of the importance of boundary geometry, however, the results would not be expected to apply to rectangular pump sumps. Prosser (1) gives a good review of designs for special applications including sewage pump sumps, small cylindrical wet well sumps (see also ref. 76) and single or multiple intakes drawing from a large forebay or reservoir.

It is the last type of horizontal intake which has received most attention. Gordon (77) in a study of 29 existing hydro-electric intakes, four of which had vortices, deduced that the minimum submergence to design for was given by

$$S = k_s V_d d^{\frac{1}{2}}$$

where k_s was 0.3 for symmetrical approach flow, and 0.4 for intakes with a lateral approach flow. This relationship is confirmed by prototype data in ref. 78, k_s however must depend on the forebay and intake geometry. Gorden compares his data with that of Denny (67) and attributes the disagreement to scale effect. However, the mechanisms of vorticity generation are different in the two cases and are thus not strictly comparable. The vertical intake used by Denny gave higher critical submergences than the horizontal intakes for a given intake velocity.

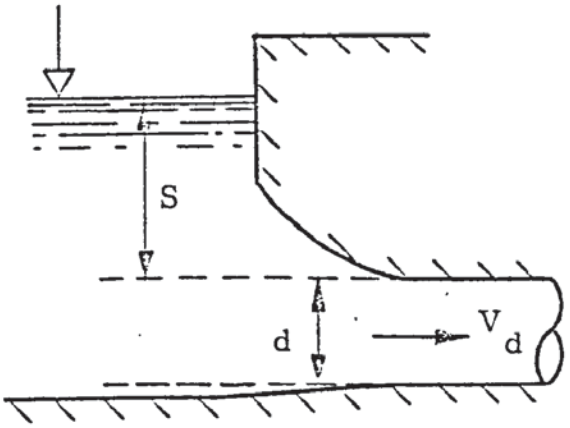

Reddy and Pickford (79) assume no Reynolds number dependence for vortex formation, and suggest that $S/d = V_d/(gd)^{\frac{1}{2}}$ for vortex free operation when anti-vortex devices are fitted, otherwise $S/d = 1 + V_d/(gd)^{\frac{1}{2}}$. This reduces to the form proposed by Gordon, and implies Froude scaling for vortex formation.

The other form of intake which should be mentioned is one with a circular forebay, though there is little published literature on this. The Central Electricity Generating Board (80) have developed a circular pump-

house arrangement for recycling cooling tower water whereby water enters an annular moat tangentially and is then drawn off by vertical spindle pumps arranged on a central island within the moat. Vortex problems may arise with this design, but model studies can ensure satisfactory performance down to very low submergences.

A development of this is reported by Dutkiewicz and Ham (81) in which water enters a circular forebay tangentially at the perimeter and is drawn off tangentially at a lower level by pumps also arranged round the perimeter. The flow patterns consisted of an outer annulus of water rotating with uniform velocity equal to the inlet velocity, together with an inner core of water rotating as a solid body. Air-entraining vortices formed at the boundary of these two flows, but were eliminated by an annular roof placed just above the level of the inlets.

4.5 Discussion and conclusions

The papers reviewed above cover a wide range of intake size and geometry, though prototype data is noticeably scarce. Detailed data on various vortex parameters have been obtained for stable vortices formed in cylindrical tanks but not for the more practical situation of a vertical intake at the end of a rectangular channel, where air-entraining vortices tend to be less stable, both with time and position.

Nevertheless, design guides for hydraulic intakes exist, which give recommended dimensions for various geometric parameters. Some differences between the recommendations inevitably exist not only between refs. 1 and 2 but also those of individual pump manufacturers. Furthermore, there is little data available on the variation of critical submergence

with intake velocity and its sensitivity to small changes about the optimum. More detailed information on these could lead to considerable savings in the civil engineering works for an intake scheme.

In dealing with the scaling of air-entraining vortices, the available literature, in general, recommends exaggeration of flow velocities above Froude scale on the model to achieve the correct levels of turbulence and viscous effects, though some authors found that Froude scale was satisfactory provided the model Reynolds number exceeded a certain critical value. However, there is still uncertainty over the exact degree of flow exaggeration necessary.

The following chapters describe the work carried out at BHRA recently in an attempt to fill some of the gaps described above in our existing knowledge of vortex formation at hydraulic intakes.

CHAPTER 5

EXPERIMENTAL STUDY

5.1 Description of programme of experiments

As stated in the introduction, there has only been a small amount of systematic work carried out on realistic sump designs, most of which covers a narrow range of geometry and physical size. This can be seen from fig. 4.11 given in the literature review of the previous chapter. Hence, experimental rigs were designed based on a commonly found sump configuration, and free surface vortex formation was observed over a wide range of conditions, in order to achieve the last three aims of this project, i.e.

— to investigate the mechanisms responsible for vortex formation

— to provide comprehensive data on various aspects of intake design

— to derive satisfactory scaling laws for free surface vortices.

Four geometrically similar rigs were built labelled 1.5", 3", 6" and 12". rigs for convenience. (These are the nominal suction pipe diameters). Further details of the rigs are given in the next section.

The majority of the experimental data on the effect of various geometric changes on critical submergence, S_c, was obtained from the 6" rig which had a 6" (nominal) suction pipe with a bellmouth, diameter, D, of 244mm. This size is in the lower end of the range of typical prototype sizes, whilst at the same time being convenient to operate and modify as necessary. A few tests were then repeated on the 12" (D = 488mm), 3" (D = 122mm) and 1.5" (D = 61mm) rigs to derive scaling laws.

Fig. 6.15 in the next chapter shows the various conditions tested. The values of C/D, X/D and W/D were chosen to coincide with those most commonly found in practice. (see fig. 5.1 for definition diagram).

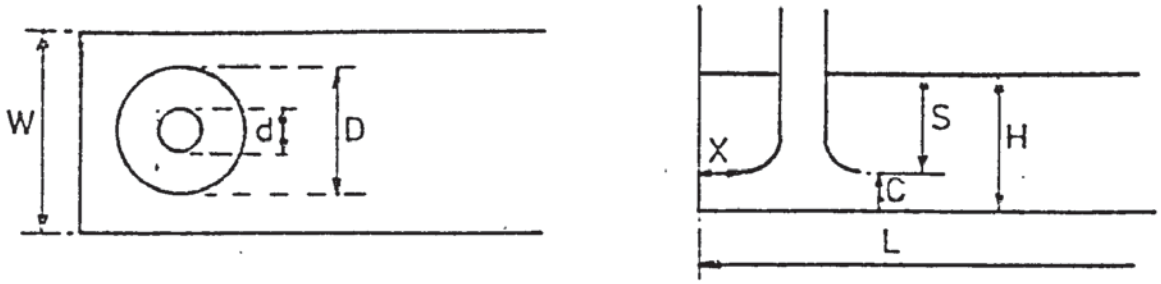

Fig. 5.1 Definition diagram of rectangular sump geometry.

Other aspects which were considered were the use of corner fillets as anti-vortex devices, and the effect of upstream boundary changes. These are all discussed further in chapter 6.

In conjunction with this experimental work on a single sump design, tests were made on a 1 : 15 scale model of a multiple pump sump, which had been built for an actual scheme and which was adapted to provide further information relevant to this project. This work is described in chapter 7.

5.2 Description of experimental rigs

The basic sump geometry, common to all size rigs, is shown in fig. 5.2*, with dimensions marked for the 6" size. It consists of a short, straight section followed by a contraction which leads to a long closed rectangular channel. The initial design just consisted of the contraction

---

* Figures for the remaining chapters are to be found at the end of each chapter.

plus rectangular channel, but this led to visible flow separation at the entry to the contraction, so the sump was extended to the line of the screens, which gave more uniform approach conditions. At the end of the channel is a vertical suction pipe with a bellmouth intake placed symmetrically on the pump centreline. Figs. 5.3 to 5.7 show general views of three of the rigs.

Figs. 5.8 to 5.10 are photos of the bellmouths, whilst Fig. 5.11 gives details of the bellmouth used in the 6" rig. The bellmouths used on the other rigs were geometrically similar models of this one with a slight variation in the external geometry, which was, however, considered insignificant. The position of the intake relative to the boundaries could be varied as required, except that in the 12" rig, only the floor clearance could be changed. In the 6" rig, one sidewall was movable so that the sump width could also be varied. In each case the channel was built inside a larger rectangular tank. Fig. 5.12 gives details of the major dimensions and flow variables of the rigs.

Water was drawn through the intake by a centrifugal pump, and returned to the channel via the discharge line of the pump to a discharge manifold. To complete the flow circuit the water then passed through a combination of perforated metal screens and 'hairlok' (a mat of closely knit fibre) to smooth out any large-scale asymmetry in the approach flow.

The flow rate was measured by an orifice plate, made and fitted according to the recommendations of the British Standard BS 1042 (ref. 82), in the discharge line of the pump with a manometer to measure the pressure difference across the tappings on the orifice plate. In the 1.5" rig, rotameters were used.

Whilst there was close agreement between mean velocities measured by a miniature propeller meter (fig. 5.13) and the orifice plate for the 6" rig, a large discrepancy of about 30% was found between these two measurements for the 12" rig, with the orifice plate giving the higher reading for the mean channel velocity. The implication of this was that the actual discharge coefficient on the rig was lower than that taken from BS 1042 for ideal approach conditions upstream of the orifice plate. At first, it was thought that air leakage on the suction side was responsible for the discrepancy, and so the metal pipework with its numerous flanged joints on the suction side of the pump was replaced by a 180^{o} bend made in one piece out of fibre glass, as shown in fig. 5.6. This led to only a slight improvement, so the second possible source of error, i.e. swirl caused by the impeller on the discharge side of the axial pump was tackled. Ref. 83 gives data on deviations from the ideal discharge coefficient due to swirl which are consistent with the 30% differences found here for an orifice plate of area ratio 0.63.

It was necessary, therefore, to design and construct an effective flow straightener with minimum head loss as quickly and as cheaply as possible. A "tube bundle" flow straightener met these requirements, and fig. 5.14 gives an idea of how the tubes were arranged in the 500mm discharge pipe. The flow straightener consisted of a bundle of plastic tubes of 89mm outside diameter, length 850mm secured at a distance of 700mm

downstream of the pump discharge flange with the downstream face about eight pipe diameters upstream of the orifice plate. A few lengths of outside diameter 50mm were also used to fill in any large gaps, thereby fixing the tube bundle more firmly in the pipe. This design follows the recommendations given in ref. 82. After the straightener had been fitted there was much better agreement (to within 5%) between the propeller meter and orifice plate readings .

5.3 Experimental procedure

For a particular geometry, the experimental procedure consisted of fixing the water level at a certain value and then observing free surface vortex formation for certain values of suction bellmouth velocity, V_D, starting from a high value and working down to low velocities. The types of vortices which formed were classified into type 1 to 5 in order of increasing severity, see fig. 6.9. The water level was adjusted to the original level each time. The reverse procedure of starting from a low V_D and working up to a high V_D with constant submergence was tried in a few cases, but there was no change compared with the original procedure in the velocity at which a particular type vortex first appeared. Perspex windows in the endwall and one sidewall allowed ready observation of the flow conditions. For each particular flow setting, observations were taken over a period of ten minutes on average after flow conditions had settled down. The classification used to distinguish between the types and severity of vortices corresponds to the different stages of development described in 6.2.3 and shown in fig. 6.9.

Fig. 5.15 shows a typical full plot where observations of vortex formation for one geometry have been plotted in detail with non-dimension-

alised submergence, S/D, along the vertical axis and bellmouth velocity, V_D, along the horizontal axis. This is a fairly common method of plotting the results, giving a ready indication of the types of vortices which form for values of two important parameters, S/D and V_D, which govern vortex formation. The bellmouth diameter, D, has been used to non-dimensionalise S as well as all the other geometric dimensions, since recommended sump dimensions are usually given in terms of D. Furthermore, for a given discharge, D determines the intake velocity and hence the acceleration field local to the bellmouth. The alternative is to use suction pipe diameter, d, but in practice, the external geometry of pump casings and columns is not in the form of a straight vertical cylinder so that it is difficult to define a meaningful value for d in any particular case.

The curve (bold line) in fig. 5.15 enclosing all fully air entraining (type 4) vortices defines the critical submergence, S_c, for these experiments, i.e. the submergence at which an air entraining vortex with a fully developed air core first occurs. This definition was chosen as it represents a definite event, and it is thus easier to identify its occurrence as compared with a type 2 or 3 vortex. However, it should be noted that this definition differs from that of some authors (see 4.3.2). Thus the bold curve divides the graph into two regions, one below the curve in which fully air-entraining vortices occur, and one above with less severe surface vortices.

Curves for S_c/D against V_D were obtained for a wide range of boundary clearances by adjusting the appropriate clearance to the required value and then repeating the above procedure. For the majority of cases, sufficient readings to determine the limit of type 4 vortices only were taken, and the curves derived from these readings are discussed in the

next chapter. Detailed plots of vortex types at the various flow conditions tested are given in Appendix A.

The effect of one type of anti-vortex measure, i.e. 45° corner fillets positioned as in fig. 5.16 was investigated for the 6" rig set at a channel width of 2D. Furthermore, tests were done with a quarter-width ($\frac{1}{2}$D) baffle inserted at various upstream stations (fig. 5.17) within the channel. This was repeated on the 1.5" and 12" rigs for an upstream station 6D from the endwall.

Before any vortex observations were made, a velocity contour plot was obtained to check that the approach flow distribution was reasonably uniform. This was done by taking point velocity measurements with the miniature propeller meter along several verticals in a plane 3D from the endwall, non-dimensionalising these velocities by the mean channel velocity, and drawing contour lines through points of equal velocity.

5.4 Discussion of experimental accuracy

In general, observations were made at various velocities in steps of between 0.1 to 0.2m/s, with changes in submergence in steps of between 0.1 and 0.2D. These steps were chosen as a compromise between spending excessively long times on one configuration (since at least ten minutes were required for one reading) whilst obtaining a sufficient number of points to determine the value of S_c/D with reasonable accuracy. Even so, twenty to thirty flow settings were necessary to be able to draw a curve defining the limit of type 4 vortices over the range of levels and velocities available, (see fig. 5.12). The error in S_c/D using this procedure is estimated to be about $\pm$ 10% for low submergences less than 1D, dropping to $\pm$ 5% for higher submergences between 1.5D and 2D. One particular

geometry was tested three times on different occasions, and no significant difference was found between the $S_c/D - V_D$ curves, within the limits of experimental error.

Flow measurement by orifice plates is a well-established and relatively simple technique. However, their accuracy depends on the area ratio, correct measurement of pipe diameter, and correct fitting with the requisite upstream and downstream lengths of straight pipe as specified in ref. 82.

Taking account of this as well as random errors in reading the manometers, the estimated accuracy of flow measurement with the orifice plates used is $\pm$ 5%.

The water used in the experiments was either fresh from the laboratory mains supply or continuously cleaned by a sand filter. The water temperature obviously varied depending on the time of year, but this would give a variation in kinematic viscosity, and hence Reynolds number of less than 10%, which was not considered significant.

In the analysis in chapter 6, values of V_D are taken for given values of S_c/D. Given the discussion above on estimated errors, the error on the values of the velocity ratio, V_m/V_p, will be $\pm$ 10% approximately.

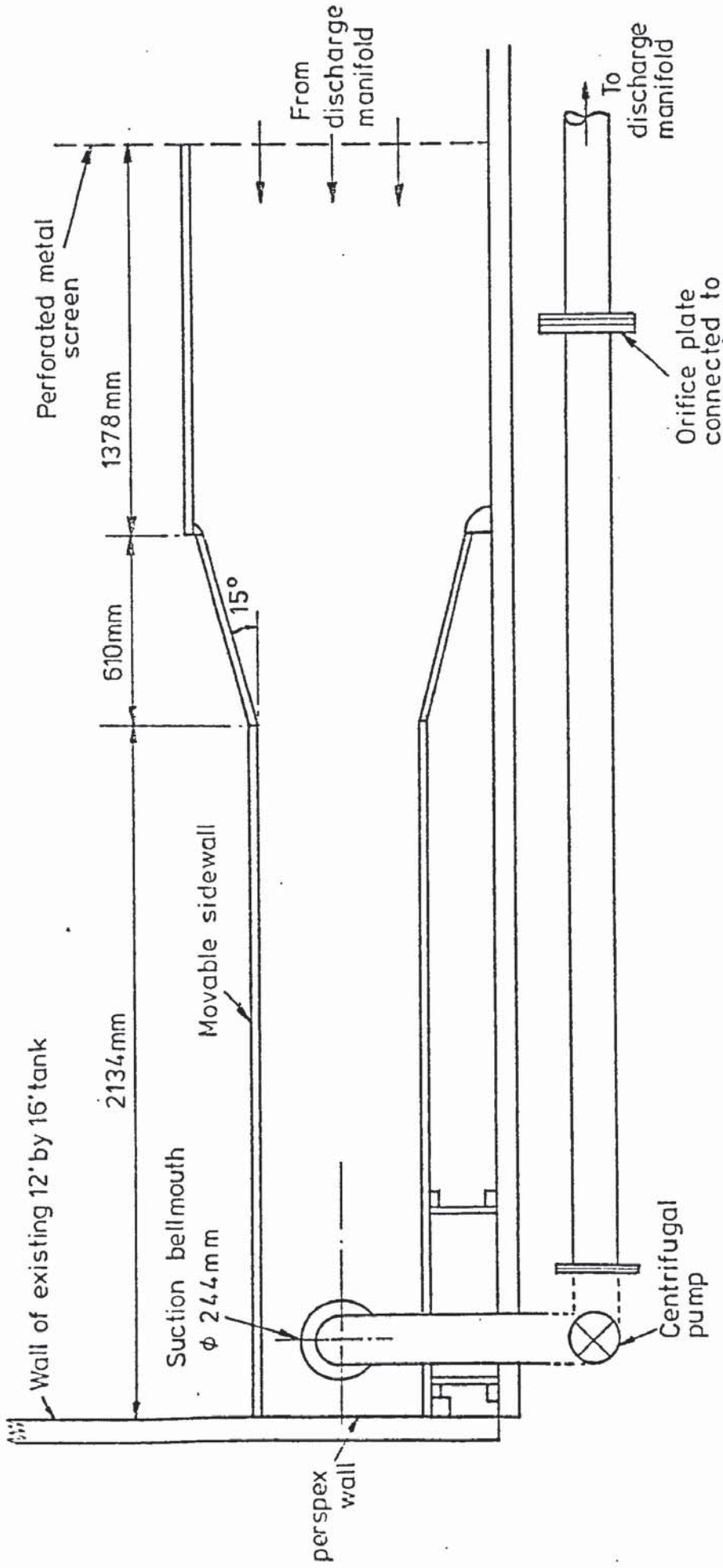

Fig. 5.2 Plan view of 6" experimental rig, showing approach channel geometry, location of bellmouth intake and associated pumping system.

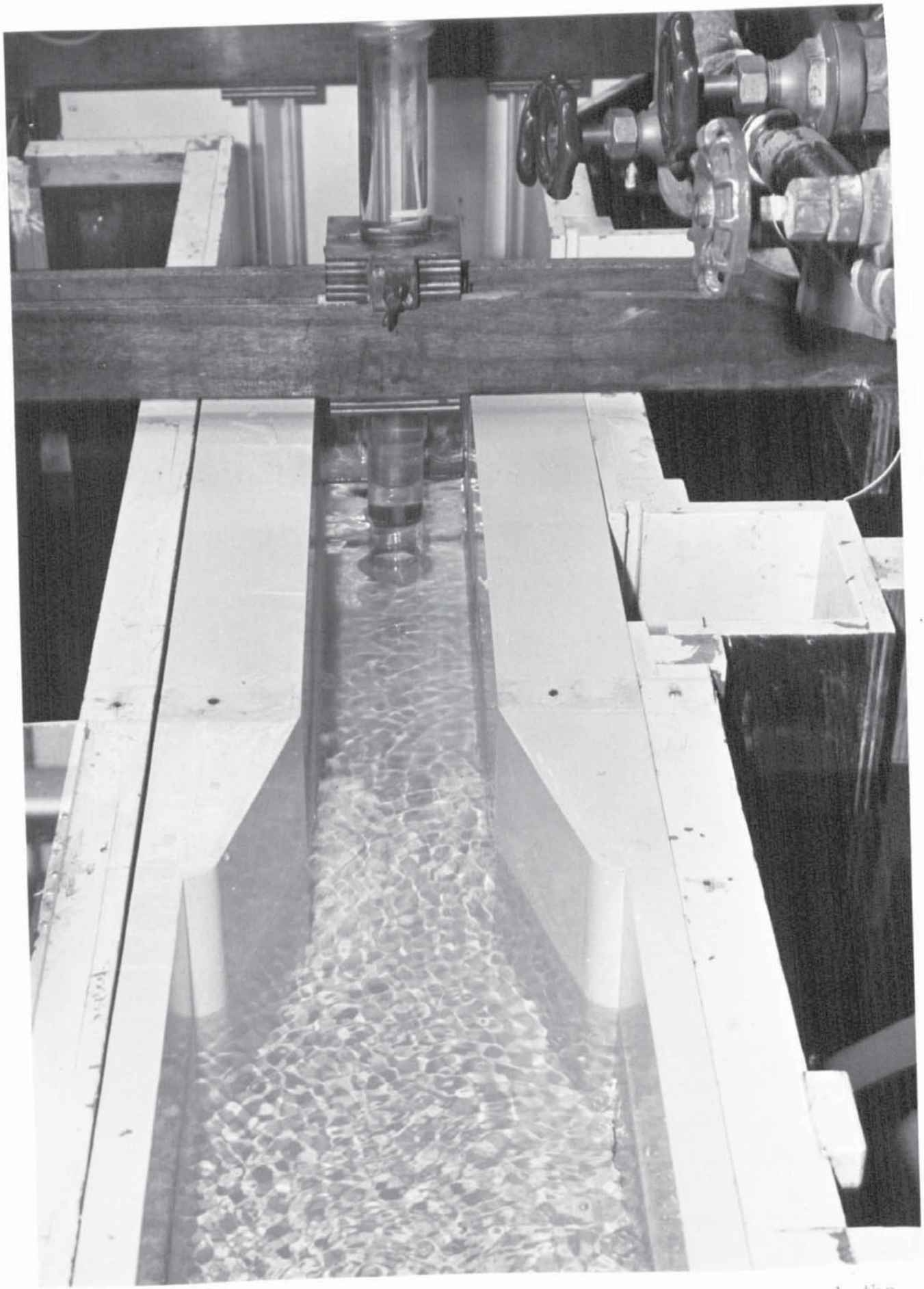

Fig. 5.3 View looking downstream from perforated screens towards the suction pipe of the 1.5" rig, channel width 122 mm.

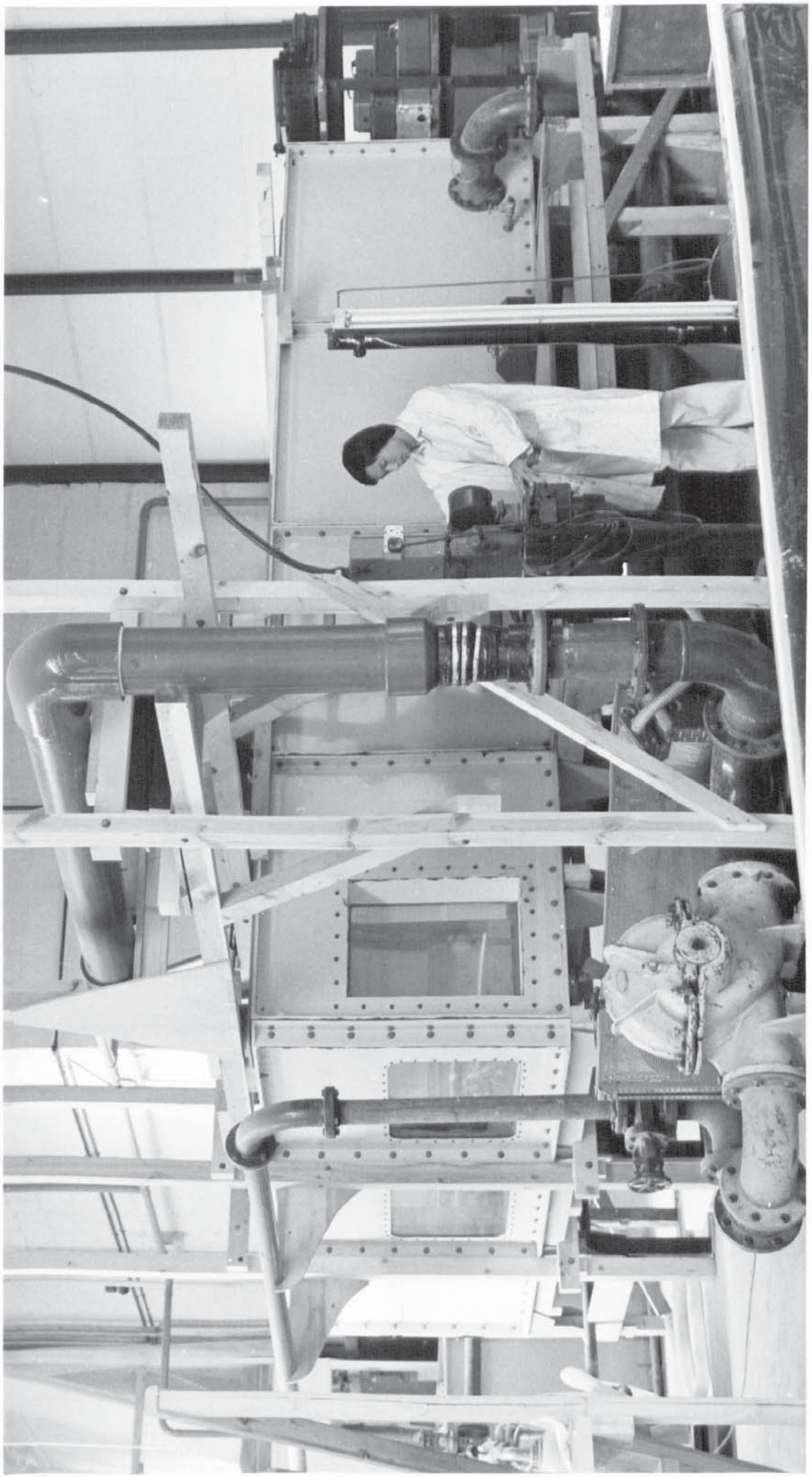

Fig. 5.4 View of 12' x 16' tank containing the 6" rig, together with the 6" radial flow pump, associated pipework and single limb manometer.

Fig. 5.5 View looking downstream of 6" rig approach channel, channel width 488 mm.

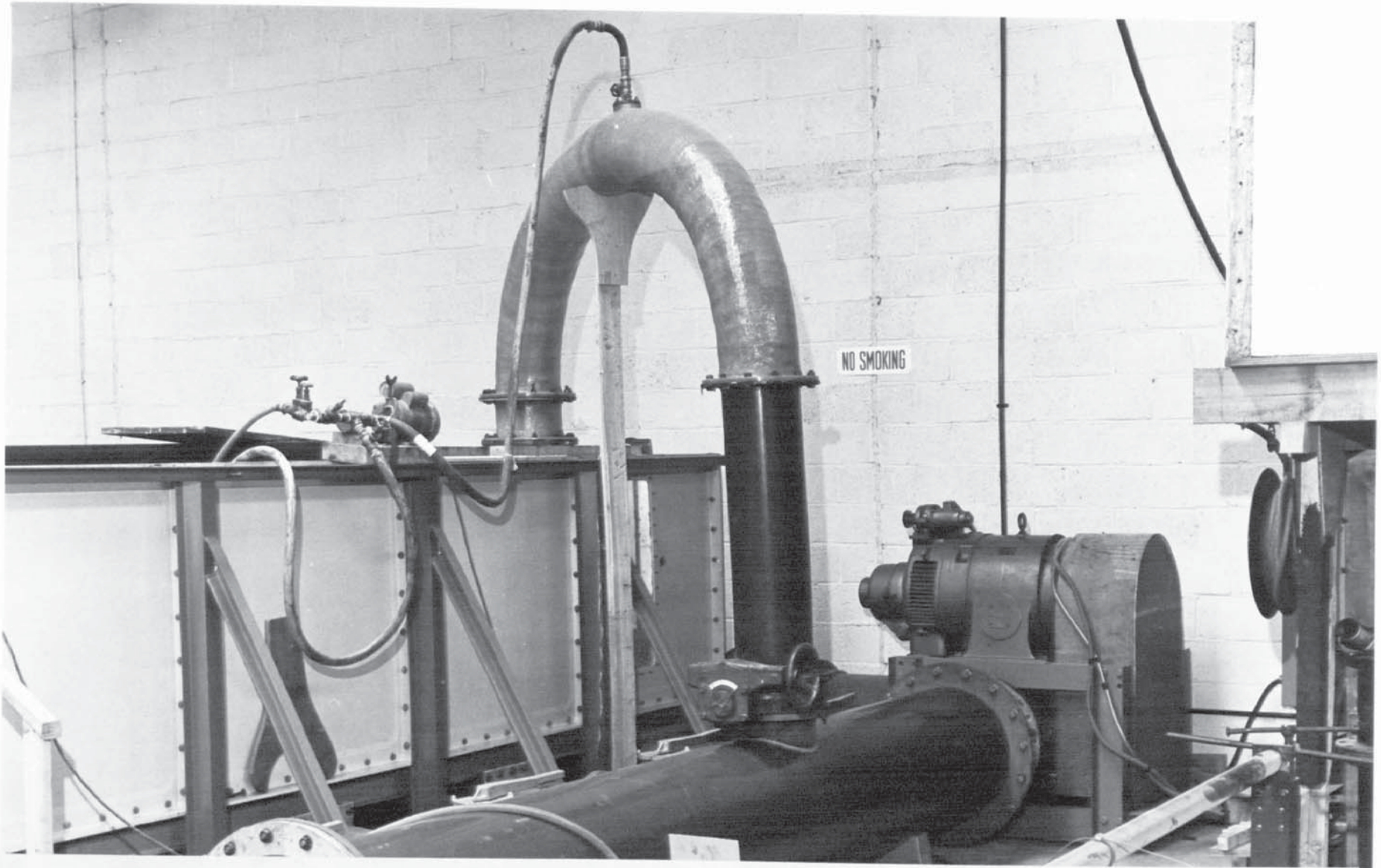

Fig. 5.6 View of the 12" rig from behind the endwall, showing the 180° fibre glass suction bend, of diameter 300 mm, 18" axial flow pump and pump priming system.

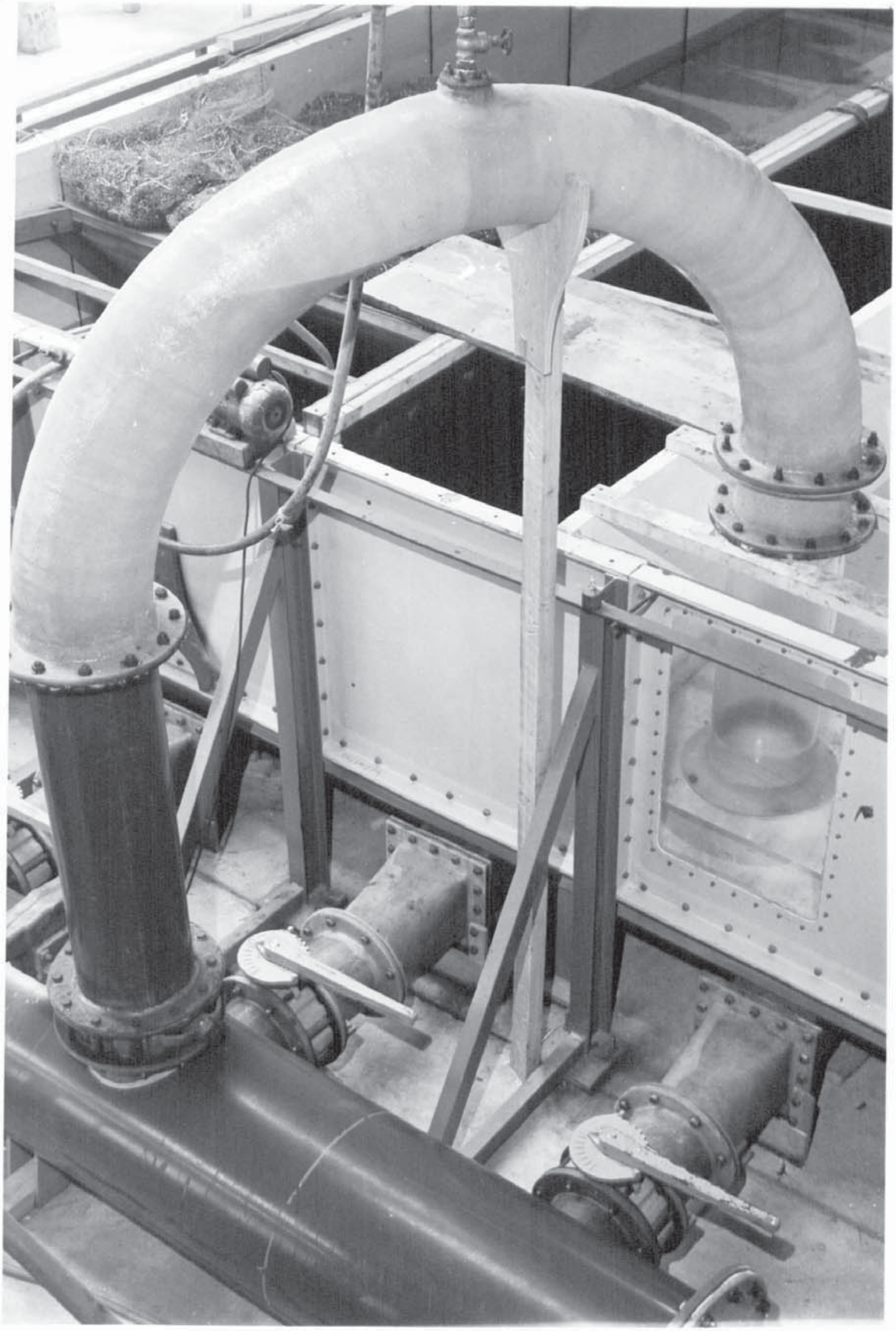

Fig. 5.7 View of the end of the 12" rig approach channel, channel width 976 mm.

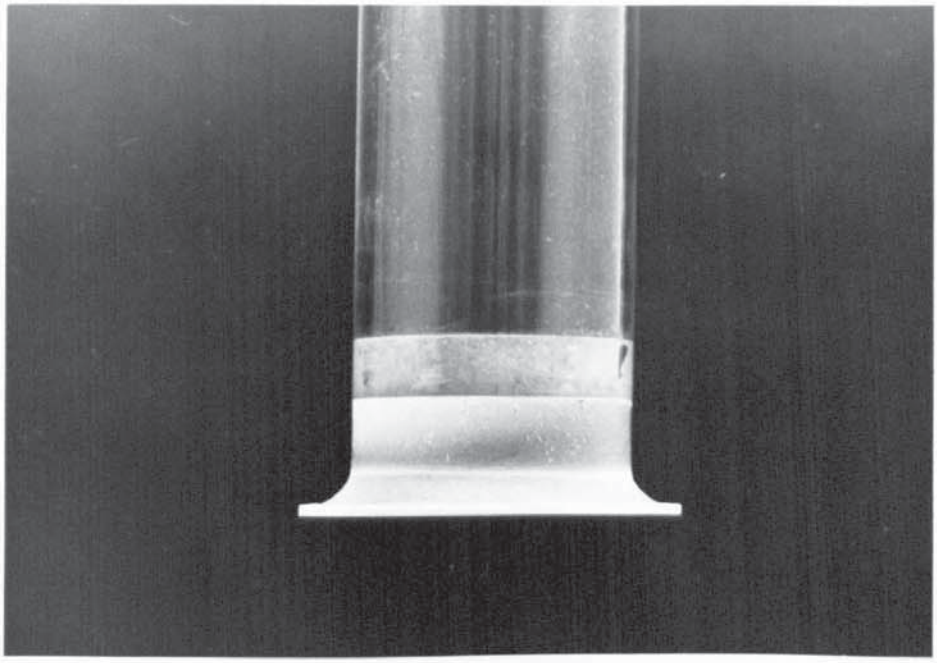

Fig. 5.8 View of the 61 mm diameter bellmouth (1.5" rig).

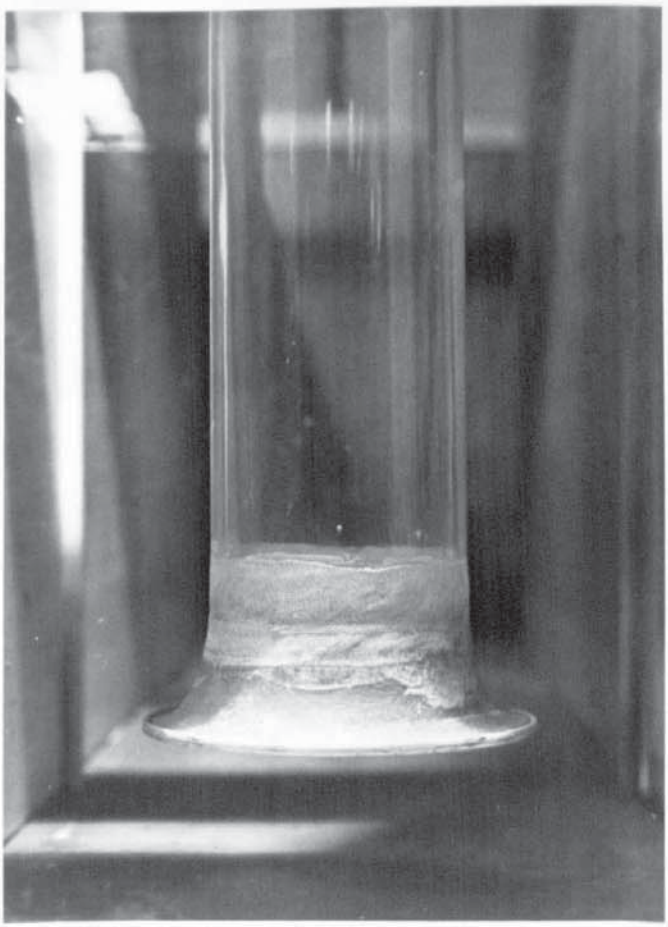

Fig. 5.9 View of the 244 mm diameter bellmouth (6" rig).

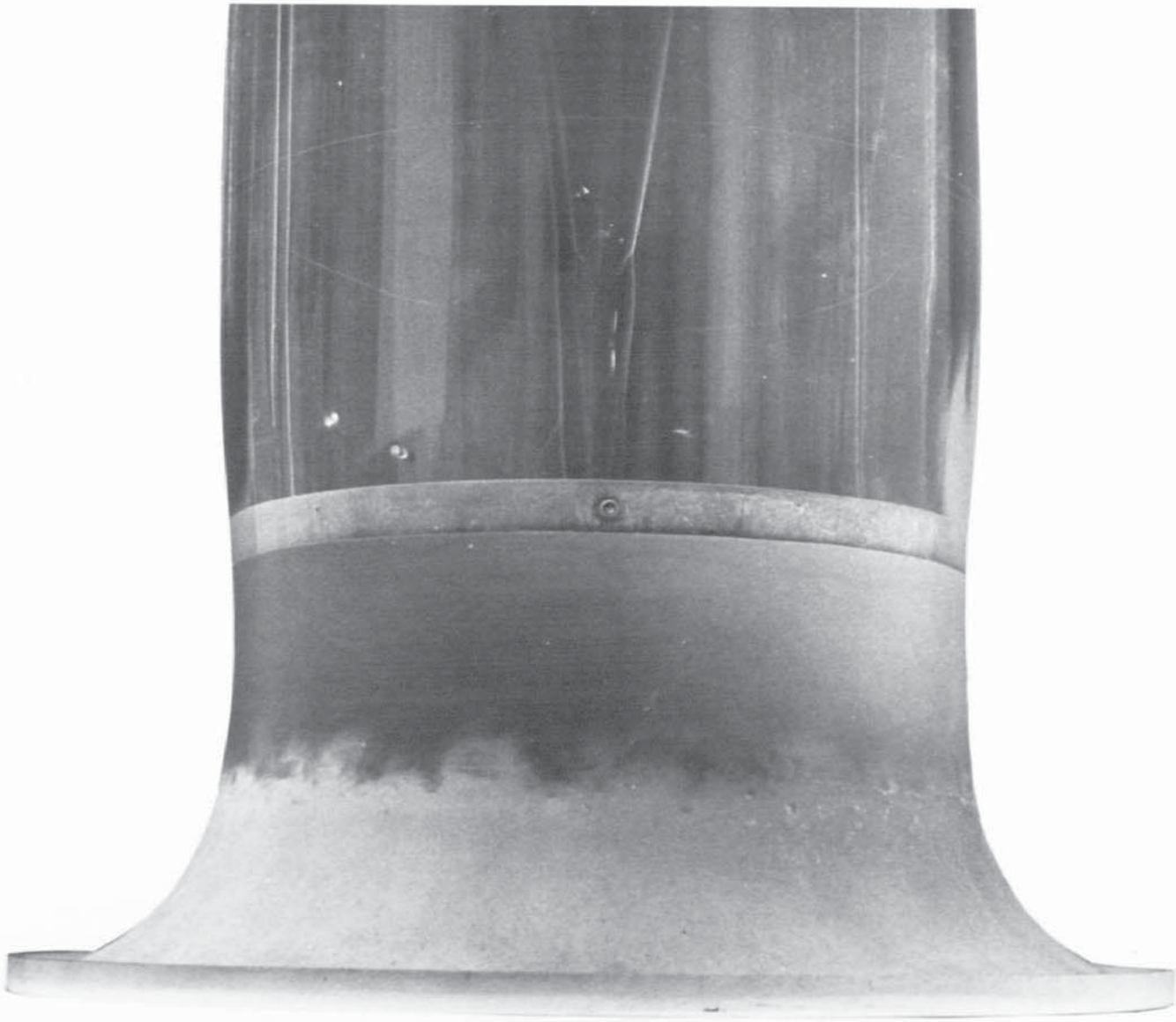

Fig. 5.10 View of the 488 mm diameter bellmouth (12" rig).

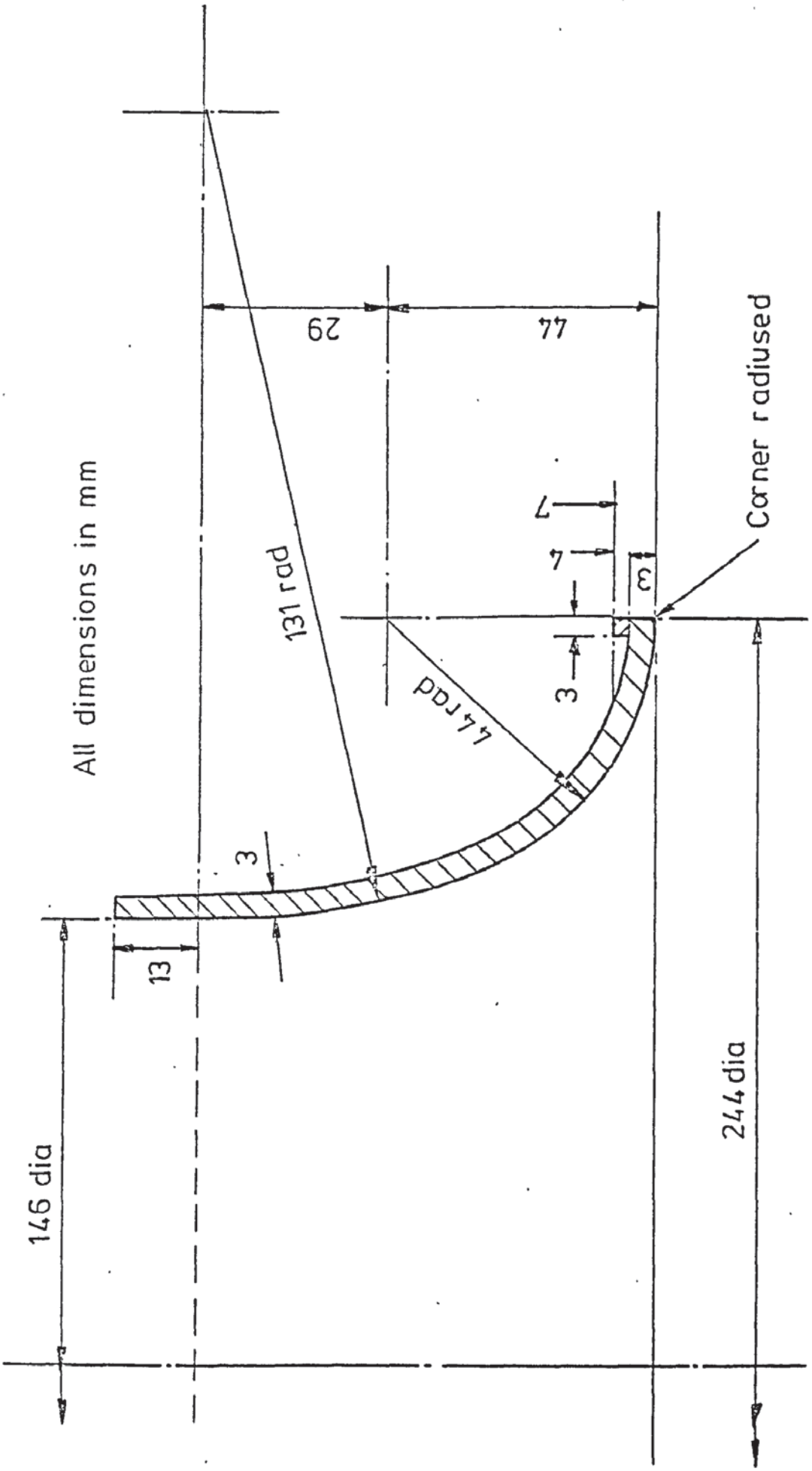

Fig. 5.11 Details of the 244mm diameter bellmouth

Fig. 5.12 **Data on Major Features of the Experimental Rigs.**

	1.5"	3"	6"	12"
D mm	61	122	244	488
d mm	44	85	160	337
Pump	3" radial flow	6" radial flow	6" radial flow	18" axial flow running in reverse
Flow measurement	Rotameter	Orifice plate, corner tappings, area ratio 0.54	Orifice plate, corner tappings, area ratio 0.55	Orifice plate, flange tappings, area ratio 0.63
Manometer Fluid	-	Water	Tetrabromo-ethane (Rel. density 2.96)	Water
Range of V_D tested m/s	0.2 to 1.6	0.2 to 1.6	0.2 to 1.2	0.2 to 1.3
Range of V_d tested m/s	0.5 to 4.1	0.5 to 4.1	0.5 to 3.3	0.5 to 3.4
Range of Q tested m^3/hr	2.1 to 16.8	8.4 to 67	34 to 202	134 to 875
Range of $R_D = \frac{V_D D}{\nu}$	1.1 to 8.9 x 10^4	2.2 to 18 x 10^4	4.4 to 27 x 10^4	8.9 to 58 x 10^4
Max. H/D available	3.8	3.6	3.8	2.1

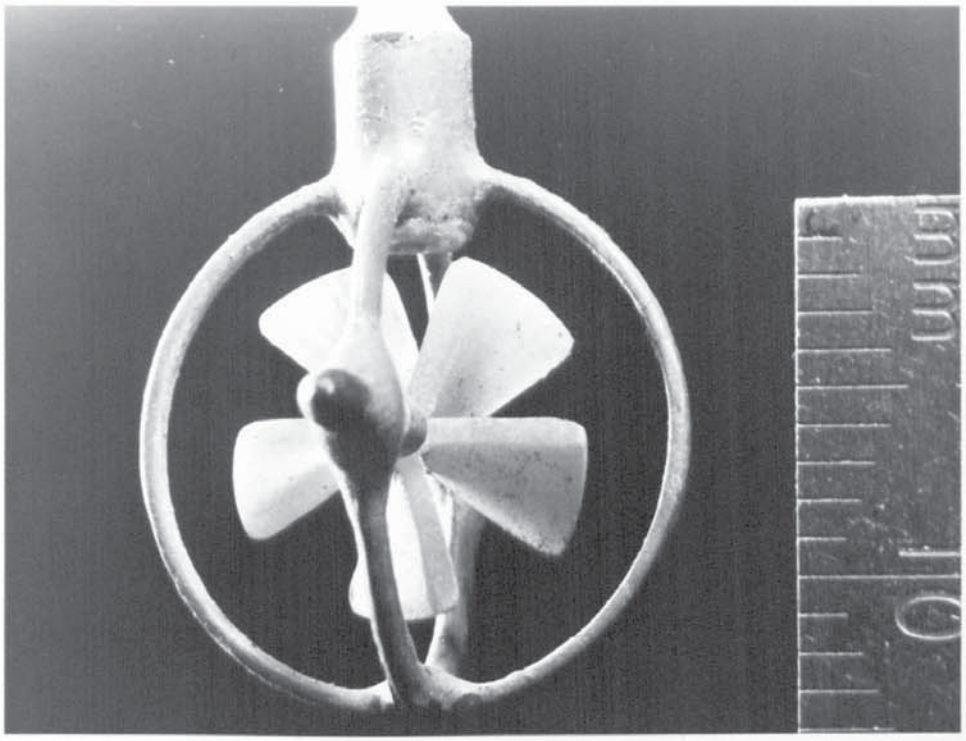

Fig. 5.13 Miniature propeller meter used in flow measurement

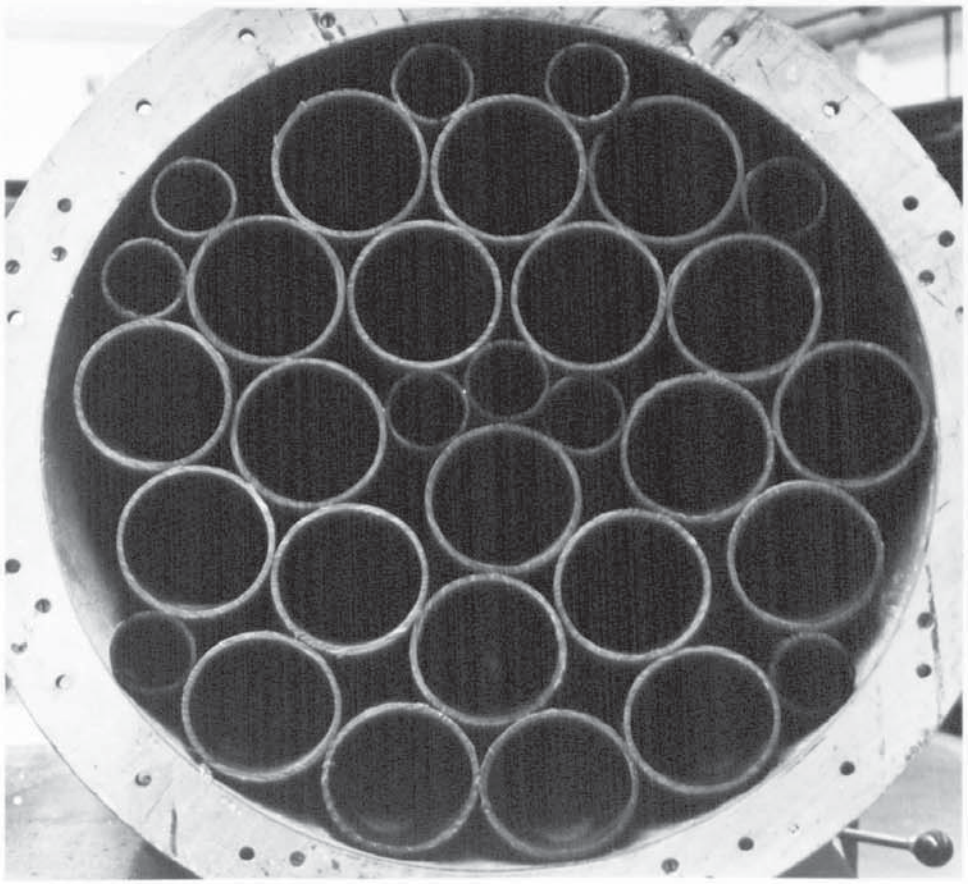

Fig. 5.14 'Tube-bundle' flow straightener installed in the 500 mm discharge pipe of the 12" rig, 8 pipe diameters upstream of the orifice plate to eliminate swirl from the pump propeller.

Notes on symbols used in Fig. 5.15

a) **surface vortices** - classification into types 1 to 4 is explained in 6.2.3 and Fig. 6.9

- O indicates no surface vortex seen.

- subscript 's' indicates a stable vortex lasting for 5 secs or more (model time).

- parentheses () indicate sporadic vortices, occurring only once in 5 mins. say.

- where a vortex seemed to alternate between two different types, both types, separated by an oblique stroke, were recorded.

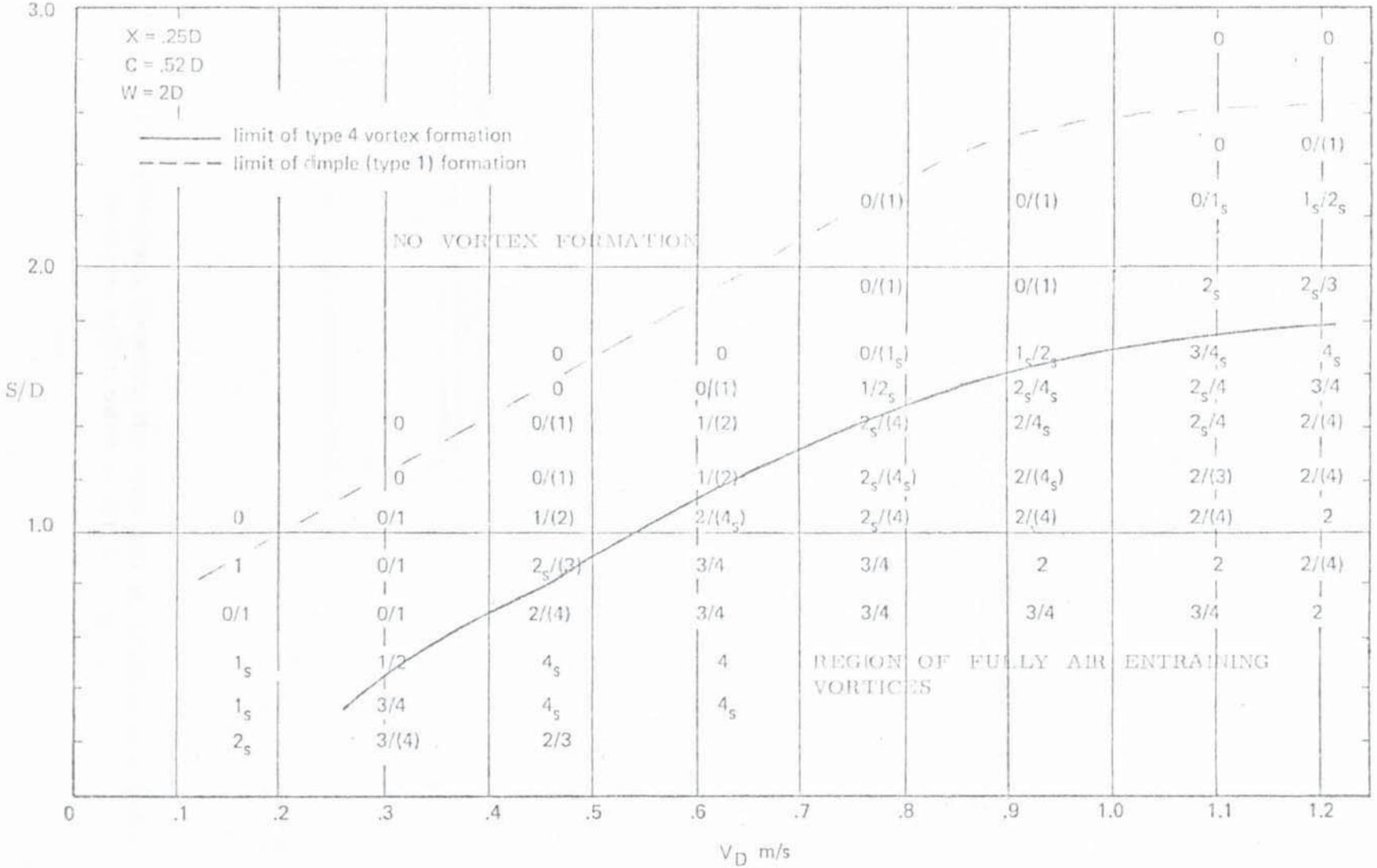

Fig. 5.15 Full plot of vortex types at various values of submergence S/D and bellmouth velocity V_D for the 6" rig, with backwall clearance X/D = 0.25, floor clearance C/D = 0.52 and width W/D = 2, (see opposite for notes on notation.) Dotted line curve divides no-vortex region from vortex region, whilst bold curve divides region of fully air-entraining vortices from less severe vortex types.

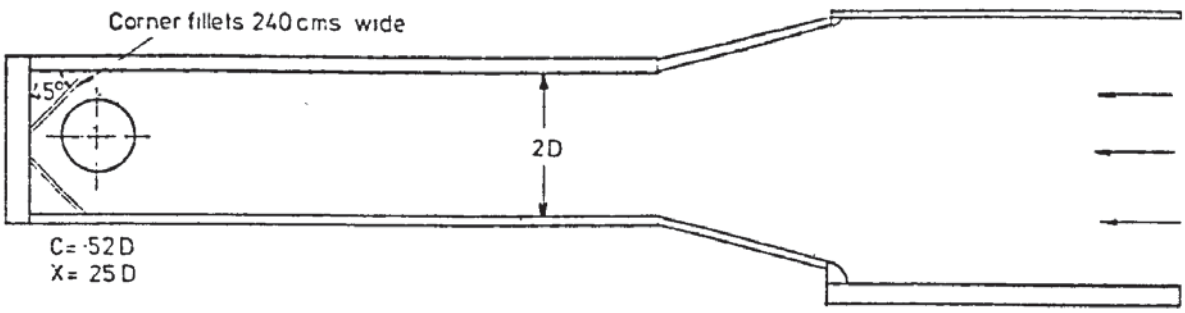

Fig. 5.16 Diagram showing the size and location of corner fillets used in the 6" rig.

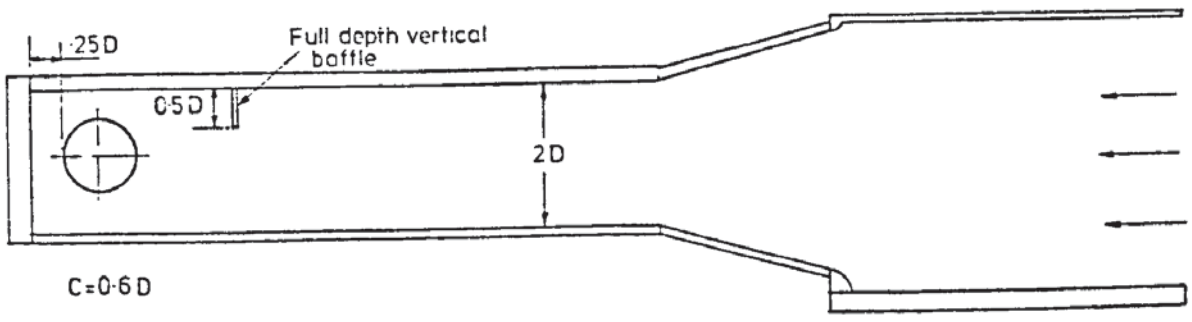

Fig. 5.17 Diagram showing the size and location of the solid upstream baffle used in the 6" rig.

CHAPTER 6

RESULTS, ANALYSIS AND DISCUSSION

6.1 Summary

This chapter gives details of the experimental results obtained from the four rigs, sizes 12", 6", 3" and 1.5". The first section describes the flow patterns near the bellmouth. The second section then gives experimental results from the 6" rig describing the effect of various sidewall and floor clearances, corner fillets and baffles on critical submergence, S_c. Values of bounding submergence S_B are inferred and compared with the theoretical predictions. The results are also discussed from the point of view of optimum sump design to ensure satisfactory hydraulic performance at minimum cost. The results generally confirm the recommendations of ref. 1 which was published during the course of experimental tests.

The third section covers the work done in relation to the final aim of the project, i.e. the derivation of satisfactory scaling laws for predicting the occurrence of free surface vortices by means of scale models. The degree of correlation with the theoretical considerations of section 3.6 is also discussed. The results suggest that the scaling laws vary with scale ratio s and submergence, S_c/D. For the range of sizes tested, it is deduced that the model velocity has to be several times Froude scale velocity.

6.2 General description of flow behaviour near the bellmouth

6.2.1 Uniformity of approach flow

The approach flow velocity distribution was checked on all the rigs

for a particular sump geometry (C/D = 0.6, X/D = 0.25, W/D = 2) and with similar mean channel velocities at a plane 3D from the endwall. Non-dimensionalised velocity contours are shown in Figs. 6.1 to 6.4. The channel width and depth was 2D in each case (500mm or 2.05D for the 6" rig).

The velocity distribution was very uniform across the whole width and depth of the channel for all the rigs. A typical profile for each contour plot is shown in Fig. 6.5, taken at a depth of 1.2D below the free surface.

These plots should be compared with the case when a $\frac{1}{2}$D baffle was inserted 6D from the endwall, Fig. 6.6. Here, a significant region of reverse flow exists and there are correspondingly higher velocities in the forward direction. Consequently, the velocity profile shows a marked asymmetry and this subsequently affects the variation of critical submergence with bellmouth velocity when compared with the "no baffle" case (see 6.3.4).

6.2.2 Flow patterns near the bellmouth

The flow patterns near the bellmouth are complex due to the three-dimensional nature of the flow in this region. There is only one plane of symmetry, that which bisects the channel along its length. Thus, in general, flow approaching the bellmouth in one half of the channel stays in that half right up to the time that it enters the bellmouth. However, any slight asymmetry or perturbation in the approach flow can produce asymmetric conditions at the intake. Any rotation which appears, however slight, affects the flow field such that the asymmetry is accentuated. This, together with the fact that the bellmouth may draw fluid preferentially from one direction, favours the rapid formation of vortices in one half only.

An analogy can be drawn with the situation where a stationary ball is placed at the top of a convex surface. This is a state of unstable equilibrium, whereby any small perturbation in any direction causes the ball to roll down the surface with ever-increasing velocity.

Fig. 6.7 attempts to show instantaneous pathlines of the flow at various positions across the channel width in the main body of the fluid for a channel depth of 2.1D, channel velocity, V_W = 0.4m/s (C/D = 0.6, X/D = 0.25, W/D = 2). These were obtained by injecting small quantities of dye (potassium permanganate solution) into the flow and observing the subsequent paths of the dye. The flow was unsteady in the bellmouth region, but the figures are representative of the flow patterns near the bellmouth.

In conclusion, it can be seen that various points of separation exist on the suction pipe, at the sidewalls, the endwall and the floor. At these points, boundary layer fluid leaves a boundary surface and is eventually drawn into the bellmouth. The boundary layer fluid which separates from the suction pipe travels downstream and entrains fluid from the main flow, thus forming a wake region behind the pipe. This process is further aided by the presence of the endwall which serves to deflect the oncoming flow towards this wake and hence into the intake. Thus the continual inflow of rotational, and hence vorticity-bearing fluid into this region seems to be the main mechanism for vortex development in this particular sump geometry. These observations agree with the theoretical predictions of Chapter 3. Fig. 6.8 shows in diagrammatic form the various flow regions near the bellmouth.

6.2.3 Description of vortex development

The development of an air-entraining vortex is described in Fig. 6.9 where the submergence, S/D, is gradually decreased with bellmouth velocity, V_D, constant. Figs. 6.10 to 6.13 are photos of a similar development process from types 1 to 4 for the 1.5" rig, but with a constant submergence of 0.8D and V_D increasing from 0.52m/s to 1.42m/s. The development process is by no means continuous. The position of the vortex, the time taken for it to develop and to collapse are all erratic, so the figures give only a static view of the whole process.

In general, vortices tended to form on prediminantly one side, sometimes changing to the other at lower submergences. At even lower submergences of about 0.5D and below, two vortices were often formed with opposite directions of rotation. The sense of rotation was always consistent with that expected from the common phenomenon of vortex shedding from a circular cylinder, so this seems to be the major source of vorticity as expected from the theoretical considerations in 3.4.4. Also, it was observed that in this range of low submergence, the position of the vortices moved from their location behind the suction pipe to points further upstream on either side of the pipe.

Mass rotation and submerged vortices were present at submergence values S/D of less than 0.4, and an example of this is shown in Fig. 6.14. This seems to be a flow regime quite distinct from types 1 to 4, and certainly vorticity from the suction pipe can no longer be a major contribution. Vortex formation at these low levels was not studied in detail since this situation is of little practical interest. However, it should be noted that with bad approach conditions, submerged vortices can occur at higher S/D values, and would then give rise to noise and vibration in the pump.

The types of vortices which were observed to form for a given submergence S/D and bellmouth velocity V_D, have been plotted with S/D along the vertical axis and V_D on the horizontal axis (see Fig. 5.15). Curves were then drawn separating the type 4 (fully air-entraining) vortex region below the curve from the other less severe types which occur in the region above the curves, hereinafter called the S_c/D-V_D curves (see Fig. 6.16, for example, which shows S_c/D-V_D curves for various values of floor clearance, C/D).

The general form of the S_c/D-V_D curves is in line with those obtained by previous authors. Extrapolation of the curves at the low submergence end suggests the existence of a threshold velocity which must be exceeded before air-entrainment, probably through surface drawdown rather than surface vortex formation, can occur. This is because surface tension has to be overcome first. At the high submergence end the curves flatten out showing that S_c/D has little dependence on V_D in this flow region. The curves tend to an asymptotic value of S_c/D which Swainston has called the bounding submergence S_B/D. The velocity at which this value of S_B/D is reached varies considerably. Detailed data for S_B/D has now been obtained for various geometries (Figs. 6.15 and 6.29) and these are discussed further in 6.3.2.

6.3 Effect of changes in sump geometry

6.3.1 Effect of changes in floor clearance C/D, endwall clearance X/D and width W/D

In this section, the results of changes in C/D, X/D and W/D are discussed one by one, from the point of view of the origin of vorticity and the growth of vortices. Their application to sump design is discussed later in 6.3.5. The comprehensive results were obtained from observations on

the 6" rig. Fig. 6.15 shows the various conditions tested, together with estimated values of bounding submergences, S_B/D. The experimental results and curves are given in the following figures :

Fig. 6.16 Variation of S_c/D with C/D (X = 0.25D, W = 2D)

Fig. 6.17 Variation of S_c/D with C/D (X = 0.5D, W = 2D)

Fig. 6.18 Variation of S_c/D and H_c/D with C/D at selected V_D values (X = 0.25D, W = 2D)

Fig. 6.19 Variation of S_c/D and H_c/D with C/D at selected V_D values (X = 0.5D, W = 2D)

Fig. 6.20 Variation of S_c/D with X/D (C = 0.5D, W = 2D)

Fig. 6.21 Variation of S_c/D with X/D at selected V_D values (C = 0.5D, W = 2D)

Fig. 6.22 Variation of S_c/D with W/D (X = 0.25D, C = 0.5D)

The effect of changing only the floor clearance, C/D is shown in Figs. 6.16 to 6.18. First of all it can be seen that for any given value of C/D, the value of critical submergence increases gradually with bellmouth velocity V_D. Secondly, as C/D is increased from 0.2D to 0.6D, there is a large drop in critical submergence, S_c/D, for any given value of V_D, followed by a small rise as C/D is increased further from 0.6D to 0.8D. This trend of a minimum in S_c/D has been observed by one other author (see Fig. 4.12). Furthermore, the value of total depth H_c (= $S_c/D + C/D$) is relatively constant over the range of floor clearance, C/D, considered, with a small increase for C/D greater than 0.6D. The latter trend is in agreement with the results of previous work shown in Fig. 4.12.

In order to explain the form of the curves, it is necessary to compare the variation in the amount of vorticity generated with the amount of vorticity required to produce a fully-air-entraining vortex. The general

rising form of the curves, shown for example in Fig. 6.16, is expected from the theoretical considerations of 3.4. There, it was suggested that as submergence increases, the amount of vorticity required to produce air-entrainment also increases. This extra vorticity can only be generated by increasing the flow past the suction pipe, i.e. by increasing the channel velocity V_W and hence V_D also. The fact that V_W and V_D do increase with critical submergence is shown in Appendix B.

The reason why the curves do not increase indefinitely with bellmouth velocity V_D, is probably related to the correlation length of the vortices shed by the pipe, as discussed in 3.4. Above a certain submergence, the vorticity generated is not sufficiently organised over a sufficient depth of water to form an air-cored vortex, irrespective of how high V_D is, and so this gives rise to the existence of a bounding submergence, S_B/D.

In considering the variation of the critical submergence with floor clearance, it can be seen from Fig. 6.18 that for a given bellmouth velocity, S_c/D decreases in the range of C/D up to 0.6 after which it increases. The initial decrease means that there is less vorticity required and hence less vorticity generated, so that a type 4 vortex does not form until lower values of submergence. However, it can also be seen that the critical depth is fairly constant for C/D up to 0.6, which means that for a given V_D, V_W is also fairly constant, and hence the vorticity generated by the pipe is constant. Yet there is less total vorticity generated, as stated earlier. One explanation for this is that there is another source of vorticity present which decreases in magnitude as the floor clearance is increased. This other source is probably the boundary layer developed along the sump floor, so that as the suction pipe is raised further and further from the sump floor, the contribution of this sump floor boundary layer to the total vorti-

city generated becomes smaller and smaller.

There comes a point, however, when, as S/D decreases, the total vorticity generated is greater than is required to overcome the static head and hence form a type 4 vortex. This point is reached at about C/D = 0.6, above which the critical submergence increases. This has the dual effect of both increasing the vorticity required for air-entrainment as well as decreasing the channel velocity and hence the vorticity generated, so that the vorticity required again balances the vorticity generated.

The variation of critical submergence, S_c/D with endwall clearance, X/D, (Figs. 6.20 and 6.21) does not show such a consistent trend, and the spread in S_c/D values is not as great as for the range of floor clearance, C/D, values tested. This shows that air-entraining vortex formation is less sensitive to changes in X compared with changes in C. X/D = 0 gives the lowest values of S_c/D over a wide range of suction velocities, and shows the importance of the endwall in suppressing air entrainment by a) providing a solid boundary which retards and often completely stops any rotational motion which might develop and b) disrupting the formation of a wake region behind the pipe so that vortices do not have either time or space to grow. It would be reasonable to assume, then, that as the endwall clearance, X/D was increased, type 4 vortices would form more readily, i.e. that S_c/D would increase. This trend was followed experimentally for values of V_D less than 0.5m/s (Fig. 6.20) but above this velocity, the curves cross each other so that S_c/D is less for X/D = 0.5 and 0.75 than for 0.25. This occurred because with the higher bellmouth velocities as well as X/D values, there was sufficient space behind the suction pipe for incipient vortices to be washed downstream away from the immediate vicinity of the bellmouth, thus preventing the development of a

fully air-entraining core.

When the channel width increased from 2D to 4D, there was a marked drop in S_c/D (Fig. 6.22). As the width is increased the sidewall boundary layers have less and less influence and so there is less vorticity opposing that developed by the pipe. It might be expected, then, that S_c/D values should be higher as W/D increased. However, increasing the width also decreases the value of V_W for a given V_D, and hence decreases the amount of vorticity generated by the suction pipe. Thus, type 4 vortices form at lower levels of S_c/D as the width increases, so that V_W and hence vorticity generation is high enough to produce air entrainment.

To sum up, then, the critical submergence is dependent on floor clearance, C/D, endwall clearance, X/D, and channel width, W/D. In discussing the experimental results from the 6" rig, the importance of the suction pipe as a source of vorticity has been shown, with the sump floor playing a subsidiary role when C/D is varied. In each case, a type 4 vortex will form when the total vorticity generated equals the vorticity required to produce air entrainment at the particular value of submergence in question. Consideration of these two quantities of vorticity has led to an explanation of the form of the experimental results. Furthermore, it would be expected that the so-called dry-well arrangement shown below where the intake does not obstruct the flow would lead to reduced vorticity and hence less vortex activity. The incidence of surface vortex formation in such a configuration is an area of intake design requiring further study.

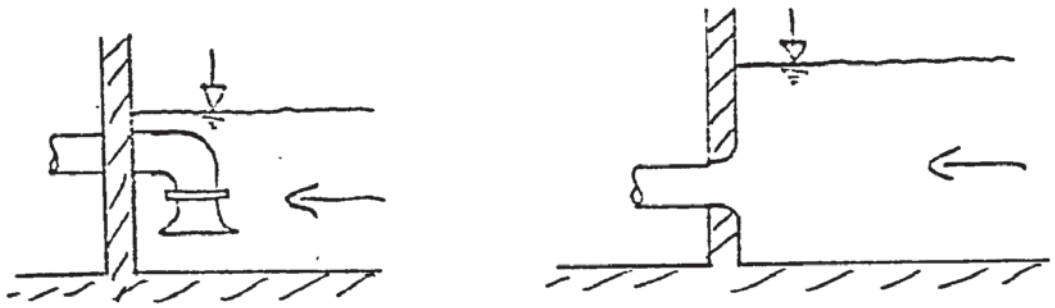

Sketch of two possible dry well arrangements

6.3.2 Dependence of bounding submergence, S_B, on geometric parameters

Swainston (3b) obtained the variation of S_B with geometric parameters from his mathematical model. He chose to non-dimensionalise the parameters by the absolute value of endwall clearance, X, rather than d or D, since he "considered the pipe diameter has a relatively small effect on the flow pattern within the sump." This is true when the pipe diameter is small relative to the sump dimensions so that the effect of the suction pipe can be represented mathematically by a point sink. However, it has been found that this is not applicable to the rigs used in this research project since the sump boundaries are relatively close to the bellmouth intake.

Values of S_B/D and S_B/X have been estimated by extrapolating the S_c/D—V_D curves in Figs. 6.16, 6.17, 6.20 and 6.22, and there is consequently a large element of error due to this subjective procedure. These values are given in Fig. 6.15 and plotted in Fig. 6.23 for comparison with Swainston's graph. It can be seen that there is very little similarity between the two, with values of S_B/X several times higher than Swainston's. This implies higher values of S_C which could arise from the large contribution to the vorticity from the suction pipe, which is not considered in

Swainston's model. Furthermore, the curves show a decrease in S_B/X with C/X which agrees with Denny's experimental results, but not with Swainston's predicted results. However, in the case of W = 4D where the influence of pipe size should be smallest, the experimental results do follow the trend of Swainston's curves and show an increase in S_B/X with C/X, though absolute values of S_B/X do not agree.

Thus the general conclusion from the limited number of results available is that there is qualitative agreement between theory and experiment provided W/D is at least equal to 4. However, for values less than this, the influence of the flow past the suction pipe as a source of vorticity renders the mathematical model inapplicable for this particular sump geometry.

6.3.3 Effect of corner fillets

Two 45° corner fillets were fitted for one geometry on the 6" rig (see Fig. 5.16) and the effect on S_c/D is shown in Fig. 6.24. There is a significant decrease in S_c/D, especially at higher values of V_D. The usual explanation for this is that the corner regions are regions of relatively stagnant fluid where the main flow has separated from the wall when turning through 90°. This is then a prime site for the development of vortices, and so, by filling in this stagnant zone there should be less likelihood of vortices. However, the corner vortices that have actually been observed appear to be very weak and too far away from the intake to entrain air. Thus, this explanation fails to consider the strong vortices formed in the wake region behind the suction pipe.

A more reasonable explanation for the effectiveness of the fillets in suppressing air-entrainment is that the relatively large corner fillets dis-

rupt the wake formation behind the suction pipe so that the normal, undisturbed vortex development is hindered. This disruption is aggravated by the de-stabilising effect of the higher local velocities behind the pipe which results from the more restricted space available for the flow. Thus, these two effects together inhibit the organisation of the vortex generated so that air-entraining vortices do not form until lower submergences, where less vorticity is required to cause air-entrainment.

6.3.4 Effect of $\frac{1}{2}$D baffle

All the experiments described above were carried out with a uniform approach velocity distribution across the width of the channel, so that there were no obvious physical sources of vorticity apart from the straight boundary walls. However, one set of tests was done on three of the rigs with a $\frac{1}{2}$D ($\frac{1}{4}$ channel width) baffle placed at right angles to the flow direction (see Fig. 5.17). For the 6" rig this was placed at various distances from the endwall, and the effect on S_c/D is shown in Fig. 6.25. The results from all the three rigs are compared in 6.4.3.

The separation of the flow downstream of the baffle provided an obvious source of organised vorticity, and created a distorted approach velocity distribution, with higher velocity fluid in that half of the channel not containing the baffle, and slower moving fluid with flow reversal directly downstream of the baffle (see Fig. 6.6 for velocity profiles). For a given value of V_D, type 4 vortices occurred at greater depths as the baffle was moved closer to the intake. This shows the increasing contribution made by the baffle to the total vorticity. However, the effect of the baffle was attenuated by the turbulence it created and also by the strong, submerged vortices which continuously removed incoming vorticity, so that the increase

in S_c/D is not as great as might be expected. For example, when the baffle was 3D from the endwall, the increase in S_c/D over the no baffle case was from 1.6D to 1.8D at V_D = 1.2 m/s. The measurement of the turbulence produced and its effect on S_c/D was outside the scope of this project. However, the results show that the protruding baffle was a very effective source of vorticity.

6.3.5 Relevance to sump design

The design of any pump sump should ensure steady, uniform approach flow to each pump intake. This is especially true for high specific speed axial flow pumps which are particularly sensitive to undesirable flow phenomena such as air entrainment, submerged vortices and swirl. These can cause significant head losses and a drop in efficiency as well as mechanical damage.

The elimination of surface air entrainment is one important aspect of sump design and depends on a) uniform approach flow conditions; b) correct positioning of the pump intake relative to the sump walls and floor, and c) sufficient submergence of the intake at minimum excavation cost. There is a lot of published literature on b) and c) but this mainly applies to specific schemes. The only comprehensive, published design guides have already been reviewed in 4.3.4. and differences exist amongst these two as well as individual pump manufacturers' design data, as already mentioned earlier. The information gained from the experimental work described above is intended to help sump designers, and is discussed in this section in relation to b) and c), taking floor clearance C/D, endwall clearance X/D and width W/D in turn.

Fig. 6.18 shows that although the value of C/D has a marked effect on S_c/D, the variation in H_c/D, which is more important because it determines the floor level, is not significant except at the higher values of C/D. Thus for minimum excavation cost for a sump, the value of C/D should not be greater than 0.7.

There seems to be no consistent variation of S_c/D with X/D (Fig. 6.21) over the range of velocities tested. A value of X/D = 0 gave the lowest value of S_c/D for bellmouth velocities less than 0.8m/s. However, persistent submerged vortices starting from the endwall just below the bellmouth level also appeared for this configuration and these would be undesirable in a real pump sump. The other disadvantage of zero endwall clearance is the severely restricted access available for maintenance and servicing on site. At the higher end of velocities tested, the optimum value of X/D is 0.75. Thus, the optimum value of endwall clearance , X/D, increases with velocity and this should be borne in mind in sump design.

It can be seen from Fig. 6.22 that a sump width greater than 2D gives decreased S_c/D. This is only a definite advantage if the total sump volume is also decreased to minimise excavation costs. The best way of comparing the required sump volumes for a variety of geometric parameters is to calculate ($W/D \times H_B/D$) which represents the sump volume per unit length of channel. This has been done in the last column of Fig. 6.15, using the estimated values of $S_B/D + C/D$ to give H_B/D. It should be noted that these values have been obtained by extrapolation, and so would only apply for high bellmouth velocities.

From Fig. 6.15 it can be seen that for W/D = 2, X/D = 0.25, the min-

imum sump volume occurs for C/D = 0.5 to 0.6 whilst overall, for the unmodified rectangular channel, the minimum volume occurs for W/D = 2, X/D = 0.75, C/D = 0.5. Thus, from the point of view of minimising sump volume these dimensions would give the optimum sump geometry for a single pump sump. There does not seem to be any advantage in going to widths greater than 2D since the sump volume is then greater. However, minimum excavation costs for a given volume are determined by local ground conditions and it may be cheaper to excavate a wide shallow pit rather than a narrow deep one. There is a constraint, anyway, on the minimum volume desirable. This is because when the sump level changes continually so that the electric motor driving the pump frequently starts up and cuts out, then considerable heat energy is generated in the motor which will not have a chance to dissipate if the sump volume is too small. There is thus a minimum cycle time depending on the pump/motor combination, which puts a lower limit on the sump volume required (see ref. 84 for further details).

Two other aspects of sump design have also been investigated: corner fillets and upstream boundary changes. It was seen in Fig. 6.24 that corner fillets greatly reduced S_c/D and this explains why these are a common feature in sump design. However, their actual size has to be chosen carefully. If they are too small they have little effect whereas if they are too large and hence too close to the intake, they provide surfaces for the development of submerged vortices (72).

The effect of a $\frac{1}{2}$D baffle at various upstream positions gives an indication of the effect of a boundary discontinuity on the occurrence of air entraining vortices. At a distance of 3D from the endwall, the baffle increases S_B/D by 10% whereas at 6D, the increase is only about 3%.

This implies that flow conditions at the intake could be acceptable if there was a length of straight channel of at least 6D before any boundary discontinuity occurred. As this length is reduced, then vortices form at ever-increasing submergences, and also tend to be stronger and more persistent. It should be noted, however, that with such a drastic discontinuity as the solid baffle, swirl and submerged vortex activity inevitably increase.

In conclusion, systematic data on sump design has been obtained for the most important geometric parameters using a single, vertically suspended 244mm bellmouth intake at the end of a long rectangular channel. This configuration was chosen since it is the one most commonly found in both single and multiple pump sumps. Although it has definite economic advantages over the dry well arrangement discussed in 6.3.1, it is not necessarily the best from a purely hydraulic point of view. However, as discussed above, it is possible to improve on the hydraulic performance by correct positioning of the pump intake relative to the sump boundaries, by using corner fillets and by locating upstream disturbances far from the intake.

The main conclusions on optimum sump design are summarised in the table below, and compared with recommendations given in ref. 1. The experimental results generally confirm the design recommendations and show the dependence of some parameters on bellmouth velocity, a factor not considered in (1). The greatest difference arises from an increase in the optimum value of X/D with bellmouth velocity so that a value of 0.75 has been found to be the best at higher bellmouth velocities, compared with the recommended value of 0.25. Values of submergence, and hence depth, also vary with V_D. Bounding submergence values are

mostly greater than 1.5D, so this should be taken as the minimum to allow for in a rectangular sump. The configuration which gave the lowest overall sump volume was W/D = 2, X/D = 0.75 and C/D = 0.5

Geometric Parameter		Ref. 1	Conclusions from experimental results
Floor clearance	C/D	$\frac{1}{2}$ to $\frac{3}{4}$	less than 0.7 to minimise sump depth
Endwall clearance	X/D	$\simeq \frac{1}{4}$	up to 0.75, depending on bellmouth velocity
Width	W/D	2 to 3	2 to 4 depending on excavation costs
Approach channel length	L/D	at least 4	at least 6 for an upstream solid baffle
Submergence	S/D	at least 1.5	at least 1.5 for W = 2D, depending on bellmouth velocity.
Total sump depth	H/D	at least 2	at least 2.1 for W = 2D, depending on C/D

6.4 Comparison of results from the different size rigs

6.4.1 General description of the form of the results

Results from all four rigs were obtained for a restricted range of geometries, i.e. W/D = 2.0, X/D = 0.25, with floor clearance, C/D = 0.4, 0.6 and 0.8. It was considered that the full set of S_c/D - V_D curves for these would give sufficient data for analysis. Also, in the case of C/D = 0.6, a test with a $\frac{1}{2}$D baffle was done on the 12", 6" and 1.5" rigs to look at the scaling of this kind of vorticity generation, and the results discussed in 6.4.3.

Figs. 6.26 to 6.28 show the three sets of curves for C/D = 0.4, 0.6 and 0.8 respectively. For C/D = 0.4, there is a large separation

between the 12" and the 6" results and the 3" and 1.5" results. For C/D = 0.6, there is crossing and re-crossing of the curves, whereas with C/D = 0.8, the curves only cross below $S_c/D = 0.9$ and there is no longer any order in the relative positions of the curves, with the 6" lying above the 12" curve and the 3" and 1.5" lying below the 12". As a consequence of this, it can be seen that the value of S_B/D is different for each size, and Fig. 6.29 gives estimates of S_B/D obtained by extrapolation. It can also be seen that the threshold velocity at zero submergence varies both with geometry and size.

The following sections describe the analysis of these results in an attempt to derive general scaling laws for free surface vortices. The methods used follow those proposed in 3.6, treating the 12" size as the "prototype" from which to take values of V_p.

6.4.2 Analysis of results

Applying the extended principle of similarity (section 3.6.2), graphs of log S_c/D against log V_D at constant D were drawn as shown in Fig. 6.30 for C/D = 0.4. For any particular size of D, a straight line could be drawn through the points, but the gradient of this line varies both with D and C/D. Furthermore, the second graph necessary to find x and y, i.e. log S_c/D against log D at constant V_D does not produce a straight line for all values of V_D but curves instead. Fig. 6.31 shows a typical set of curves for C/D = 0.4 and various values of V_D together with values of S_B/D which apply at large values of V_D. This method was therefore not pursued further, and the implication is that the scaling law is not simply a function of the product of powers of the Froude and Reynolds numbers.

The analysis of section 3.6.4 based on the new consistent combination law was then applied to the experimental results. For a particular value of C/D and S_c/D, the corresponding values of bellmouth velocity for each size rig were taken to give values of V_6/V_{12}, V_3/V_{12} and $V_{1.5}/V_{12}$, corresponding to $f(\frac{1}{2})$, $f(\frac{1}{4})$ and $f(\frac{1}{8})$ respectively. Detailed results for these are tabulated in Fig. 6.32.

Some interesting features arise from this. Firstly, it can be seen that for a given geometry and scale ratio, s, the value of f(s) is not constant, but generally increases with submergence. This trend agrees with recent work reported in ref. 75. Various alternative forms of plotting the results were tried, but it was not possible to obtain constant values of f(s) over the range of S/D and V_D tested.

Secondly, the value of f(s) also varies with C/D. These two points are illustrated by the graph in Fig. 6.33 for $s = \frac{1}{4}$. This dependence on S/D and C/D is not entirely unexpected (see 6.3.1) but is something which is not taken account of in practice. It is important to note, therefore, that a scaling law used for a particular hydraulic model could vary according to the submergence or floor clearance in the intake design.

In order to obtain the variation of the Froude scale multiplying factor k, with scale ratio, it is first necessary to consider a particular value of C/D and S_c/D. This is shown in Fig. 6.34 for various C/D and S_c/D values with 1/s along the abscissa. The curves have been drawn to pass through the point (1,1). The rising trend agrees with the theory of 3.6.5. However, as can be seen from the detailed results in Fig. 6.32, the f(s) and k values do not correspond to a single value of b.

In other words, what has been obtained in Fig. 6.34 is the value of

k and hence scaling factor for a range of C/D and S/D over a scale range from 1 : 2 to 1 : 8, based on a 12" prototype. These should have direct application in operating models of rectangular pump sumps in this size range. The curves seem to flatten out as 1/s increases to give an asymptotic k value for small size models, but further work with larger models as the prototype would be needed to confirm this. Furthermore, it seems that more analysis along the lines suggested in 3.6.4 will not lead to a unique value of b and hence to a generally applicable scaling law which depends on scale ratio only. The possible reasons for this are discussed below in 6.4.3.

A slightly different approach to give scaling laws for a limited range of conditions has also been tried by first 'removing' the variation of f(s) with S_c/D. This was done by using a corrected velocity instead of actual velocities in the velocity ratio V_m/V_p, a method suggested by the different values of threshold velocity for the different size rigs, as seen in Figs. 6.26 to 6.28.

Thus, if the velocities for a particular rig are corrected by an amount v related in physical terms to the value of the threshold velocity, then, although V_m/V_p is not constant for a given C/D, it may be possible to make

$$\frac{V_m - v}{V_p - v} = \text{constant} = B$$

by finding a suitable value of v. This can be done by re-arranging the above equation :

$$\frac{V_m}{V_p} = B - \frac{v(B - 1)}{V_p}$$

If now a graph of V_m/V_p against $1/V_p$ is plotted, then the intercept on the abscissa gives the value of the constant B and the gradient gives the required value of v.

This procedure has been tried for a few representative cases, and the results given in Appendix C. Since the values of B are not constant over a wide range of velocities the laws have only limited use. Furthermore, there is no obvious correlation between the values of v or B from which to extend the laws to other scale ratios, so this method was not pursued further.

6.4.3 Tests with $\frac{1}{2}$D baffles on three rigs

One particular geometry (C/D = 0.6, W/D = 2, X/D = 0.25) was tested with a $\frac{1}{2}$D baffle placed 6D from the endwall for the 12", 6" and 1.5" rigs. The purpose of these tests was to compare the scaling laws for vortices produced by the organised vorticity arising from this kind of boundary discontinuity with the laws derived for the unmodified rectangular channel where the vortices are produced by the separation of vorticity-bearing fluid from the boundary surfaces.

Figs. 6.35 to 6.38 show photographs of flow conditions in the three rigs. Surface vortex formation always occurred on that side to which the baffle was fixed. Although type 4 vortices were obtained on the 1.5" and 6" rigs, no definite air core was formed in the 12" rig. Instead, the tail of a developing vortex would suddenly break into lots of small bubbles, some of which were subsequently entrained. It seems that on the 12" rig, where absolute depths were larger, the baffle did not generate sufficiently high rotational velocities over the whole depth of water to form a coherent air core. This also happened to a lesser extent on the other two rigs.

Fig. 6.39 compares the results from the 1.5" and 6" rigs. There is insufficient overlap between the readings to derive any general scaling law for this particular scale ratio but certainly the velocity ratio values, $V_{1.5}/V_6$, are higher than for the "no baffle" case, having a value of 3.0 for $S_c/D = 0.8$ (compared with 1.5 for the "no baffle" case). This is close to the value of 4 which would be expected for Reynolds number scaling. Thus, because of the different mechanism for vorticity generation, a different value of b and hence scaling law is required for modelling vortex formation caused by upstream boundary discontinuities such as a $\frac{1}{2}$D baffle. On the basis of the limited results available, it is concluded that Reynolds number scaling is appropriate in this case.

6.4.4 Discussion of results from the four rigs

The general form of the S_c/D - V_D curves for the different size rigs shown in Figs. 6.26 to 6.28 does not agree with the requirements of the consistent scaling law discussed in 3.6.5. Although values of k -factor have been obtained whose variation with s agrees with the theory, the variation of b with geometric parameters and scale ratio has led to the rather limited analysis above. Some of the points arising from the analysis are discussed below.

The original assumption that the velocity ratio V_m/V_p was simply a function of s only has been found to be invalid over the range of flow conditions tested. V_m/V_p varies not only with the position of the intake within the sump, but also with the submergence S/D. This variation can be deduced from the results of refs. 67 and 75, and has been discussed in 3.4.4 and 6.3.1 in terms of the origin of vorticity in the flow and the absolute depth of water which a surface vortex has to penetrate. Denny (67)

attributed the form of his results to scale effect, and then went on to propose a scaling law independent of submergence, whereas the scale effect could be interpreted as representing a dependence on submergence.

The curves of S_c/D - V_D do not lie one above the other in order of size. The only consistent trend between the three values of C/D tested seems to be the variation of S_B/D with size, the order of increasing S_B/D being 1.5", 3", 12" and 6". Taking the 12" rig as the prototype, this order is consistent with an increasing k -factor as the scale ratio s decreases. In other words, whilst some of the 6" results are close to once Froude scaling of the 12" rig, the lower positions of the curves for the 3" and 1.5" rigs imply increasing values of k for s = $\frac{1}{4}$ and s = $\frac{1}{8}$ and hence different Reynolds number contributions. Generally speaking, the b values are larger for s = $\frac{1}{4}$ and $\frac{1}{8}$ than for s = $\frac{1}{2}$ (see Fig. 6.32), showing the increasing effect of Reynolds number, and hence viscous effects, as s gets smaller.

It seems, therefore, that the most likely explanation for the larger k values as s decreases is the increasing importance of viscous forces at lower Reynolds numbers. This has the effect of reducing the high rotational velocities needed at a vortex core to produce a type 4 vortex. This, in turn, inhibits the formation of air-cored vortices and progressively depresses the S_c/D - V_D curves. This would give higher values of model velocity, V_m for a given S_c/D for the smaller rigs and hence higher k values, as found from the experimental results. Hence, it is this variation of Reynolds number contribution with size which leads to the discrepancy between the theory (where b was assumed constant) and experiment.

Given the variation of k with scale ratio, it can be seen from Fig. 6.34 that whilst once Froude-scale modelling applies at a scale ratio around 1 : 2, there is increasing deviation from this as the scale ratio decreases to 1 : 8. To see the error that can arise from using a once-Froude scaling law, it is best to consider a specific example. In order to understand this more clearly the figure below shows the S_c/D - V_D curves for the 12" prototype and for a model, in this case the 3" rig.

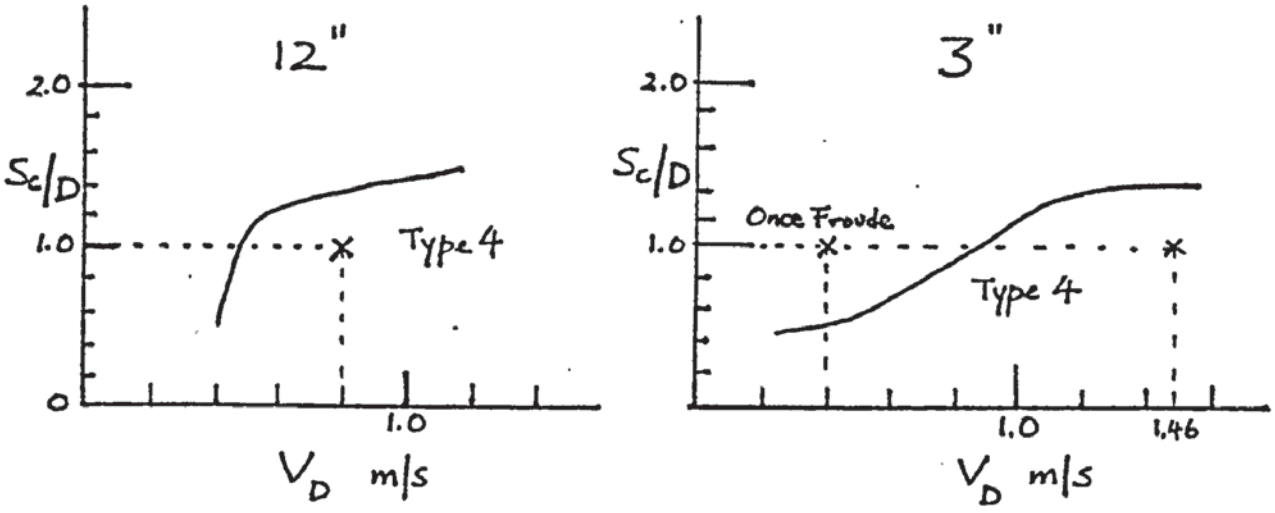

The usual problem is: given a particular submergence, S/D, and bell-mouth velocity V_D on a prototype whose behaviour is unknown, use the model to predict whether or not a type 4 vortex will occur on the prototype. If the prototype S/D is 1.0, and V_D is 0.8 m/s, then a once-Froude law says that a 1 : 4 scale model should be run at $\frac{1}{2}$ of the prototype velocity, i.e. at 0.4 m/s, with S/D the same at 1.0. It can then be seen from the S_c/D - V_D curve for the 3" rig that the model operating point is outside the fully air-entraining vortex region, and so the model predicts no type 4 vortex. However, from the prototype 12" curve, the operating point lies below the curve, and hence a type 4 vortex exists on the prototype. Thus, a once-Froude law in this case under-estimates the severity of the prototype vortex, and the degree of deviation from once-Froude scaling varies

with s, as can be seen in Fig. 6.34.

Using the data on scaling factors from Fig. 6.34, a k-factor of 3.64 is required for this sump geometry and scale ratio. Thus the model velocity should be 3.64 x 0.4 m/s = 1.46 m/s. The model then predicts a type 4 vortex as required.

As a further point of interest, the time required to organise the generated vorticity into a coherent vortex has also been considered to see if this has a size dependence. An estimate of the organisation time required can be made by assuming that the vortex-forming process follows that of regular vortex-shedding from a cylinder in a steady flow. In this case, for the range of pipe Reynolds number, R_d, under consideration (10^3 to 10^5) vortex shedding occurs at a constant Strouhal number, S, so that the frequency of shedding, n, is given by :

$$n = \frac{S V_W}{d}$$

Thus the organisation time required $\approx \frac{1}{n} \propto \frac{d}{V_W}$ for constant S

On the other hand, the time available for vortex formation before the fluid is drawn into the intake is approximately equal to the distance travelled by an element of water in going from the surface to the intake, divided by its velocity. An estimate of this is $\frac{S}{V_W}$

By analogy with the Keulegan-Carpenter number, which gives a measure of the time available for a wake to form behind a cylinder in the presence of waves, a measure of the likelihood of vortex formation and hence its stability is given by the ratio N :

$$N = \frac{\text{time available for vorticity organisation}}{\text{time required}}$$

$$= \frac{SV_W}{V_W d}$$

$$= \frac{S}{d}$$

Thus the larger the value of S/d, the greater the chances of organising the vorticity into a type 4 vortex. Conversely, for a given S/d, the value of N is constant irrespective of size because it is a non-dimensional parameter, and so this time factor would not be expected to affect the behaviour of the different size rigs.

The outcome of this discussion, then, is that vortex formation in the different size rigs is more complex than originally assumed in the theory developed in 3.6. There is a variation in the Reynolds number contribution as measured by the value of b, for a given size rig with different sump geometry and submergence. Even for a given geometry and submergence, the value of b varies with size. Mathematically, this means that instead of the simple theory used in Chapter 3 based on

$$\frac{V_m}{V_p} = f(s)$$

it has been found that

$$\frac{V_m}{V_p} = f(s,\ b,\ \text{geometric parameters})$$

Nevertheless, it has been possible to obtain scaling laws (Fig. 6.34) from the experimental results, which give the required degree of exaggeration above Froude scale (i.e. the k factor) over a limited size and scale range. These k values can then be directly used for scaling vortices in hydraulic models in this range. It is uncertain, however, to what extent these values

apply to larger prototype sizes met in practice, and more prototype data is therefore needed to investigate this. It has also been shown that the use of a once-Froude scaling law can lead to underestimation of the severity of the vortex which will occur on a prototype.

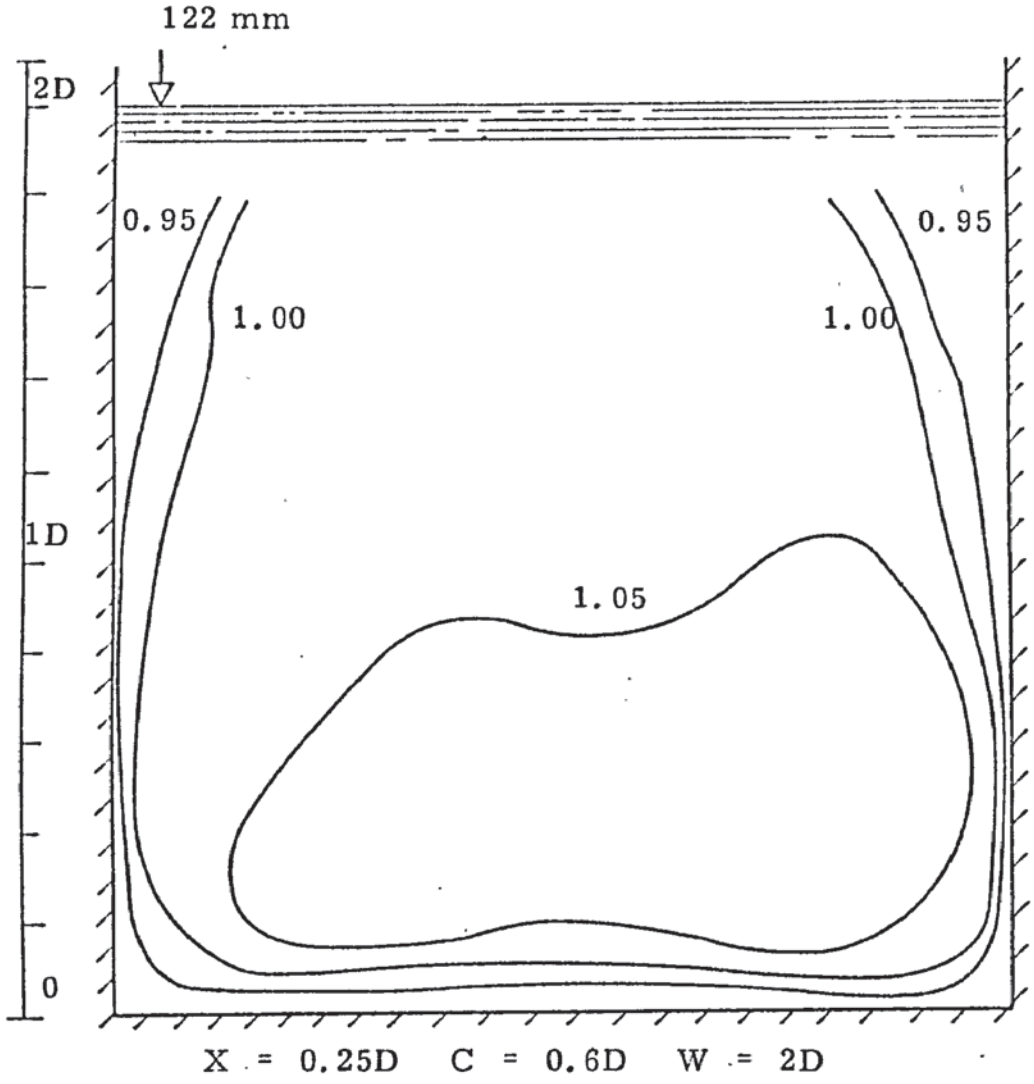

Fig. 6.1 Non-dimensionalised velocity contours for the 1.5" rig at a plane 3D from the endwall with water depth 2D (122mm)

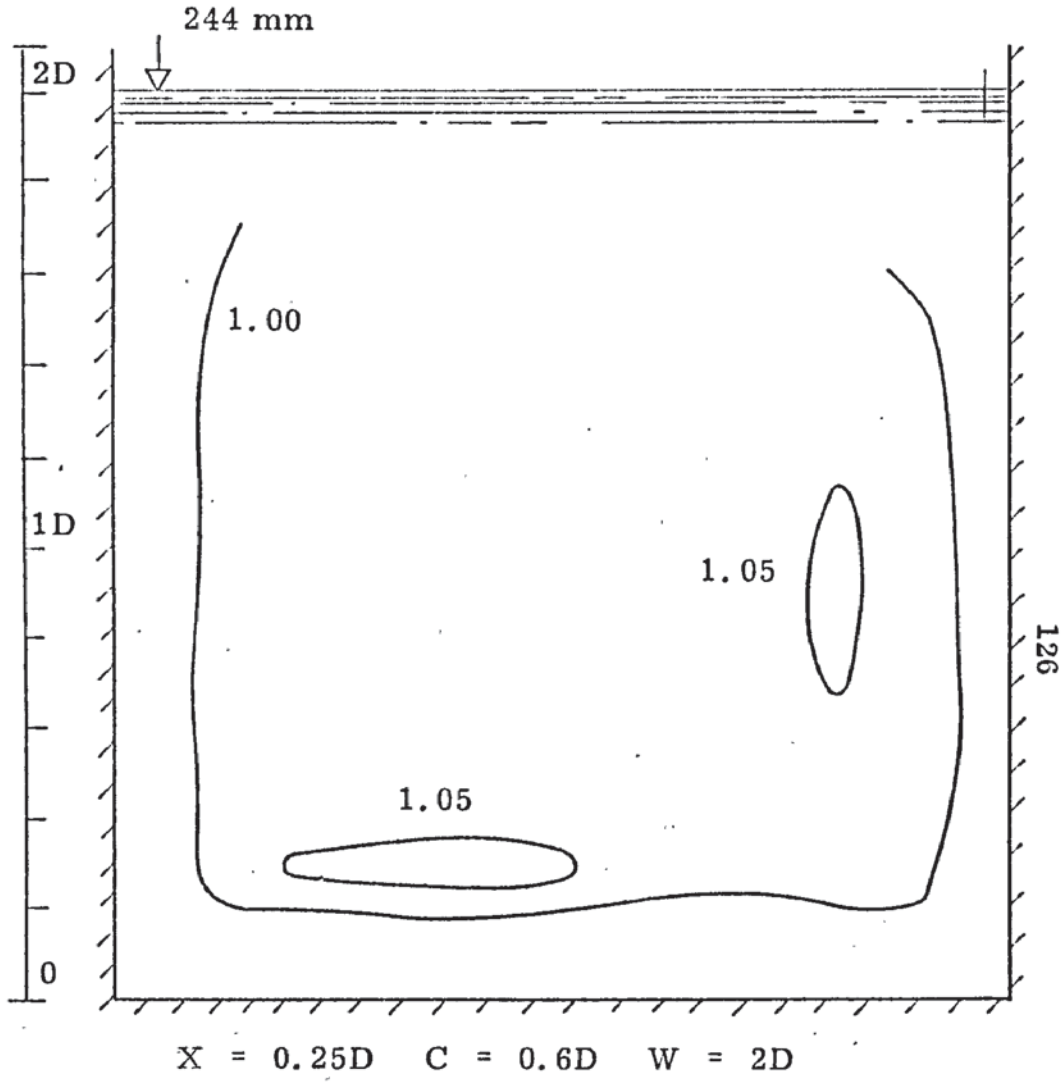

Fig. 6.2 Non-dimensionalised velocity contours for the 3" rig at a plane 3D from the endwall with water depth 2D (244mm)

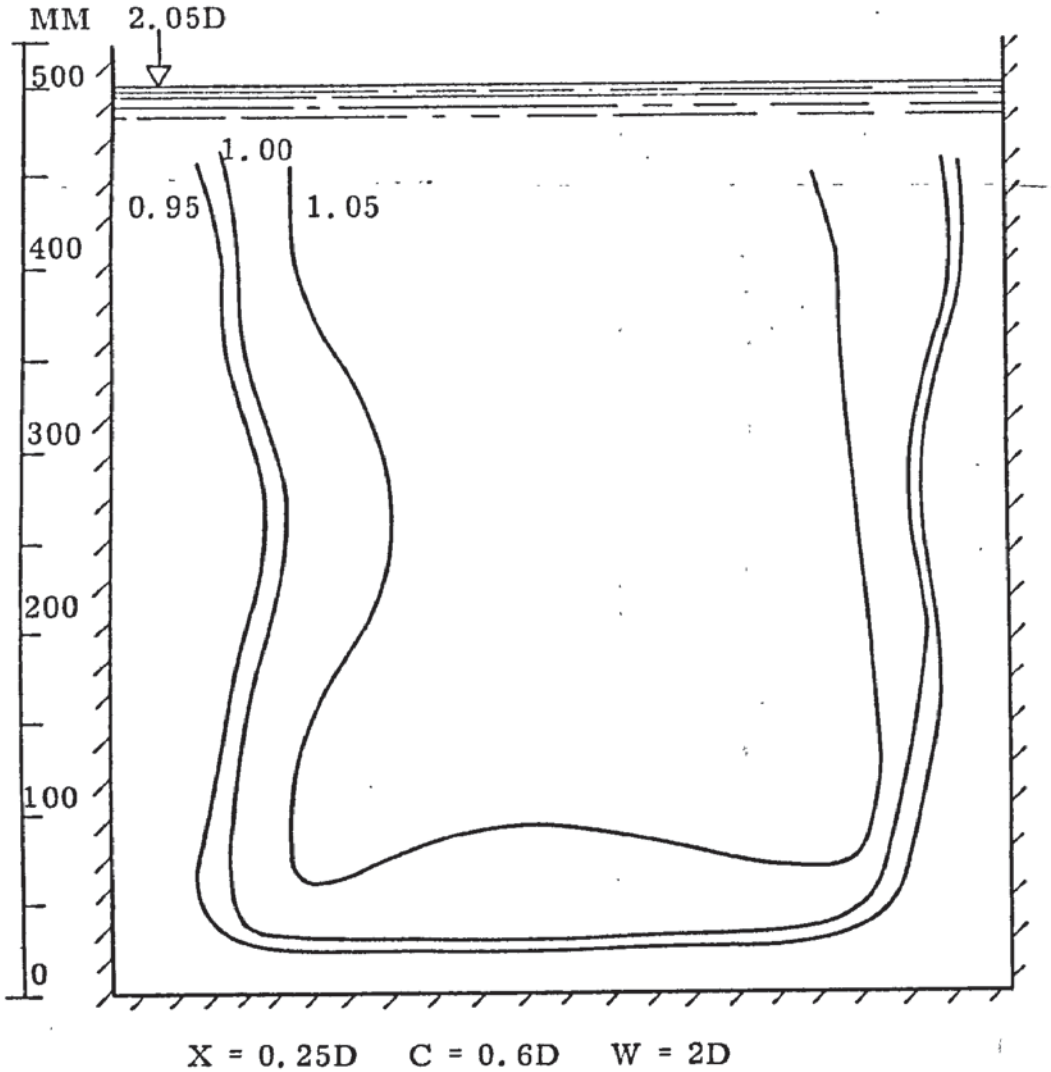

Fig. 6.3 Non-dimensionalised velocity contours for the 6" rig at a plane 3D from the endwall with water depth 2.05D (500mm)

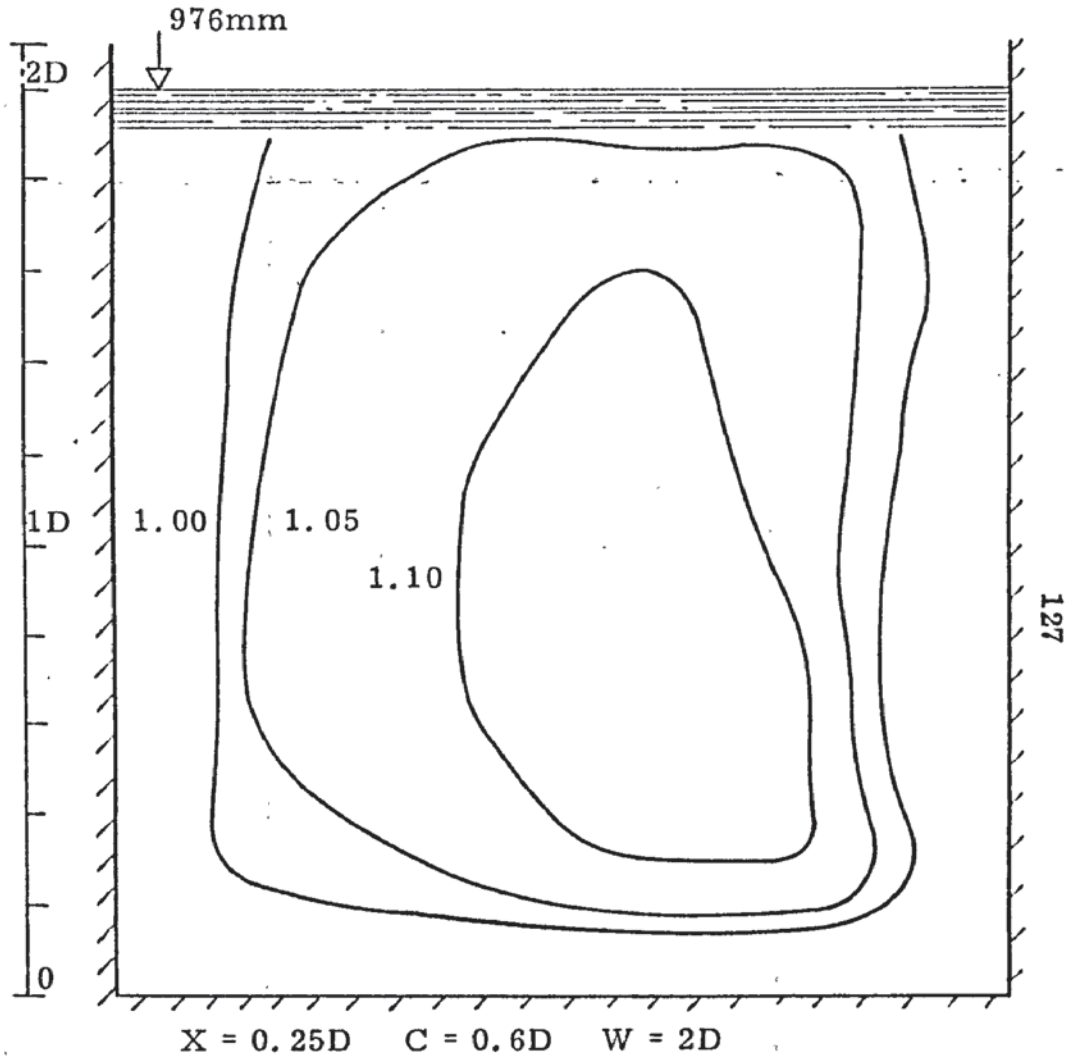

Fig. 6.4 Non-dimensionalised velocity contours for the 12" rig at a plane 3D from the endwall with water depth 2D (976mm)

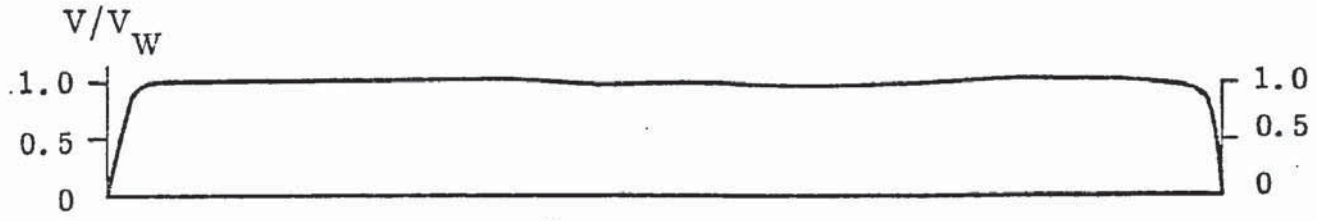

a) 1.5" rig

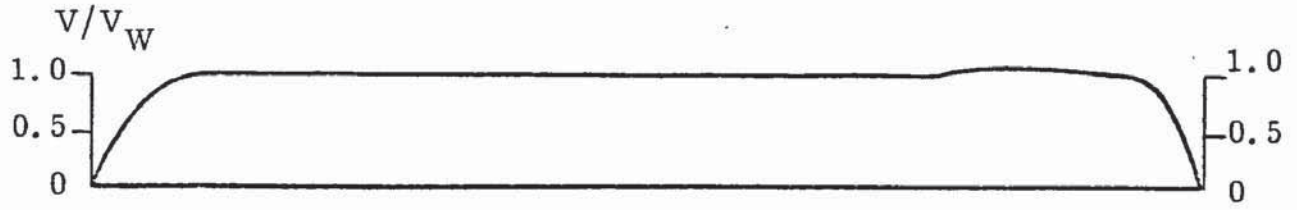

b) 3" rig

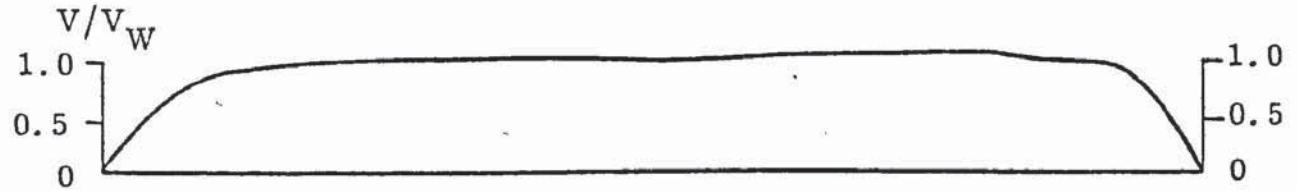

c) 6" rig

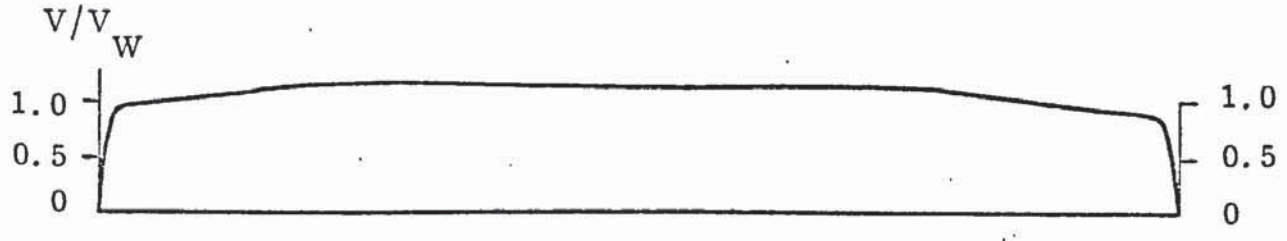

d) 12" rig

Fig. 6.5 Velocity profiles across the channel at a depth of 1.2 bellmouth diameters below the water surface, constant channel width of 2 bellmouth diameters.

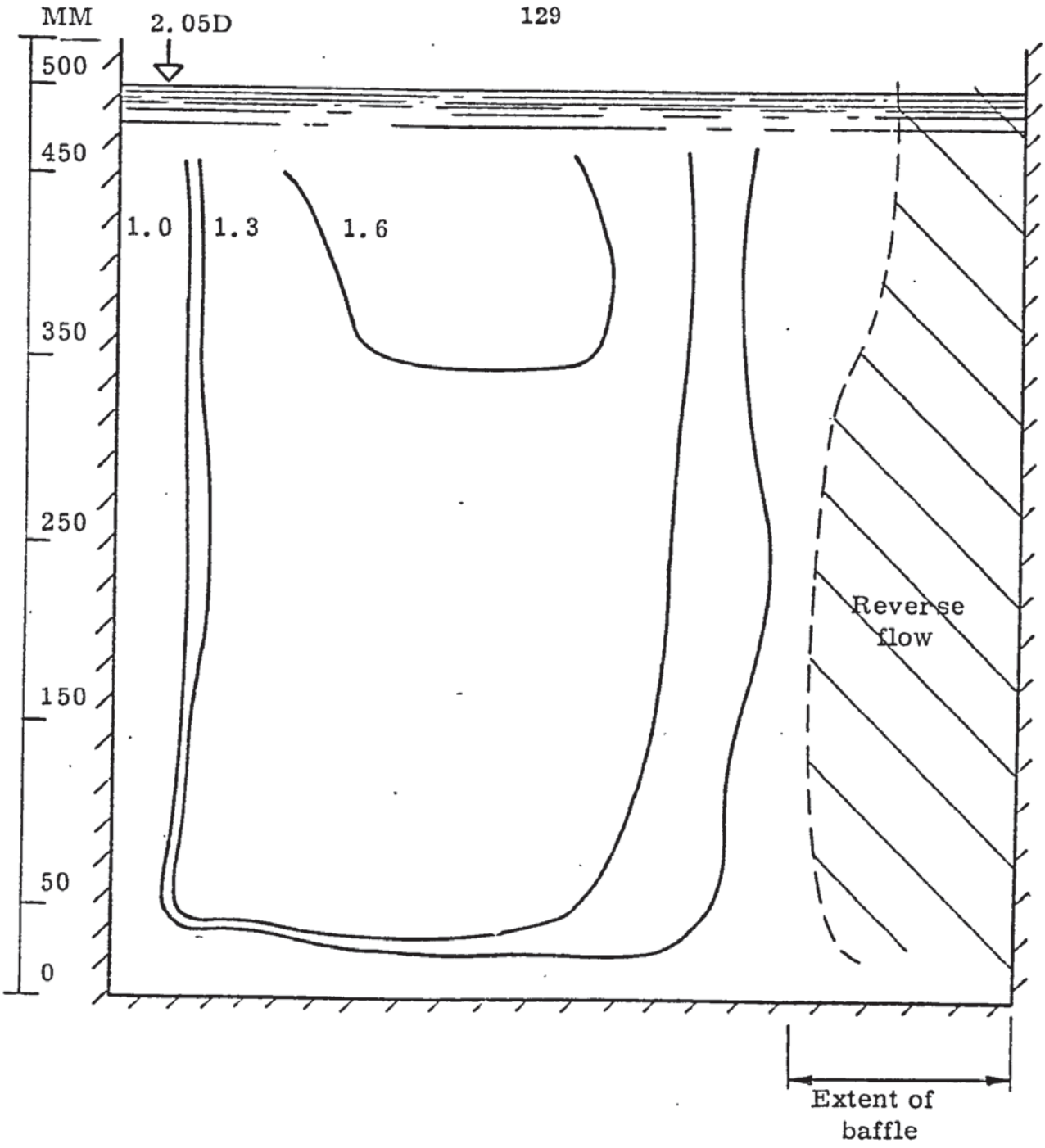

Fig. 6.6(a) Non-dimensionalised velocity contours for the 6" rig with a $\frac{1}{2}$D wide baffle placed 6D from the end-wall, water depth 2.05D, (500mm)

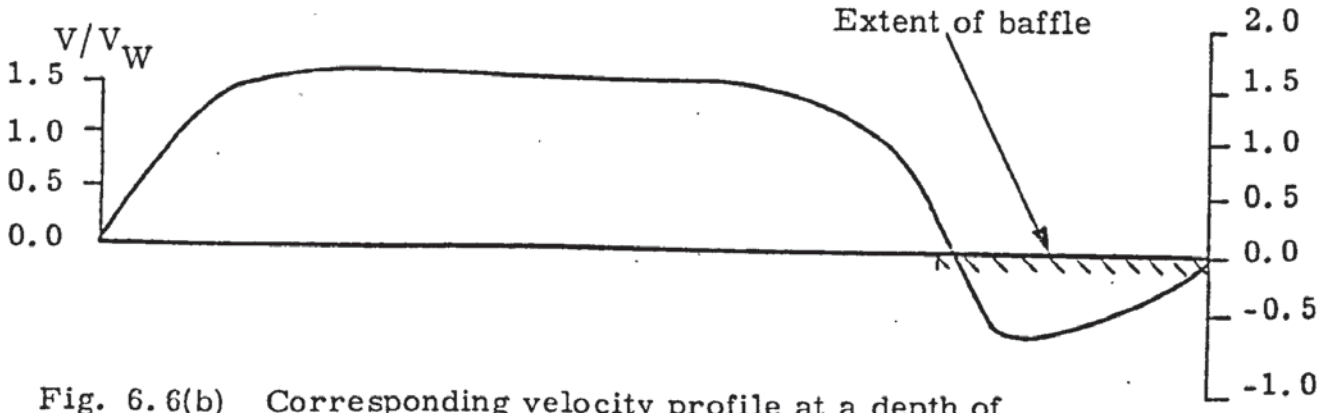

Fig. 6.6(b) Corresponding velocity profile at a depth of 1.2D below the water surface.

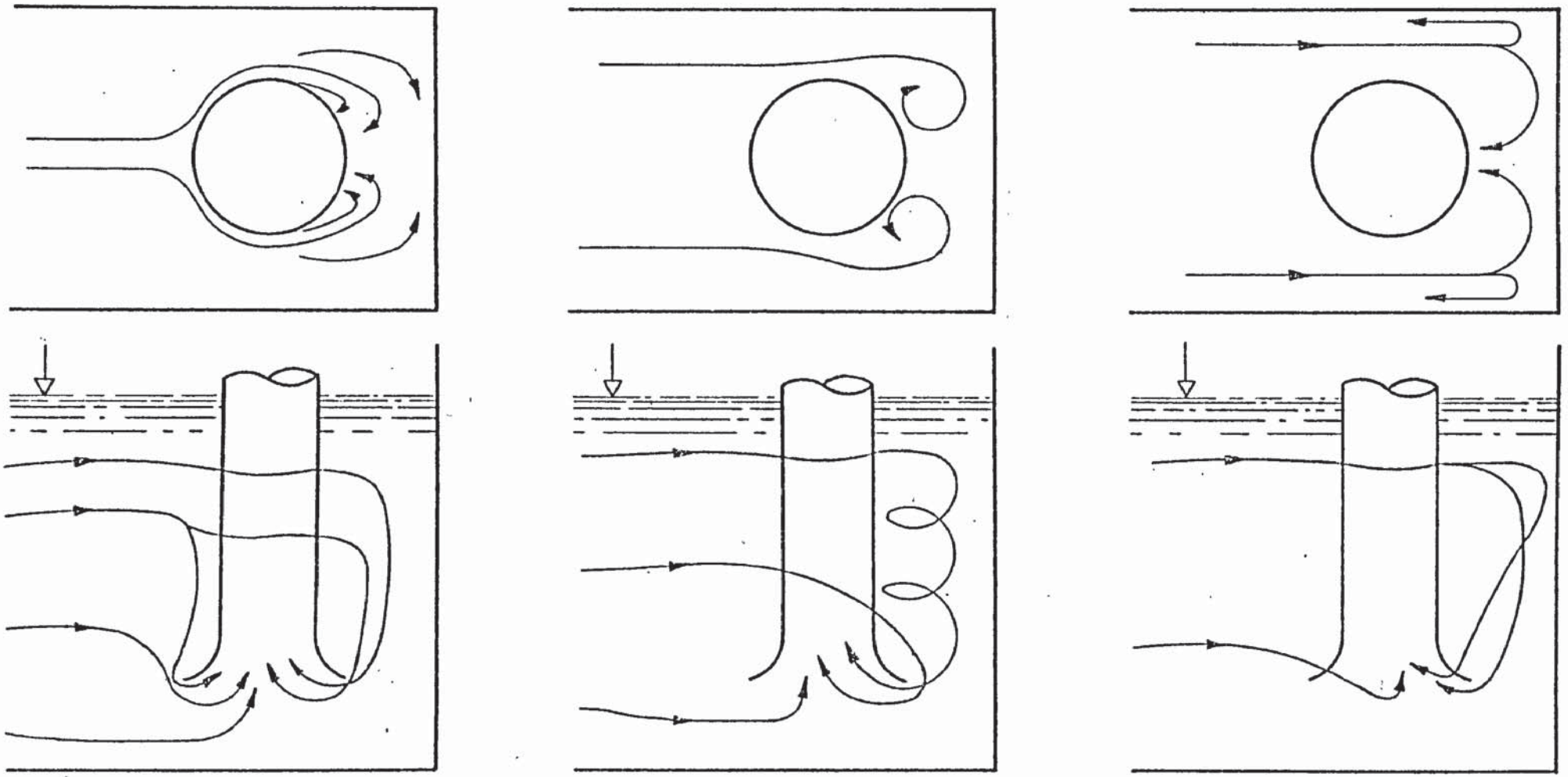

Flow at centre of channel

Flow midway between centreline and sidewalls

Flow along sidewalls

Fig. 6.7 Flow patterns near the bellmouth taken from the 6" rig at various positions across the channel width, showing both plan and elevation, Water depth 2.13D (520mm)

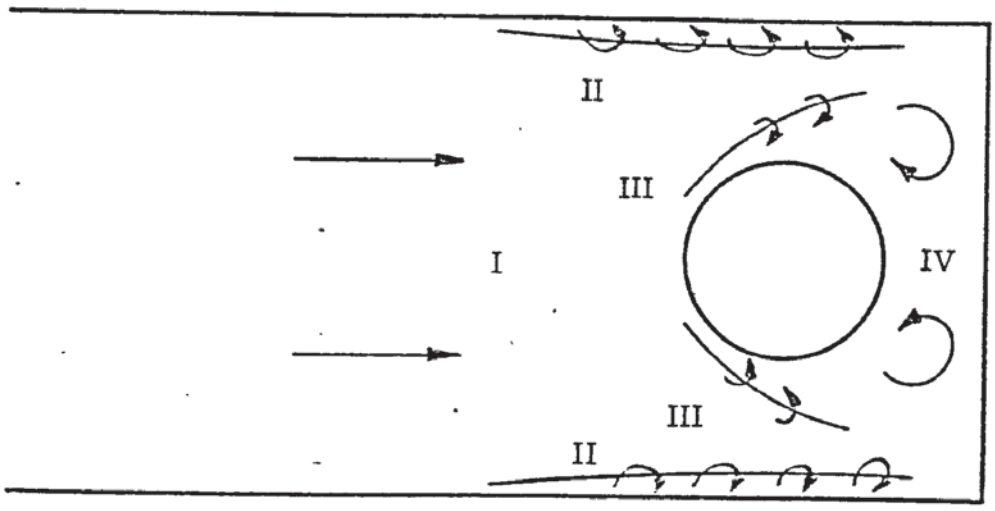

I Main flow (irrotational)

II Boundary layer from sidewalls

III Boundary layer from suction pipe

IV Wake region behind pipe

Fig. 6.8 Flow regions near the bellmouth

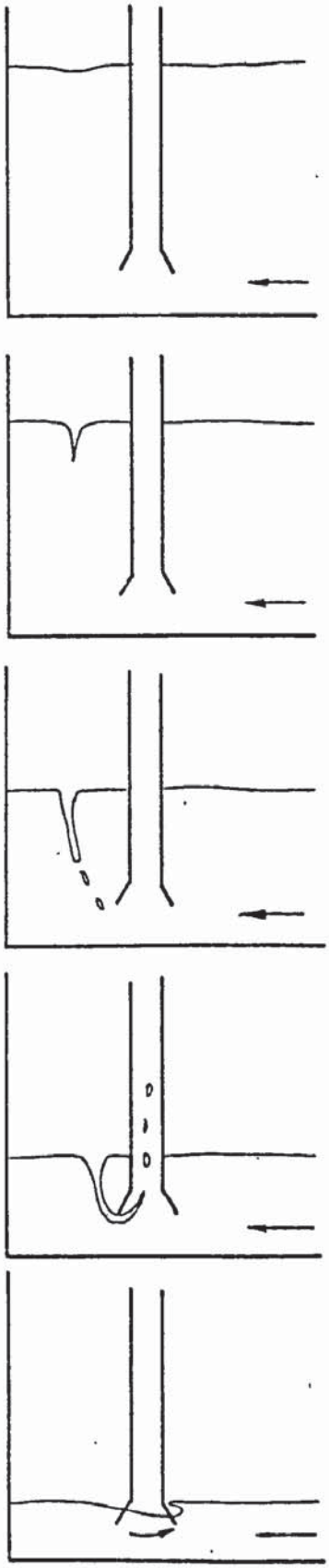

Type 1. At high submergences and low velocities, there is little surface movement. The only visible sign of a vortex is a surface dimple. No air is entrained at this stage.

Type 2. As the dimple grows, a distinct 'tail' appears, which may or may not have a rotating core of water beneath it. If sufficiently strong, the vortex can ingest small surface debris even at this stage.

Type 3. At this stage, distinct bubbles start to break off from the tail and can be drawn into the suction pipe, hence starting the air-entrainment process. This stage of development results in intermittent air-entrainment.

Type 4. At the height of its development, the vortex forms an open air core with the tail extending into the suction pipe to produce continuous air-entrainment, often accompanied by a loud gurling sound. The surface profile follows a hyperbolic form but is also corrugated, due to surface waves at the air-water interface.

Type 5. At very low submergences, the flow pattern changes to mass rotation of the water round the intake, and surface drawdown causes large volumes of air to be entrained. A submerged vortex may also develop. Although it is easy to produce this condition in the laboratory, in practice the submergence would not normally be allowed to reach such low values.

Fig. 6.9 Development of air-entraining vortices.

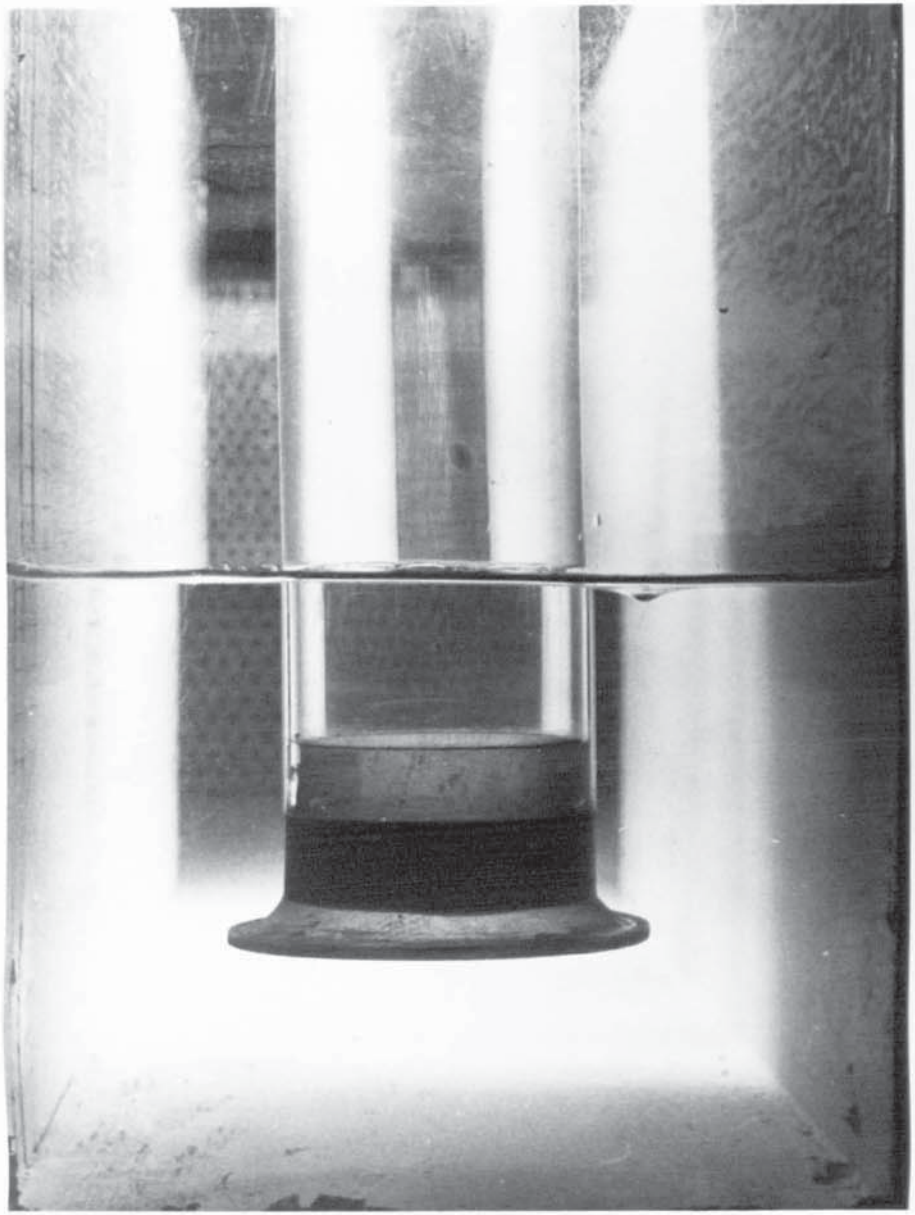

Fig. 6.10 Type 1 vortex on the 1.5" rig, submergence 0.8D, bellmouth velocity V_D = 0.52 m/s.

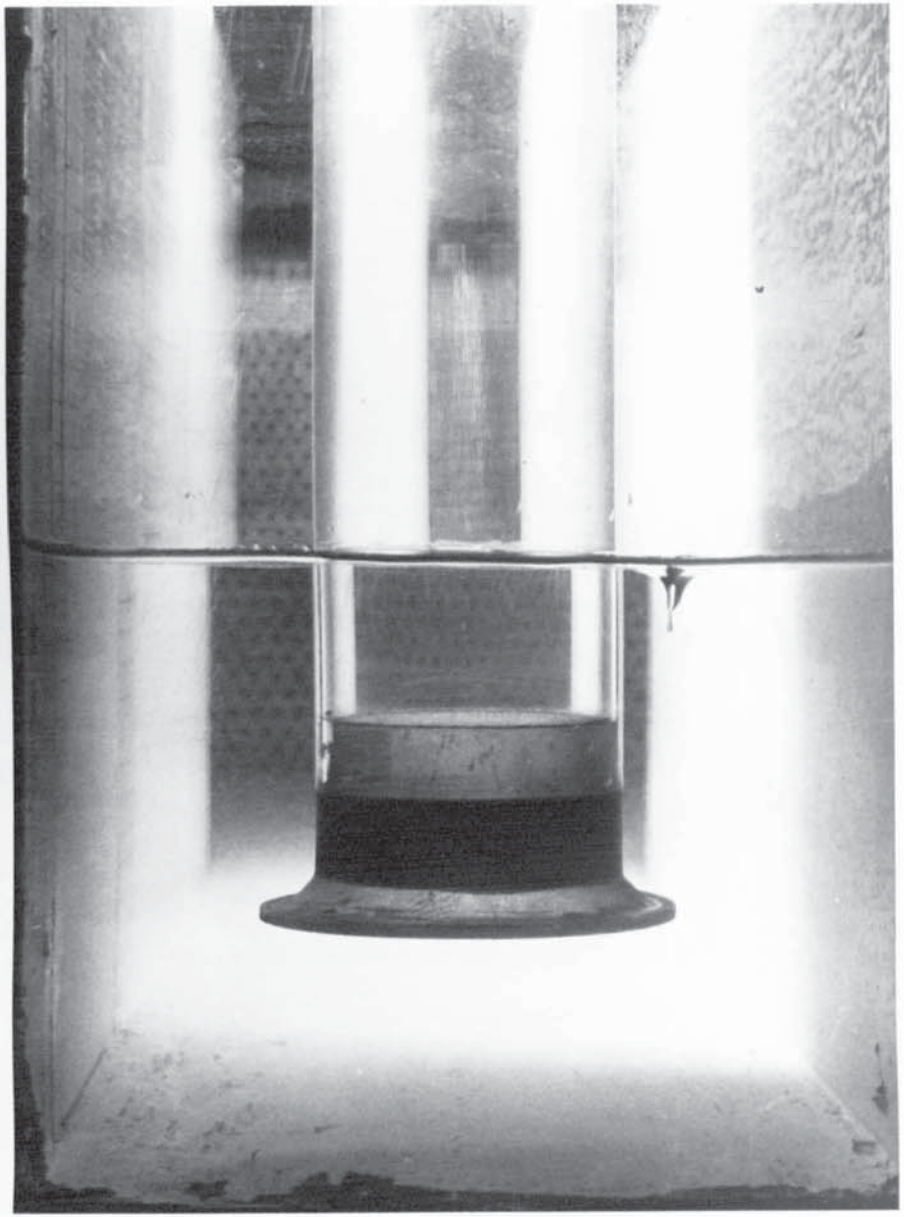

Fig. 6.11 Type 2 vortex on the 1.5" rig, submergence 0.8D, bellmouth velocity V_D = 0.78 m/s.

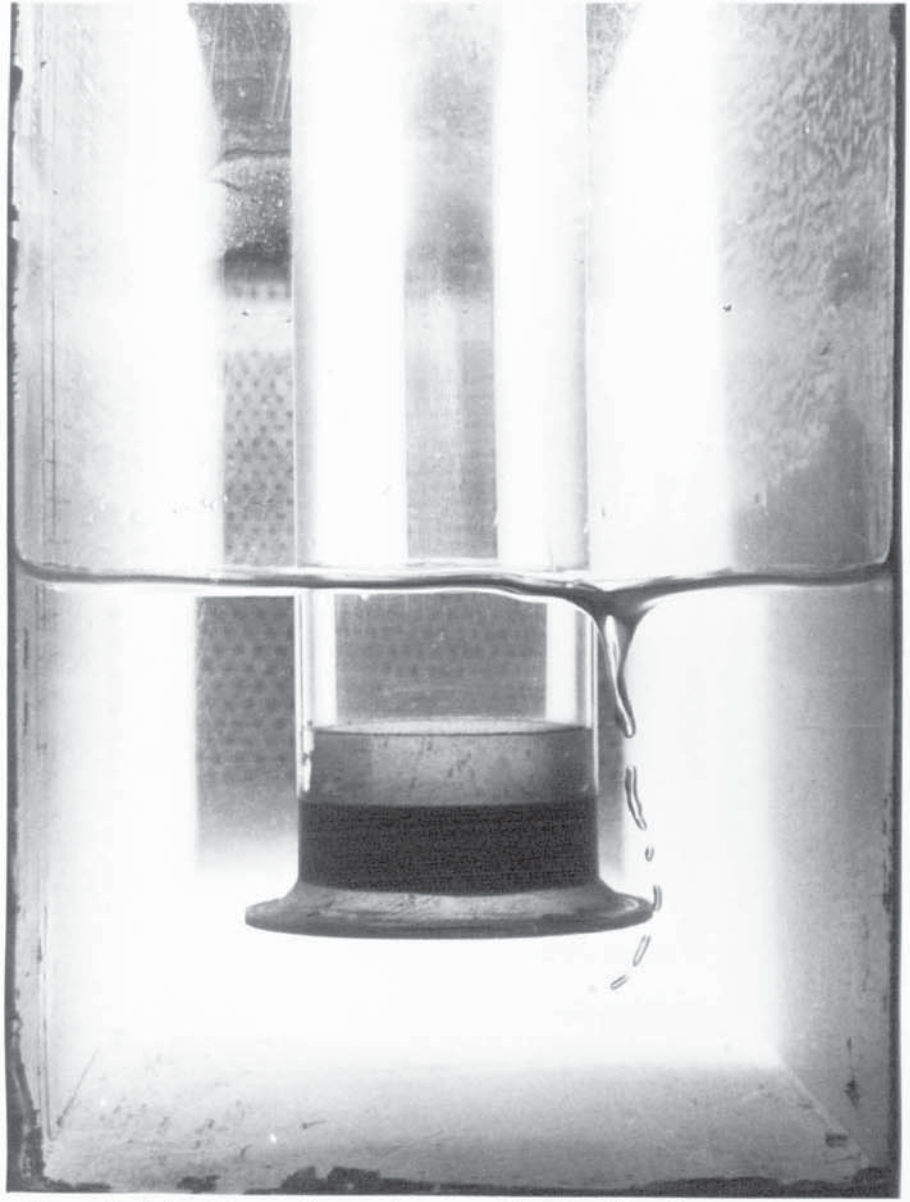

Fig. 6.12 Type 3 vortex on the 1.5" rig, submergence 0.8D, bellmouth velocity V_D = 1.04 m/s.

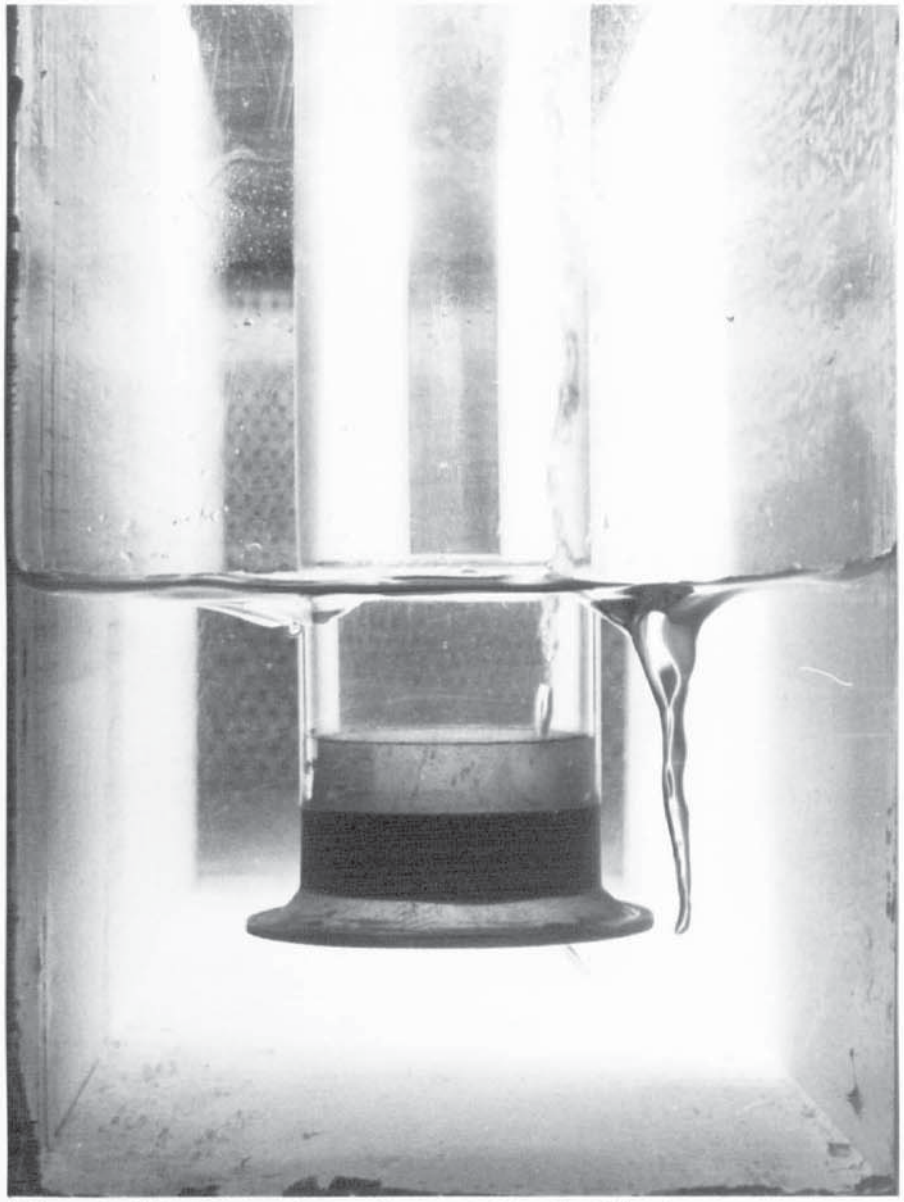

Fig. 6.13 Type 4 vortex on the 1.5" rig, submergence 0.8D, bellmouth velocity V_D = 1.42 m/s.

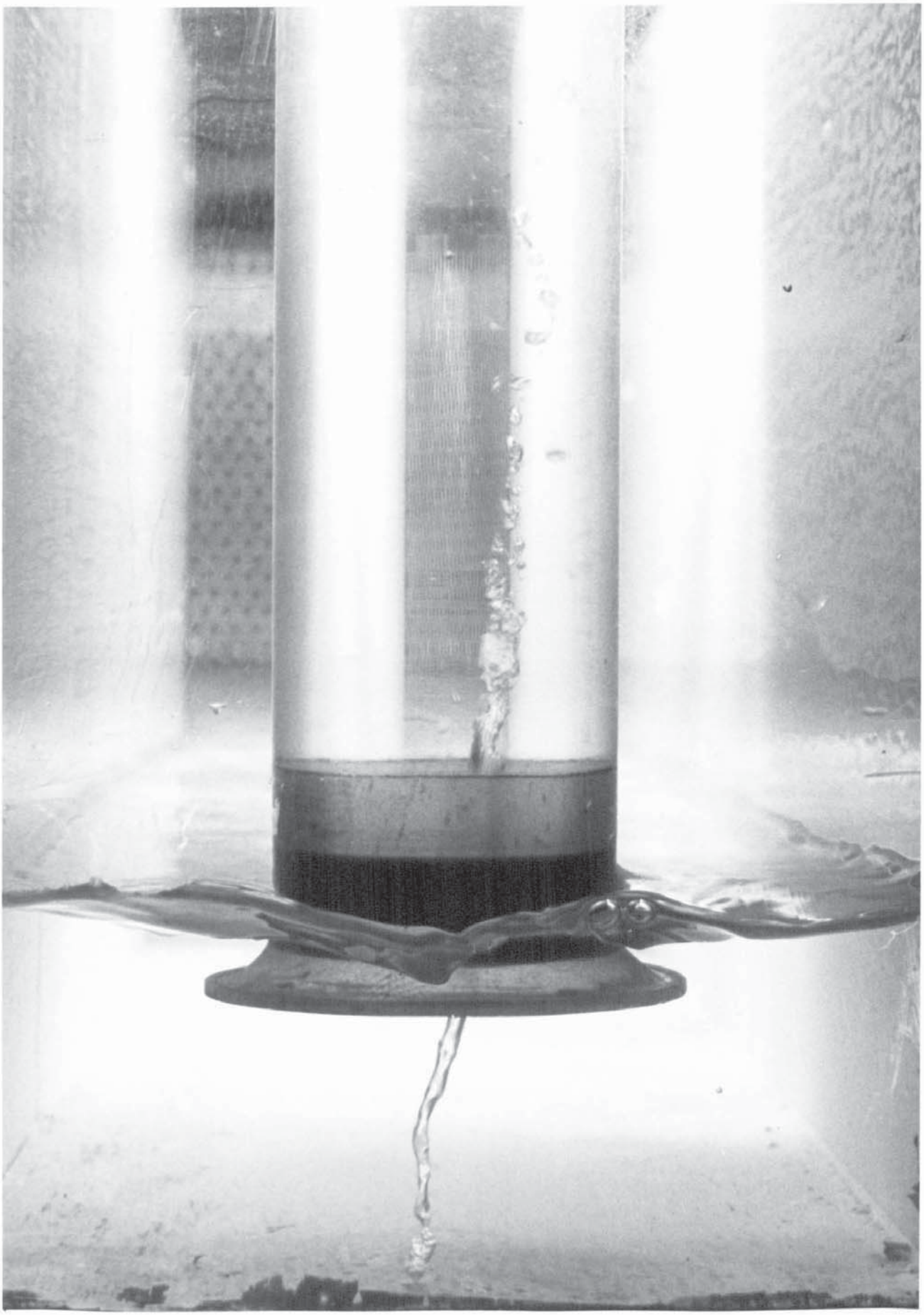

Fig. 6.14 Type 5 vortex (submerged) on the 1.5" rig, submerged .2D bellmouth velocity V_D = 0.78 m/s.

Fig. 6.15 Table of geometric conditions tested, and experimentally derived values of S_B/D and sump volume for 6" rig.

W/D	X/D	C/D	S_B/D	H_B/D	W/D x H_B/D
2.0	0.0	0.5	1.6	2.1	4.2
	0.25	0.2	2.2	2.4	4.8
		0.3	2.1	2.4	4.8
		0.4	2.1	2.5	5.0
		0.5	1.8	2.3	4.6
		0.6	1.7	2.3	4.6
		0.7	1.8	2.5	5.0
		0.8	1.8	2.6	5.2
	0.50	0.3	2.1	2.4	4.8
		0.4	1.9	2.3	4.6
		0.5	1.7	2.2	4.4
		0.6	1.6	2.2	4.4
	0.75	0.5	1.5	2.0	4.0
3.0	0.25	0.5	1.1	1.6	4.8
4.0	0.25	0.5	0.7	1.2	4.8
2.0	0.25	0.5 + corner fillets	0.8	1.3	2.6
		0.6 + baffle at 3D	1.8	2.4	4.8
		4D	1.7	2.3	4.6
		6D	1.7	2.3	4.6

Fig. 6.16 Graph of critical submergence S_c/D against bellmouth velocity V_D for values of floor clearance C/D. The area below each curve defines the region where fully air-entraining (type 4) vortices occur.

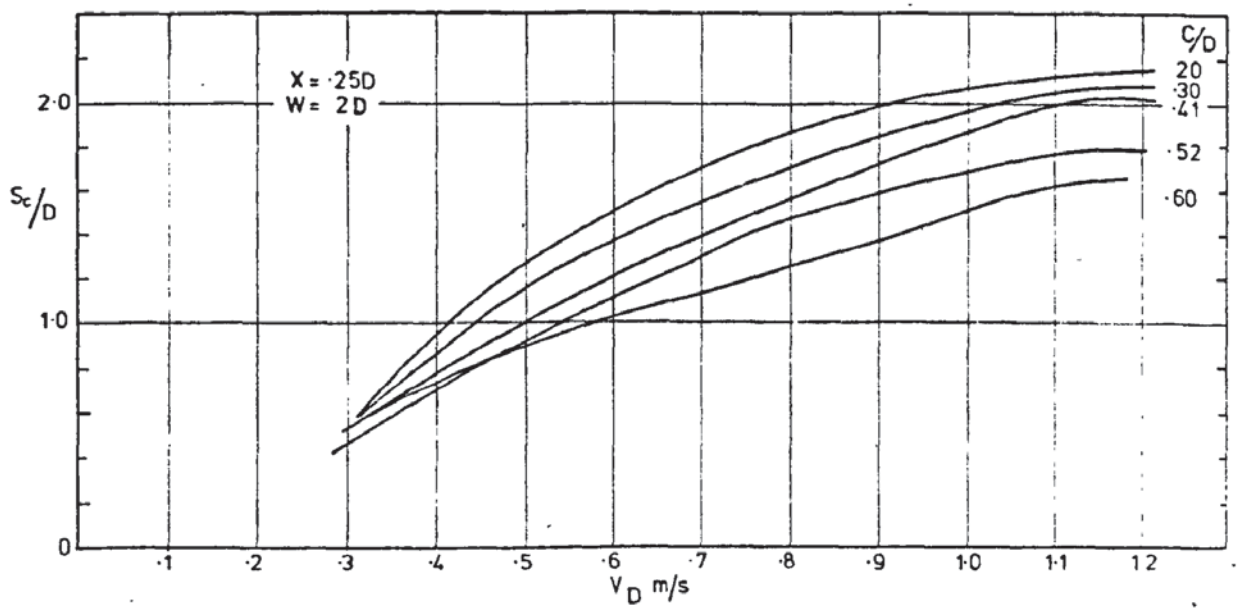

Fig. 6.16(a) C = 0.2D to 0.6D

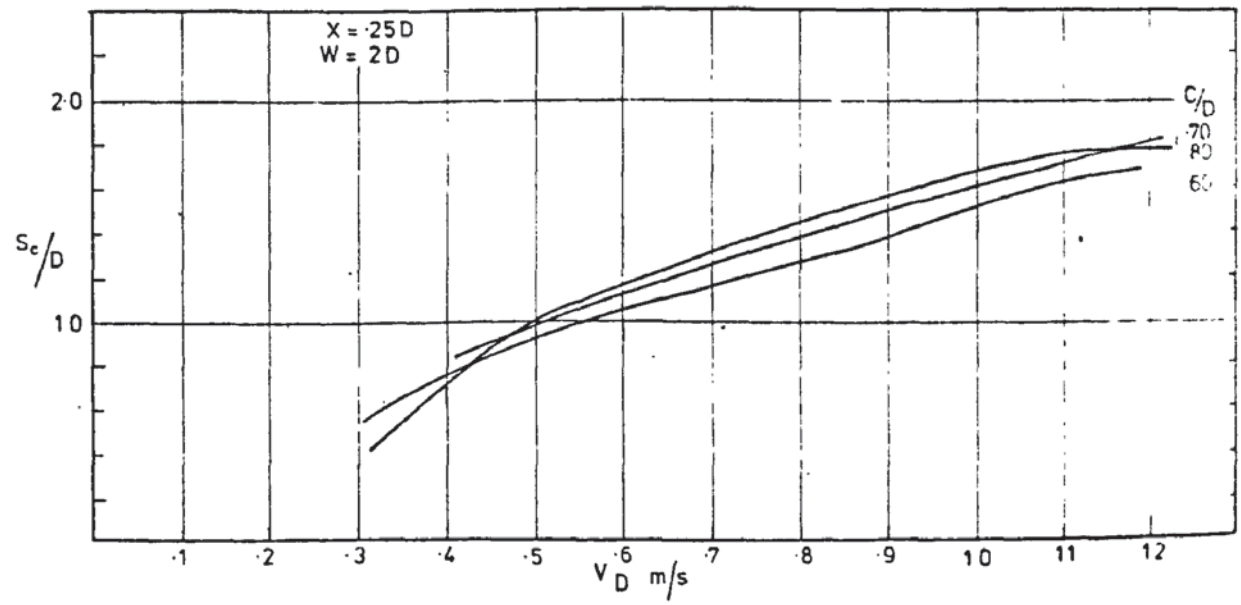

Fig 6.16(b) C = 0.6D to 0.8D

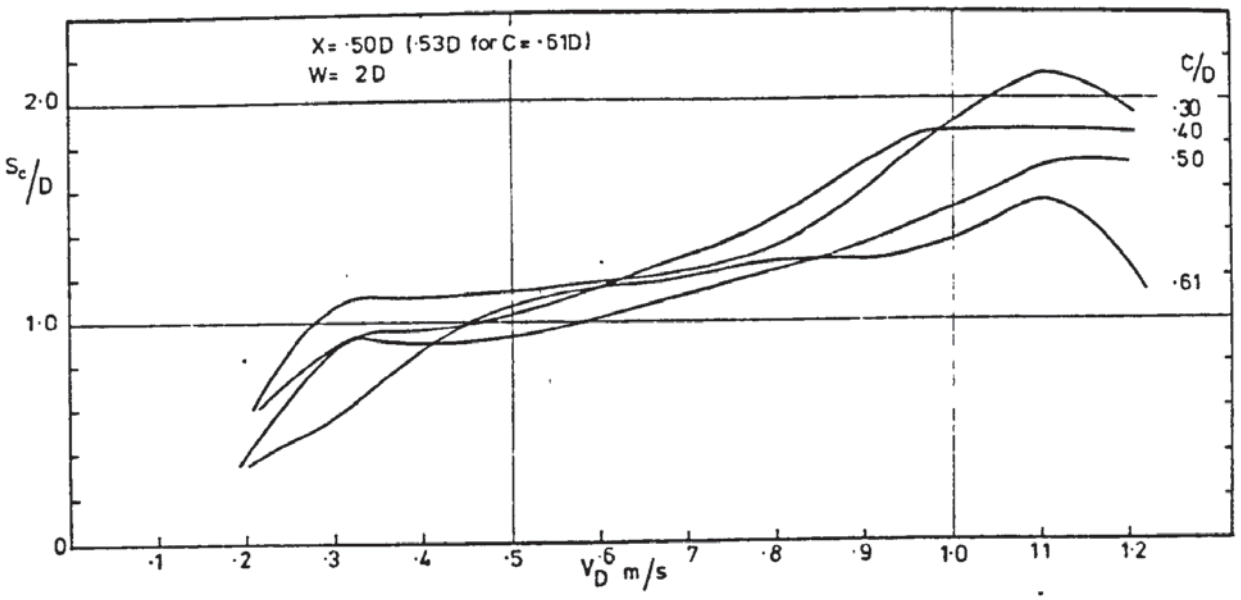

Fig. 6.17 Graph of critical submergence S_c/D against bellmouth velocity V_D as in 6.16, but with $X/D = 0.5$ and C/D in the range 0.30 to 0.61.

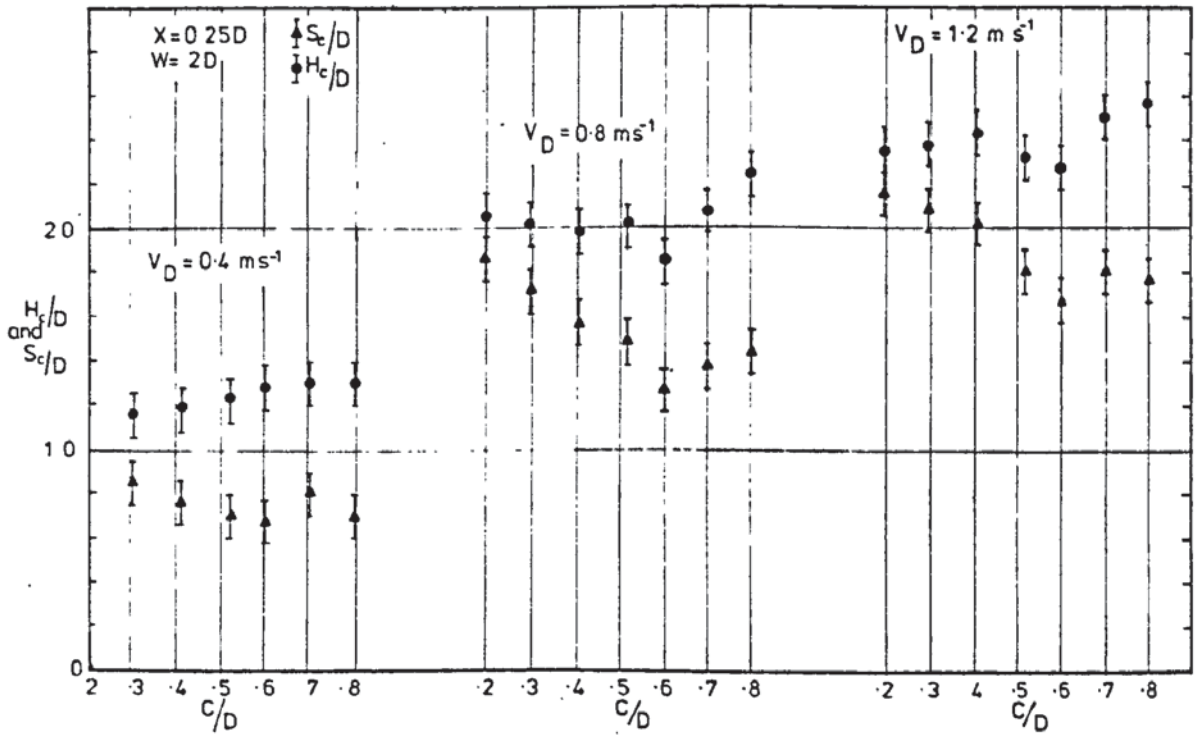

Fig. 6.18 Variation of critical submergence S_c/D and critical depth H_c/D with floor clearance, C/D, at values of bellmouth velocity V_D of 0.4, 0.8 and 1.2 m/s.

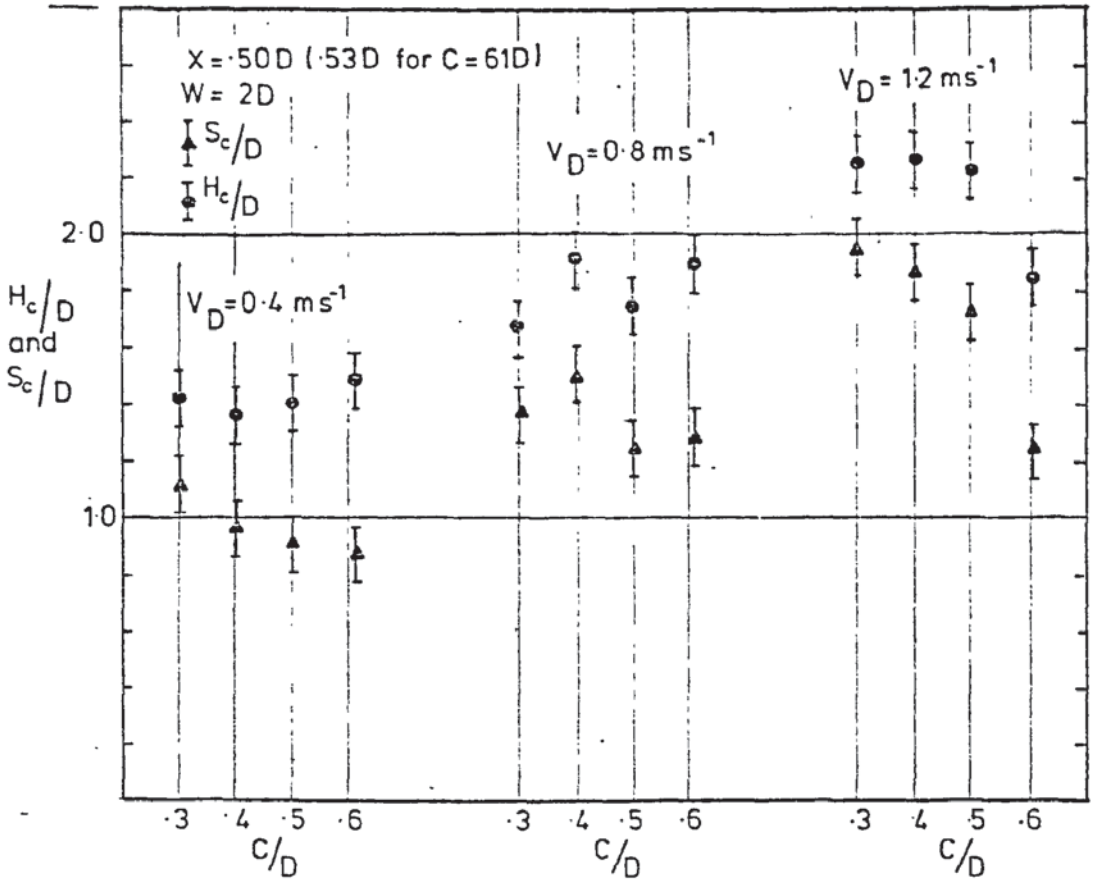

Fig. 6.19 Variation of S_c/D with H_c/D with C/D, as in 6.18 but with X/D = 0.5

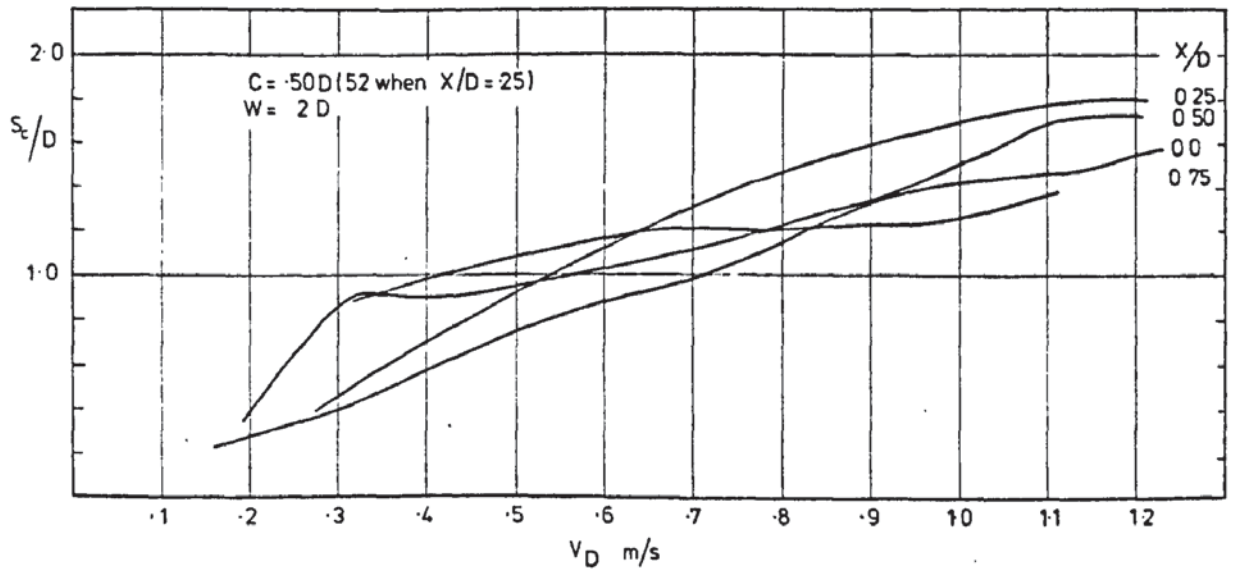

Fig. 6.20 Graph of critical submergence S_c/D against bellmouth velocity V_D for values of endwall clearance X/D in the range 0 to 0.75.

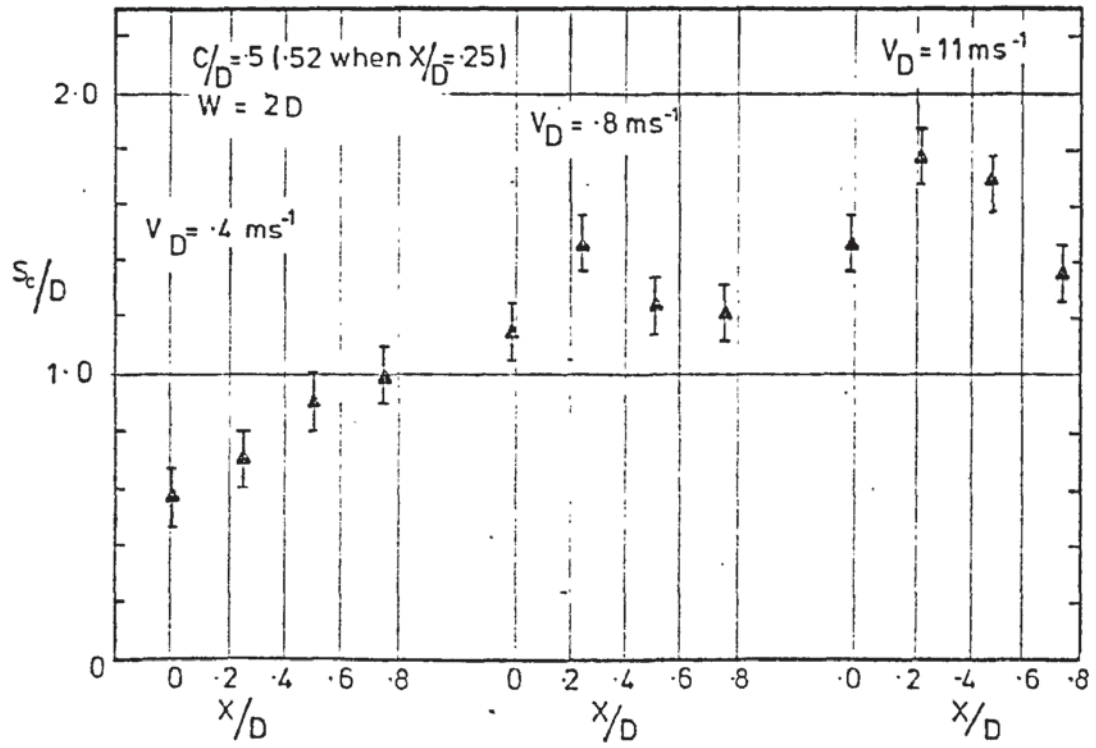

Fig. 6.21 Variation of critical submergence S_c/D with endwall clearance X/D at values of bellmouth velocity V_D of 0.4, 0.8 and 1.1 m/s.

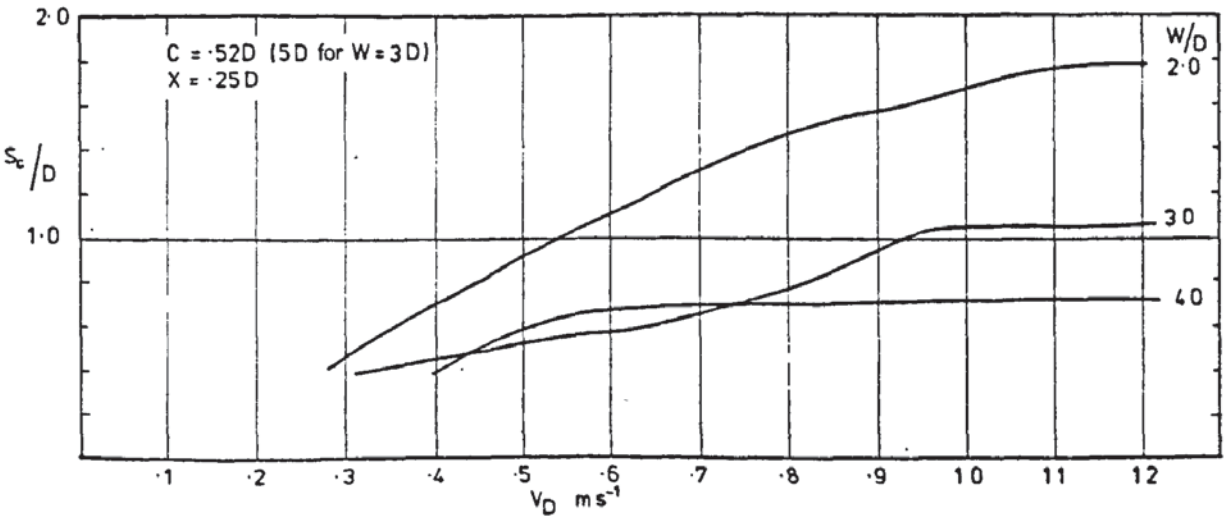

Fig. 6.22 Graph of critical submergence S_c/D against bellmouth velocity V_D for various values of channel width W/D.

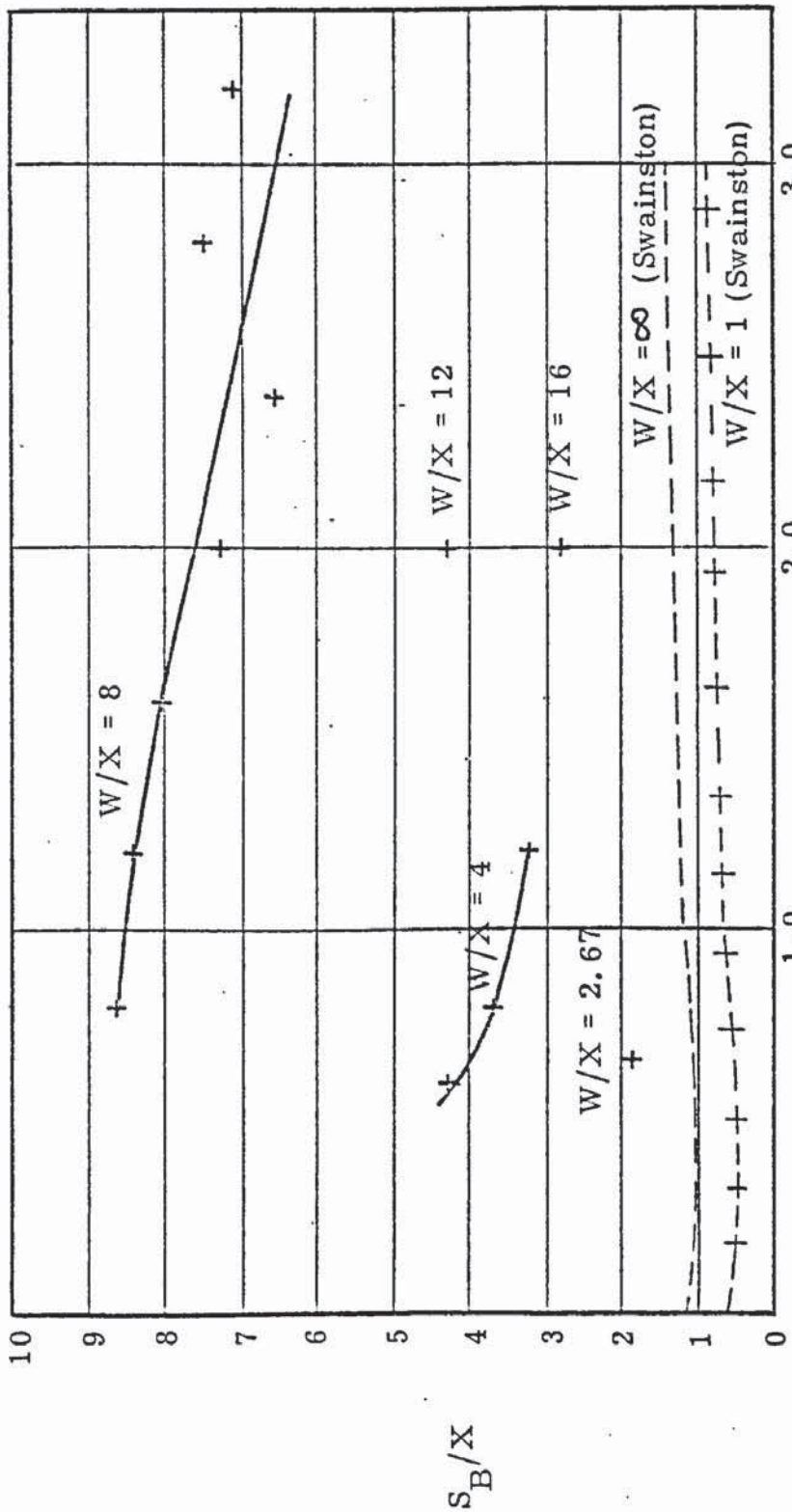

Fig. 6.23 Graph of non-dimensionalised bounding submergence S_B/X against non-dimensionalised floor clearance C/X for various values of width W/X. Results from Swainston (3) shown by dotted line.

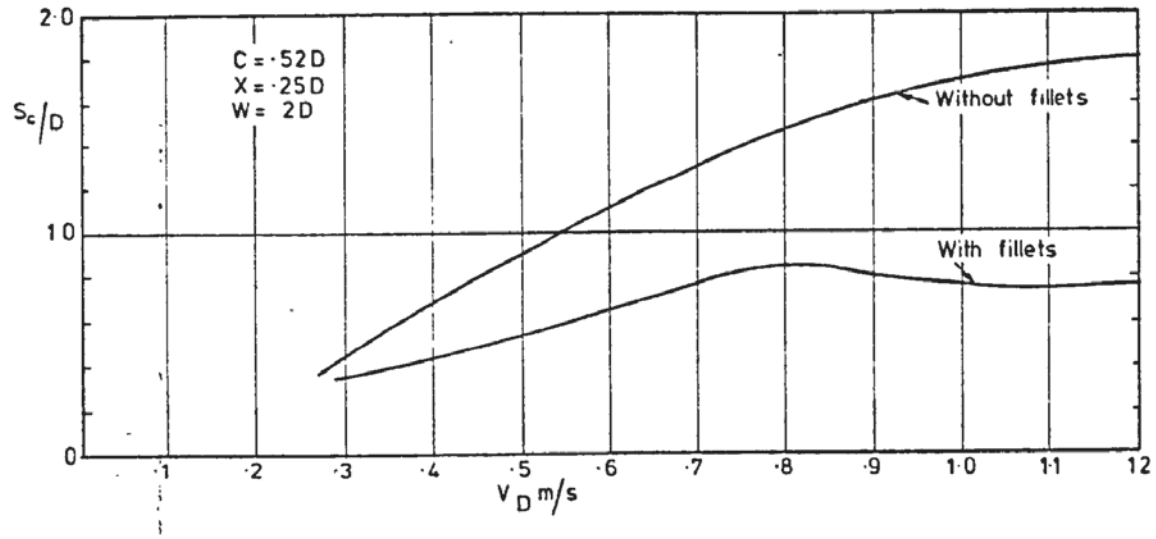

Fig. 6.24 Effect of corner fillets on the critical submergence - bellmouth velocity curve.

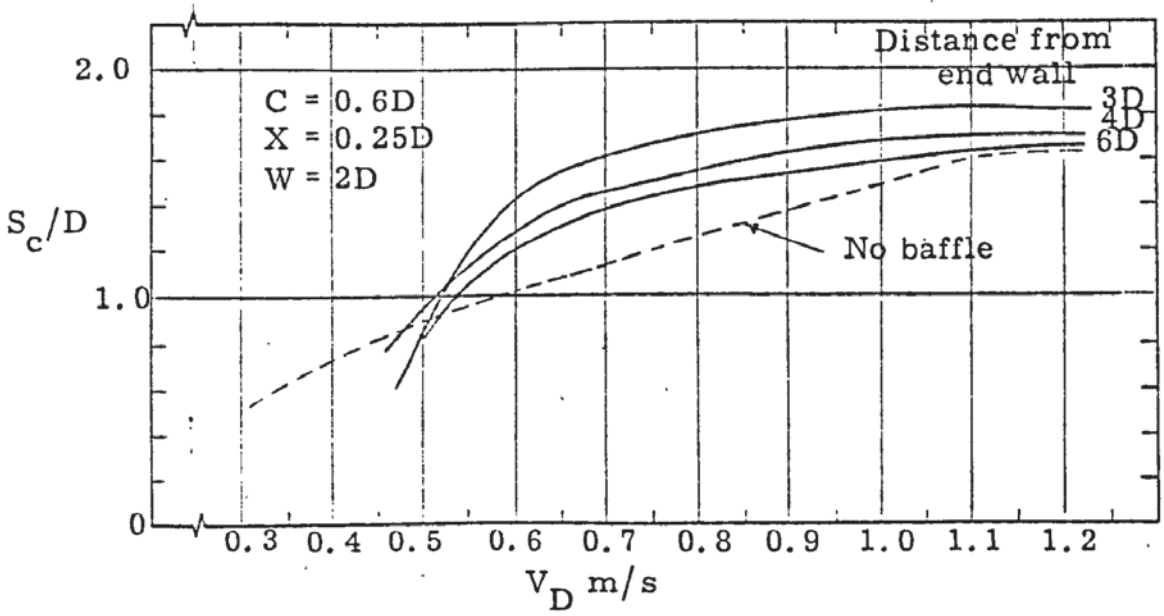

Fig. 6.25 Effect of a $\frac{1}{2}$D baffle placed at various positions upstream of the endwall on the critical submergence-bellmouth velocity curve.

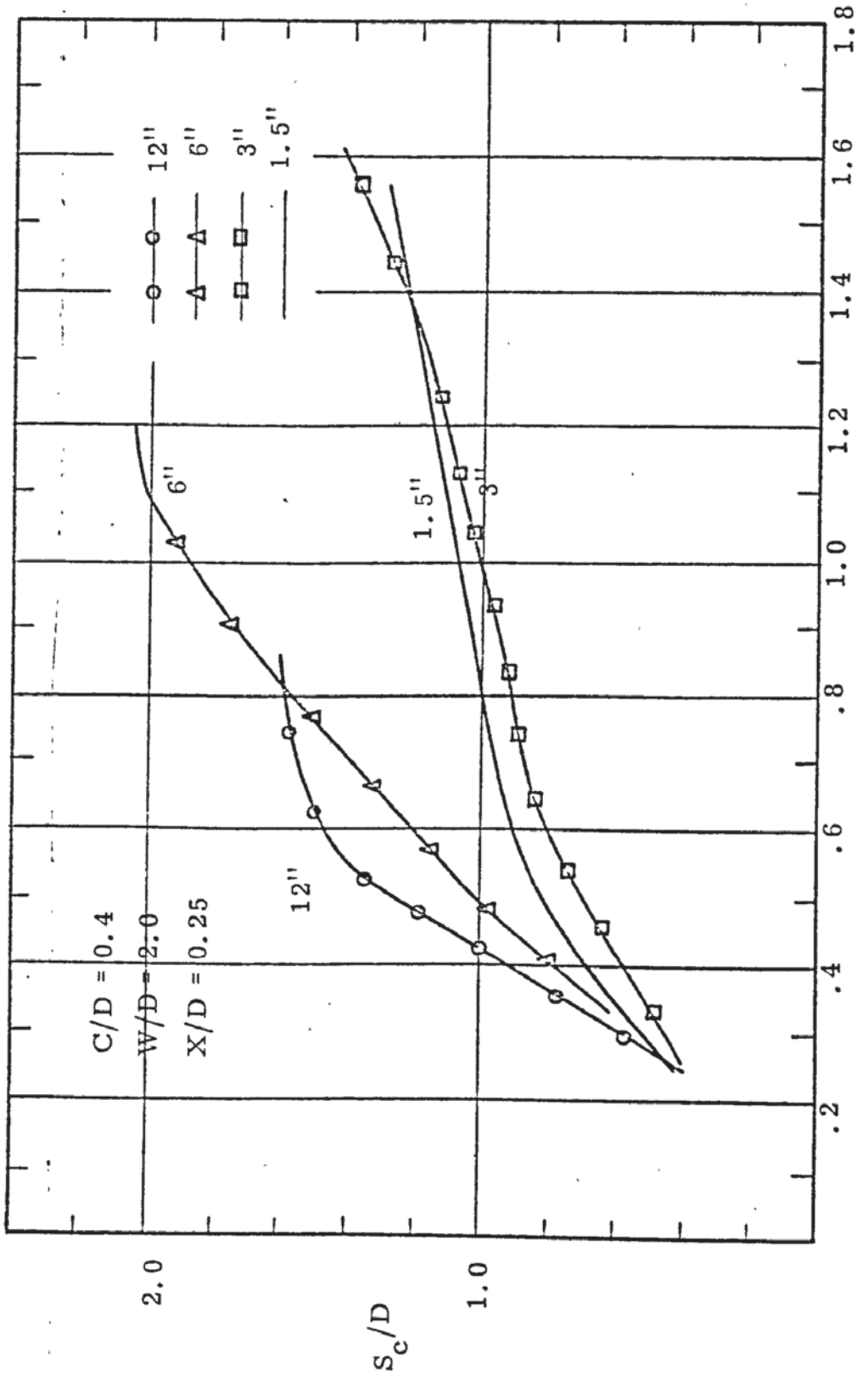

Fig. 6.26 Graph of critical submergence S_c/D against bellmouth velocity V_D for the four rigs, C/D = 0.4

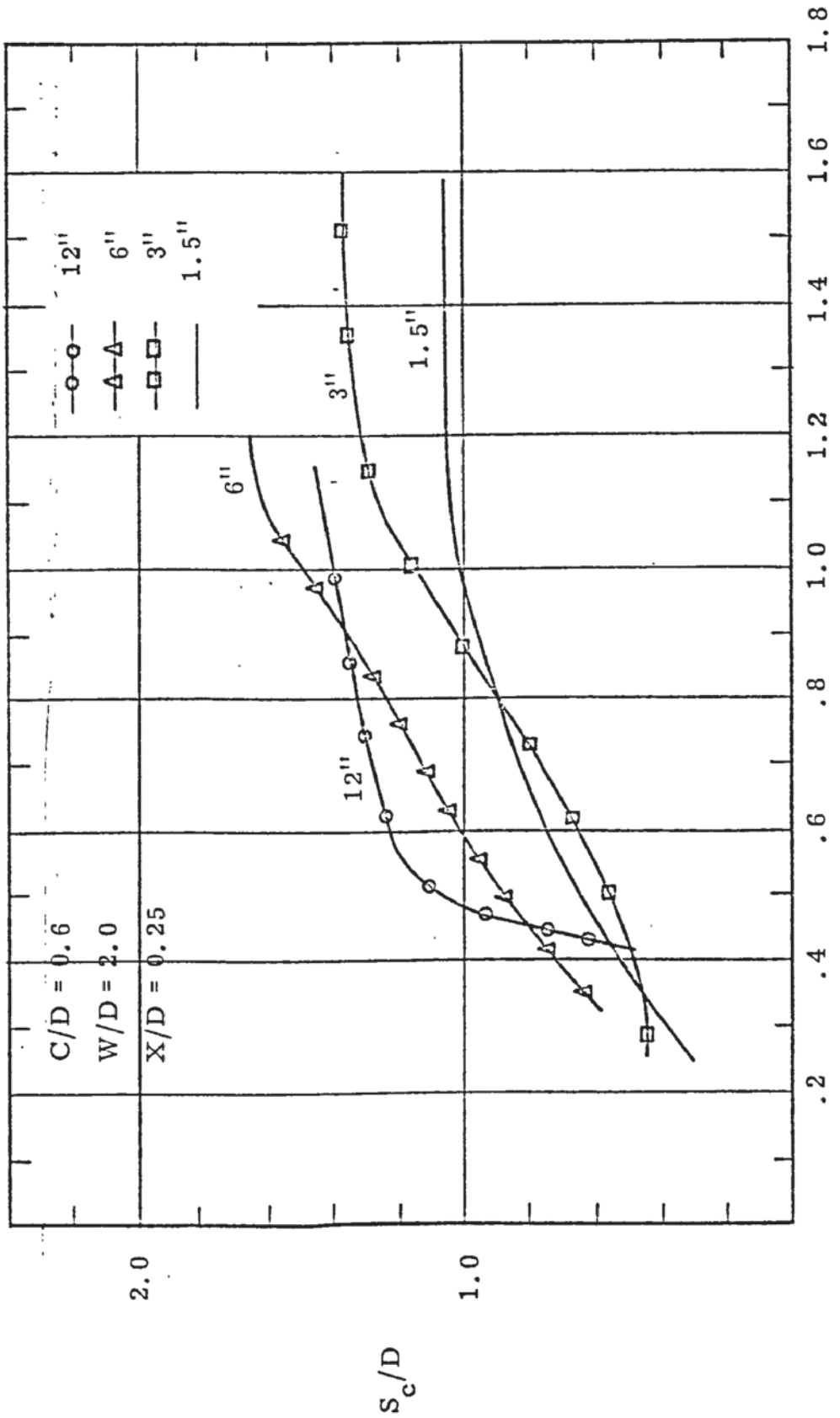

Fig. 6.27 Graph of critical submergence S_c/D against bellmouth velocity V_D for the four rigs, C/D = 0.6

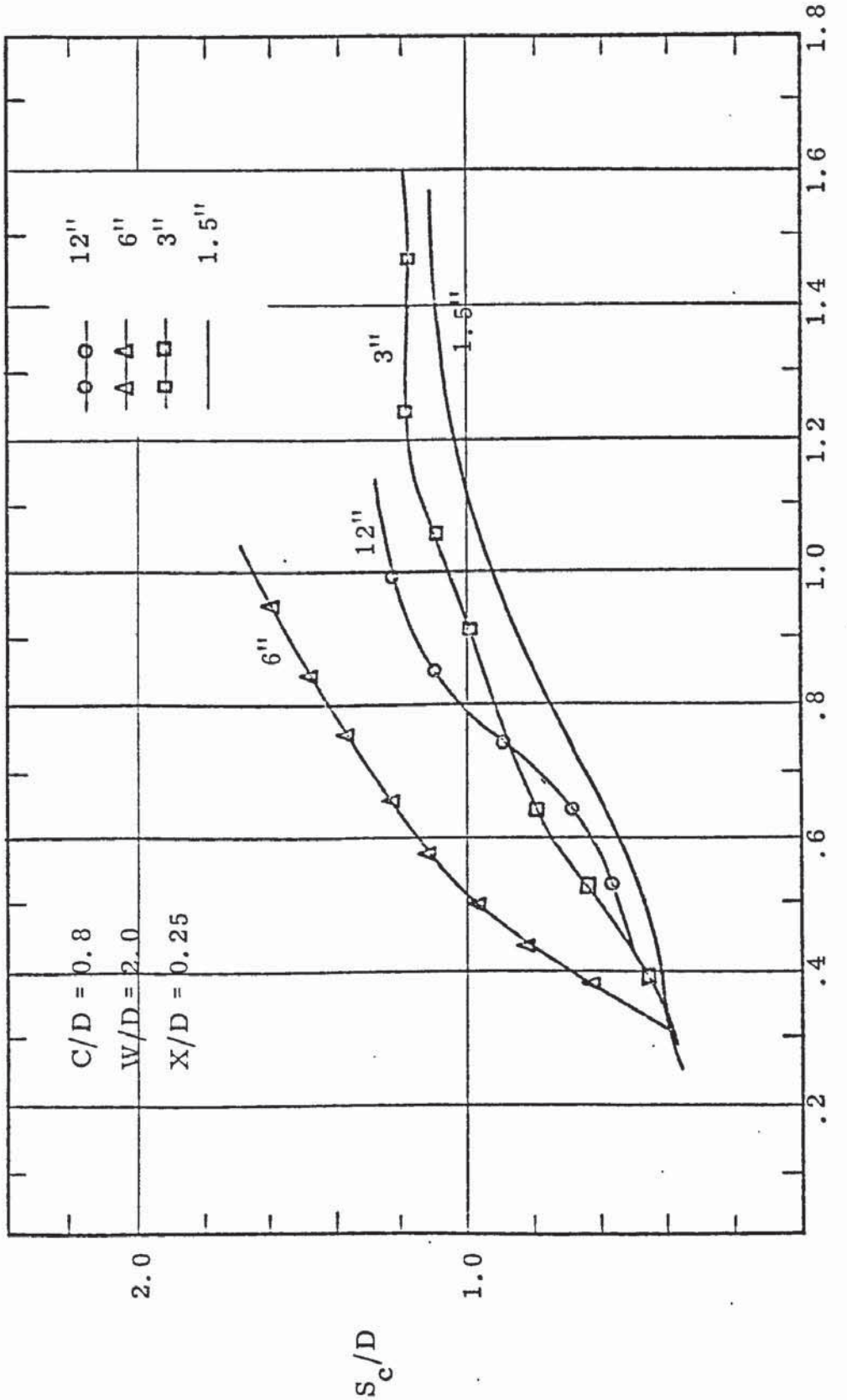

Fig. 6.28 Graph of critical submergence S_c/D against bellmouth velocity V_D for the four rigs, C/D = 0.8

Fig. 6.29 Comparison of bounding submergence S_B/D for the four rigs, width W/D = 2.0, endwall clearance X/D = 0.25

C/D	Rig Size	S_B/D	H_B/D
0.4	1.5"	1.4	1.8
	3"	1.5	1.9
	6"	2.1	2.5
	12"	1.6	2.0
0.6	1.5"	1.1	1.7
	3"	1.4	2.0
	6"	1.7	2.3
	12"	1.6	2.2
0.8	1.5"	1.1	1.9
	3"	1.2	2.0
	6"	1.8	2.6
	12"	1.4	2.2
0.6 + baffle at 6D	1.5"	1.0	1.6
	6"	1.7	2.3

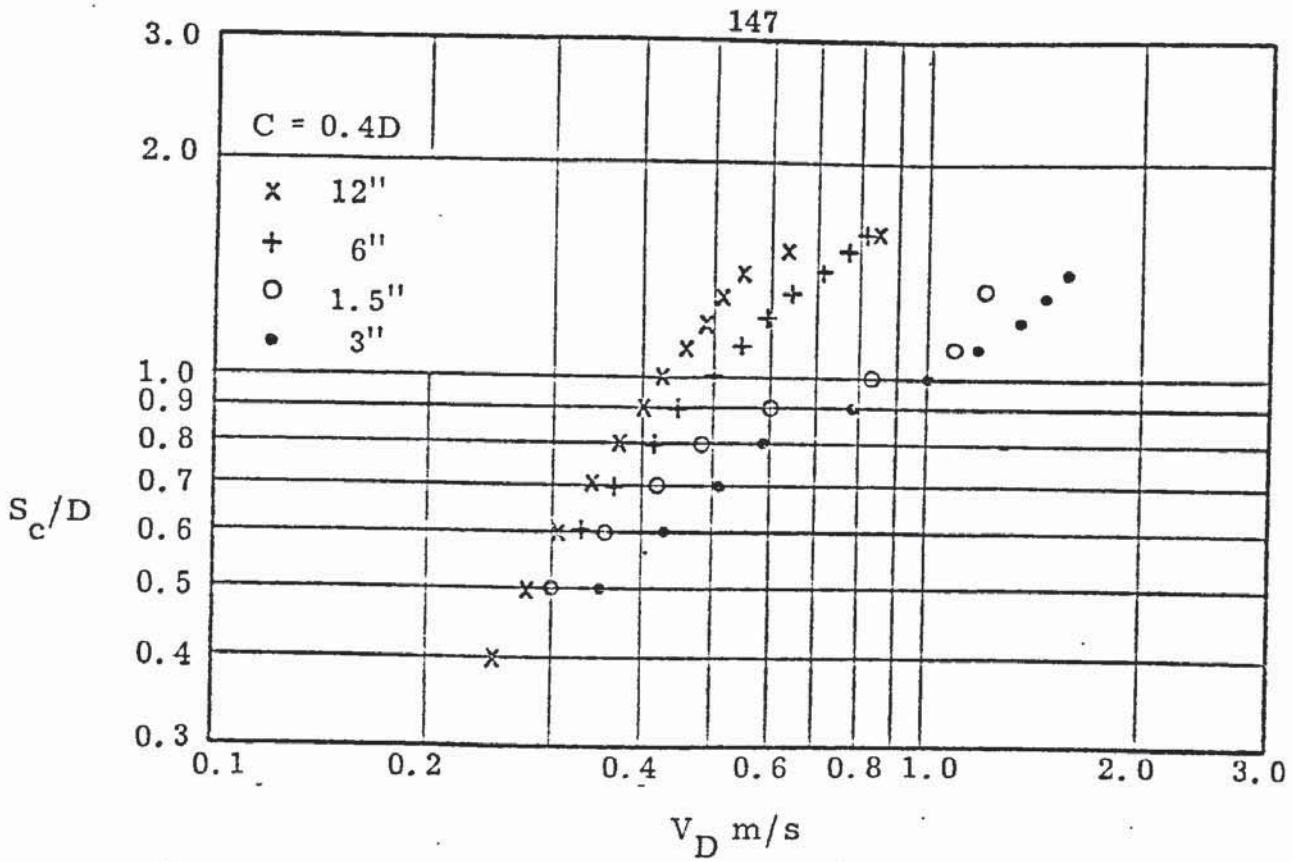

Fig. 6.30 Graph of log S_c/D against log V_D for the various size rigs and hence various values of bellmouth diameter D.

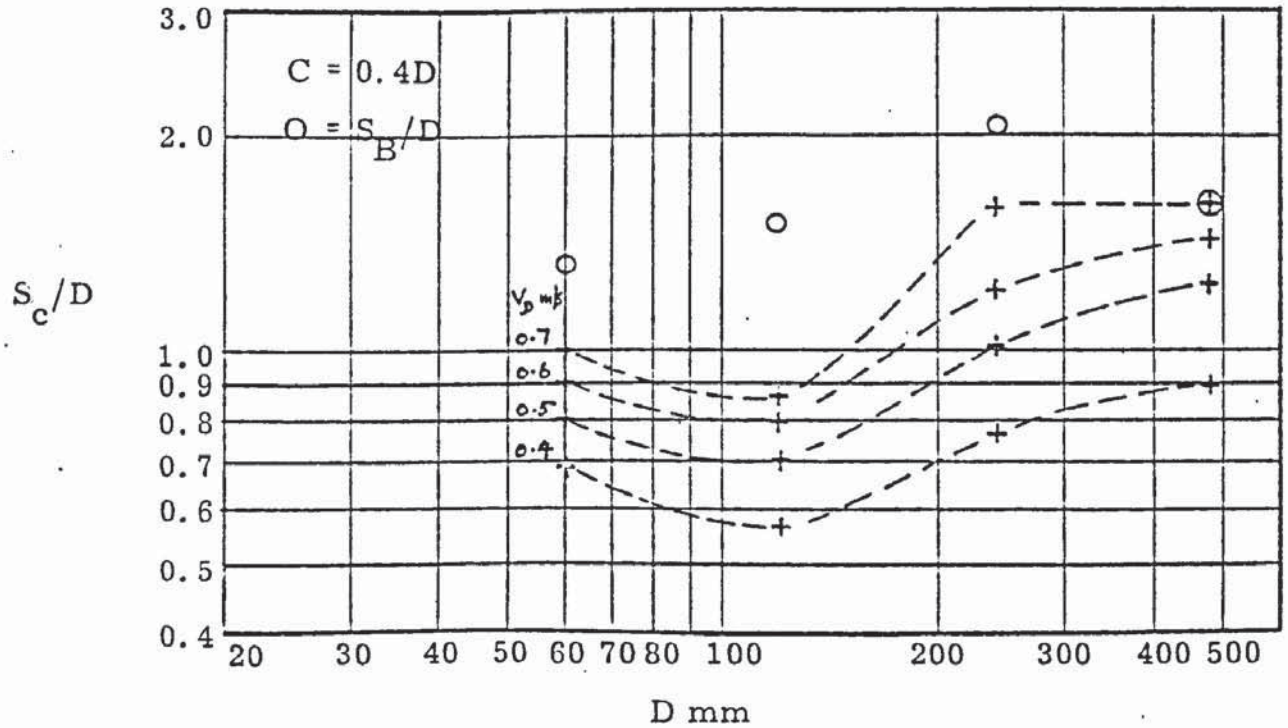

Fig. 6.31 Graph of log S_c/D against log D for various values of bellmouth velocity V_D. Values of bounding submergence S_B/D have been plotted by circles O.

Fig. 6.32 Table of values of velocity ratio $V_m/V_p = f(s)$, $k(s)$ and b for values of critical submergence S_c/D in the range 0.6 to 1.2 and floor clearances C/D of 0.4, 0.6 and 0.8.

	S_c/D						
	0.6	0.7	0.8	0.9	1.0	1.1	1.2
C/D = 0.4							
$f(\frac{1}{2})$	1.06	1.09	1.14	1.13	1.16	1.20	1.22
$f(\frac{1}{4})$	1.39	1.50	1.59	1.98	2.33	2.59	2.76
$f(\frac{1}{8})$	1.16	1.24	1.32	1.53	1.95	2.39	2.76
$k(\frac{1}{2})$	1.54	1.54	1.61	1.60	1.64	1.70	1.73
$k(\frac{1}{4})$	2.78	3.00	3.18	3.96	4.66	5.18	5.52
$k(\frac{1}{8})$	3.28	3.51	3.73	4.33	5.52	6.76	7.81
$b(\frac{1}{2})$		0.71			0.91		
$b(\frac{1}{4})$		1.13			3.11		
$b(\frac{1}{8})$		0.62			1.26		
C/D = 0.6							
$f(\frac{1}{2})$	0.77	0.86	0.98	1.07	1.18	1.31	1.36
$f(\frac{1}{4})$	1.26	1.43	1.60	1.72	1.82	1.90	1.86
$f(\frac{1}{8})$	1.07	1.23	1.47	1.72	1.97		
$k(\frac{1}{2})$	1.09	1.22	1.39	1.51	1.67	1.85	1.92
$k(\frac{1}{4})$	2.52	2.86	3.20	3.44	3.64	3.80	3.72
$k(\frac{1}{8})$	3.03	3.48	4.16	4.86	5.57		
$b(\frac{1}{2})$		0.23			1.00		
$b(\frac{1}{4})$		1.02			1.71		
$b(\frac{1}{8})$		0.62			1.27		
C/D = 0.8							
$f(\frac{1}{2})$	0.65	0.61	0.61	0.62	0.64	0.67	0.67
$f(\frac{1}{4})$	0.75	0.76	0.90	1.04	1.18	1.25	1.26
$f(\frac{1}{8})$	1.14	1.12	1.20	1.30	1.44	1.61	
$k(\frac{1}{2})$	0.92	0.86	0.86	0.88	0.91	0.95	0.95
$k(\frac{1}{4})$	1.50	1.52	1.80	2.08	2.36	2.50	
$k(\frac{1}{8})$	3.22	3.17	3.39	3.68	4.07	4.55	
$b(\frac{1}{2})$	-0.70	-0.12	-0.10	-0.08			
$b(\frac{1}{4})$		0.23		0.68			
$b(\frac{1}{8})$		0.53		0.79			

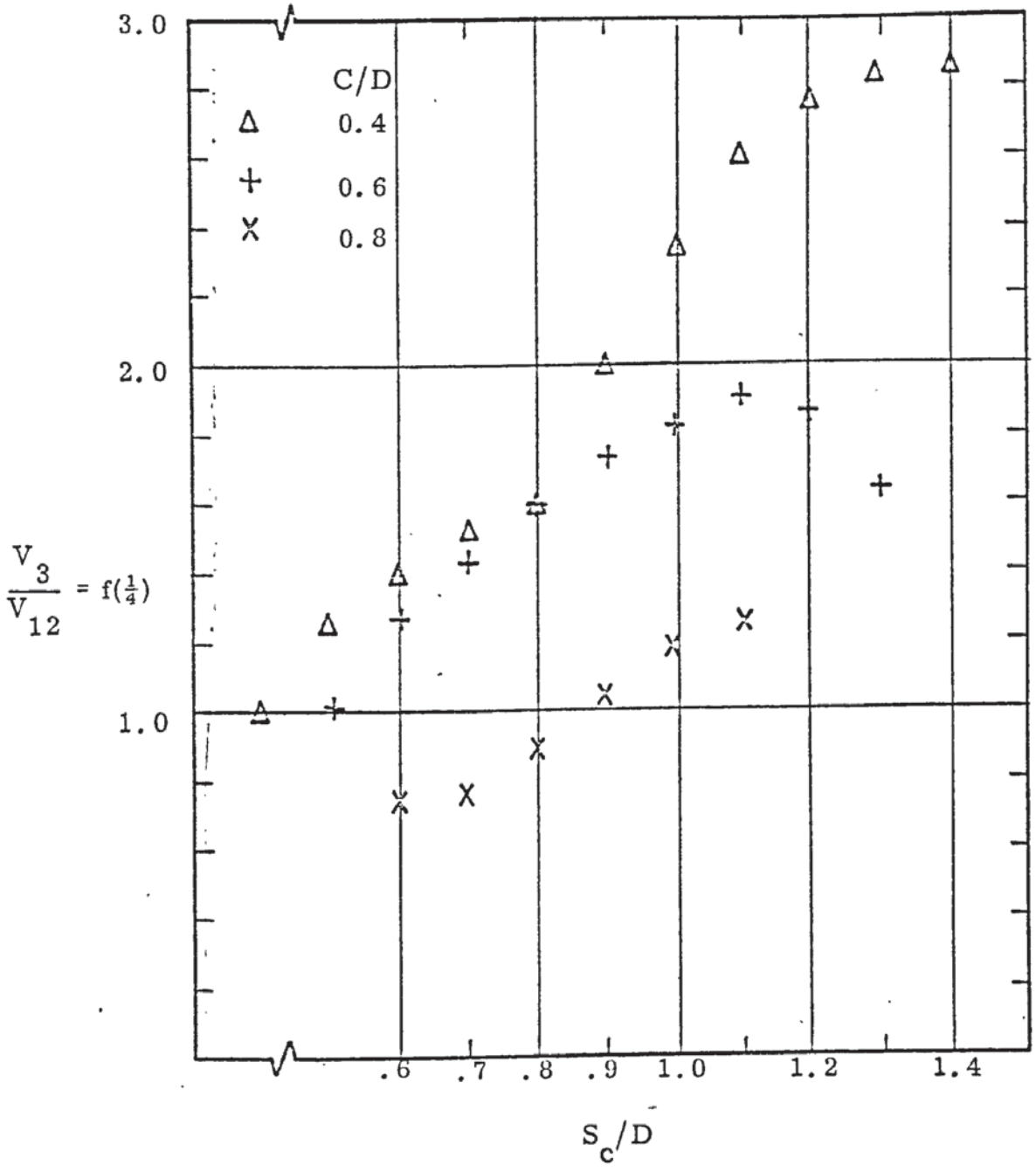

Fig. 6.33 Plot of velocity ratio $V_3/V_{12} = f(\frac{1}{4})$ against critical submergence for values of floor clearance C/D of 0.4, 0.6 and 0.8.

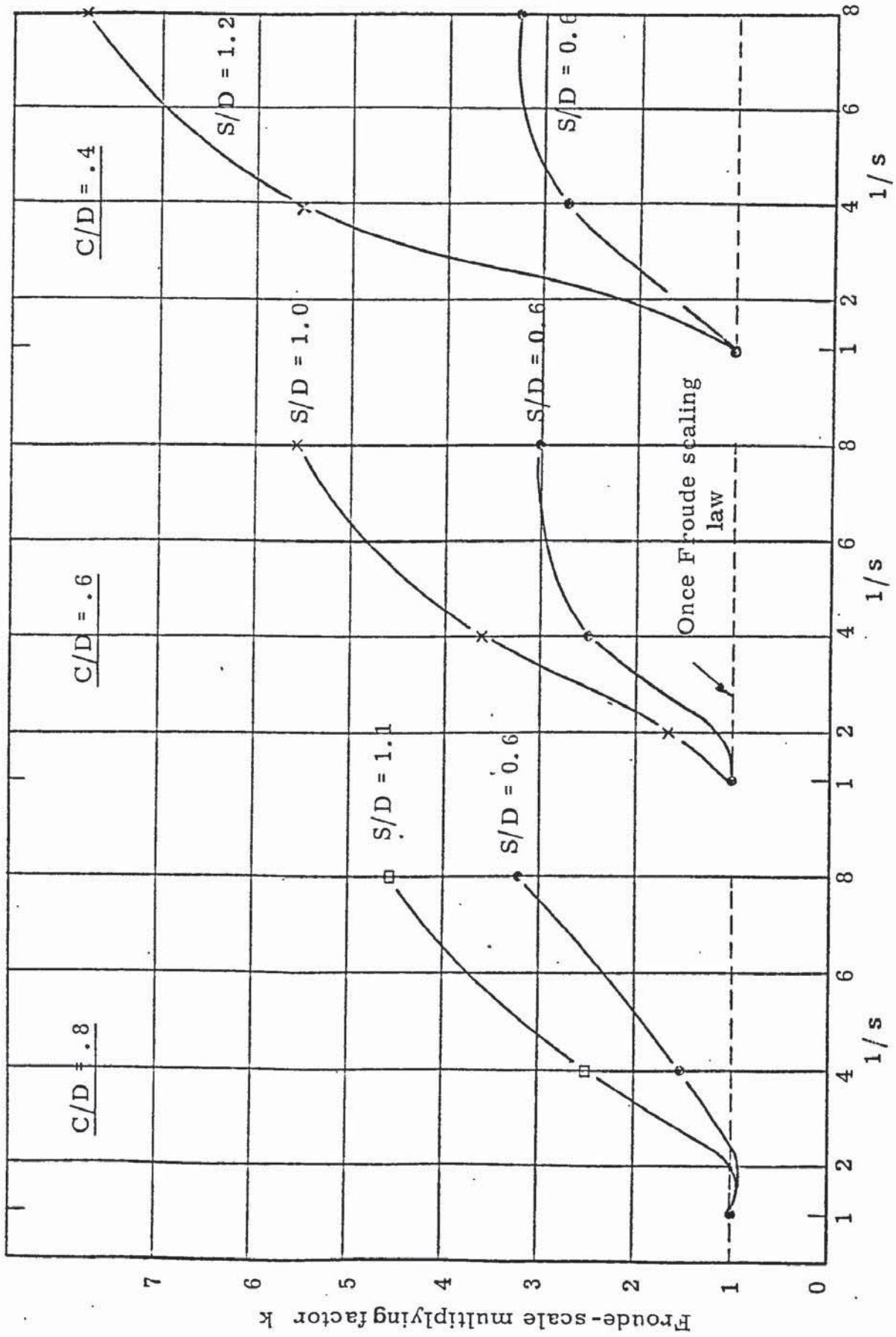

Fig. 6.34 Graph of the Froude-scale multiplying factor k against the inverse scale ratio 1/s for a range of submergences S/D and floor clearances C/D.

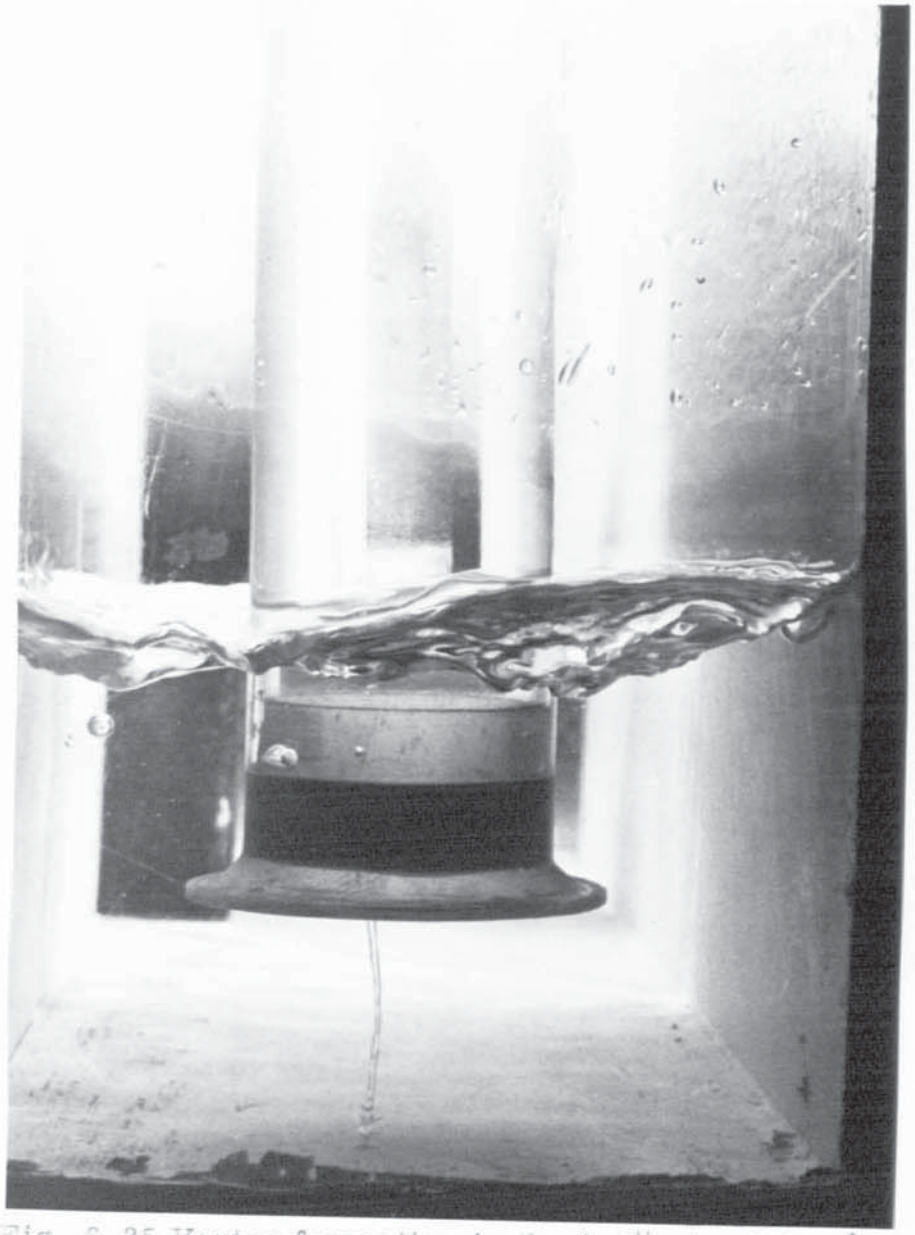

Fig. 6.35 Vortex formation in the 1.5" rig with a $\frac{1}{2}$D baffle placed 6D upstream of the endwall, (left hand wall in photo). S/D = 0.6, V_D = 1.04 m/s.

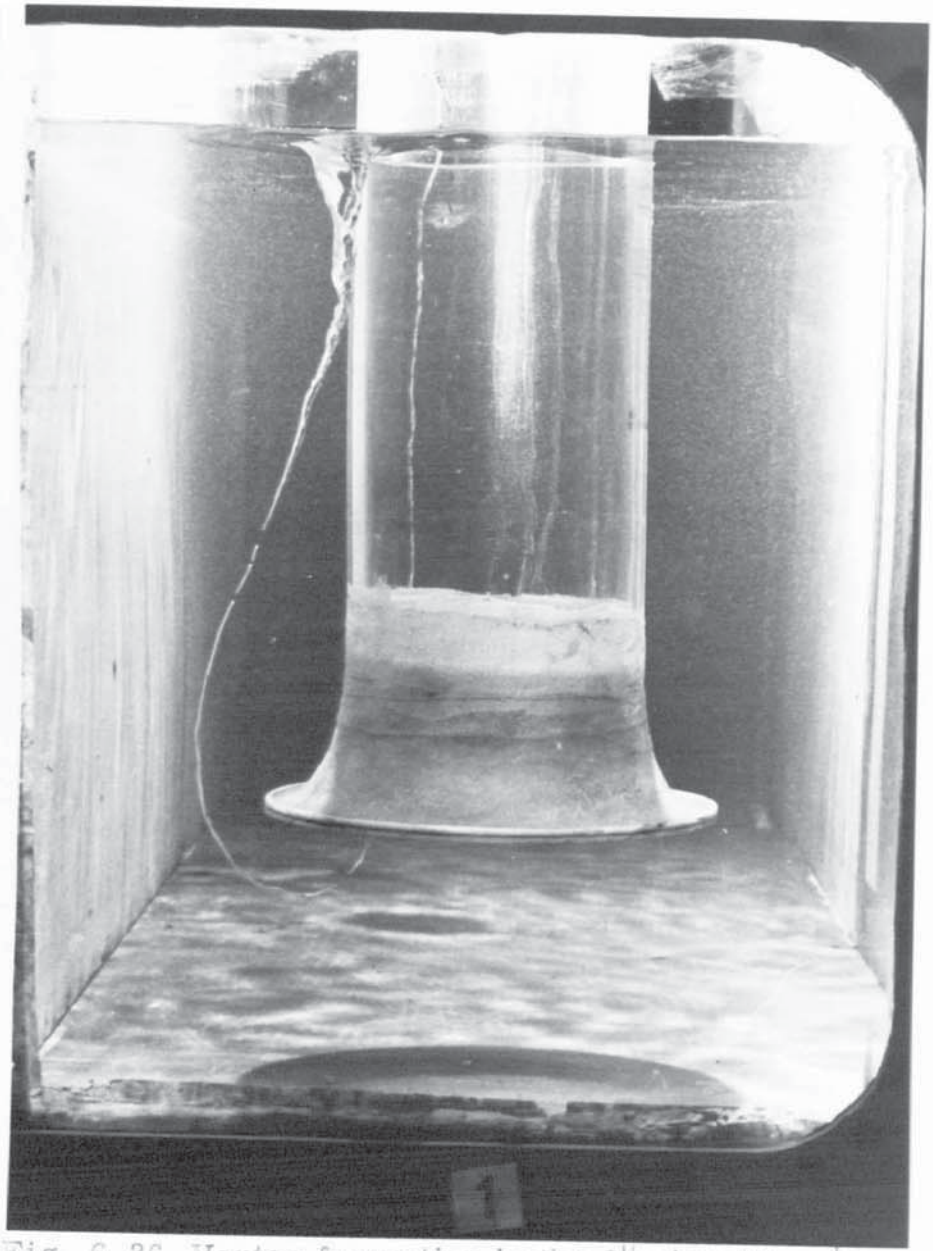

Fig. 6.36 Vortex formation in the 6" rig with a $\frac{1}{2}$D baffle placed 6D upstream of the endwall (left hand side in photo) S/D = 1.4, V_D = 1.04 m/s.

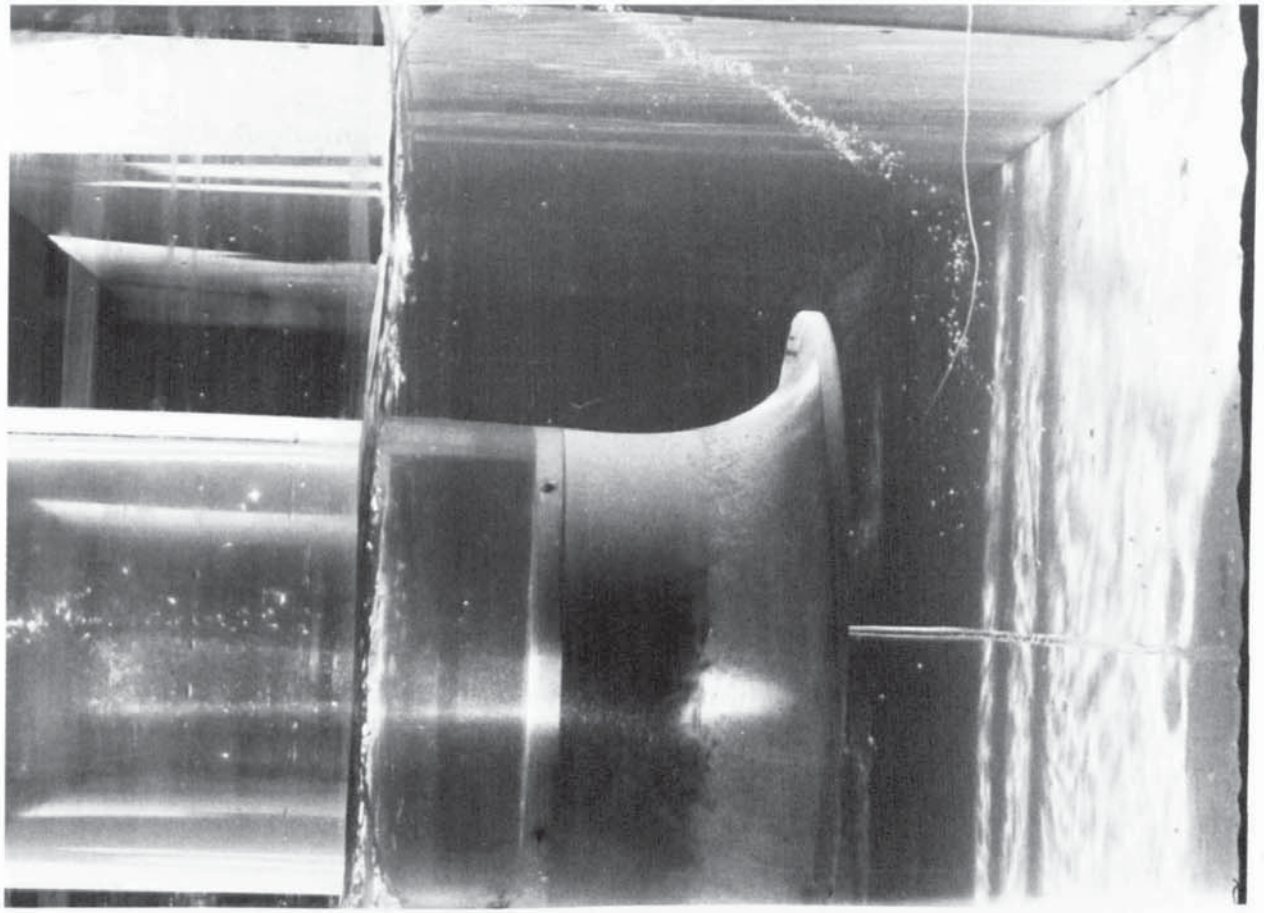

Fig. 6.38 Vortex formation in the 12" rig with a $\frac{1}{2}$D baffle placed 6D upstream of the endwall (right hand side in photo), S/D = 0.6, V_D = 1.04 m/s.

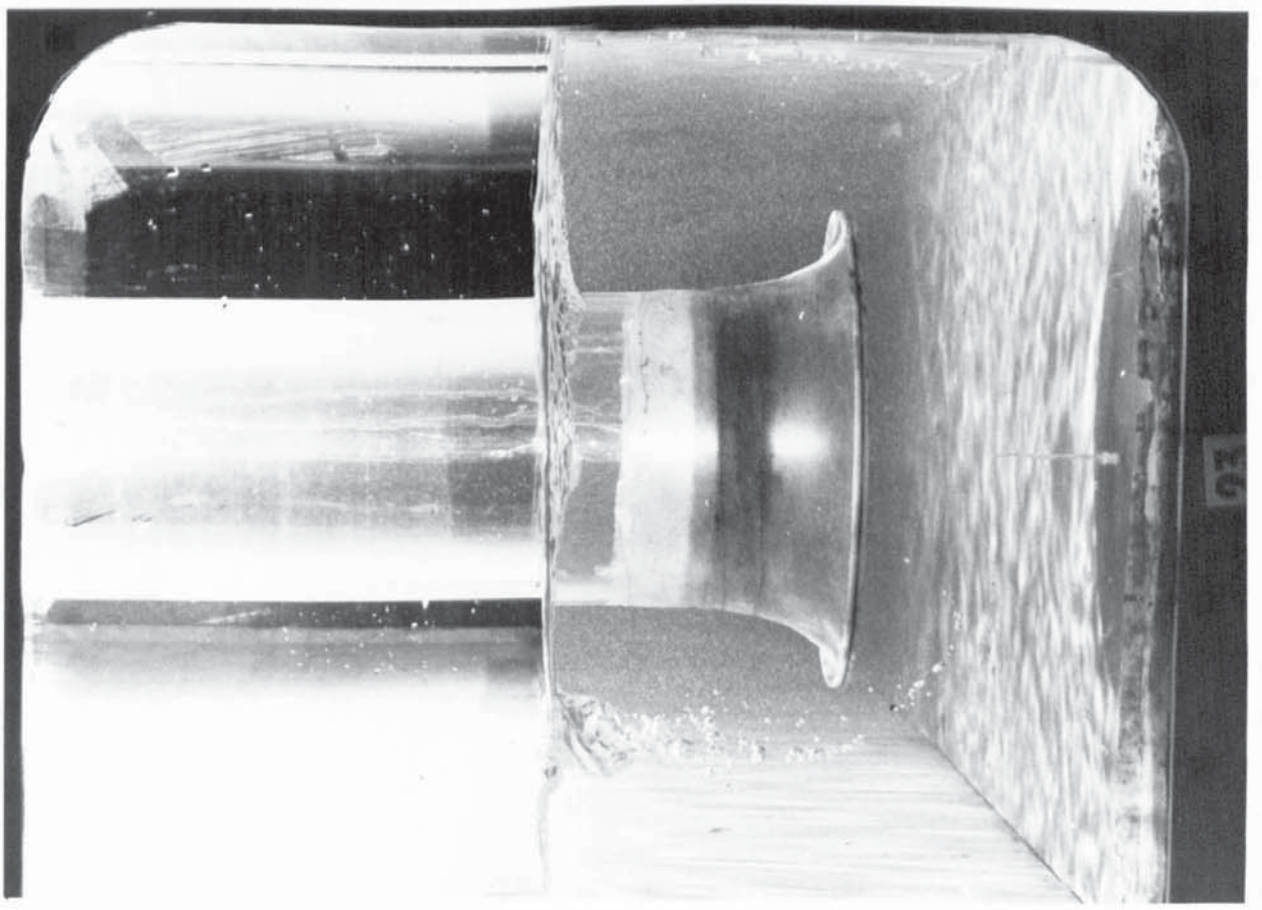

Fig. 6.37 Vortex formation in the 6" rig with a $\frac{1}{2}$D baffle placed 6D upstream of the endwall (left hand side in photo), S/D = 0.6, V_D = 1.04 m/s.

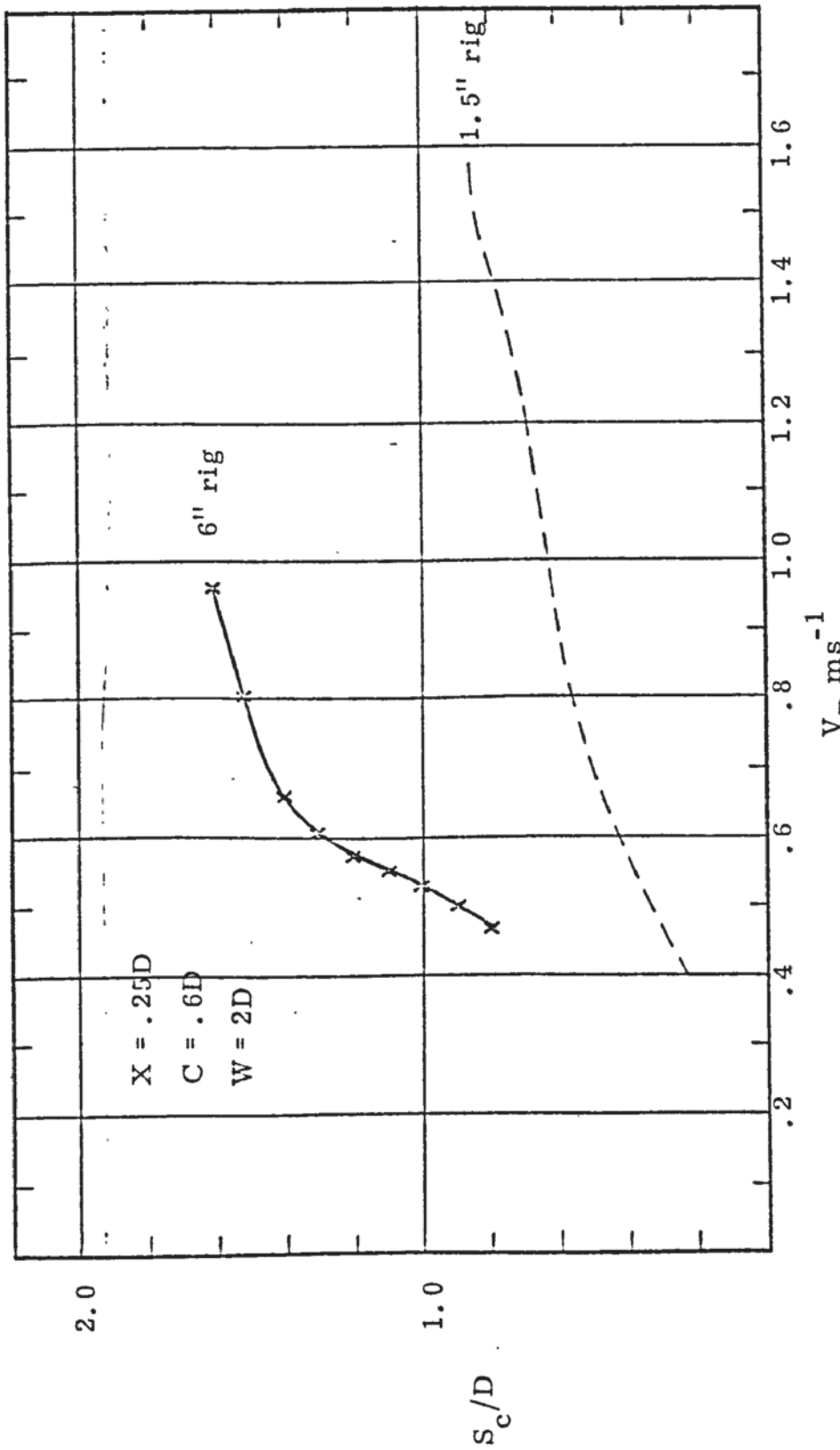

Fig. 6.39 Graph of critical submergence S_c/D against bellmouth velocity V_D for the 1.5" rig and 6" rig, both with a $\frac{1}{2}$D baffle 6D upstream of the endwall.

CHAPTER 7

EXAMPLE OF A MODEL STUDY

7.1 Introduction

The practical problems encountered in an actual model study are discussed in this chapter. The study concerns the recirculating cooling water intake structure at the Kori nuclear power station and is reported in more detail in refs. 17 and 72. There were two sumps involved, unit 1 and unit 2, and both involved aspects of multiple pump sump design and free surface vortex formation relevant to the general research programme. A photograph of the combined model, which was built to a scale 1:15, is shown in Fig. 7.1 with unit 1 on the right-hand side and unit 2 on the left.

7.2 Description of Kori unit 2

This unit is discussed first, since it is an illustration of the more usual and preferred order of events: initial design → model study → design modifications → prototype construction. In actual fact, unit 1 was built first, so the design of unit 2 was influenced to a certain extent by the existing structure for unit 1. In unit 2, sea water flows through two rectangular culverts (bottom, centre Fig. 7.1) into a common forebay which serves both units. The flow then passes through four vertically suspended pumps to a discharge culvert. The nominal duty of each pump when all four pumps are in operation is 141,000 UK gpm (10.7 m^3/s), increasing to 181,000 UK gpm for one-pump operation. It was assumed that the bell-mouth diameter would be 90" (2.3m) as for unit 1.

At the initial design stage, it was decided that a unitised sump design would be preferable to an open design, since each pump "cell" would then

be unaffected by different combinations of pump and bandscreens in operation. The various geometric parameters for the sump (see 4.3.4) closely follow those recommended in refs. 1 and 2. The channel length was a compromise between good approach flow and minimum excavation costs. A plan view of the initial model design is shown in Fig. 7.2, and it can be seen that the design of each pump bay is similar to that used in the experimental rigs described in Chapter 5.

The model was built to a linear, undistorted scale of 1 to 15. Materials used were plywood and perspex to allow easy observation of flow conditions. The shape of the bandscreens and their exit ports were correctly modelled and wire mesh of 50% blockage was used to model the prototype screen material. Each of the four pumps was represented by four vertical lengths of perspex pipe, each having a geometrically scaled fibreglass bellmouth (fig. 7.3). A vortometer was placed in each pipe just above the bellmouth to indicate the degree of swirl in the approach flow to the pump impeller.

In order to model vortex formation, past experience at BHRA suggested that a velocity exaggeration above Froude scale of 1.5 times Froude scale velocity would be adequate for this model scale, i.e. the multiplying factor $k = 1.5$ and

$$\frac{V_m}{V_p} = 1.5\,(1/15)^{\frac{1}{2}} = 0.39$$

and

$$\frac{Q_m}{Q_p} = 1.5\,(1/15)^{5/2} = 0.0017$$

Thus, for any given pump combination, the model flow rates, Q_m and bellmouth velocity V_D, were fixed. Observations were made of

surface vortices, submerged vortices and swirl for various water levels covering the normal tidal range expected on the prototype. The most detailed tests were done at the lowest level where vortices would be most severe.

It was found that the initial sump design gave very little surface vortex activity. However, there was a high degree of swirl and strong submerged vortices due to the high velocity jets issuing from the bandscreens. These attached to one side of the pump chamber, leading to asymmetric approach flow. This shows the importance of uniform approach flow, even when sump dimensions follow recommended design practice.

The final design (Figs. 7.4 and 7.5) incorporated a bandscreen splitter wall to give a more uniform velocity distribution across the chamber and a bellmouth splitter to reduce submerged vortex activity. The short diffusers at the bandscreen exits were not effective and thus removed. Also, it is interesting to note that in this sump design, the corner fillets encouraged the formation of submerged vortices and were thus also removed. The usual reason for fitting corner fillets is to reduce the critical submergence, but in this case, there seemed to be sufficient submergence anyway at the lower level to prevent air-entraining surface vortices.

7.3 Description of Kori unit 1

This unit was the first one to be built on site. It was designed without the aid of a model study and on commissioning of the pumps, there was considerable noise and vibration reported, together with gearbox failure. Since there were some doubts about the hydraulic design, BHRA was asked to conduct a model study to investigate and improve on the hydraulic conditions in the existing sump. Extensive modifications were required, and

these, together with stiffening of the motor supports, eventually enabled the power station to reach 100% generating capacity. The economic implications of bad hydraulic design have been discussed in Chapter 2.

The original design of unit 1 is shown in Fig. 7.6. Water in the forebay passes through five travelling bandscreens into an open sump. Then, four vertically suspended, mixed flow pumps discharge the water into a discharge culvert. The nominal duty of each pump is 138,000 UK gpm (10.5 m^3/s), with a bellmouth diameter 90" (2.3m). Because of the open design, the effect of closing any one bandscreen, together with different combinations of 4, 3, 2, or 1 pump in operation, was pronounced, and therefore all 66 possible combinations were tested in the final design at the lowest storm tide level.

The model scale was again 1 to 15, and its construction was similar to that of unit 2. Also, most tests were done at 1.5 times Froude-scale velocity, though selected check tests were also made at other velocities.

It was found that a major factor responsible for the unacceptable hydraulic conditions in the sump was the short distance between the bandscreens and the pump centreline. This meant that the expanding jets from the bandscreen outlets did not have sufficient distance to dissipate excess energy and even out non-uniform velocity distributions before reaching the pumps. Furthermore, the large clearance of 1.37D between the pumps and the endwall allowed surface vortices and swirl to develop. Also, the three roof support pillars were very close to the line of the pumps so that when there was flow past the pillars, vortices were shed which could enter the pump-intake.

The final recommended sump geometry is shown in Figs. 7.7 and

7.8. This design emerged after numerous intermediate modifications had been tested and found to be unacceptable in one way or another.

The main features of the final design are :-

a) Decreased rear wall clearance - the distance between the rear wall and the bellmouth lip is 0.3D, D being the bellmouth diameter, compared with 1.37D in the original design.

b) Rectangular bays - these are of width 2D (slightly narrower for pumps A and B), height 9.0' (2.74 m) and help to achieve symmetry in the flow approaching each pump, regardless of the combinations of pumps and bandscreens in operation.

c) Horizontal shelf - this lies on top of the bays and acts as a horizontal roof, 9.0' from the sump floor. To facilitate removal of the complete pump unit, an annular gap exists between the pump column and the shelf. The shelf reduces the occurrence near the pumps of strong surface vortices whose tails would otherwise enter the bellmouth and entrain air continuously.

d) Vertical bar screen - it was also found necessary to fix a screen of 50% blockage across the entrance to each pump bay. This reduces the intensity of, and breaks up the 'tails' of the remaining vortices which cannot be completely eliminated. Furthermore, the screens are effective in reducing the turbulence and non-uniformity of the flow conditions to each pump.

7.4 Relevance to the hydraulic design of multiple pump sumps

The above two sections on units 1 and 2 bring out several interesting features that arise in an actual model study, and influence sump design for multiple pump sumps. Firstly, it was seen that not only surface vortices

have to be eliminated but also submerged vortices and swirl. It is uncertain to what extent the latter two affect pump performance, but they should be minimised as far as possible. A recent paper (85) concluded that intermittent submerged vortices gave rise to only slight vibrations in the lower pump casing of about 4 mm at a frequency of 10 Hz. This was based on prototype measurements and observations of a 1 to 10 scale model run at once-Froude scale velocity. It was not considered necessary in this case to eliminate the submerged vortices.

Secondly, the model study shows the importance of having a uniform approach flow. The various recommendations given in design guides will only give all-round satisfactory hydraulic performance if there is uniform approach flow; hence the desirability of a unitised design in situations where one or more pumps and/or the bandscreens may be out of operation. In addition, a large distance between the bandscreen exit ports and the line of the pumps is necessary in order to obtain uniform flow. In more severe cases, as in unit 1, a full-width vertical grid may also be necessary.

In the unitised sump design, the length of straight channel required for uniform flow is very sensitive to the first upstream disturbance (6.3.5) and will vary for different bandscreen designs (1). It seems that with the design used in units 1 and 2 where the approach flow turns through two right-angles and enters the pump chamber as a high velocity jet, an excessively long channel is needed for uniform approach flow. A better design would be a full-width, through-flow bandscreen where the flow direction is not turned from its original direction. Subsidiary tests in unit 1 (17) showed that a compromise design between an open sump and unitised sump, whereby each pump bay wall is full-depth and extends for a straight length of 2D (as in Fig. 7.7 but without the vertical grid) is not satisfactory.

Air-entrainment from vortices shed off the bay nosings becomes a problem together with submerged vortices for asymmetric pump/bandscreen combinations. Thus it is important to have an adequate length of pump bay.

Limited tests on submergence requirements and the effect of varying the endwall clearance, X/D, were made, the former for unit 2 and the latter for unit 1 (original design), in order to compare the behaviour of multiple pump sumps with the single "cell" described in the previous chapters. Fig. 7.9 shows the variation of critical submergence S_c/D, with bellmouth velocity V_D, for one pump running in the multiple pump sump of unit 2, with the bandscreen removed and a simulated pump casing as opposed to the straight suction pipes used in the experimental rigs. As with the single pump sump, S_c/D increases with increasing V_D but at the higher velocity limit of these test results, no definite type 4 vortices were observed due to surface disturbance and high turbulence levels. It is interesting to note that at 1.5 times Froude-scale velocity (V_D = 1.24 m/s), the critical submergence $S_c/D \simeq 1D$ which is substantially lower than the minimum available submergence of 1.9D and the value of 1.5D recommended in ref. 1. This implies that the floor level need not have been set so deep and that a model study at the design stage, after determining the optimum floor level, could have significantly reduced excavation costs. It is uncertain what the effect of the shape of the pump casings is, and this is an area needing further work.

The effect of changing X/D from 0.35 to 0.67 is shown in Fig. 7.10, obtained from the original open sump design of unit 1, with all bandscreens removed and replaced by a full-width perforated metal screen at the entrance to the bandscreen chambers and with the three support pillars also removed. All four pumps were running, and the occurrence of a type 4 vortex at any

pump was recorded. The results show an increase in S_c/D as the end-wall clearance is increased, showing the importance of minimising X/D to eliminate surface vortices in this design.

7.5 Discussion on scaling laws for free surface vortices

Scale models can be used to obtain information on scaling laws. The procedure would be to obtain a comprehensive S_c/D - V_D curve on the model, and then to repeat this as far as possible for the prototype. In practice, V_D is fixed on the prototype by the operating duty point of the pumps, so it is only possible to observe vortices with a variation in S/D. Plans are in preparation for this for the Steenbras pumped storage scheme, which has been extensively model tested (21) though prototype tests will concentrate on optimising the size of the installed anti-vortex grids, as discussed in Chapter 2.

A limited amount of prototype information is available on the initial behaviour of Kori unit 1 from reports of engineers who were present on site at that time (86). Pump A, running by itself failed first after only a few hours running, followed by C by itself after 200 hours. The only other combination tried was B and D together which was also unsatisfactory. However, it should be noted that no accurate information is available on the type of vortex that was present (since the sump is covered over by a concrete roof), the flow rates or the water levels during this commissioning period. Furthermore, one possible reason for the failure of the pumps was faulty gearbox construction and design.

Nevertheless, when these four observations are compared with results from the model (original design) for various scale velocities, shown in Fig. 7.11, it can be seen that type 3 and type 4 vortices occurred

on the model for velocities of 1.5 Froude scale and above for pump A alone, and at Froude scale and above for pumps B and D together. They were not observed for pump C alone. The tentative conclusion is that for a scale ratio of 1 to 15, a minimum model velocity of 1.5 times Froude scale is required to model air-entraining vortices, assuming these are the major cause of failure. This conclusion is not inconsistent with the scaling laws given in Fig. 6.34.

Another point of interest is to see if the scaling laws derived in 6.4.2. can be applied to this 1 to 15 scale model. The experimental results shown in Fig. 6.34 only extend to a scale ratio of 1 to 8, but extrapolation of the curves to higher scale ratios suggest k-factors considerably higher than the value of 1.5 actually used. Fig. 6.34 would be expected to apply to unit 2 where the unitised design is similar to the sump geometry used in the experiments, and it may well be that, provided the free surface was not excessively distorted and turbulent, the higher k values would be correct for vortex modelling. However, in this situation where the first upstream disturbance is due to a bandscreen, an excessive head drop across the bandscreen would develop as the model velocity was increased, thus artificially disturbing the free surface and suppressing vortex formation.

The geometry of unit 1, and hence the source of vorticity is quite different from that in the experiments. Asymmetry in the approach flow is the major factor, and so the scaling laws plotted in Fig. 6.34 would not apply.

Thus on the basis of limited data on prototype performance of unit 1, it has been found that a minimum model velocity of 1.5 times Froude scale was necessary to model air-entraining vortices for a scale ratio of

1 to 15. This k-factor of 1.5 is, however, less than that found from extrapolating the experimental results of Fig. 6.34. This discrepancy is to be expected for unit 1 because of the different source of vorticity as compared with the experimental rigs.

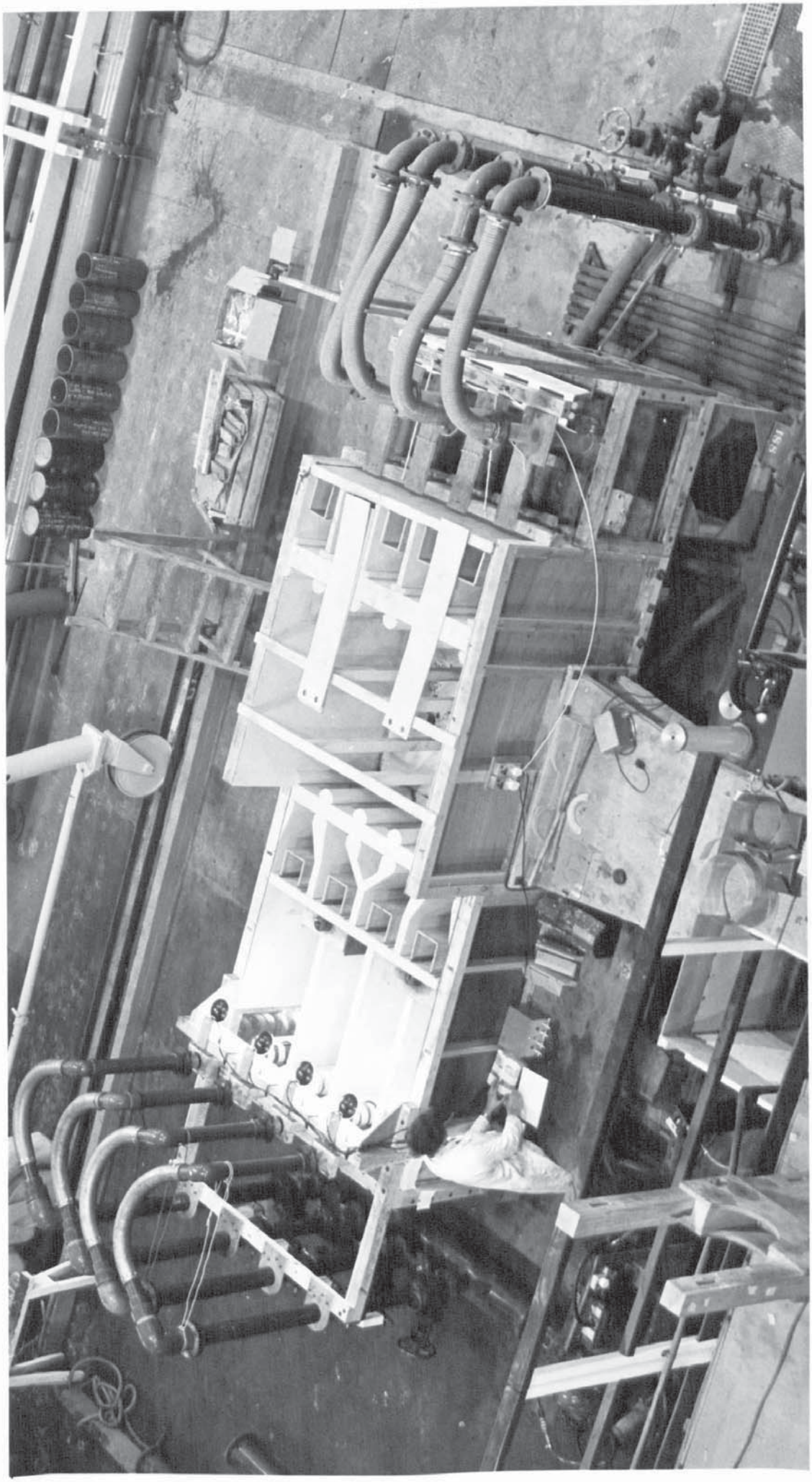

Fig. 7.1 Photo of model of combined Kori pump sump, No.1 unit (right hand side) and No.2 unit (left hand side). Seawater inlet culverts shown at bottom, centre.

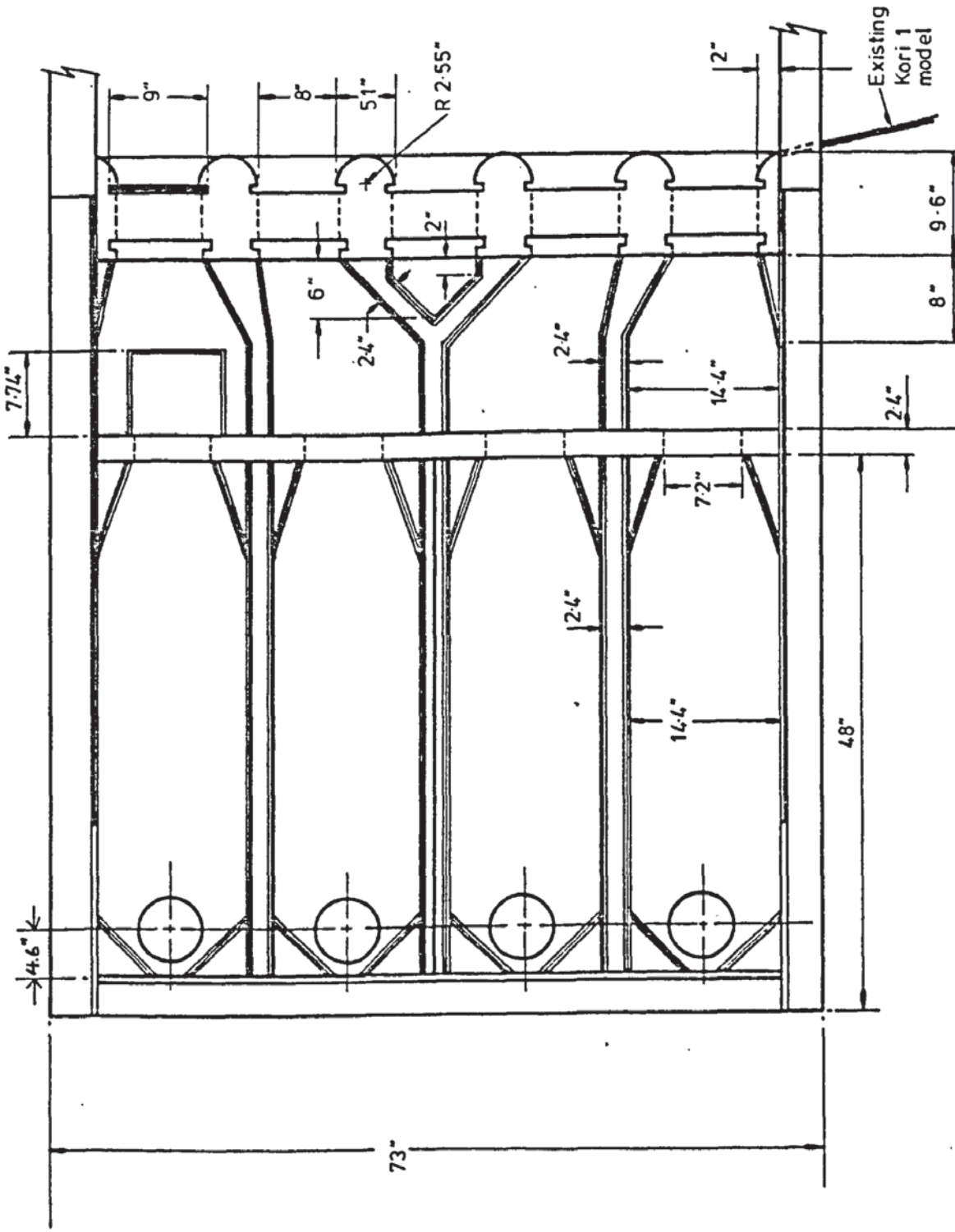

Fig. 7.2 Plan view of initial model design of No. 2 unit, showing unitised design.

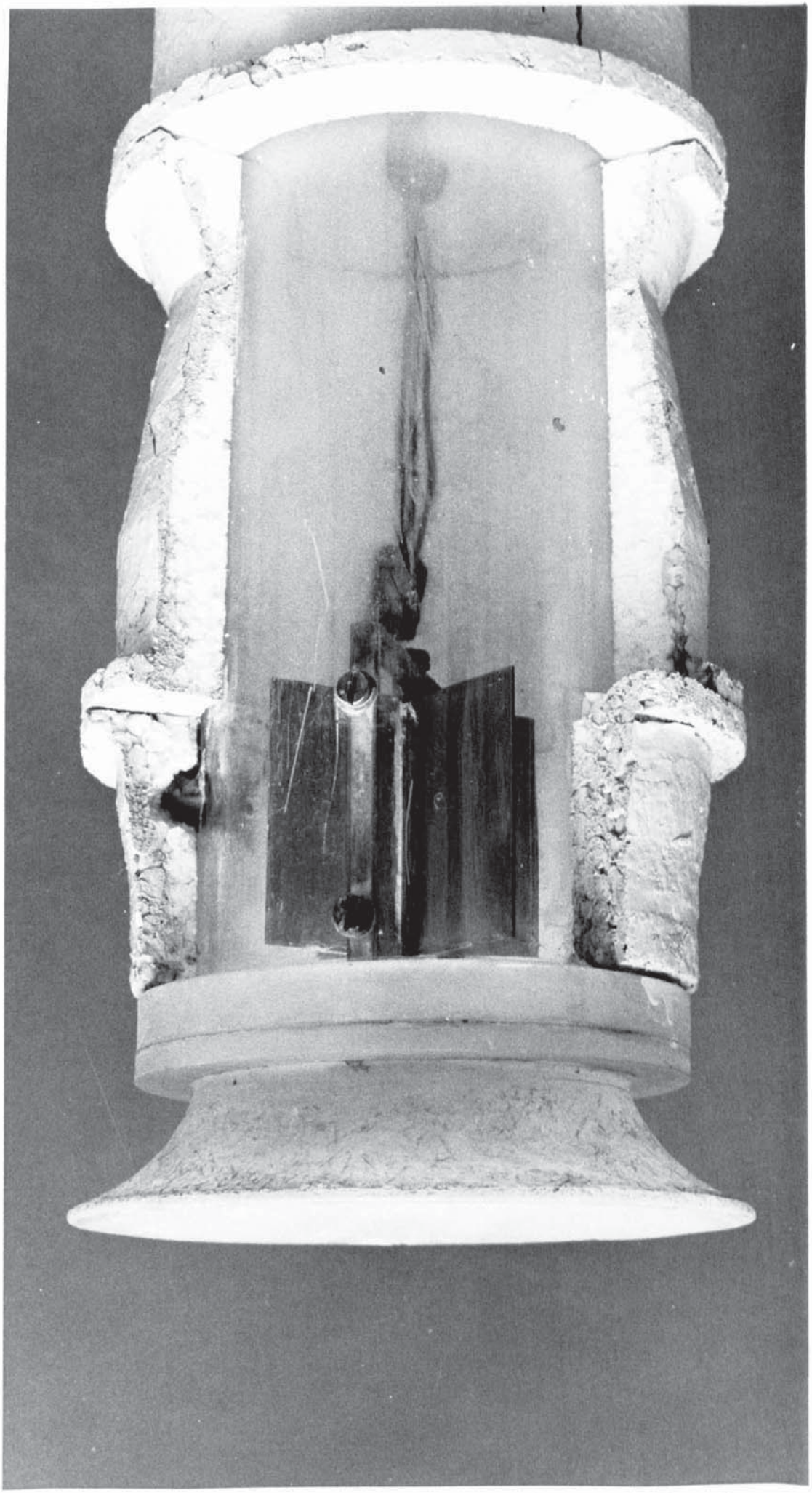

Fig. 7.3 View of bellmouth and pump casing partially cut away to show the vortometer (used for measuring swirl).

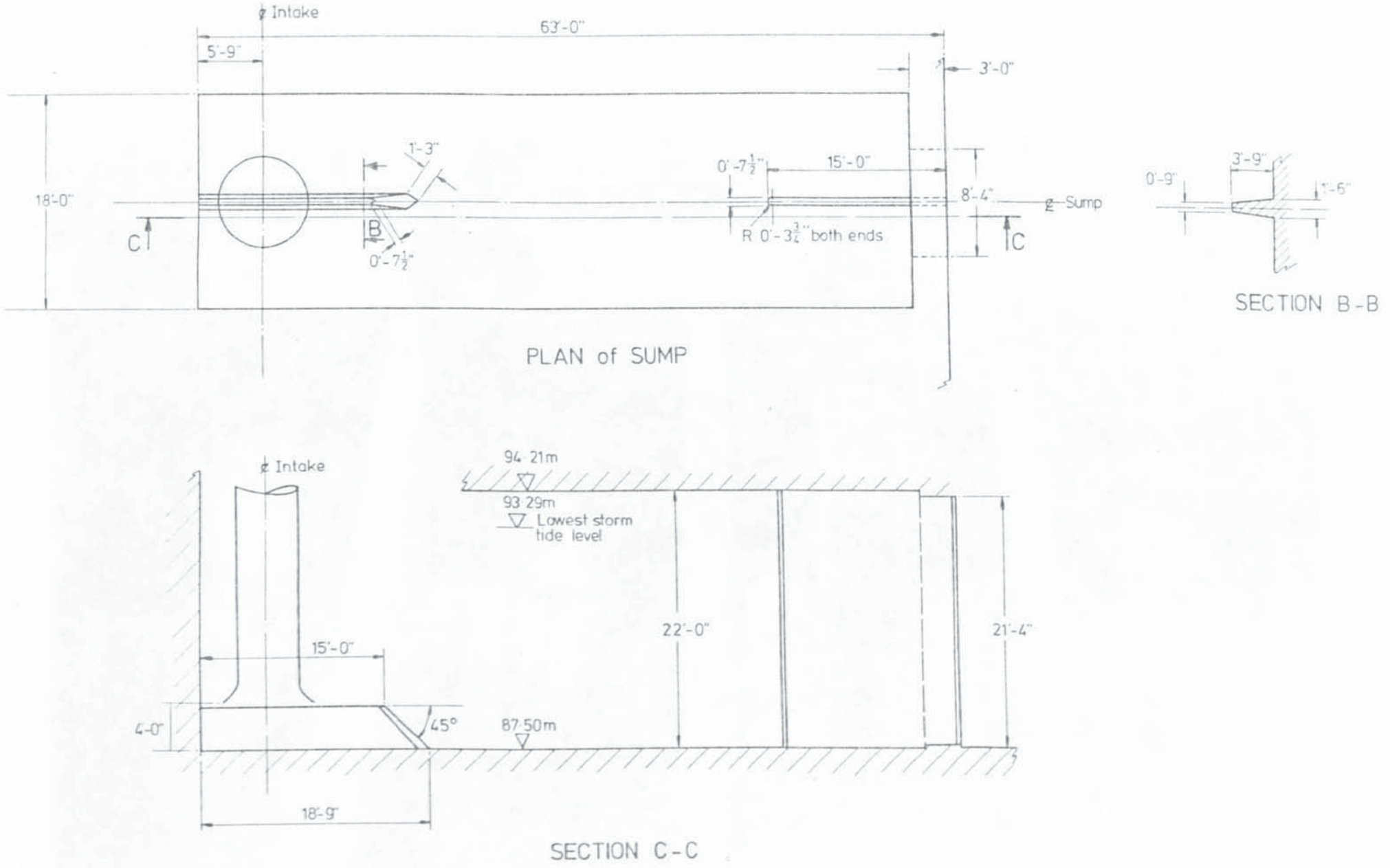

Fig. 7.4 Plan view and section of final design of one pump bay (No. 2 unit)

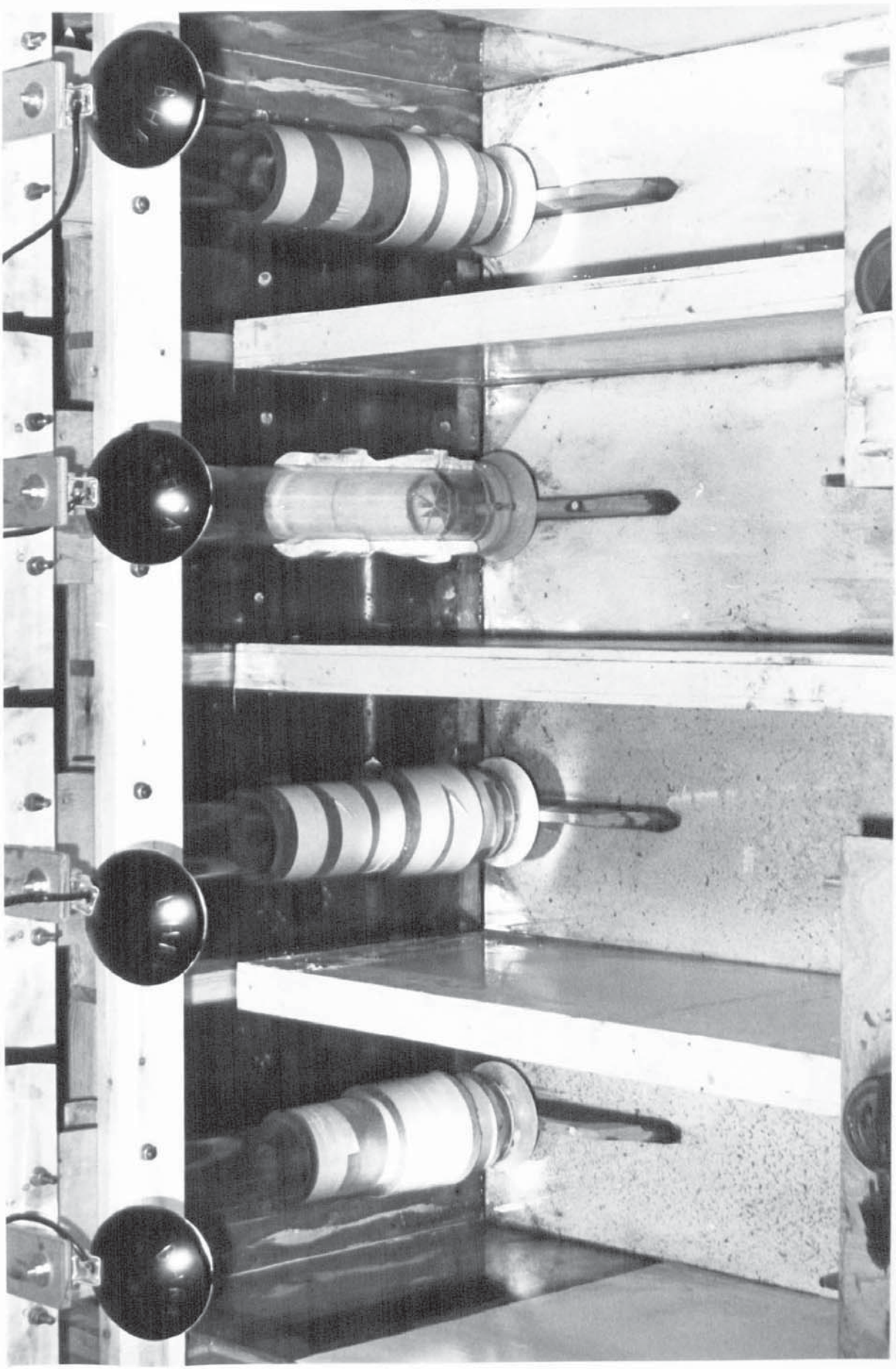

Fig. 7.5 Photo of final design of No. 2 unit, showing central splitters underneath each bellmouth, and splitter walls at each bandscreen outlet.

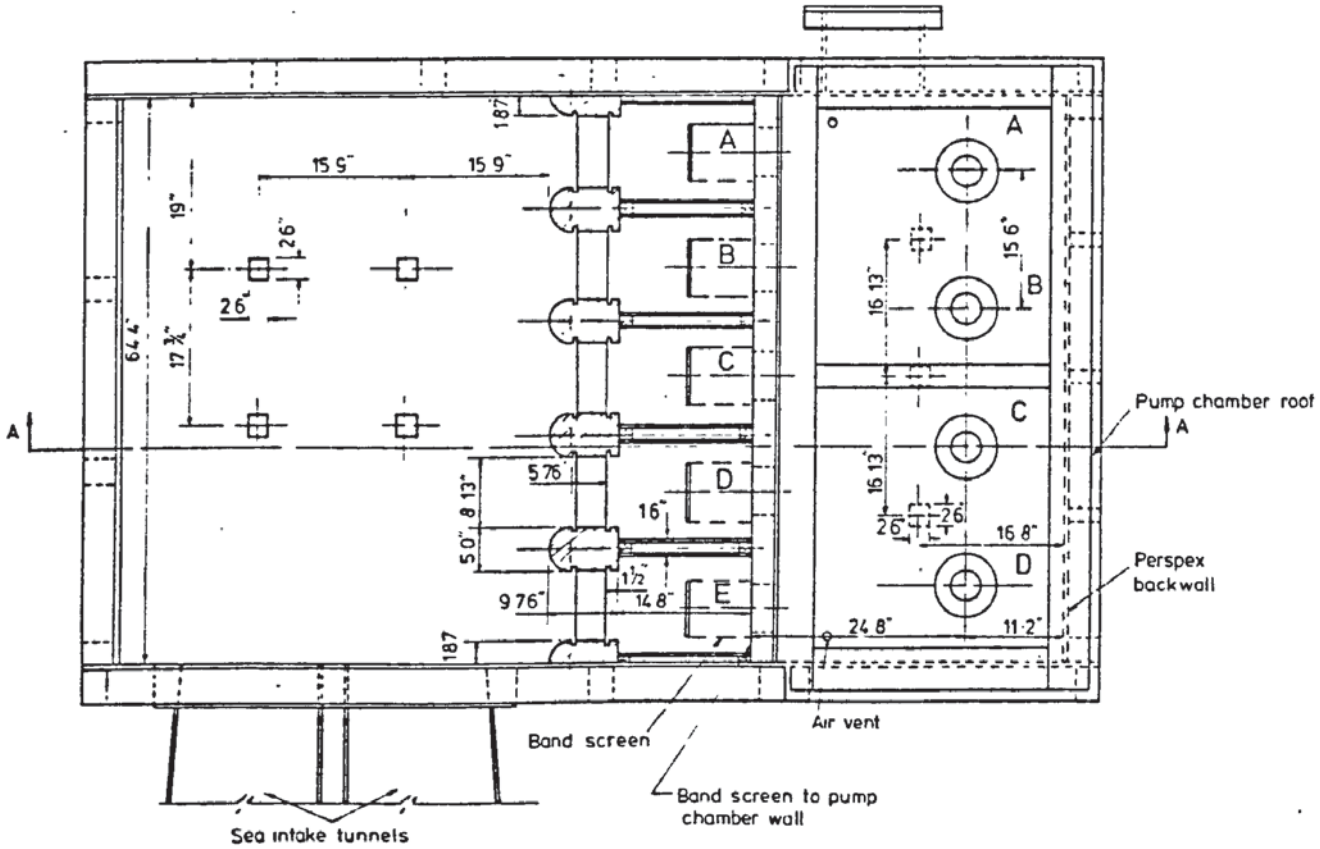

PLAN

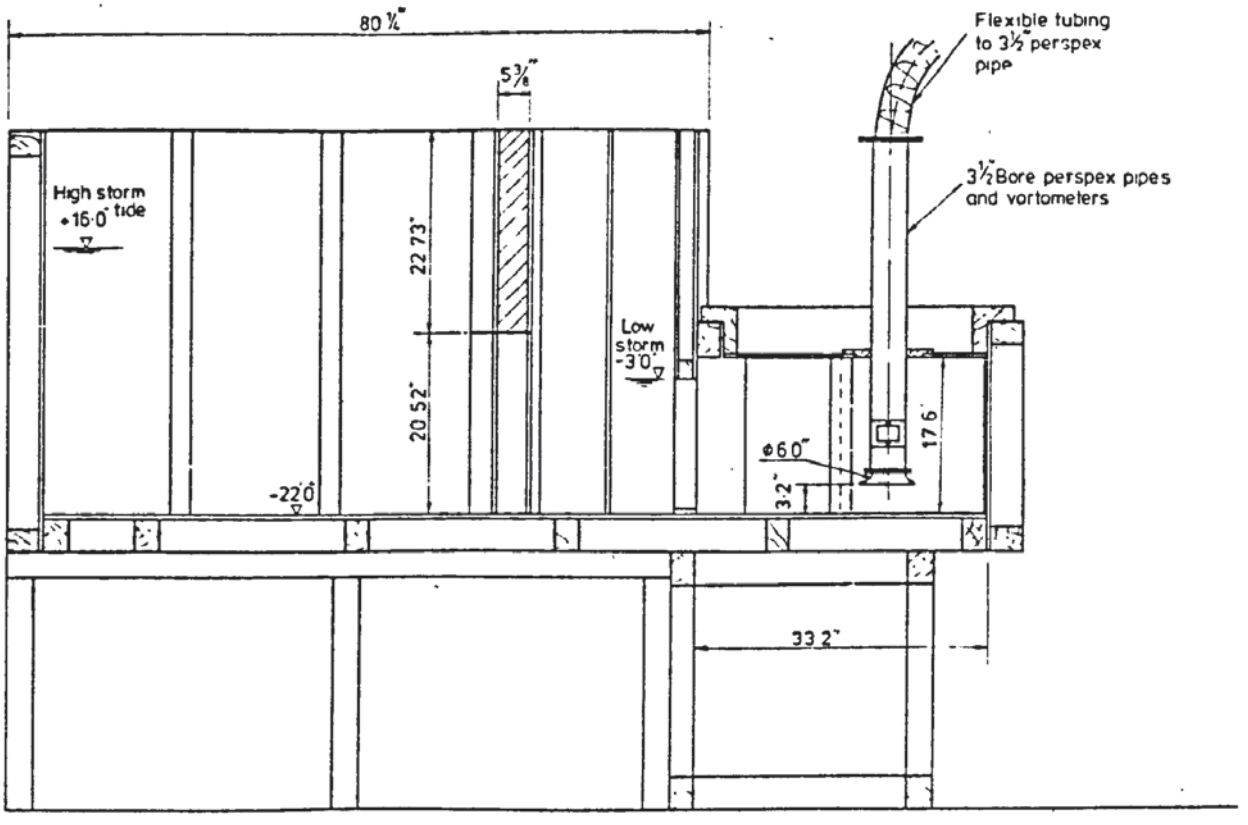

SECTION A-A

Fig. 7.6 Plan and elevation of model of original design of No. 1 unit.

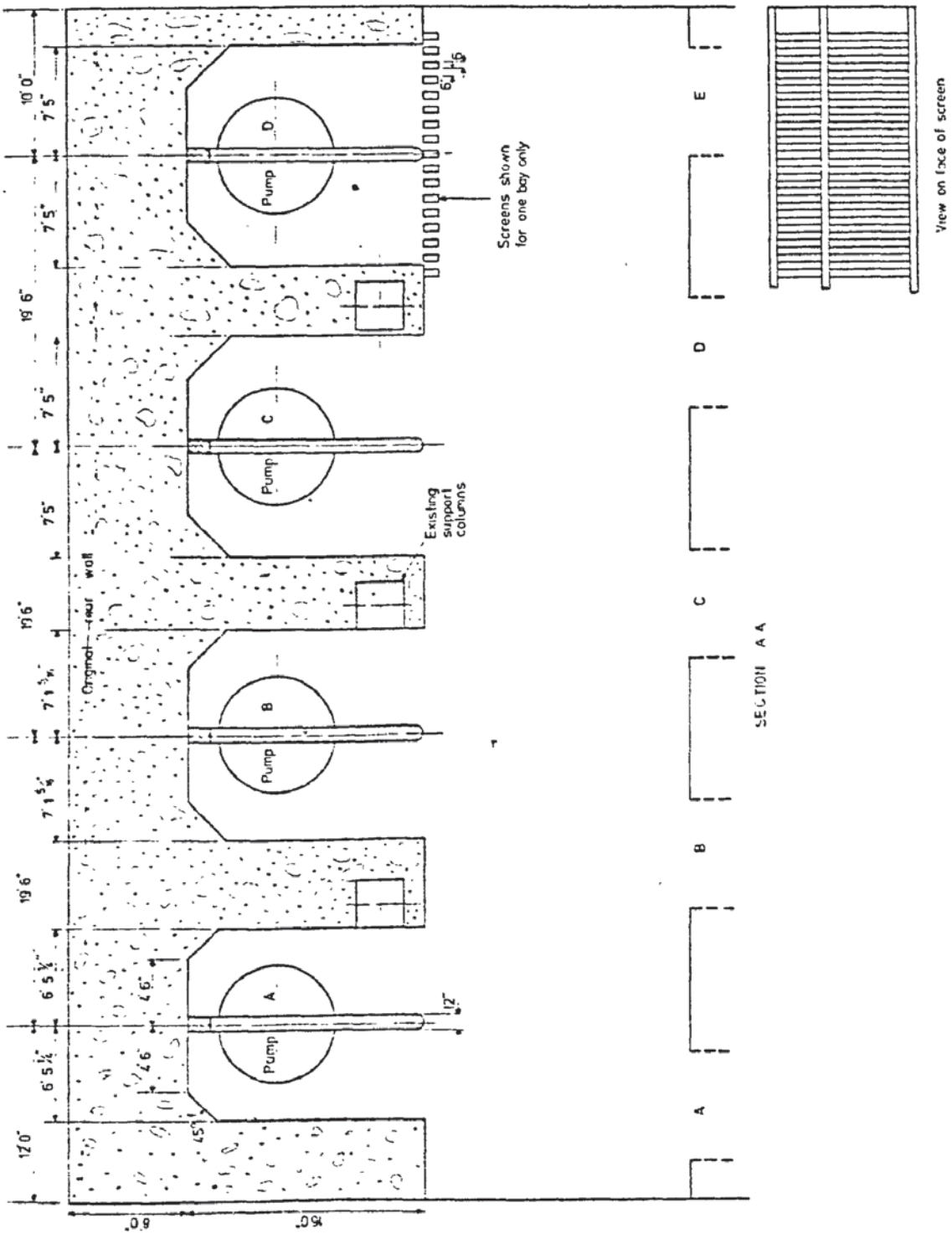

Fig. 7.7 Plan view of final design of No.1 unit (Horizontal shelf not shown).

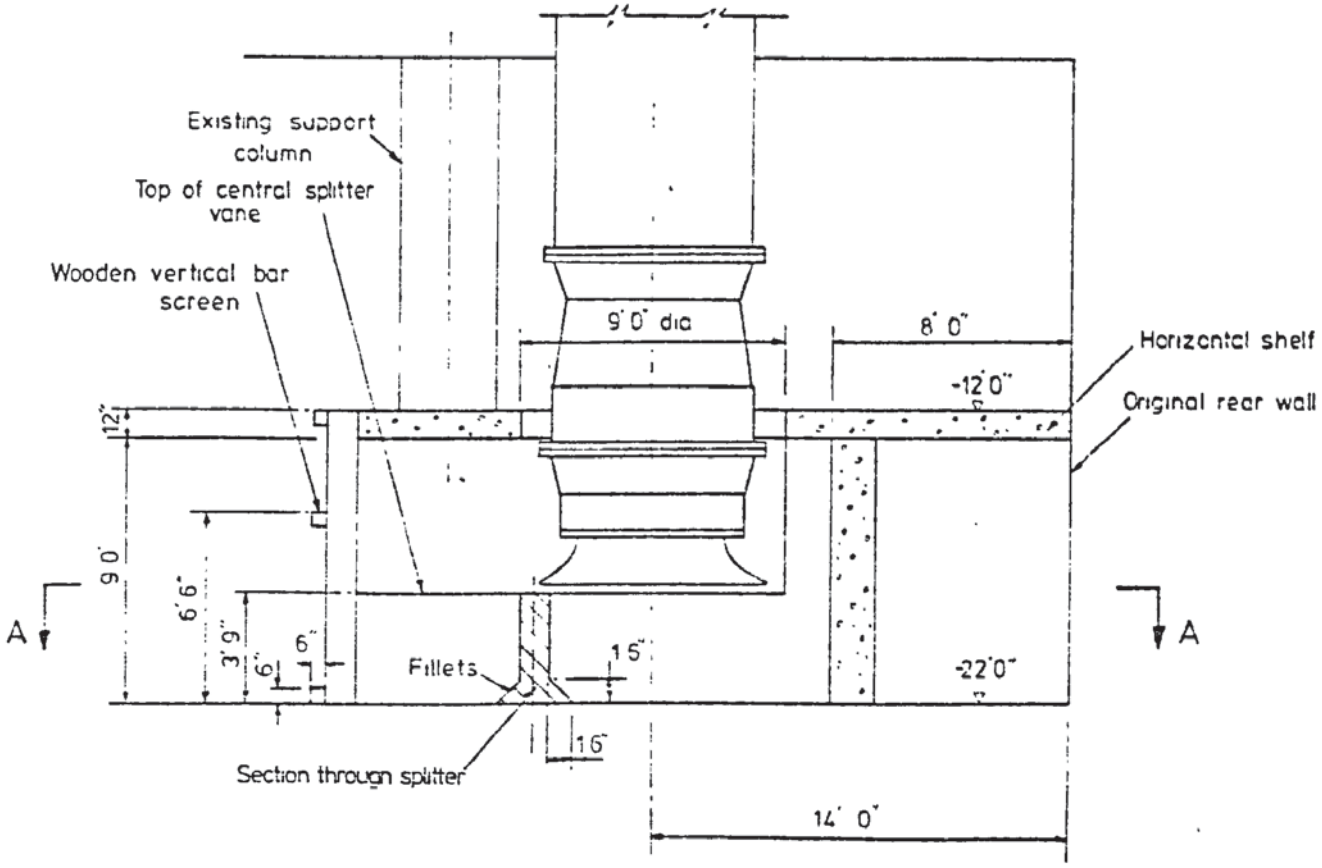

Fig. 7.8 Typical section through one pump bay of final design of No. 1 unit.

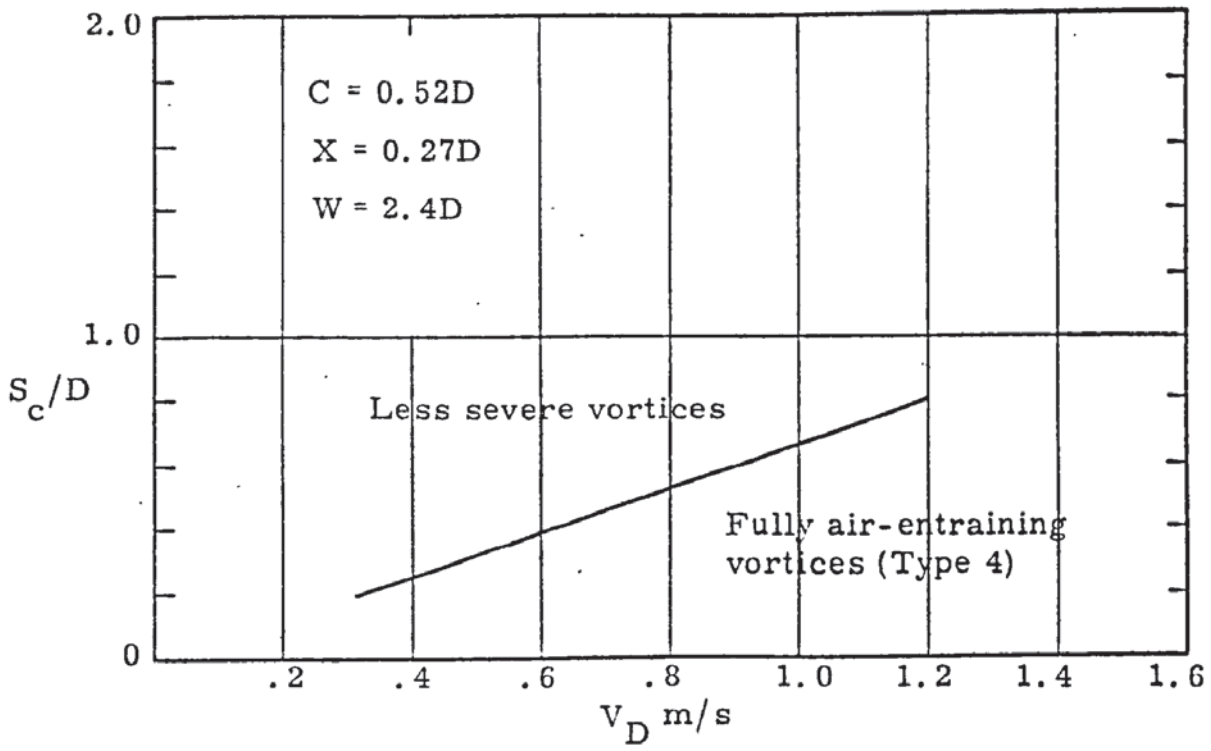

Fig. 7.9 Variation of critical submergence, S_c/D, with bellmouth velocity for No. 2 unit, bellmouth diameter 152 mm.

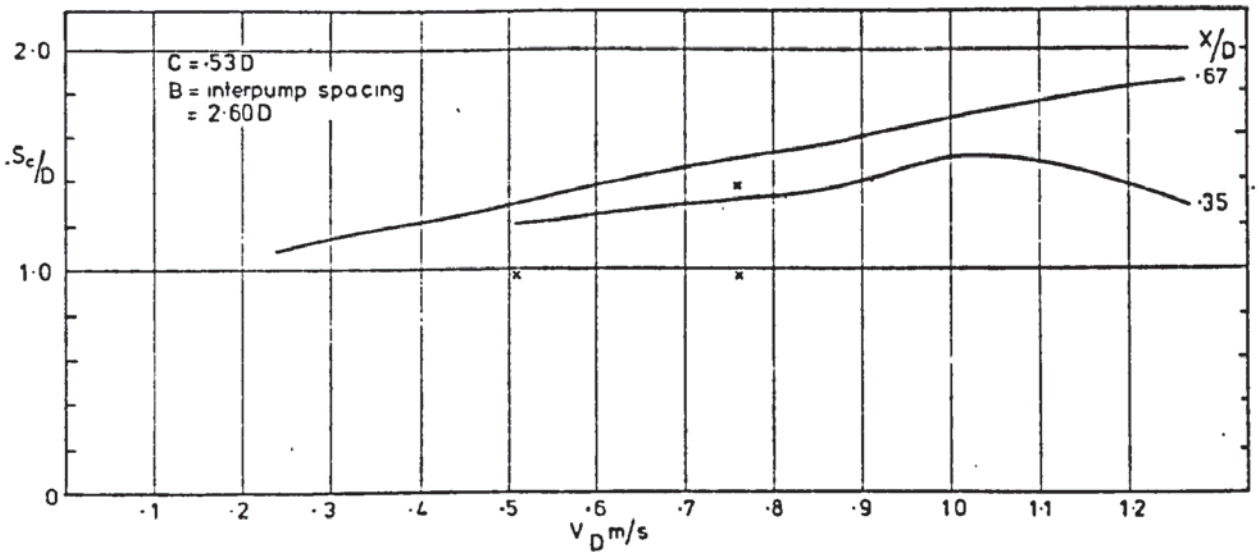

Fig. 7.10 Effect of reducing endwall clearance, X/D, on critical submergence (No. 1 unit)

Fig. 7.11 Tests on original design of No. 1 unit for various Froude scale velocities and pump combinations at a constant submergence, S/D, of 2.0

Pump Combination		Scale velocity	Surface Vortices	Submerged vortices (No. of cores in 1 min)	Swirl in RPM	
A		1.0Fr	0/1	None	15	(A)
		1.5Fr	2/(4_s)	"	37	
		2.0Fr	2/3	"	40	
		2.5Fr	2/3	"	50	
		3.0Fr	3/4	"	63	
B		1.0Fr	0	None	29	(A)
		1.5Fr	0/1 + wispy tail	"	29	
		2.0Fr	3/ (4)	"	49	
		2.5Fr	3/ (4)	"	50	
C		1.0Fr	0/ (1)	None	12	
		1.5Fr	1/ (2)	"	3	
		2.0Fr	1/ (2)	"	6	
		2.5Fr	1/ (2)	"		
D		1.0Fr	1/ (2)	None	3	
		1.5Fr	1/2 + wispy tail	"	4	
		2.0Fr	3/ (4)	"	9	
		2.5Fr	3/4	"	9	
EC	B	1.0Fr	2/ (4)	None		(C)
	C		0	"	45	(A)
	B	1.5Fr	2/ (3)	None		
	C		2/ (3)	Transient, distinct	150	
	B	2.0Fr	(3/4)	None	120	
	C		1/2	Persisent, distinct	144	
BD	B	1.0Fr	0	None		(C)
	D		2/ (3)	Transient, wispy	112	(A)
	B	1.5Fr	0/1	None		
	D		2/3	persistent, distinct	168	
	B	2.0Fr	0 + odd bubble from vortex at D	None		
	D		3/4	persistent, distinct		

CHAPTER 8

CONCLUSIONS AND RECOMMENDATIONS FOR FURTHER WORK

As explained in the introductory chapter, this research programme was started in order to investigate various aspects of intake design, in particular pump sumps, and to derive scaling laws for modelling free surface vortices. This would enable the sponsoring organisation, BHRA, to provide better consultancy services and cost-effective model studies, leading to more reliable and economic operation of prototype schemes by BHRA's clients. Considerable progress has been made in meeting some of the original aims of the research programme and the conclusions from the work described and discussed in the preceding chapters, together with suggestions for further work, are given below under the headings 1) economic considerations, 2) origin of vorticity, 3) hydraulic intake and sump design 4) scaling laws, and 5) further work.

8.1 Economic considerations

It has been shown in Chapter 2 that it is important to get the hydraulic design correct at an early stage, even if it forms only a small part of a particular scheme, and that in certain circumstances, a model study is advisable to be certain of trouble-free performance of the whole scheme. Examples of the adverse effects which can occur when no model study is carried out have been discussed in terms of loss in hydraulic performance, mechanical damage and cost of delays. The consequence of one or more of these factors can give rise to financial penalties running into millions of pounds, and out of all proportion to the cost of the hydraulic intake itself. On the other hand, the cost of a model study has been shown to be only a

small percentage, usually, of the total cost of the real-life scheme, and furthermore, design recommendations arising from the model study can reduce construction costs. Thus, there are real, economic benefits in considering the hydraulic design at an early stage, and then commissioning a model study if the intake design is non-standard.

8.2 Origin of vorticity

It was suggested in Chapter 3 that the growth and separation of the boundary layer from the suction pipe was the main source of vorticity in the common rectangular sump geometry with a vertically suspended pump where there was no obvious asymmetry in the approach flow. The boundary layers developed along the sidewalls and floor play only a subsidiary role. Observation of flow patterns and the experimental results obtained for various geometric clearances have been explained using these new ideas, and they confirm that the observed direction of rotation of the surface vortices is the same as that expected from vortex shedding from a circular cylinder.

It was concluded that air entrainment would only occur if the net vorticity derived from the boundary layers was sufficiently organised to produce rotational motion which was capable of reducing the local pressure within the fluid to atmospheric. With increasing submergence, the vortex strength would therefore have to be increasingly large and this was found to be the case in practice. The existence of a bounding submergence, however, suggests that the vorticity is no longer organised over the whole depth, as the depth and channel velocity increase, and this is attributed to the finite correlation length of shed vortices.

Comparison of extrapolated values of bounding submergence with

predicted values from Swainston's mathematical model shows substantial discrepancies, and is explained by the fact that the mathematical model, in representing the suction flow by a point sink, does not take into account the effect of the suction pipe itself, a factor which has been shown to be of major importance in a rectangular sump geometry. Thus, whilst the mathematical model is a useful contribution in describing vortex formation in a large, stepped sump, it cannot be directly applied to the case of a suction pipe placed at the end of a narrow rectangular channel.

8.3 Intake and sump design

This has been considered with reference to a commonly found sump configuration, that of a vertically suspended pump placed at the end of a rectangular channel. Comprehensive data on sump design has been obtained for the most important geometric parameters using a suction pipe with a bellmouth of diameter 244 mm. This rig was designed to cover the range of bellmouth velocities and water depths (non-dimensionalised) met in practice. These results have been plotted to show the variation of critical submergence with bellmouth velocity.

The experimental data generally confirm the recommendations of ref. 1, but some of the optimum values found from experiment depend on bellmouth velocity, a factor which is not considered in ref. 1. For example, it was found that a pump position close to the endwall gave least submergence requirements at low bellmouth velocities, but at higher velocities a value of 0.75D for the endwall clearance was best. The effectiveness of corner fillets as an anti-vortex device has also been demonstrated, together with the effect of upstream boundary changes. Thus, the data given in Chapter 6 provides useful information for sump designers

and for BHRA when advising on sump design.

One further point arises from the conclusion given in the previous section that the suction pipe (or pump column in real-life) is the major source of vorticity. If this is so, then it would be expected that a horizontal intake placed in the endwall so that there would be no suction pipe obstructing the flow, would lead to reduced surface vortex formation and hence, reduced submergence requirements.

This is borne out by one of the recommendations in ref. 1 for a horizontal intake specifying a minimum submergence of one bellmouth diameter (as opposed to 1.5 bellmouth diameters for a vertically suspended bellmouth intake). However, more detailed work is required in this area to see which configuration gives the least sump depth requirement and construction costs.

8.4 Scaling laws

The original aim was to derive a general scaling law for modelling free-surface vortices. The approach adopted was to use four geometrically similar models with bellmouth diameters 61 mm, 122 mm, 244 mm and 488 mm, and to record vortex formation on each rig. A new mathematical form of scaling law has been developed, based on a Froude and Reynolds number contribution which provides the theoretical basis for a general scaling law. This mathematical function was chosen so that it was internally consistent, i.e. it could be used both to scale up as well as scale down. This requirement is necessary for any scaling law if it is to have any physical meaning.

It was decided to formulate the law as a velocity ratio of model to prototype velocity, since this would be the form most convenient for

immediate application to any scale model. Based on past experience at BHRA, it was assumed that this velocity ratio was a function of scale ratio, s, only i. e.

$$\frac{V_m}{V_p} = f(s) = k(s)\, s^{\frac{1}{2}}$$

where k is the Froude scale multiplying factor. The form of f(s) and k(s) is dependent on a quantity called b which was to be found experimentally from the results of the four rigs.

From analysis of the results of the four rigs, it was found that a unique value of b did not exist for the flow conditions and scale range tested. Furthermore, the value of the velocity ratio was found to depend not only on s but also on geometric parameters such as floor clearance and submergence, i. e.

$$\frac{V_m}{V_p} = f(s,\ b,\ \text{geometric parameters})$$

It was not possible to correlate the various values of V_m/V_p and b to obtain the form of the function f.

However, what has been obtained is a set of curves giving the appropriate k-factor for a scale ratio up to 1 : 8 for various floor clearances and submergences. These will have direct application to models operated in this size range, though application to larger prototype sizes will require further work on prototype data collection. Limited prototype data given in Chapter 7 give a minimum value for k which is not inconsistent with the values deduced from the experimental work.

8.5 Further work

Although this thesis has made a contribution to an understanding of the origin of vorticity, no attempt has been made to give a rigorous mathematical analysis. However, this will be necessary in order to obtain values of vorticity in a fluid, and hence to predict the onset of air entrainment. Further work is needed in this area, together with careful measurements of vortex parameters in a practical configuration such as a rectangular pump sump. This should be possible with the increasing use of high speed computers for numerical analysis as well as more sophisticated technology such as the laser doppler anemometer.

The work on scaling laws has been mainly experimental, with some theoretical considerations based on a physical understanding of hydraulic modelling. However, the scope of the results is limited by the size of the largest rig, which in turn is restricted by laboratory space, facilities, ease of operation, and cost. Thus, further practical work in this area should concentrate on collecting prototype data on vortex formation for comparison with model data and this is being planned by the author for the Steenbras pumped storage scheme (21). Where it is not possible to actually see the degree of air-entrainment of a surface vortex, then noise and vibration measurements at the pump itself would be necessary.

The experimental work has concentrated on type 4 vortices, i.e. fully air entraining vortices. Further extension of the work is suggested to cover less severe types of vortices, since in some applications, no air-entrainment is permissible at all and so a scaling law for non-air-entraining vortices or those just on the verge of entraining air, is required.

In the area of sump design, the logical extension to the work already

carried out would be to test a horizontal intake, the so-called "dry well" sump, and to investigate its submergence requirements over a range of velocities and sump geometries to see if it is a better design hydraulically than the vertical, suspended intake. In addition, because of the conclusion that the suction pipe is the main source of vorticity, it would be worthwhile investigating the effects of different shapes of pump casing and the effects of fins and roughening elements added to the surface of the suction pipe. These could prove useful in reducing vortex activity and so aid the design of the common rectangular sump with a vertical suspended pump.

This thesis has concentrated on surface vortices, whereas it has already been noted that submerged vortices and swirl are also a problem at hydraulic intakes. The effect of sump geometry on these two phenomena should therefore be investigated in order to establish what degree of submerged vortex activity and swirl is acceptable to any given prototype pump, and then to correlate this with observations on a model.

Lastly it should be noted that the pump and its casing have been represented simply by flow through a suction pipe. However, it is possible that the presence of a rotating pump impeller can influence flow conditions upstream, and hence aggravate swirl or vortex strength. Thus, tests with a model pump in the suction should be carried out, and the results compared with the "no-pump" case to see if there are any pre-rotation effects. If all this can be done, then it will be possible to predict the behaviour of a prototype intake with greater accuracy and confidence than at present.

Appendix A RECORD OF EXPERIMENTAL OBSERVATIONS

A1 - A18	6" rig	A23 - A25	3" rig
A19 - A22	1.5" rig	A26 - A29	12" rig

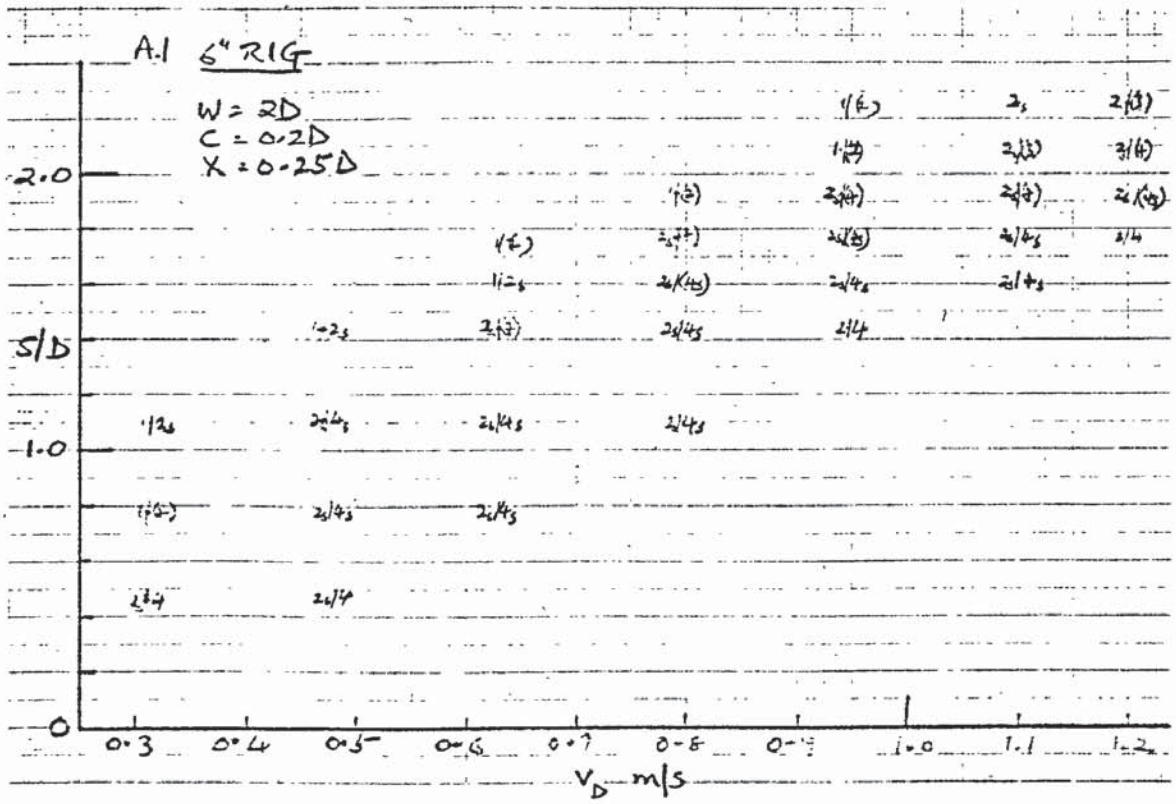

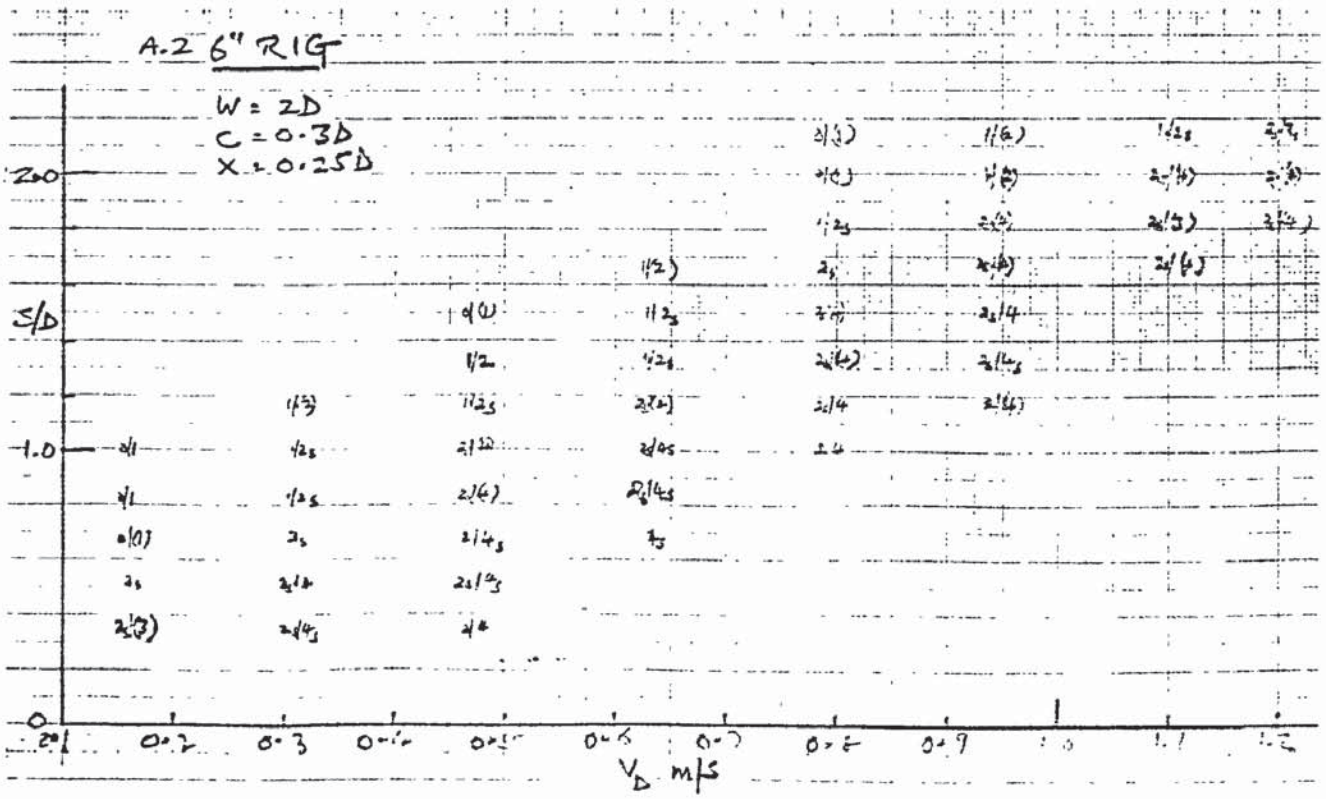

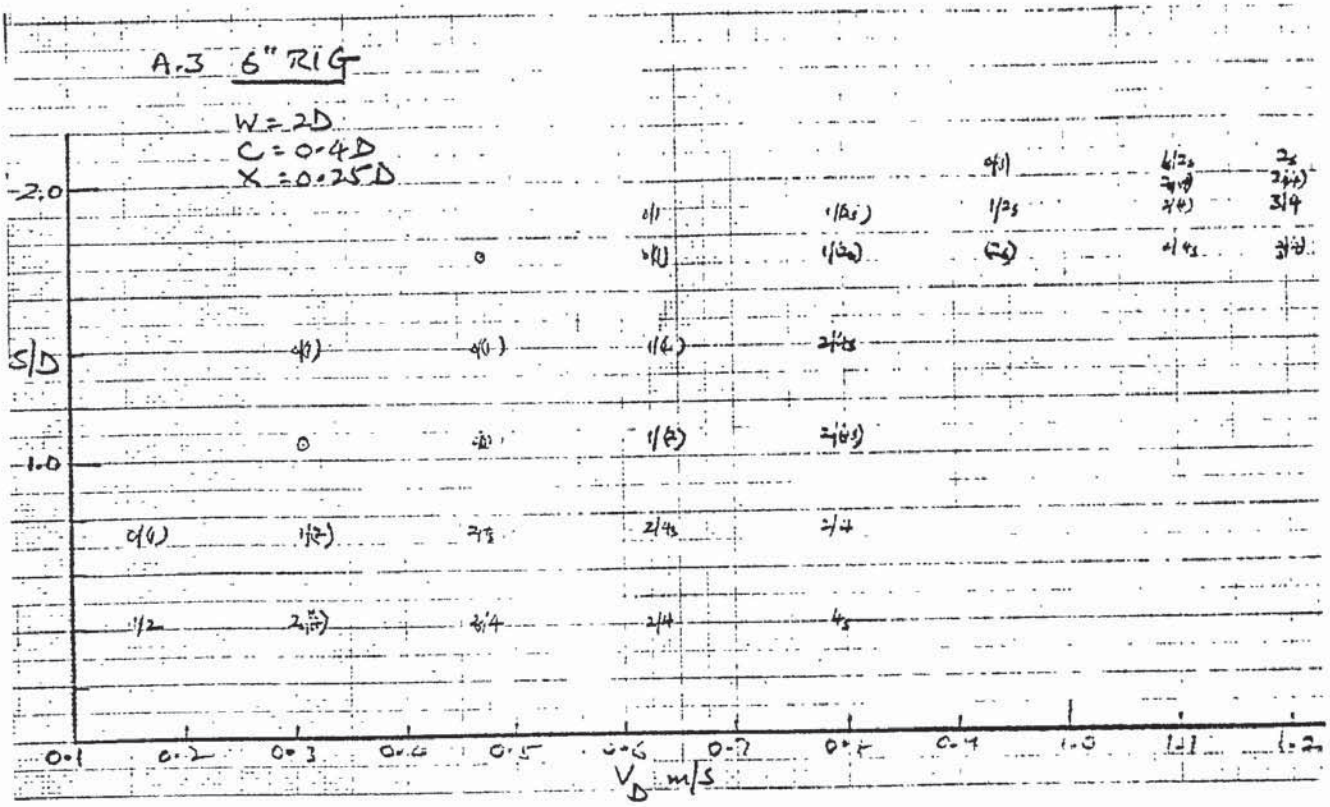
A.3 6" RIG
W = 2D
C = 0.4D
X = 0.25D
2.0
S/D
1.0
0.1
0.2
0.3
0.4
0.5
0.6
0.7
0.8
0.9
1.0
1.1
1.2
V_D m/s

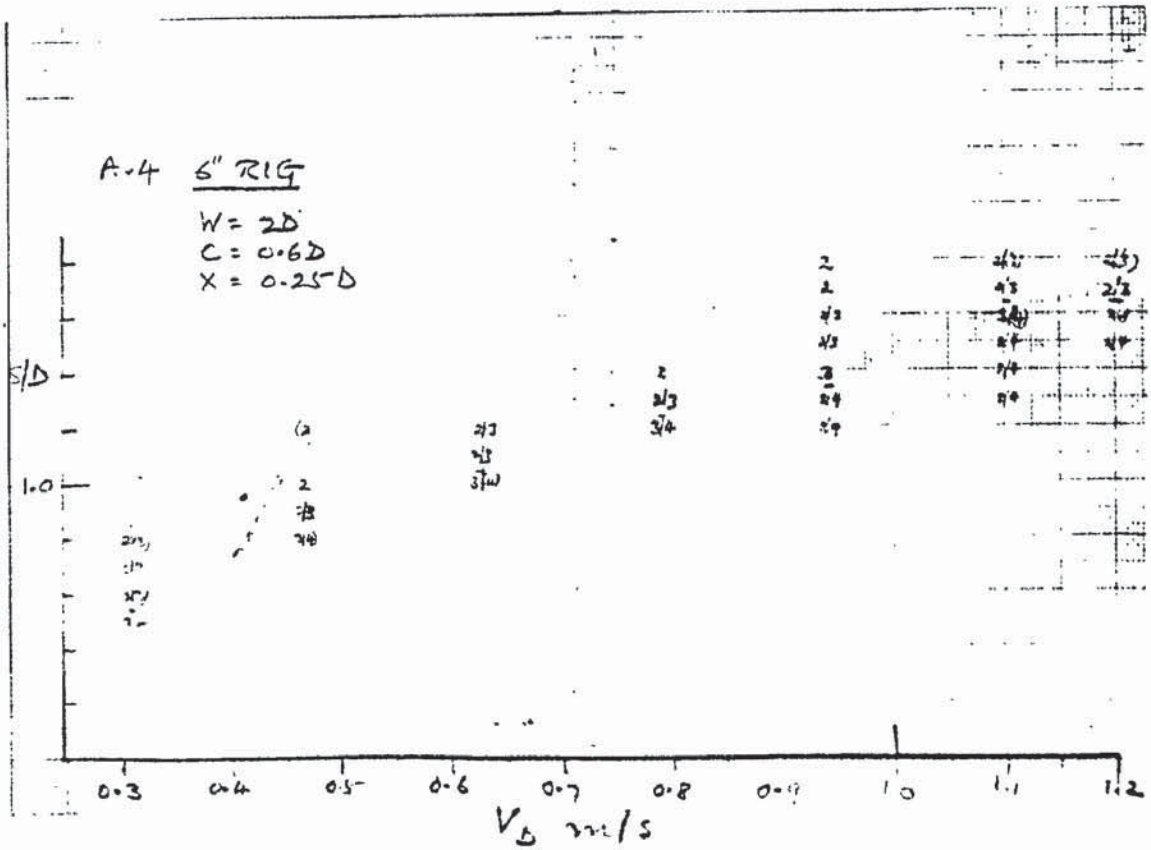
A.4 6" RIG
W = 2D
C = 0.6D
X = 0.25D
S/D
1.0
0.3
0.4
0.5
0.6
0.7
0.8
0.9
1.0
1.1
1.2
V_D m/s

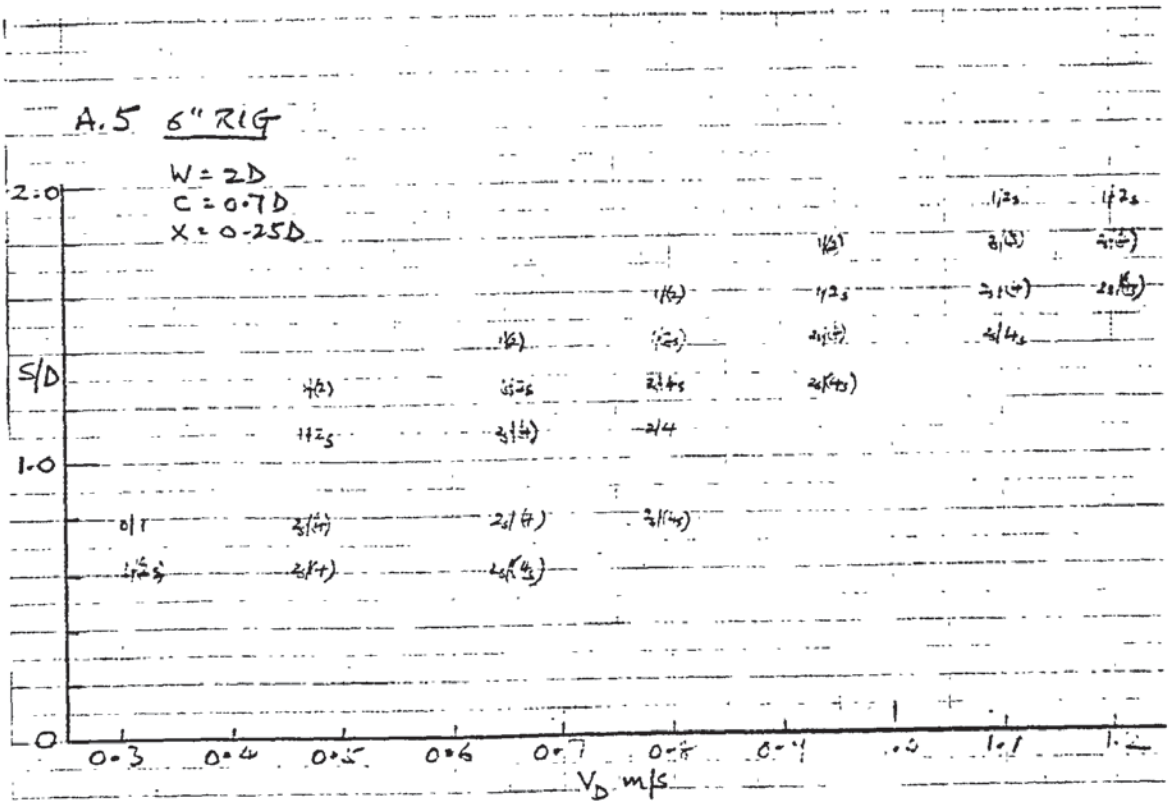
A.5 6" RIG
W = 2D
C = 0.7D
X = 0.25D
S/D
2.0
1.0
0
0.3
0.4
0.5
0.6
0.7
0.8
0.9
1.0
1.1
1.2
V_D m/s

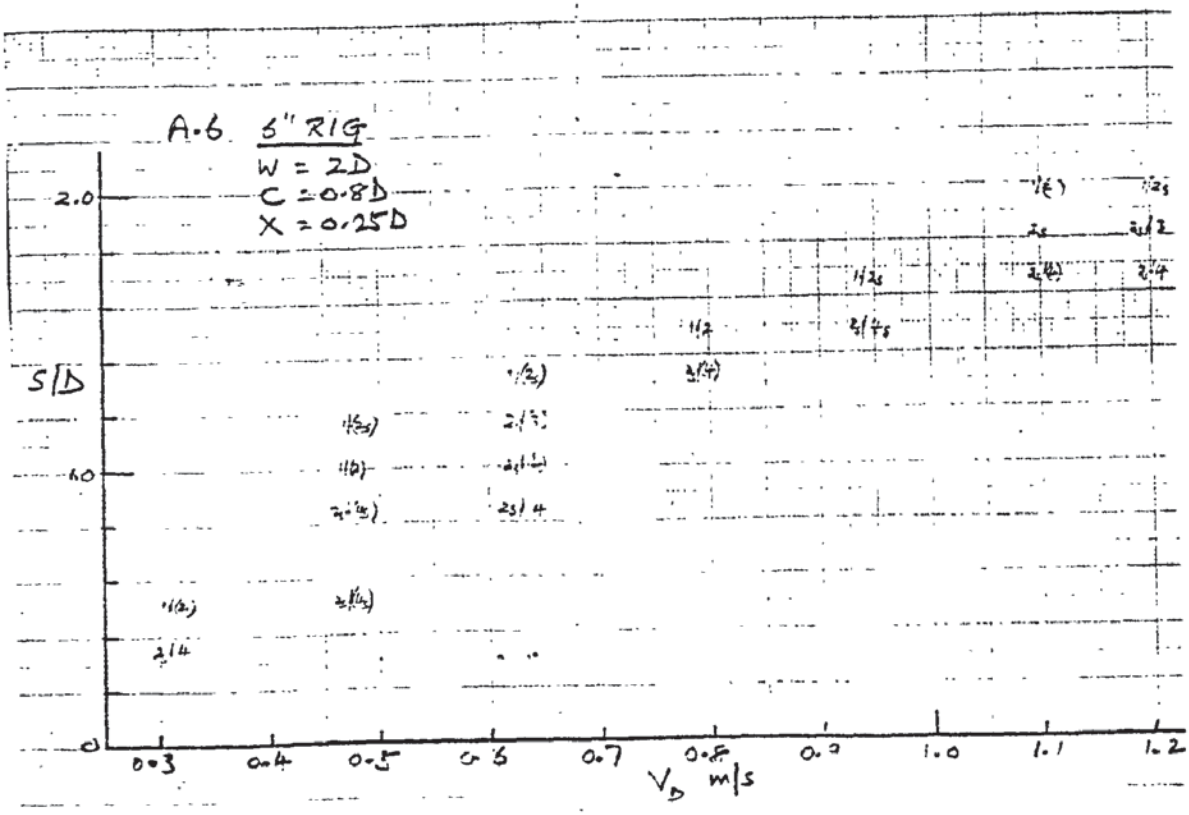
A.6 6" RIG
W = 2D
C = 0.8D
X = 0.25D
S/D
2.0
1.0
0
0.3
0.4
0.5
0.6
0.7
0.8
0.9
1.0
1.1
1.2
V_D m/s

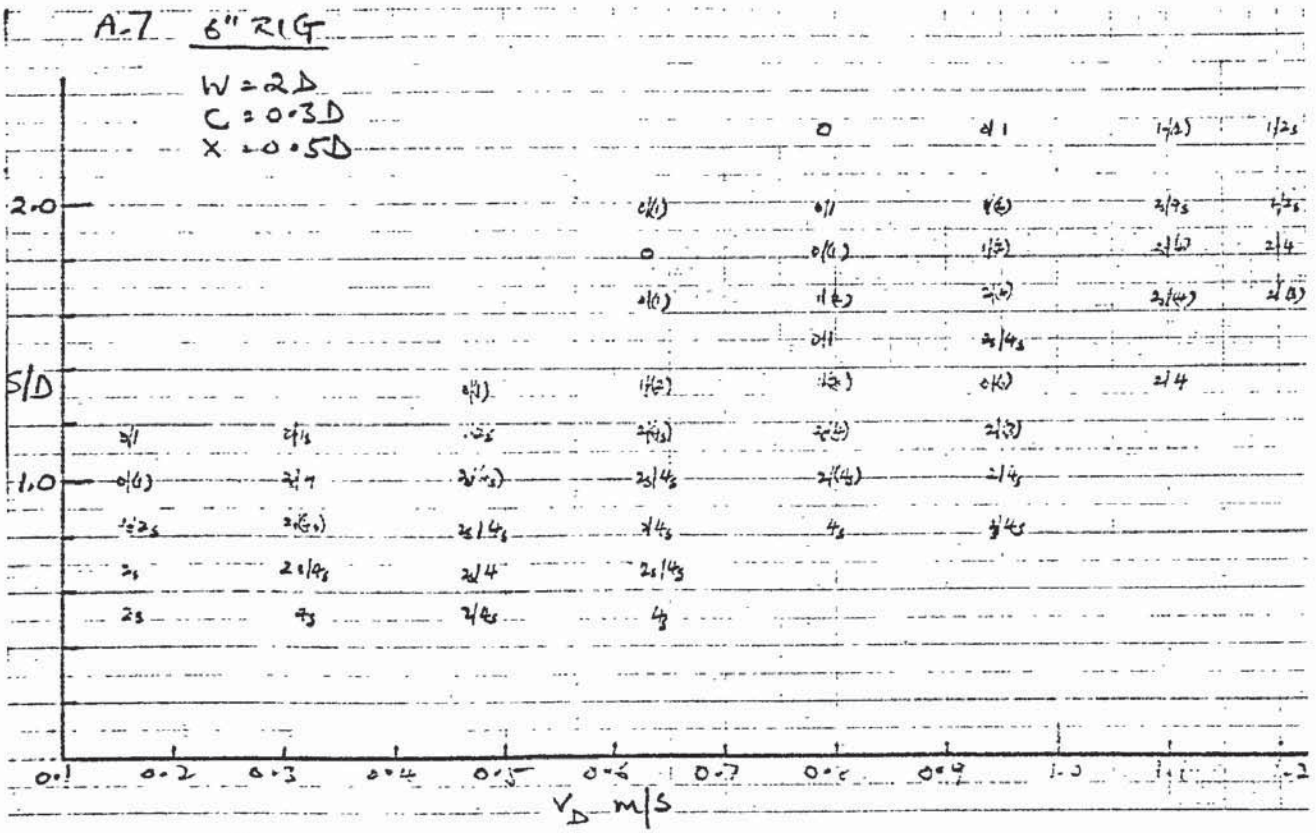
A-7 6" RIG
W = 2D
C = 0.3D
X = 0.5D
2.0
S/D
1.0
0.1
0.2
0.3
0.4
0.5
0.6
0.7
0.8
0.9
1.0
1.2
V_D m/s

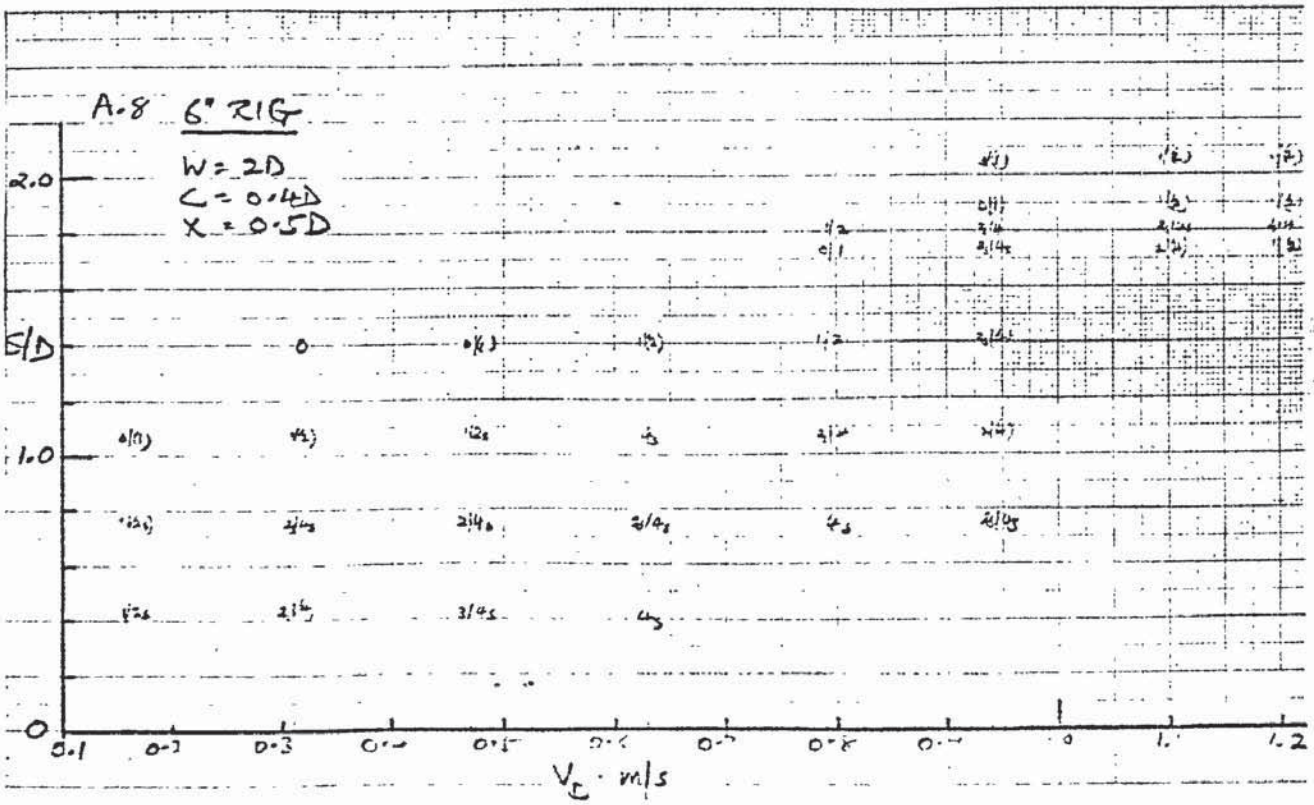
A-8 6" RIG
W = 2D
C = 0.4D
X = 0.5D
2.0
S/D
1.0
0
0.1
0.2
0.3
0.4
0.5
0.6
0.7
0.8
0.9
1.0
1.2
V_D m/s

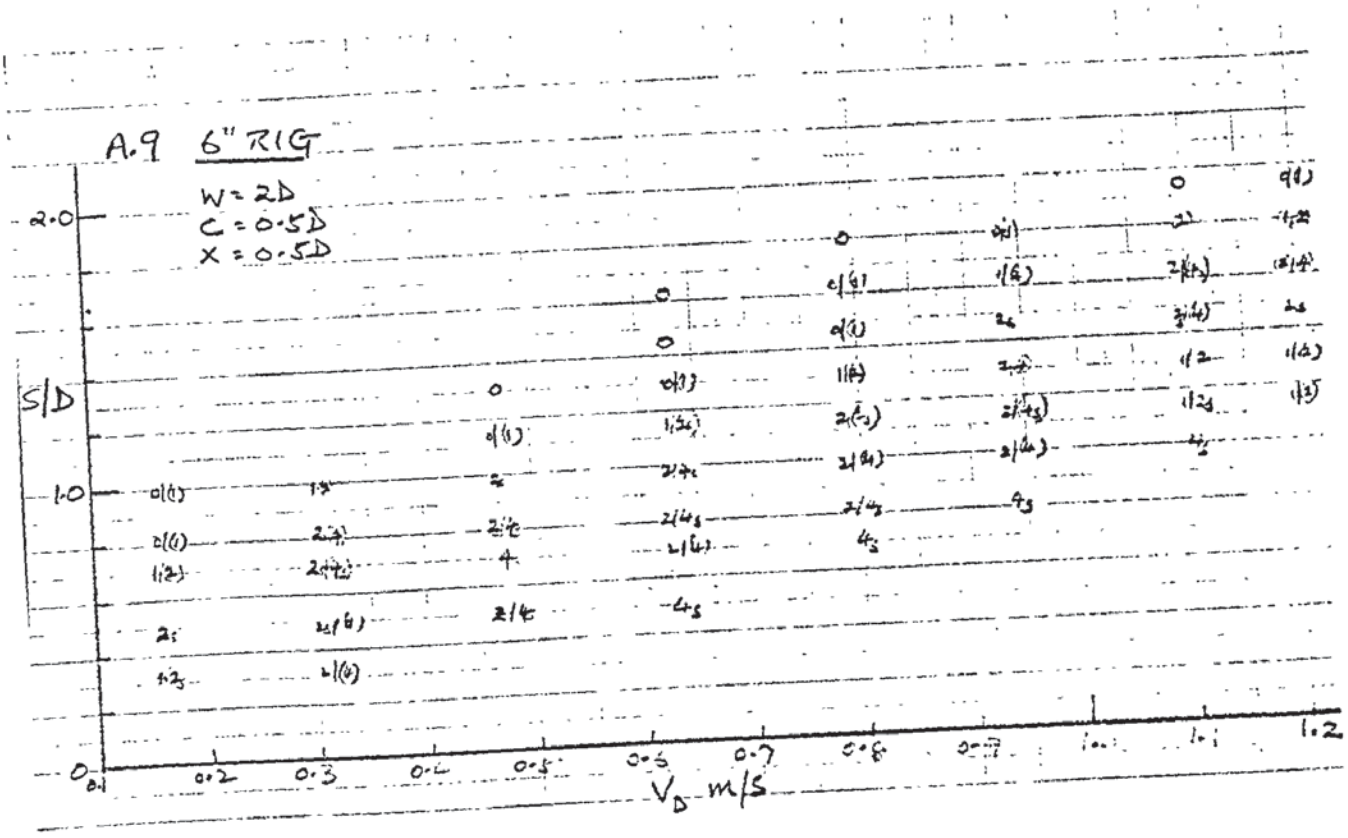
A.9 6" RIG
W = 2D
C = 0.5D
X = 0.5D
S/D
2.0
1.0
0
0.1
0.2
0.3
0.4
0.5
0.6
0.7
0.8
0.9
1.0
1.1
1.2
V_D m/s

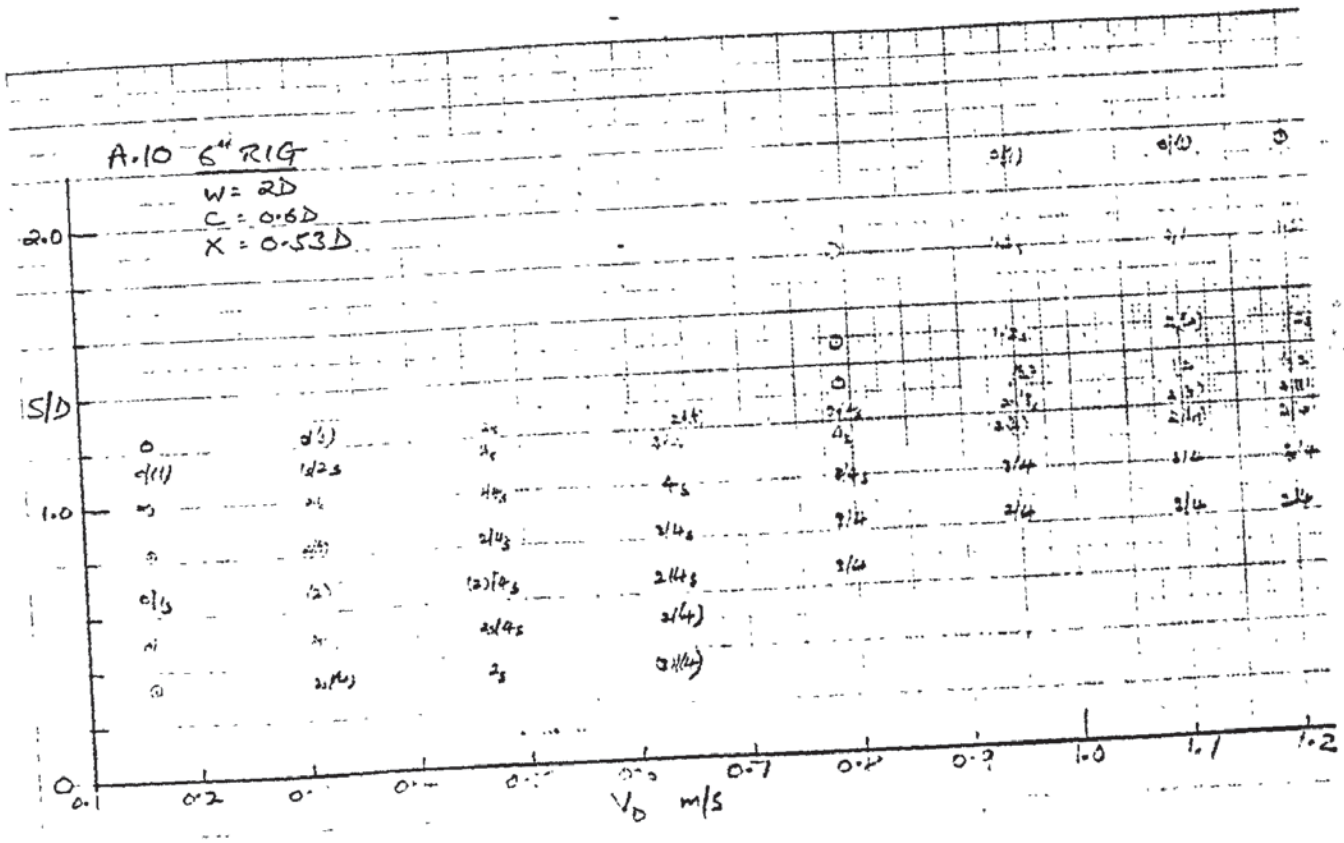
A.10 6" RIG
W = 2D
C = 0.6D
X = 0.53D
S/D
2.0
1.0
0
0.1
0.2
0.3
0.4
0.5
0.6
0.7
0.8
0.9
1.0
1.1
1.2
V_D m/s

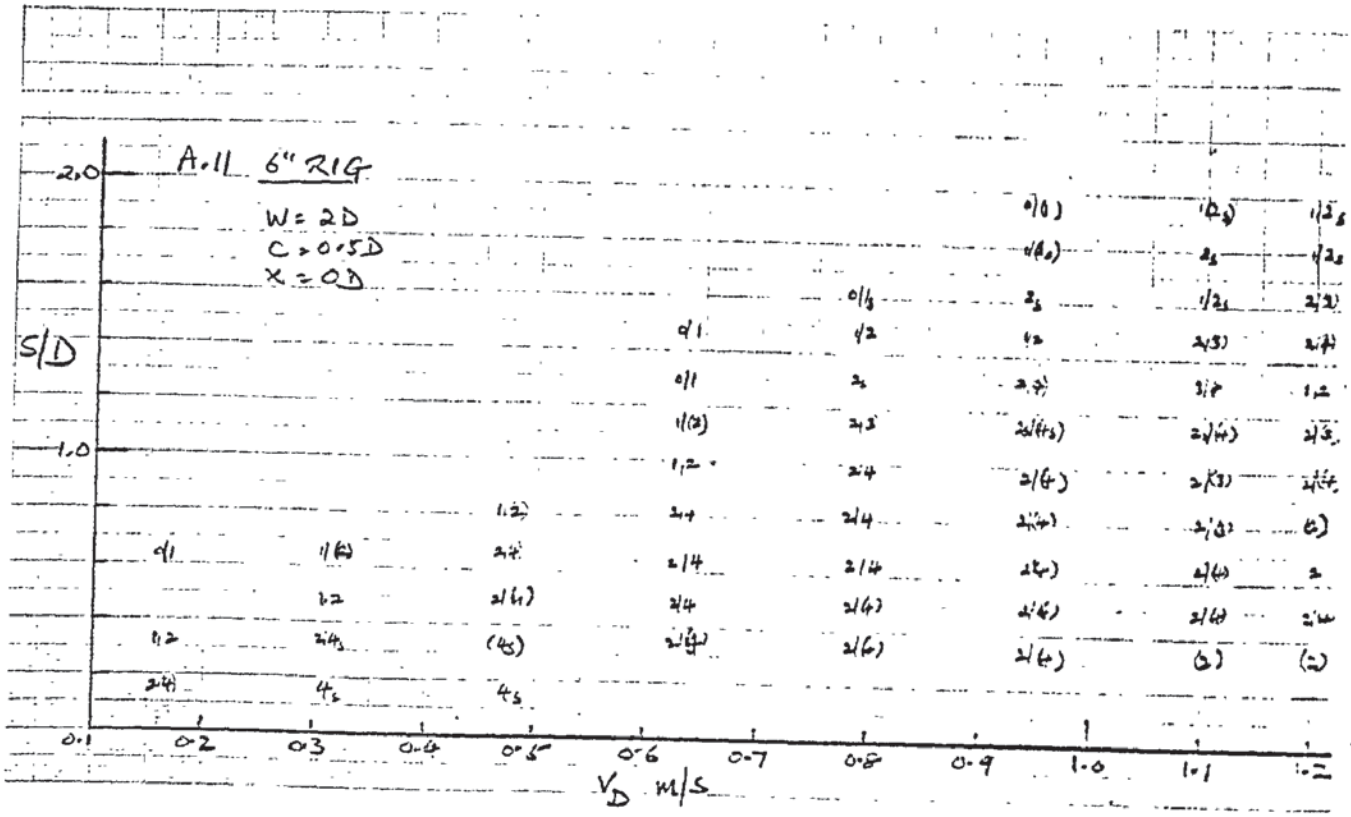
A.11 6" RIG
W = 2D
C = 0.5D
X = 0D
S/D
2.0
1.0
0.1
0.2
0.3
0.4
0.5
0.6
0.7
0.8
0.9
1.0
1.1
1.2
V_D m/s

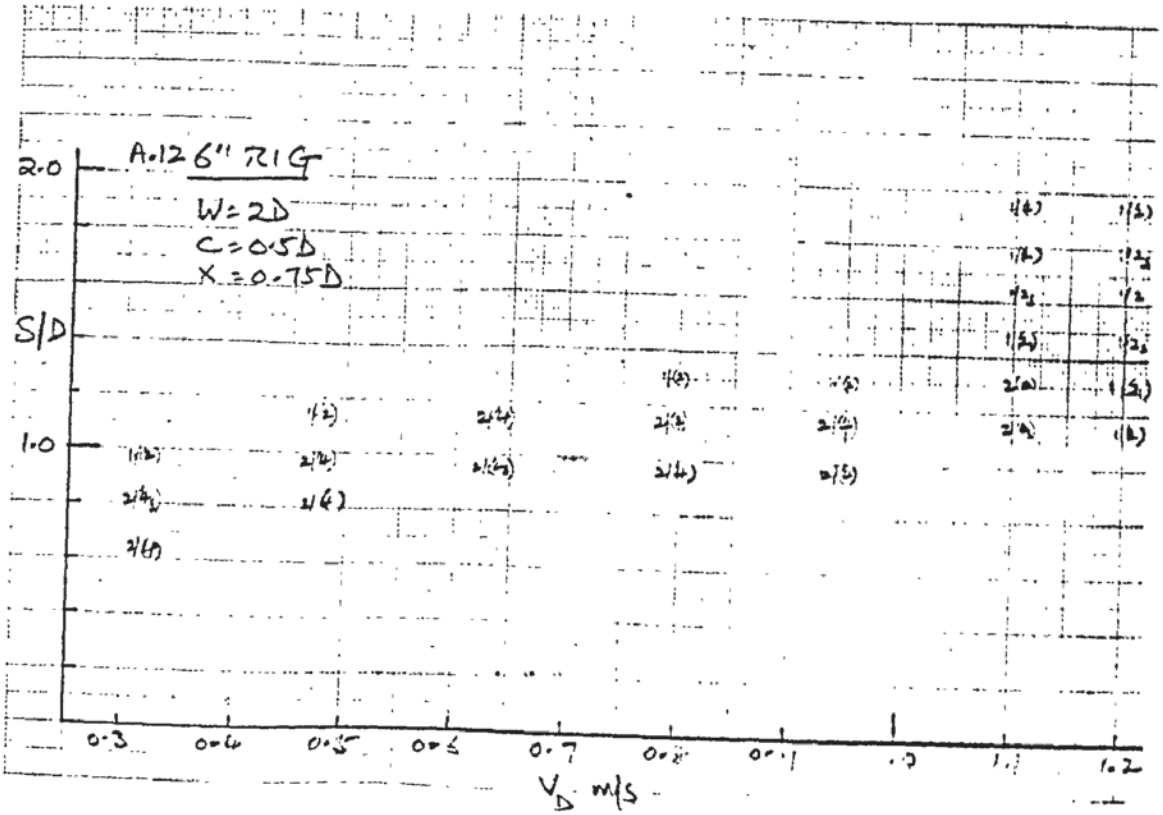
A.12 6" RIG
W = 2D
C = 0.5D
X = 0.75D
S/D
2.0
1.0
0.3
0.4
0.5
0.6
0.7
1.0
1.2
V_D m/s

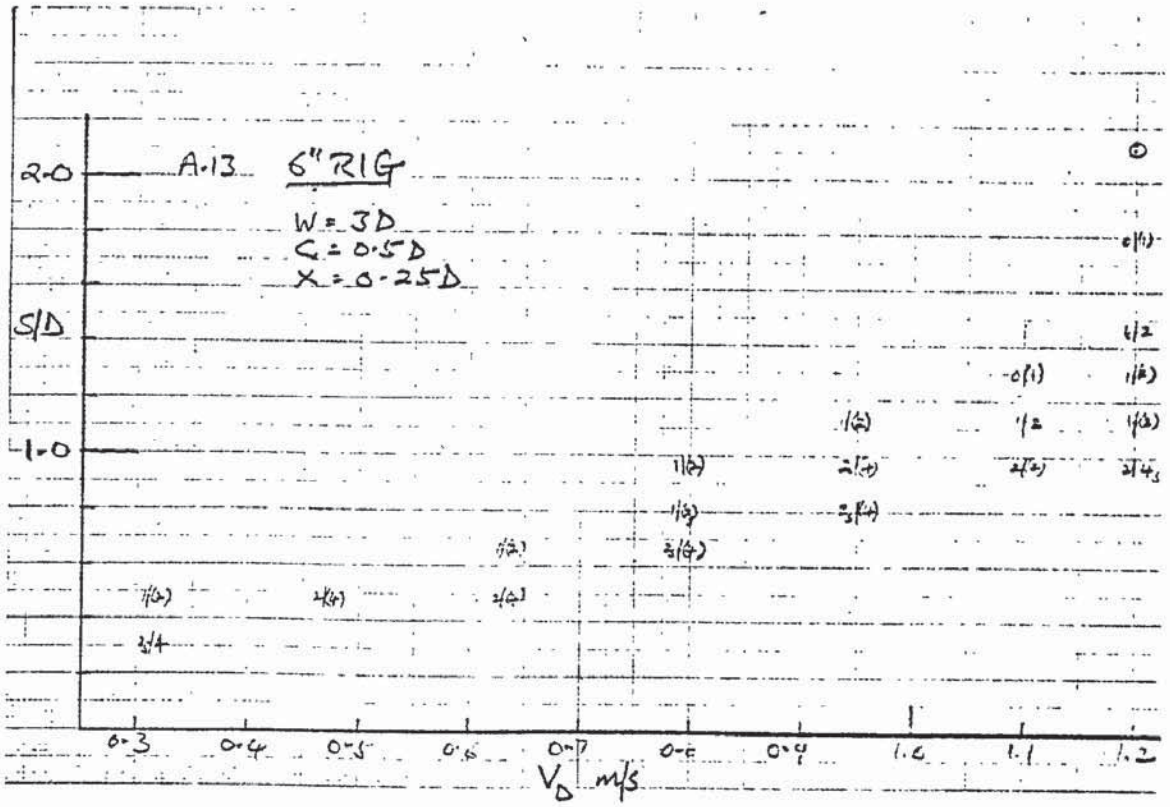
A.13 6" RIG
W = 3D
C = 0.5D
X = 0.25D
S/D
2.0
1.0
0.3
0.4
0.5
0.6
0.7
0.8
0.9
1.0
1.1
1.2
V_D m/s

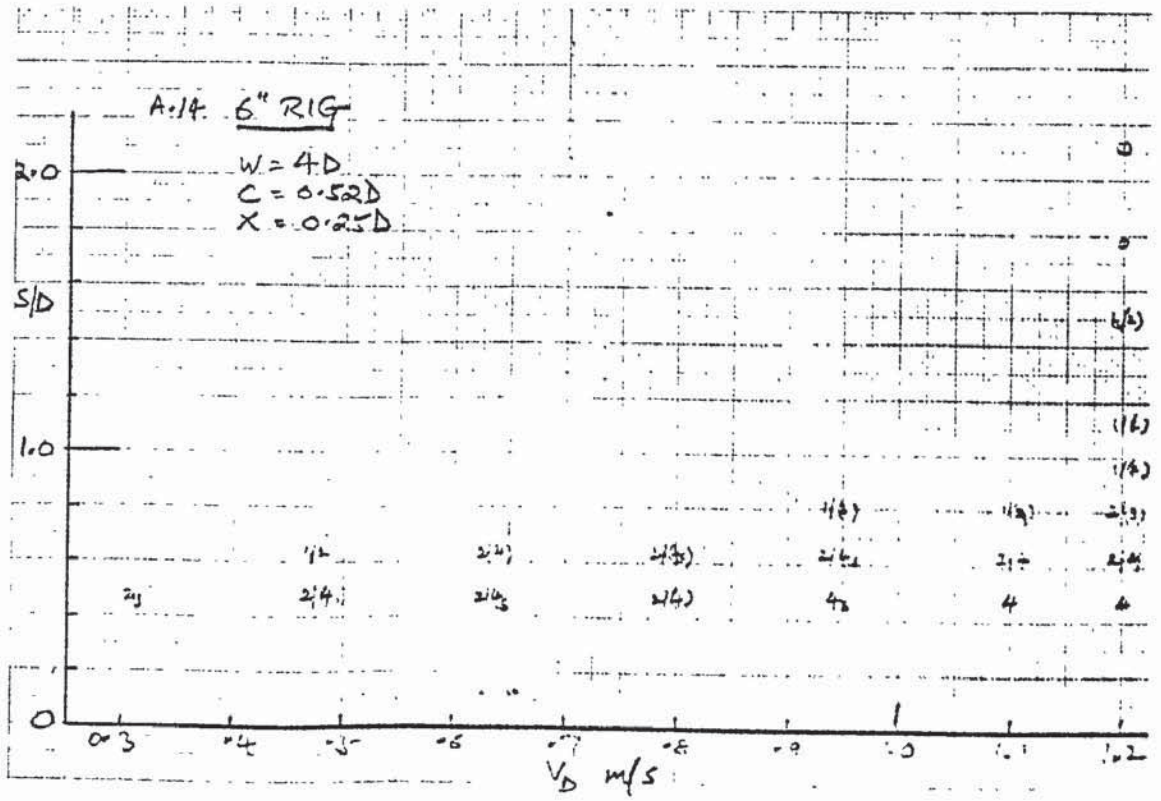
A.14 6" RIG
W = 4D
C = 0.52D
X = 0.25D
S/D
2.0
1.0
0
0.3
0.4
0.5
0.6
0.7
0.8
0.9
1.0
1.1
1.2
V_D m/s

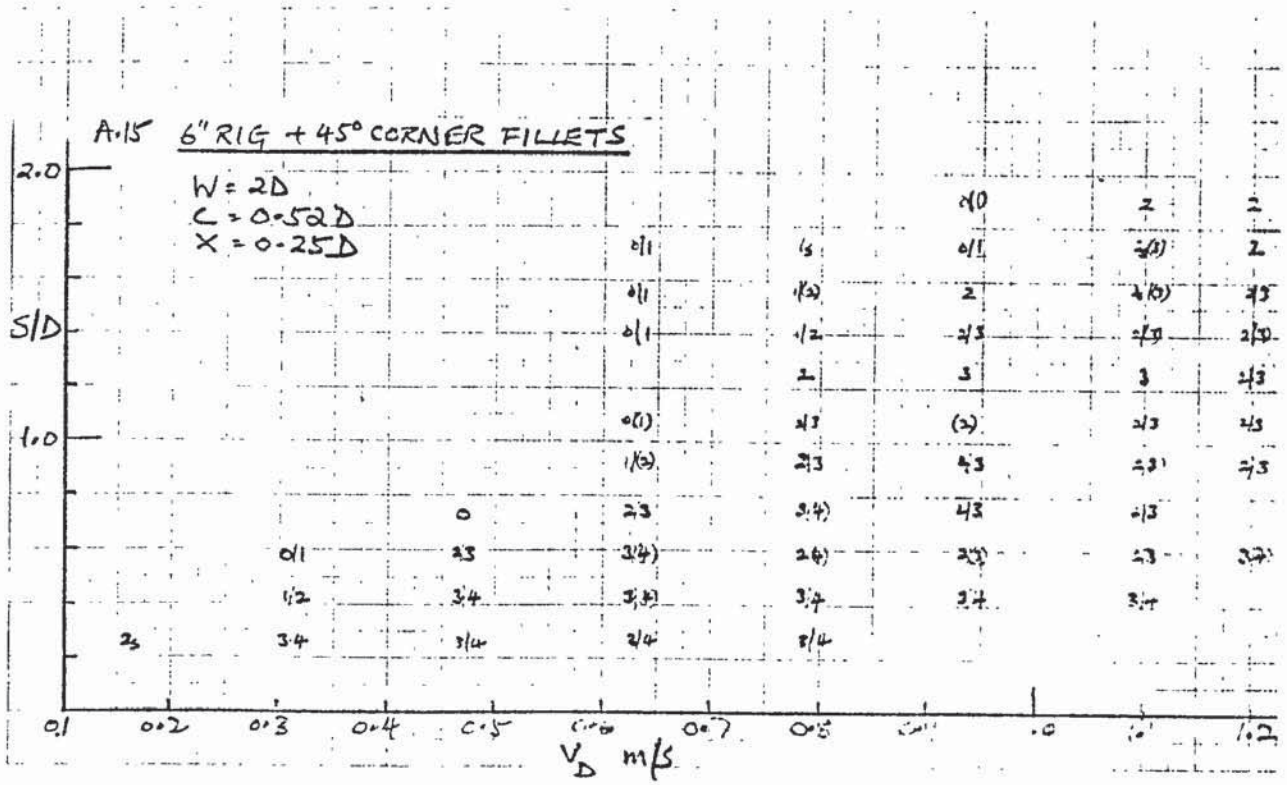
A-15 6" RIG + 45° CORNER FILLETS
W = 2D
C = 0.52D
X = 0.25D
S/D
2.0
1.0
0.1
0.2
0.3
0.4
0.5
0.7
1.0
1.2
V_D m/s

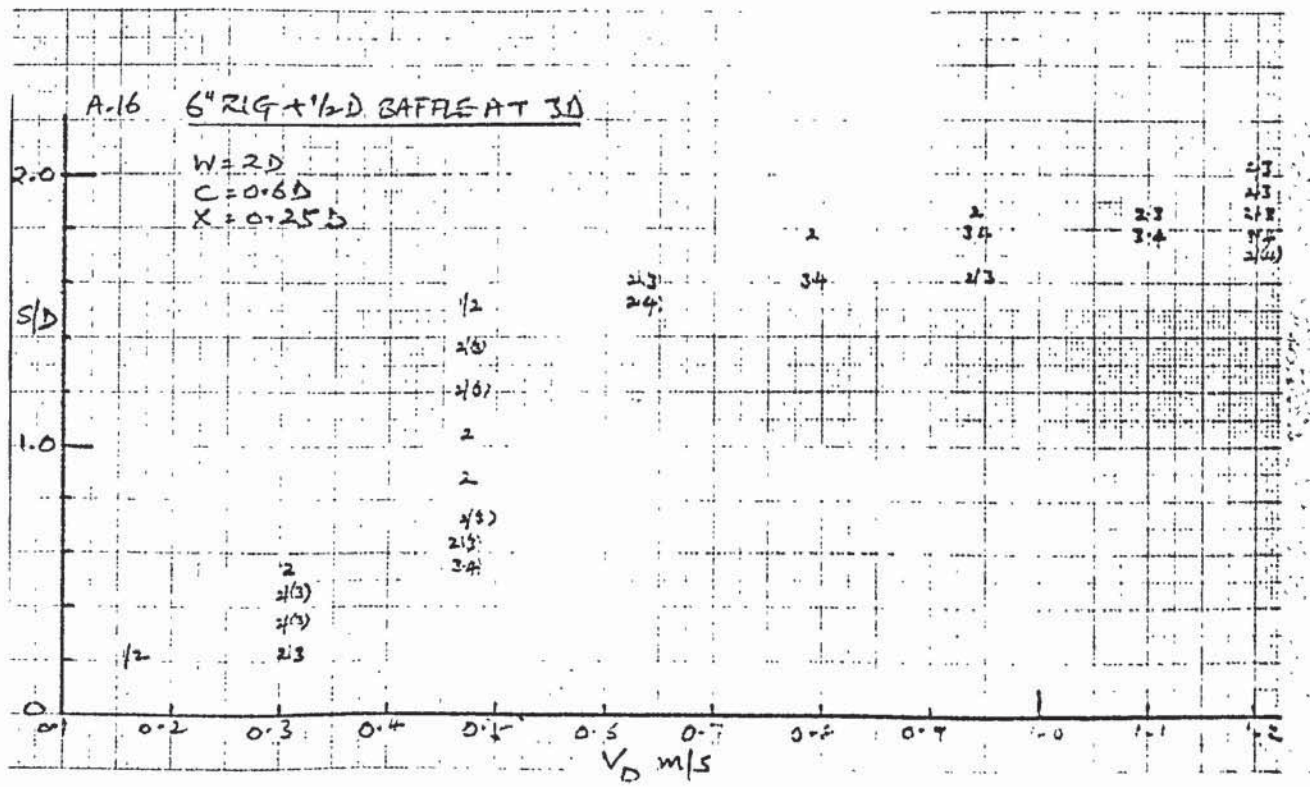
A-16 6" RIG + 1/2 D BAFFLE AT 3D
W = 2D
C = 0.6D
X = 0.25D
S/D
2.0
1.0
0
0.1
0.2
0.3
0.4
0.5
0.7
1.0
1.2
V_D m/s

A-17 6" RIG + ½D BAFFLE AT 4D

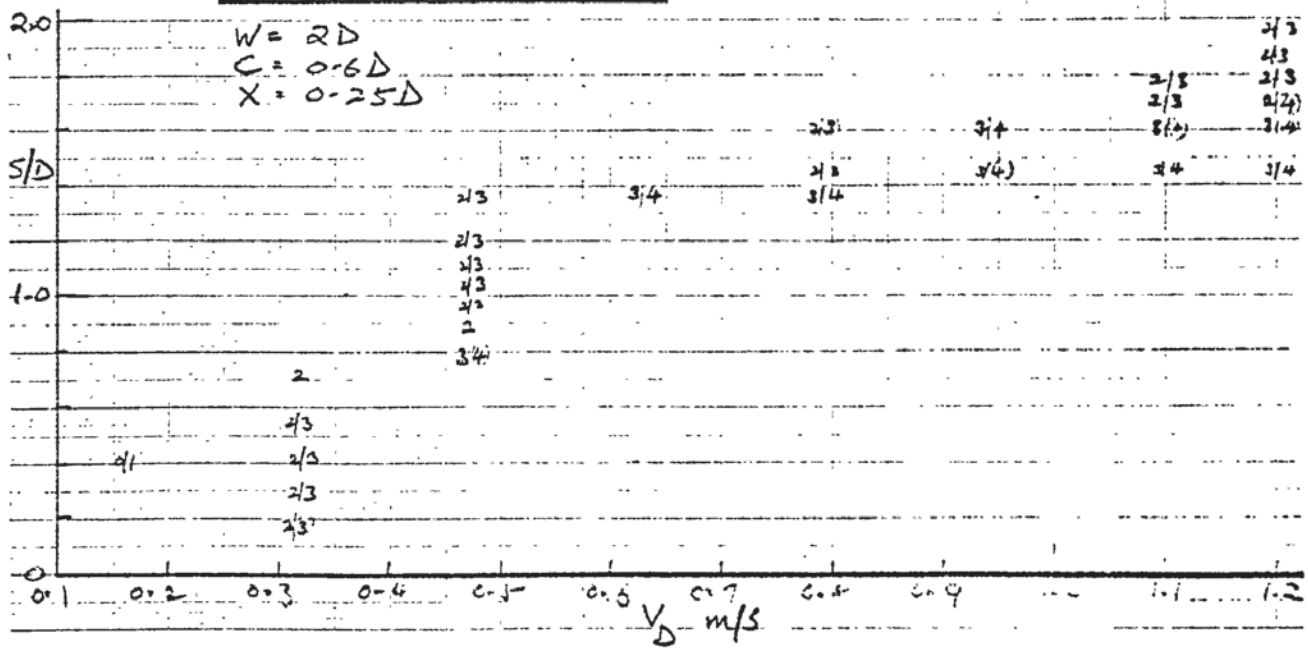

A-18 6" RIG + ½D BAFFLE AT 5D

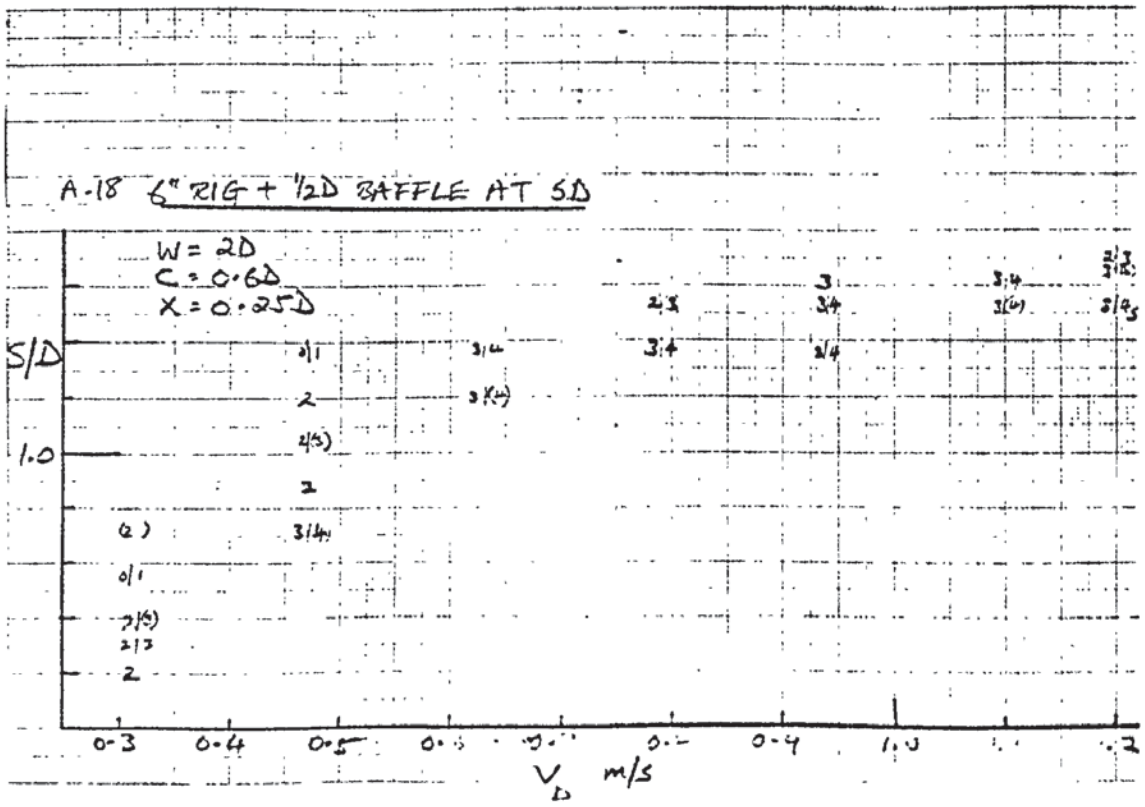

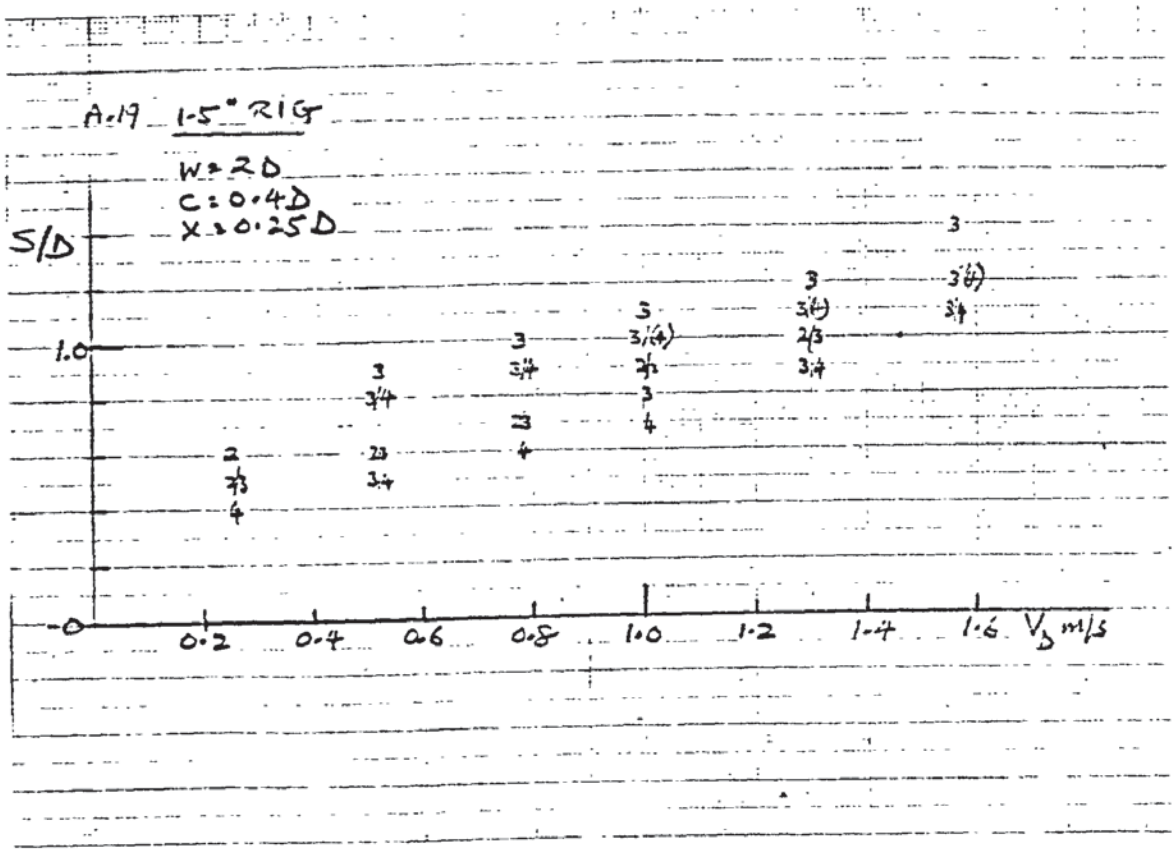
A.19 1.5" RIG
W = 2D
C = 0.4D
X = 0.25D
S/D
1.0
0
0.2
0.4
0.6
0.8
1.0
1.2
1.4
1.6
V_s m/s

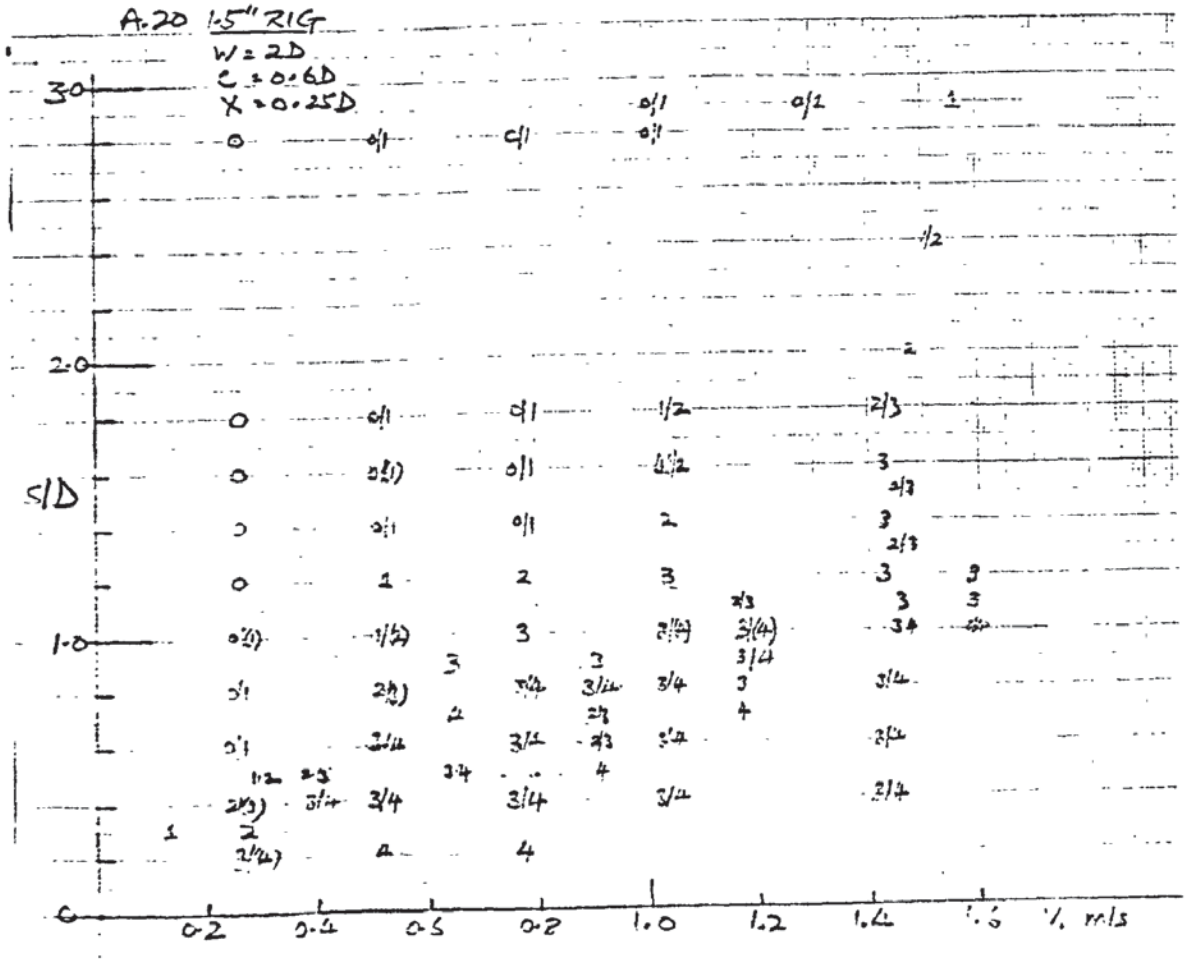
A.20 1.5" RIG
W = 2D
C = 0.6D
X = 0.25D
S/D
3.0
2.0
1.0
0
0.2
0.4
0.6
0.8
1.0
1.2
1.4
1.6
V_s m/s

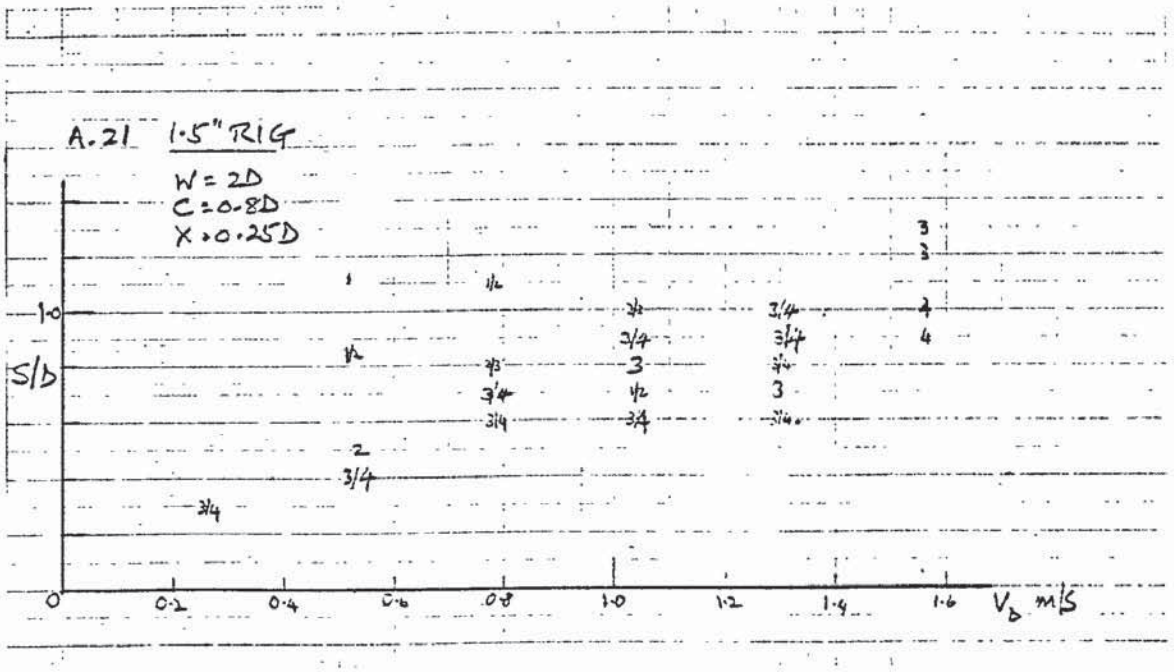
A.21 1.5" RIG
W = 2D
C = 0.8D
X = 0.25D
S/D
1.0
0
0.2
0.4
0.6
0.8
1.0
1.2
1.4
1.6
V_D m/s

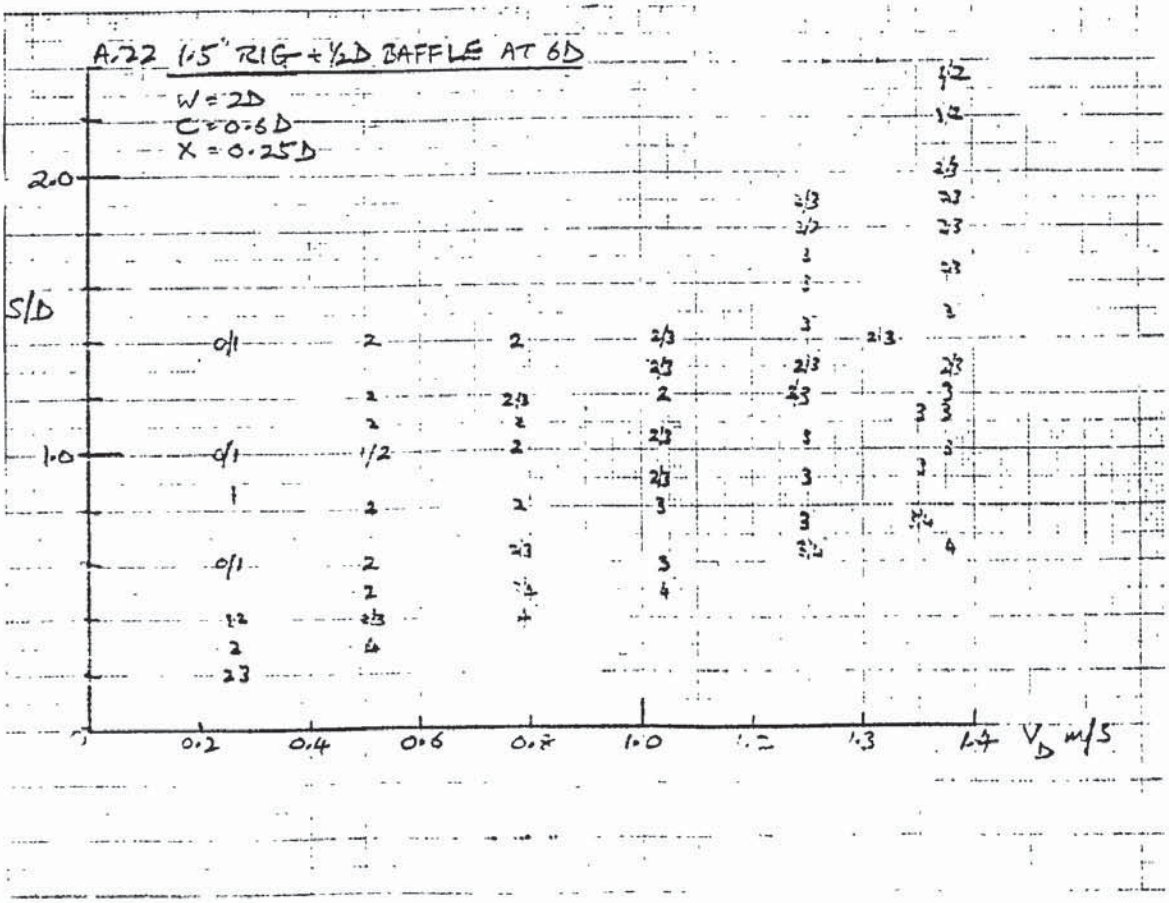
A.22 1.5" RIG + ½D BAFFLE AT 6D
W = 2D
C = 0.6D
X = 0.25D
S/D
2.0
1.0
0.2
0.4
0.6
0.8
1.0
1.2
1.3
1.4
V_D m/s

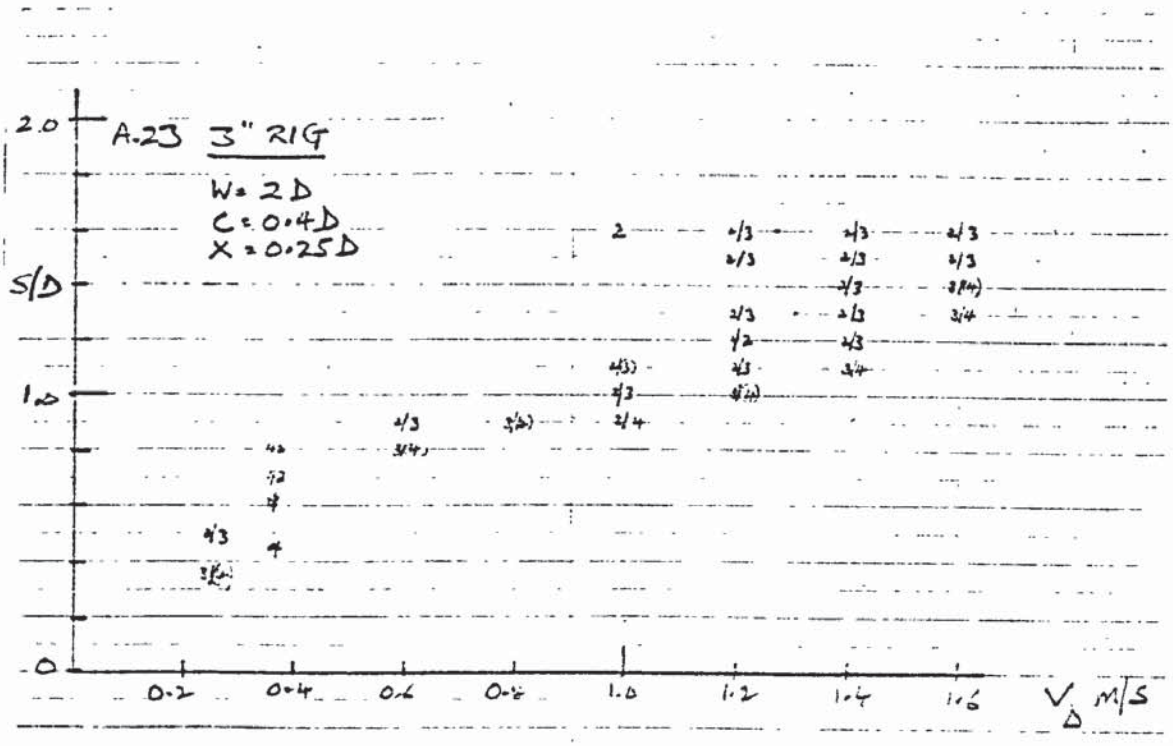
A-23 3" RIG
W = 2D
C = 0.4D
X = 0.25D
S/D
2.0
1.0
0
0.2
0.4
0.6
0.8
1.0
1.2
1.4
1.6
V_Δ m/s

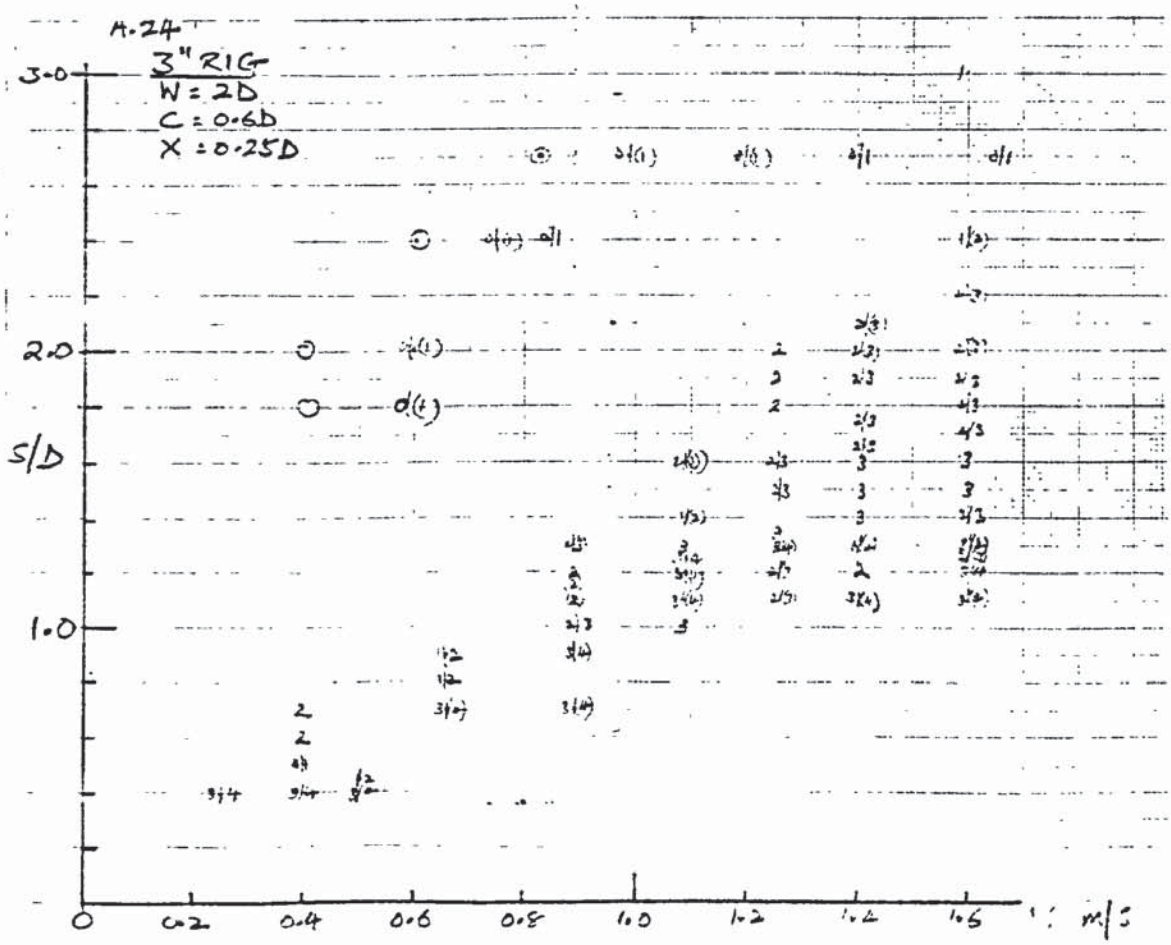
A-24
3" RIG
W = 2D
C = 0.6D
X = 0.25D
S/D
3.0
2.0
1.0
0
0.2
0.4
0.6
0.8
1.0
1.2
1.4
1.6
m/s

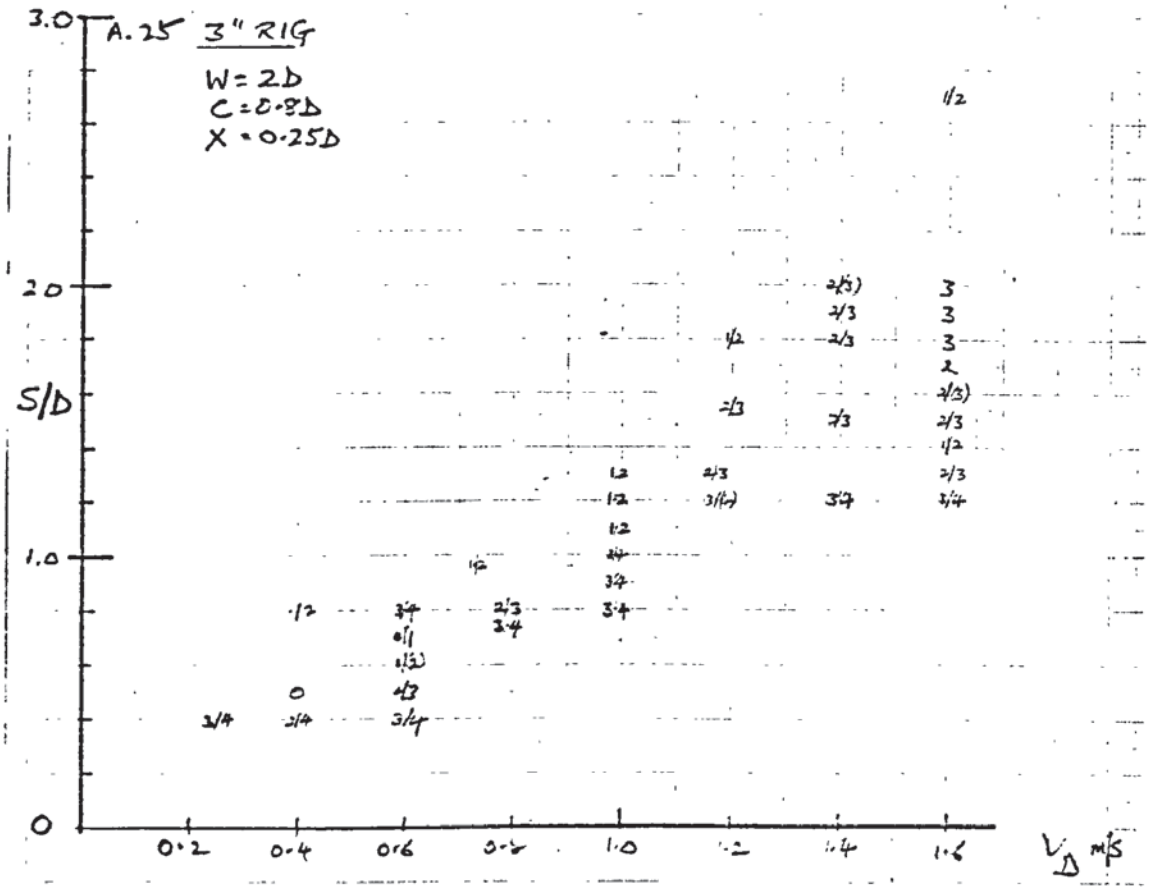
A.25 3" RIG
W = 2D
C = 0.8D
X = 0.25D
S/D
3.0
2.0
1.0
0
0.2
0.4
0.6
0.8
1.0
1.2
1.4
1.6
V_D m/s

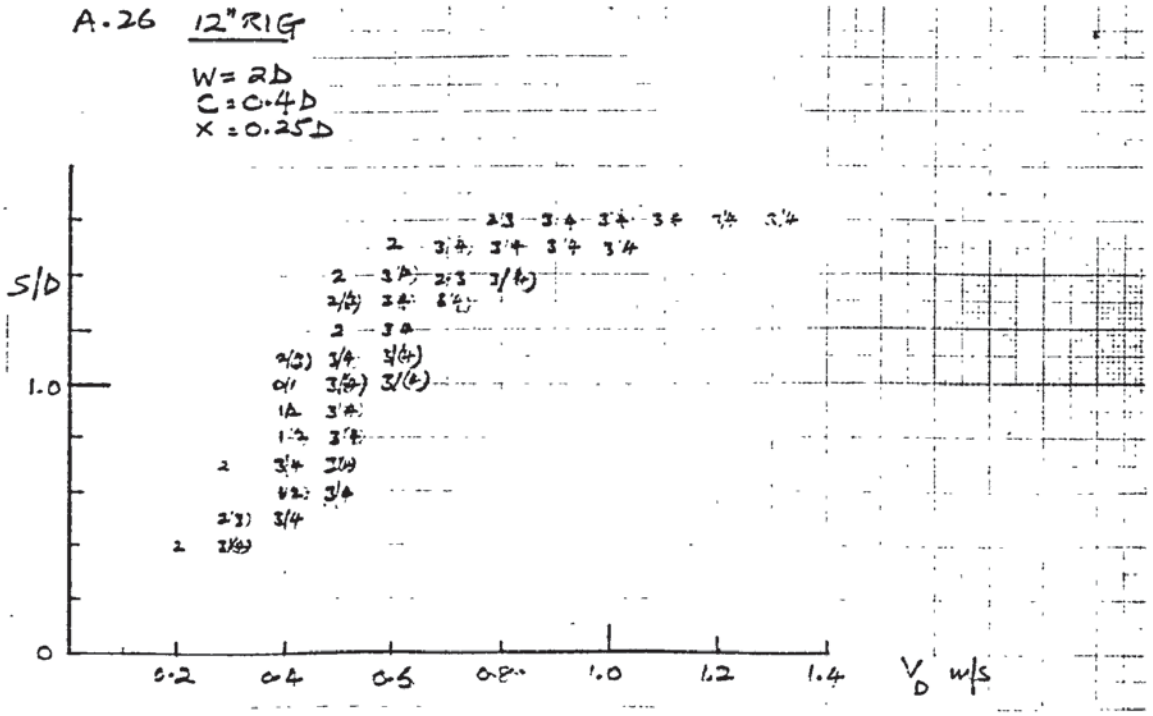
A.26 12" RIG
W = 2D
C = 0.4D
X = 0.25D
S/D
1.0
0
0.2
0.4
0.6
0.8
1.0
1.2
1.4
V_D m/s

A-27 12" RIG

W = 2D
C = 0.6D
X = 0.25D

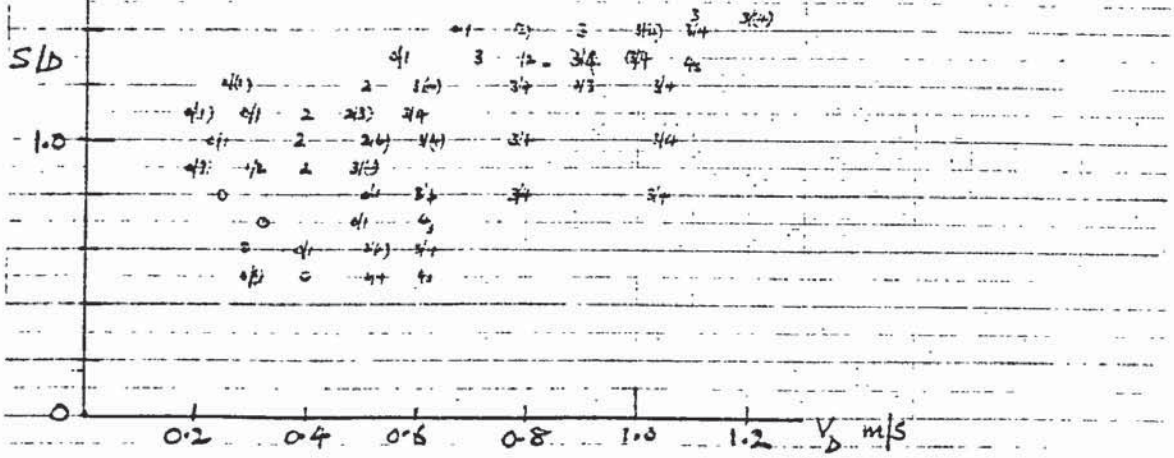

A-28 12" RIG

W = 2D
C = 0.5D
X = 0.25D

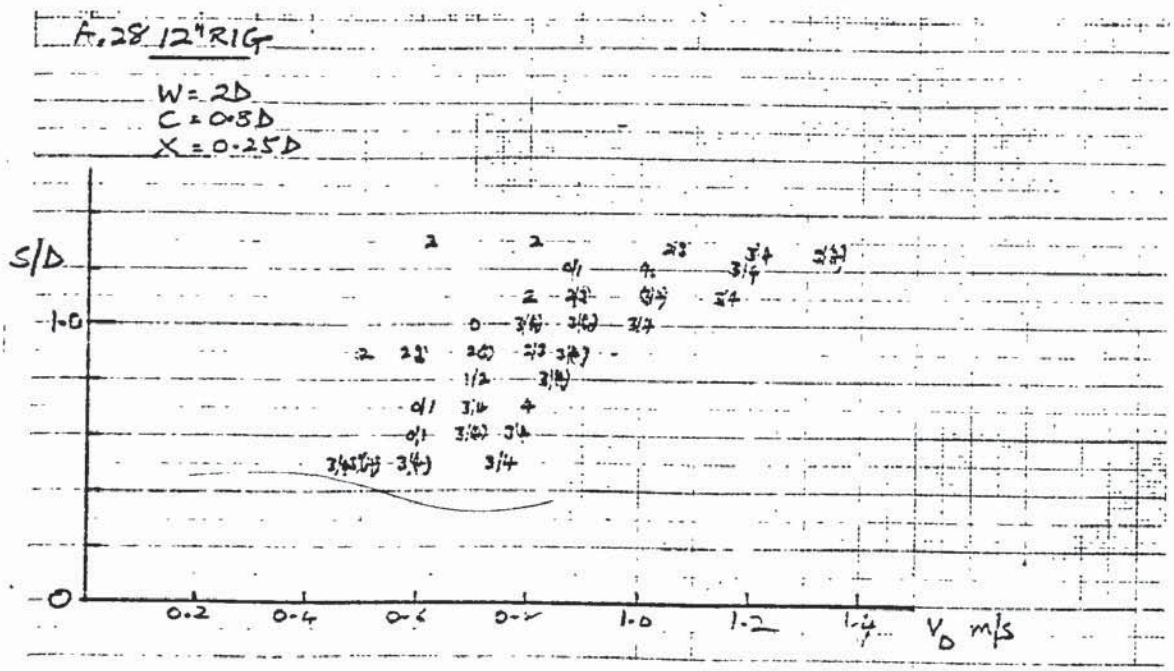

A.29 12" RIG + ½D BAFFLE AT 6D

W = 2D
C = 0·6D
X = 0·25D

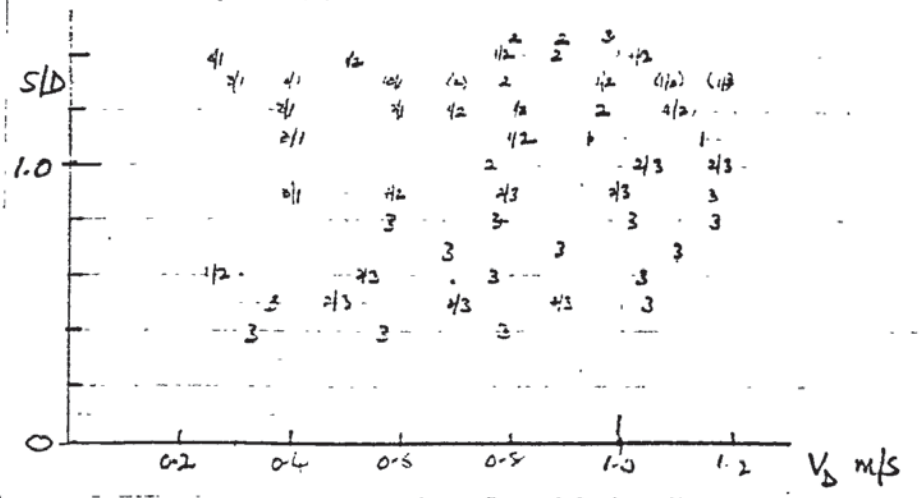

Appendix B: Table of bellmouth velocity, V_D, values and corresponding channel velocity, V_W, values.

W = 2D
X = 0.25D

		S_c/D												
		0.4	0.5	0.6	0.7	0.8	0.9	1.0	1.1	1.2	1.3	1.4	1.5	1.6
C = 0.4D														
V_D	1.5"		0.30	0.36	0.42	0.49	0.61	0.84	1.10	1.34				
	3"	0.25	0.35	0.43	0.51	0.59	0.79	1.00	1.19	1.35	1.47	1.57		
	6"			0.33	0.37	0.42	0.45	0.50	0.55	0.60	0.65	0.71	0.77	0.82
	12"	0.25	0.28	0.31	0.34	0.37	0.40	0.43	0.46	0.49	0.52	0.55	0.64	0.84
C = 0.6D														
V_D	1.5"	0.31	0.39	0.46	0.54	0.66	0.81	0.96						
	3"		0.42	0.54	0.63	0.72	0.81	0.89	0.97	1.04	1.16			
	6"			0.33	0.38	0.44	0.50	0.58	0.67	0.76	0.85	0.94	1.01	1.07
	12"		0.42	0.43	0.44	0.45	0.47	0.49	0.51	0.56	0.71	0.97		
C = 0.8D														
V_D	1.5"	0.33	0.54	0.65	0.74	0.85	0.97	1.12	1.35					
	3"		0.33	0.43	0.50	0.64	0.77	0.92	1.05	1.20				
	6"	0.31	0.34	0.37	0.40	0.43	0.46	0.50	0.56	0.64	0.70	0.77	0.85	0.94
	12"			0.57	0.66	0.71	0.74	0.78	0.84	0.95	1.13			
C = 0.4D														
V_W	1.5"		0.13	0.14	0.15	0.16	0.18	0.24	0.29	0.33				
	3"	0.12	0.15	0.17	0.18	0.19	0.24	0.28	0.31	0.33				
	6"			0.13	0.13	0.14	0.14	0.14	0.14	0.15				
	12"	0.12	0.12	0.12	0.12	0.12	0.12	0.12	0.12	0.12	0.12	0.12	0.13	0.17
C = 0.6D														
V_W	1.5"	0.12	0.14	0.15	0.16	0.19	0.21	0.24						
	3"		0.15	0.18	0.19	0.20	0.21	0.22	0.22	0.23				
	6"			0.11	0.12	0.12	0.13	0.14	0.16	0.17	0.18	0.19	0.19	0.19
	12"		0.15	0.14	0.13	0.13	0.12	0.12	0.12	0.12	0.15	0.19		
C = 0.8D														
V_W	1.5"	0.11	0.16	0.18	0.19	0.21	0.22	0.24	0.28					
	3"		0.10	0.12	0.13	0.16	0.18	0.20	0.22	0.24				
	6"	0.10	0.10	0.10	0.11	0.11	0.11	0.12	0.12	0.13	0.13	0.13	0.15	0.15
	12"			0.16	0.17	0.17	0.17	0.17	0.17	0.19	0.21			

APPENDIX C

STRAIGHT LINE FITTING USING CORRECTED VELOCITIES $(V_m - v)$ and $(V_p - v)$

As discussed in 6.4.2 an alternative method of obtaining a constant velocity ratio V_m/V_p is to correct the velocities by subtracting a quantity, v, and then take the ratio of the corrected velocities. This leads to a scaling law of the form

$$\frac{V_m - v}{V_p - v} = \text{const.} = B$$

$$\frac{V_m}{V_p} = B - \frac{v(B - 1)}{V_p}$$

The values of B and v have been found by fitting V_m/V_p and $1/V_p$ values to a straight line, using a programmable pocket calculator, and the results and data for one geometry (C/D = 0.8, X/D = 0.25, W/D = 2) are given in fig. C1. The laws are only valid for the range of V_p tested (otherwise V_m/V_p could become negative which would be meaningless in practice).

Values of the Froude scale multiplying factor, k, and Reynolds number contribution coefficient, b, have also been calculated by taking B as the value of the (corrected) velocity ratio. It can be seen that the value of b is not a constant, and furthermore, there is no obvious correlation between the values of v for correcting the velocities. Hence, this method, being more complex than the alternative discussed in 6.4.2, was not developed further.

Fig. C.1 **Scaling Laws derived from corrected velocities (V - v)**

C = 0.8D

V_{12}	$1/V_{12}$	V_6/V_{12}	V_3/V_{12}	$V_{1.5}/V_{12}$
0.57	1.75	0.65	0.75	1.14
0.66	1.52	0.61	0.76	1.12
0.71	1.41	0.61	0.90	1.20
0.74	1.35	0.62	1.04	1.30
0.78	1.28	0.64	1.18	1.44
0.84	1.19	0.67	1.25	1.61
0.95	1.05	0.67	1.26	

Scale Ratio	Derived scaling law	Other parameters
s = 1/2	$\frac{V_m}{V_p} = 0.71 - \frac{0.05}{V_p}$	v = - 2.45 B = 0.71 k = 1.00 b = 0.00
s = 1/4	$\frac{V_m}{V_p} = 2.24 - \frac{0.90}{V_p}$	v = 1.81 B = 2.24 k = 4.48 b = 2.80
s = 1/8	$\frac{V_m}{V_p} = 2.46 - \frac{0.82}{V_p}$	v = 1.68 B = 2.46 k = 6.96 b = 1.81

REFERENCES

1. **Prosser, M.J.** "The hydraulic design of pump sumps and intakes". BHRA/CIRIA, ISBN 0-86017-027-6, 48 pp. July 1977.

2. "Hydraulic Institute standards for centrifugal, rotary and reciprocating pumps". 13th ed. Cleveland. Ohio, USA, Hydraulic Institute 1975.

3a. **Swainston, M.J.C.** "Vortex formation near the intakes to turbomachinery and duct systems". Heat and Fluid Flow, I. Mech. E., 4, 2, pp. 92-100, Oct. 1974.

3b. **Swainston, M.J.C.** "Experimental and theoretical identification of air ingestion regimes in pump sumps". Proc. I. Mech. E., **190**, 59, pp. 671-678, 1976.

4. **Jenkins, J.D.** "Pumping plant". Jnl. Instn. Water Engrs. and Scientists, 30, 8, pp. 446-464, Nov. 1976.

5. **Briller, R.** "Discounted cash flow analysis to select equipment". Proc. ASCE, Jnl. Environ. Engng., **102**, EE3, pp. 595-611, Jun. 1976.

6. **Ponomareff, A.I.** "Intake tunnel design for condenser circulating pumps". ASME paper No. 50-A-138, 7 pp + 10 figs., Nov. 1950.

7. **Iversen, H.W.** "Studies of submergence requirements of high specific speed pumps". Trans. ASME, 75, pp. 635-641, May 1953.

8. **Chang, E.** "Review of literature on the formation and modelling of vortices in rectangular pump sumps". BHRA report TN 1414, 29 pp. Jun. 1977.

9. Merry, H. "Effects of two-phase liquid/gas flow on performance of centrifugal pumps". I. Mech. E. Conf. on Pumps and Compressors for Offshore Oil and Gas, Univ. of Aberdeen, Paper No. C.130/76 pp. 61-67, 29 Jun.-1 Jul. 1976.

10. Hattersley, R.T. "Hydraulic design of pump intakes." Proc. ASCE, Jnl. Hydraul. Div., 91, HY2, part 1, pp. 223-249, Mar. 1965.

11. Denny, D.F. "Experiments with air in centrifugal pumps". BHRA Report RR 465, 5 pp + 8 figs., Oct. 1953.

12. Painter, C.W. "Vortex formation in sumps of centrifugal pumps". Mining Electrical and Mechanical Engineer, 46, 1543, pp. 176-183 Jan. 1966.

13. Mayo, H.A. "The cost of inefficiency in fluid machinery". ASME Winter Annual Meeting, New York, ed. D. Japikse, pp. 19-47, Nov. 17-21, 1974.

14. Diclimente, T.J. et al "Hydraulics of cooling system backfits". Proc. Jt. Symp. Fl. Machinery, Colorado, Vol. I, pp. 475-488, June. 12-14, 1978.

15. Gardner, C.A. and Hill, H.T. "Shaft failure of large axial flow pumps". Proc. ASCE, Jnl. Power Div., 102, PO2, pp. 209-223, Nov. 1976.

16. Paterson, I.S. and Campbell, G. "Pump intake design investigations". Symp. I. Mech. E., Cranfield, pp. 3-12, April 18-19, 1968.

17. Chang, E. "Kori nuclear power station - model study of circulating water pump sump No. 1 unit". BHRA report RR 1421, 42pp. July, 1977.

18. Central Electricity Generating Board Press Office.

19. Eadie, A. Parliamentary reply, Hansard, Feb. 1978.

20. Abbott, P. "Jack rods aid slide at Steenbras". Civil Engineering, p. 12, Feb. 1978.

21. Chang, E. and Crow, D.A. "Steenbras pumped storage scheme - hydraulic and air model tests of the lower control works." BHRA Report RR 1398, 51 pp., Mar. 1977.

22. May, P. Private communication.

23. Fellerman, L. and Bruce, B.A. "Model study of the pump sump for the Marino Point project". BHRA report RR 1373, 17 pp. Sept. 1976.

24. Hall, M.G. "The structure of concentrated vortex cores". Progress in Aero Sciences, Vol. 7, ed. D. Kuchemann, pp. 53-110, 1966.

25. Burgers, J.M. "A mathematical model illustrating the theory of turbulence". Advances in Applied Mechanics, 1, pp. 171-199, 1948.

26. Rott, N. "On the viscous core of a line vortex". Zeits. Ange. Math. Phys., 96, pp. 543-553, 1958.

27. Donaldson, C. du P. and Sullivan, R.D. "Behaviour of solutions of the Navier-Stokes equations for a complete class of three-dimensional viscous vortices". Proc. 1960 Heat Transfer and Fluid Mechanics Institute, Stanford, Calif., pp. 16-30, 15-17 Jun. 1960.

28. Long, R.R. "Vortex motion in a viscous fluid". J. Meteorol., 15, 1, pp. 108-112, Feb. 1958.

29. Holtorff, G. "The free surface and conditions of similarity for a drain vortex". La Houille Blanche, 19, 3, pp. 377-384, 1964 (In French).

30. Einstein, H.A. and Li, H. "Steady vortex flow in a real fluid". La Houille Blanche, 10, 4, pp. 483-496, Aug/Sep. 1955.

31. Lewellen, W.S. "A solution for three-dimensional vortex flows with strong circulation". J. Fluid Mech., 14, 3, pp. 420-432, Nov. 1962.

32. Granger, R. "Steady three-dimensional vortex flow". J. Fluid Mech., 25, 3, pp. 557-576, July 1966.

33. Anwar, H.O. "Formation of a weak vortex". J. Hydraul. Res., 4, 1, pp. 1-16, 1966.

34. Dergarabedian, P. "The behaviour of vortex motion in an emptying container". Proc. 1960 Heat Transfer and Fluid Mechanics Institute, Stanford, Calif., pp. 47-61, 15-17 Jun. 1960.

35. Gerlach, C.R. and Dodge, F.T. "An engineering approach to tube flow-induced vibrations". Proc. Conf. on flow-induced vibrations in reactor system components, pp. 205-225, Argonne National Laboratory, 1970.

36. Schlichting "Boundary Layer Theory". McGraw-Hill, 6th edn., 747 pp. 1968.

37. Johnstone, R.E. and Thring, M.W. "Pilot plants, models and scale-up methods in chemical engineering". McGraw-Hill, 307 pp. 1957.

38. Stevens, J.C. and Kolf, R.C. "Vortex flow through horizontal orifices". Trans. ASCE, 124, paper 3004, pp. 871-883, 1959.

39. Brombach, H. "Vortex amplifiers for low control pressure ratios" 7th Cranfield Fluidics Conf. Paper C1, Nov. 1975.

40. Bradley, D. "The Hydrocyclone". Pergamon Press, 330 pp. 1965.

41. Gluck, D.F. et al "Distortion of a free surface during tank discharge" J. Spacecraft, 3, 11, pp. 1691-1692, Nov. 1966.

42. Shapiro, A.H. "Bath-tub vortex". Nature, 196, 4859, pp. 1080-1081, 15 Dec. 1962.

43. Sibulkin, M. "A note on the bathtub vortex". J. Fluid Mech., 14, 1, pp. 21-24, Sept. 1962.

44. Binnie, A.M. "Some experiments on the bath-tub vortex". J. Mech. Engng. Sci., 6, 3, pp. 256-257, Sept. 1964.

45. Springer, E.K. and Patterson, F.M. "Experimental investigation of critical submergence for vortexing in a vertical cylindrical tank". ASME paper 69-FE-49, 8 pp. Jun. 1962.

46. Daggett, L.L. and Keulegan, G.H. "Similitude in free-surface vortex formations". Proc. ASCE, J. Hydraul. Div., 100, HY11, pp. 1565-1581, Nov. 1974.

47. Quick, M.C. "Scale relationships between geometrically similar free spiral vortices". Civ. Engng. and Public Works Rev., 57, 674, pp. 1135-1138, Sept. 1962 (Part 1).

48. Toyokura T. and Akaike, S. "Vortex phenomena in a water tank". Bull. JSME, 13, 57, pp. 373-381, March 1970.

49. Seddon, A.E. and Anwar, H.O. "Measuring fluid velocities optically". Engineering, 196, pp. 318-319, Sept. 1963.

50. Berge, J.P. "Etude des phénomènes de vortex dans un liquide à surface libre. Méthodes optiques expérimentales d'étude". Bull. Centre de Recherches et d'Essais de Chatou, 13, pp. 3-23, Oct. 1965 (In French)

51. **Anwar, H.O.** "Flow in a free vortex". Water Power, 17, 4, pp. 153-161. Apr. 1965.

52. **Kelly, D.L. et al** "A further note on the bath tub vortex". J. Fluid Mech., 19, 4, pp. 539-542, Aug. 1964.

53. **Harada, M.** "On the generalized bath-tub vortex". Trans. ASME, 89, Series D, No. 3, pp. 617-623, Sept. 1967.

54. **Marris, A.W.** "Theory of the bath tub vortex". Trans. ASME, Series E, J. Appl. Mech., 89, 1, pp. 11-15, Mar. 1967.

55. **Haindl, K.** "Contribution to air entrainment by a vortex". Paper 16-D, Proc. 8th Congress IAHR, Montreal, 24-29 Aug., 1959.

56. **Kamel, M.Y.M.** "The effect of swirl on the flow of liquids through bottom outlets". ASME paper 64-WA/FE-37, 9 pp. Nov. 1964.

57. **Hughes, R.L.** Discussion to ref. 46, Proc. ASCE, HY9, pp. 1287-1289, Sept. 1975.

58. **Quick, M.C.** "Scale relationships between geometrically similar free spiral vortices". Civ. Engng. and Public Works Rev., 57, 675, pp. 1319-1320, Oct. 1962 (Part 2).

59. **Polikovski, V.I.** and **Perelman, R.T.** "The Formation of vortices in a liquid with a free surface". Gidrotechnik, 5, 1956,(In Russian).

60. **Kenn, M.J.** and **Zanker, K.J.** "Aspects of similarity for air-entraining water flows". Nature, 213, 5071, pp. 59-60, 7 Jan. 1967.

61. **Rohan, K.** "Velocity distribution in a free vortex". Vodohospod. Cas., 13, 3, pp. 345-363, 1965. (In Czech).

62. Amphlett, M.O. et al "Similarity of free-vortex at horizontal intake". Jnl. Hydr. Res., 16, 2, pp. 95-105, 1978.

63. Dicmas, J.L. "Development of an optimum sump design for propeller and mixed-flow pumps". ASME paper 67-FE-26, 8 pp., May 1967.

64. Markland, E. and Pope, J.A. "Experiments on a small pump suction well with particular reference to vortex formations". Proc. I. Mech. E., 170, 2, pp. 95-105, 1956.

65. Ragunathan, S. and Kar, S. "Performance characteristics of pump inlets". ASME paper no. 75-FE-23, 8 pp., May 1975.

66. Berge, J.P. "A study of vortex formation and other abnormal flow in a tank with and without a free surface". La Houille Blanche, 21 1, pp. 13-40, 1966. (In French- BSRA translation available no. 3166).

67. Denny, D.F. "An experimental study of air entraining vortices in pump sumps". Proc. I. Mech. E., 170, 2, pp. 106-116, 1956.

68. Wonsak, G. "Investigations of the inlet flow conditions for vertical immerged centrifugal pumps". Int. Symp. Pumps in Power Stations, Braunschweig, Session E, pp. E9-E20, 7-9 Sept. 1966.

69. Duggins, R.K. "Possible sump configurations for a small submersible pump". 4th Technical Conf. of the Brit. Pump Manufacturers. Assoc., Univ. of Durham, paper no. A3, pp. 31-39, 9-10 Apr. 1975.

70. Bqrzsonyi, A. and Kajdi, L. "Investigation of parameters characterising air turbulence phenomena in pump wells". 4th Technical Conf. of the Brit. Pump Manufacturers' Assoc., Univ. of Durham, paper no. A2, pp. 19-29, 9-10 Apr. 1975.

71. Young, L. Discussion on ref. 67, Proc. I. Mech. E., 170, 2, pp. 121-123, 1956.

72. Chang, E. and Clarke, A. "Kori nuclear power station model study of circulating water pump sump No. 2 unit". BHRA report RR 1489, 20 pp. July 1978.

73. Surek, D. "Strömungtechnische gestaltung offener einlaufbauwerke für verticale axial-und diagonal pumpen". Pumpen und Verdichter Informationen, 1, pp. 23-9, 1975. (In German - BHRA translation available).

74. Durgin, W.W. and Hecker, G.E. "The modelling of vortices at intake structures". Proc. Jt. Symp. Fl. Machinery, Vol. I, pp. 381-392, Jun. 12-14, 1978.

75. Zajdlik, M. "New checking mode of model parameters for vortex formation in pump tanks". Proc. 7th Congress IAHR, Baden-Baden, Vol. 5, pp. 379-386, 15-19 Aug. 1977.

76. Shahroody, A.M. and Davis, J.R. "Efficiency of pumping from small circular sumps". Proc. ASCE, 90, IR 1, Part 1, paper 3817, pp. 1-8, Mar. 1964.

77. Gordon, J.L. "Vortices at intakes". Water Power, pp. 137-138, Apr. 1970.

78. Rahm, L. "Flow problems with respect to intakes and tunnels of Swedish hydro-electric power plants". Trans. Roy. Inst. Tech., Stockholm, Sweden, no. 71, 219 pp., 1953.

79. Reddy, Y.R. and Pickford, J.A. "Vortices at intakes in conventional sumps". Water Power, pp. 108-109, Mar. 1972.

80. **Jones, W.G.** "Cooling water for power stations". Proc. Instn. Civ. Engrs., Part 1, **62**, pp. 373-398, Aug. 1977.

81. **Dutkiewicz, R.K.** and **Ham, A.J.** "Model studies of a circular pumphouse forebay". The S. African Mech. Engr., pp. 217-220, Jan. 1968.

82. **British Standards Institution** "Methods for the measurement of fluid flow in pipes". British Standard 1042, 1964 (Part 1) and 1965 (Part 3).

83. **Lugt, H.** "Influence of swirling flow on the discharge coefficient of standard pressure differential flowmeters". Brennst.-Wärme-Kraft, 13, (3), pp. 121-125, 1961. (In German - translation available - BHRA translation T 716, Feb. 1962).

84. **Goldschmidt, G.** "Wet-well volumes for multipump systems". Proc. ASCE, Irrig. Drainage Div., 100, IR 3, pp. 371-385, Sept. 1974.

85. **Sosa, F.** and **Baker, E.W.** "Acoustic evaluation of axial-flow propellers and their influence on pump vibratory characteristics". Proc. Jt. Symp. Fl. Machinery, Colorado, Vol. II, pp. 439-449, Jun. 12-14, 1978.

86. **Scott, B.** Private communication.

NOMENCLATURE

A	Cross-sectional area of intake
b	Coefficient of Reynolds number contribution to consistent scaling law
C	Distance from sump floor to bellmouth lip (floor clearance)
C_D	Discharge coefficient
D	Bellmouth diameter
d	Suction pipe diameter (external)
F	Froude number - $V/(gl)^{\frac{1}{2}}$
g	Acceleration due to gravity
H	Total depth (S + C) or pump head
K	Kolf number $\Gamma r/Q$
k	Froude scale multiplying factor
L	Length of approach channel
l	Characteristic length, e.g. water depth, intake diameter
p	Pressure
Q	Discharge, flow rate
R	Reynolds number Vl/ν
r, θ, z,	Cylindrical polar co-ordinates
S	Submergence (water surface to bellmouth)
$\mathcal{S}$	Strouhal number = nd/V_W, n = frequency of vortex shedding
s	Scale ratio l_m/l_p
t	Time
u	Radial velocity component
V	Velocity
v	Tangential velocity component
W	Sump channel width
We	Weber number = $V(\rho l/\sigma)^{\frac{1}{2}}$
w	Axial velocity component
X	Distance from endwall to bellmouth lip (endwall clearance)
x	Distance along sidewall
x, y, z	Rectangular co-ordinates
Γ	Circulation at radius r
δ	Boundary layer thickness
ζ	Vorticity
μ	Dynamic viscosity
ν	Kinematic viscosity
ρ	Density
σ	Surface tension
ψ	Stream function
Ω	Angular velocity

Subscripts (not included above)

c	Critical length parameter for onset of air entrainment
m	Model
p	Prototype
θ	Tangential component